Computer-assisted proofs for differential equations and dynamical systems

Maxime Breden

INSTITUT POLYTECHNIQUE DE PARIS

Habilitation à Diriger les Recherches

Computer-assisted proofs for differential equations and dynamical systems

Maxime Breden

Professeur assistant, CMAP UMR 7641, École polytechnique

30 juin 2025

Sur avis des rapports de :

Javier Gómez-Serrano
Department of Mathematics, Brown University

Marc Massot
CMAP, École polytechnique

Konstantin Mischaikow
Department of Mathematics, Rutgers University

Composition du Jury :

Clément Cancès
INRIA et LPP, Université de Lille

Javier Gómez-Serrano
Department of Mathematics, Brown University

Mioara Joldes
CNRS, LAAS

Marc Massot
CMAP, École polytechnique

Konstantin Mischaikow
Department of Mathematics, Rutgers University

Martin Vohralík
INRIA et CERMICS, Ecole nationale des ponts et chaussées

Thomas Wanner
Department of Mathematical Sciences, George Mason University

Remerciements

First of all, I want to thank Javier Gómez-Serrano, Konstantin Mischaikow and Marc Massot for taking to time to review this manuscript. Konstantin and Javier, you are both excellent ambassadors for the field of computer-assisted proofs, it is an honor to have you as reviewers for this habilitation. On the local side, thank you Marc for always being very supportive since I arrived at École polytechnique, if not for your help with getting a half-sabbatical for the first part of this year, this habilitation would probably still not be done. I am also very grateful to Clément Cancès, Mioara Joldes, Martin Vohralík and Thomas Wanner for agreeing to be part of my jury, and for the interest they have shown in my work.

I want to take this opportunity to thank once more my former PhD supervisors Laurent Desvillettes and Jean-Philippe Lessard, who both had a very positive influence on the researcher I have become. Looking back, I do not think I fully appreciated at the time how lucky I was to have you two as first examples. The next two years I spent as a postdoc in Munich with Christian Kuehn were equally fruitful. Thank you Christian for putting together such a great group, several of my current research endeavors and collaborations originate from there. Finally, the last person that acted as a kind of mentor (although unofficially, and maybe even unintentionally) is Jan Bouwe van den Berg, who has always been, in his own unassuming way, a great person for me to look up to. I am also extremely glad for the close collaboration we set up these past few years (I counted at least ten visits between Amsterdam and Paris since the end of my PhD, and I am looking forward to the next one).

More generally, my biggest thanks are for all my collaborators: you are the main reason this job is both so stimulating and so much fun. Special shout-outs to all the CAPifiers for building such a welcoming community, and in particular to Jason Mireles James for more than ten years of (ongoing) collaboration, as well as to my former TUM office mate Maximilan Engel for first dragging me into the world of random dynamical systems. I also want to specifically thank some of my younger collaborators, who trusted me to try to provide some guidance to them, thereby giving me the opportunity to actually learn how to become a better supervisor: Maxime Payan (who is in fact the main reason why this habilitation is being done now rather than eventually) and Olivier Hénot, as well as Matthieu Cadiot and Hugo Chu, whom I look forward to welcoming at École Polytechnique in the coming months.

Despite my research being somewhat exotic and not quite fitting into any of the existing teams at CMAP, I was very well welcomed there. Thank you to all the colleagues who contribute to the great research and teaching environment there (even though we like to complain about it), and particularly to all the support staff from the lab and the department, who, despite sometimes difficult working conditions, go out of their way to make our own job as easy as possible.

Contents

Foreword

The purpose of this manuscript is to describe the work I have carried out since completing my PhD, in the field of computer-assisted proofs for differential equations and dynamical systems. As such, it is inevitably way too biased to constitute a proper survey of the field, but I hope it still provides an informative overview of some of the recent and still ongoing developments, and extensive references to related works are provided throughout the manuscript.

The aim of Chapter 1 is to give a gentle introduction to the field of computer-assisted proofs in nonlinear analysis, and hopefully to provide a good entry-point for researchers not yet familiar with computer-assisted proofs. Some of the essential tools and their different variations are presented in full details, and a relatively simple but still non trivial example is discussed in a self-contained manner, and solved using two different computer-assisted approaches. None of the material contained in this first chapter is new, but the presentation is sometimes slightly more modern or simplified compared to the existing literature. For the readers already familiar with computer-assisted proofs, this first chapter describes what will be taken for granted in the remainder of the manuscript, and is used as a reference point in subsequent chapters, to explain when and how we depart from the already well-established techniques.

Chapter 2 is based on [B3, B10], and describes two computer-assisted proofs, for the Navier–Stokes equations and the so-called DPCM. The aim of this chapter is twofold. First, it provides good examples of problems that were already of interest to the mathematical community, but that could not be fully solved with traditional pen-and-paper analysis, and for which computer-assisted proofs can provide helpful answers, and pave the way to further investigations. Second, it showcases that some of the relatively simple ideas presented on basic examples in Chapter 1 can also be used successfully on significantly more complex problems.

In Chapter 3, we discuss various problems which are outside of the "traditional" framework that was described in Chapter 1, and present new approaches to study them with computer-assistance. The first topic is that of quasilinear equations, studied in [B7, B24], and for which some of the classical computer-assisted techniques developed for semi-linear equations no longer apply. We then discuss recent developments in the treatment of non-polynomial nonlinearities within computer-assisted proofs based on spectral methods, and in particular [B17], in which we revisit computer-assisted proofs for Feigenbaum renormalization operators. Finally, we present computer-assisted proofs for a class of problems on unbounded domains, for which a new setup was introduced in [B11].

Whereas the first chapters only dealt with stationary or periodic problems, Chapter 4 is focused on rigorous time-integration of parabolic PDEs, with the goal of eventually studying connecting orbits in PDEs with computer-assisted proofs. There has been a lot of recent activity around rigorous integration of PDEs, and we present our own take on this question, based on [B4, B1]. These are perhaps some of the most technical works described in this manuscript, but we present the main ideas in a general and hopefully accessible way, as some of them are of interest beyond rigorous integration problems.

Chapter 5 discusses rigorous continuation techniques, for which we recently proposed a new approach in [B8], that is significantly simpler and more efficient that previous techniques, and also generalizes in a straightforward manner to multi-parameter continuation.

Finally, Chapter 6 describes the ongoing journey I have embarked upon, with several col-

laborators from the stochastic world, whose aim is to develop computer-assisted tools to study stochastic systems in a quantitative way [B18, B19, B8, B16, B5, B12]. Of particular note are the results of Section 6.3, in which we present new techniques to precisely study Lyapunov exponents of SDEs, and in particular to prove that some stochastic systems have positive Lyapunov exponents, which is often associated with chaotic dynamics.

List of publications

The articles that were part of my PhD thesis are identified with a symbol $\star$, and are not presented in this manuscript, but some of them are mentioned when relevant. Among the other ones, [B13] is not related to computer-assisted profs, and is therefore also not discussed further in this document.

[B1] J. B. van den Berg and M. Breden. Improved validated integration of semilinear parabolic PDEs. *In preparation*, 2025.

[B2] $\star$ J. B. van den Berg, M. Breden, J.-P. Lessard, and M. Murray. Continuation of homoclinic orbits in the suspension bridge equation: a computer-assisted proof. *Journal of Differential Equations*, 264(5):3086–3130, 2018.

[B3] J. B. van den Berg, M. Breden, J.-P. Lessard, and L. van Veen. Spontaneous periodic orbits in the Navier–Stokes flow. *Journal of Nonlinear Science*, 31(2):1–64, 2021.

[B4] J. B. van den Berg, M. Breden, and R. Sheombarsing. Validated integration of semilinear parabolic PDEs. *Numerische Mathematik*, pages 1–69, 2024.

[B5] A. Blessing, A. Blumenthal, M. Breden, and M. Engel. Detecting random bifurcations via rigorous enclosures of large deviations rate functions. *Physica D: Nonlinear Phenomena*, 476:134617, 2025.

[B6] $\star$ M. Breden. Applications of improved duality lemmas to the discrete coagulation-fragmentation equations with diffusion. *Kinetic and Related Models*, 11(2):279–301, 2018.

[B7] M. Breden. Computer-assisted proofs for some nonlinear diffusion problems. *Communications in Nonlinear Science and Numerical Simulation*, 109:106292, 2022.

[B8] M. Breden. A posteriori validation of generalized polynomial chaos expansions. *SIAM Journal on Applied Dynamical Systems*, 22(2):765–801, 2023.

[B9] $\star$ M. Breden and R. Castelli. Existence and instability of steady states for a triangular cross-diffusion system: a computer-assisted proof. *Journal of Differential Equations*, 264(10):6418–6458, 2018.

[B10] M. Breden, C. Chainais-Hillairet, and A. Zurek. Existence of traveling wave solutions for the Diffusion Poisson Coupled Model: a computer-assisted proof. *ESAIM: Mathematical Modelling and Numerical Analysis*, 55(4):1669–1697, 2021.

[B11] M. Breden and H. Chu. Constructive proofs for some semilinear PDEs on $H^2(e^{|x|^2/4}, \mathbb{R}^d)$. *arXiv preprint arXiv:2404.04054*, 2024.

[B12] M. Breden, H. Chu, J. S. Lamb, and M. Rasmussen. Rigorous enclosure of Lyapunov exponents of stochastic flows. *arXiv preprint arXiv:2411.07064*, 2024.

[B13] M. Breden and L. Desvillettes. Rigorous study of the equilibria of collision kernels appearing in the theory of weak turbulence. *Archive for Rational Mechanics and Analysis*, 235(2): 1151–1176, 2020.

[B14] ⋆ M. Breden, L. Desvillettes and K. Fellner. Smoothness of moments of the solutions of discrete coagulation equations with diffusion. *Monatshefte für Mathematik*, 183(3): 437–463, 2017.

[B15] ⋆ M. Breden, L. Desvillettes, and J.-P. Lessard. Rigorous numerics for nonlinear operators with tridiagonal dominant linear part. *Discrete & Continuous Dynamical Systems-A*, 35(10):4765–4789, 2015.

[B16] M. Breden and M. Engel. Computer-assisted proof of shear-induced chaos in stochastically perturbed Hopf systems. *Ann. Appl. Probab.*, 33(2):1052–1094, 2023.

[B17] M. Breden, J. Gonzalez, and J. Mireles James. Validated enclosure of renormalization fixed points via Chebyshev series and the DFT. *arXiv preprint arXiv:2409.20457*, 2024.

[B18] M. Breden and C. Kuehn. Rigorous validation of stochastic transition paths. *Journal de Mathématiques Pures et Appliquées*, 131:88–129, 2019.

[B19] M. Breden and C. Kuehn. Computing invariant sets of random differential equations using polynomial chaos. *SIAM Journal on Applied Dynamical Systems*, 19(1):577–618, 2020.

[B20] M. Breden, C. Kuehn, and C. Soresina. On the influence of cross-diffusion in pattern formation. *Journal of Computational Dynamics*, 8(2):213–240, 2021.

[B21] ⋆ M. Breden and J.-P. Lessard. Polynomial interpolation and a priori bootstrap for computer-assisted proofs in nonlinear ODEs. *Discrete & Continuous Dynamical Systems-B*, 23(7):2825–2858, 2018.

[B22] ⋆ M. Breden, J.-P. Lessard and J.D. Mireles James. Computation of maximal local (un)stable manifold patches by the parameterization method. *Indagationes Mathematicae*, 27(1): 340–367, 2016.

[B23] ⋆ M. Breden, J.-P. Lessard, and M. Vanicat. Global bifurcation diagrams of steady states of systems of PDEs via rigorous numerics: a 3-component reaction-diffusion system. *Acta applicandae mathematicae*, 128(1):113–152, 2013.

[B24] M. Breden and M. Payan. Computer-assisted proofs for the many steady states of a chemotaxis model with local sensing. *Physica D: Nonlinear Phenomena*, 466:134221, 2024.

Below are links to the different codes referenced throughout this manuscript, which are used for the computer-assisted parts of the proofs. I emphasize that I was not directly involved in the writing of some of them. In particular, [Code 12] was entirely written by Maxime Payan, [Code 10] and [Code 11] by Hugo Chu, and [Code 1] by Jan Bouwe van den Berg. I made some minor contributions to [Code 2], which was mostly written by Jan Bouwe van den Berg, based on some older code from Ray Sheombarsing. I made some contributions to [Code 9], which was mainly written by Jorge Gonzalez. All the other codes were written by myself.

[Code 1] J. B. van den Berg. Matlab code for "Spontaneous periodic orbits in the Navier-Stokes flow". https://www.math.vu.nl/~janbouwe/code/navierstokes/, 2019.

[Code 2] J. B. van den Berg, M. Breden, and R. Sheombarsing. Matlab code for "validated integration of semilinear parabolic PDEs". https://github.com/MaximeBreden/validated-PDE-integrator, 2024.

[Code 3] M. Breden. Matlab code for "Existence of traveling wave solutions for the Diffusion Poisson Coupled Model: a computer-assisted proof". https://github.com/MaximeBreden/DPCM, 2021.

[Code 4] M. Breden. Matlab code for "Computer-assisted proof of shear-induced chaos in stochastically perturbed Hopf systems". https://github.com/MaximeBreden/Shear-inducedChaos, 2021.

[Code 5] M. Breden. Matlab code for "Computer-assisted proofs for some nonlinear diffusion problems". https://github.com/MaximeBreden/Nonlinear_diffusion, 2022.

[Code 6] M. Breden. Matlab code for "A posteriori validation of generalized polynomial chaos expansion". https://github.com/MaximeBreden/gPC_expansions, 2023.

[Code 7] M. Breden. Matlab code for "Detecting random bifurcations via rigorous enclosures of large deviations rate functions". https://github.com/MaximeBreden/LDPforFTLE, 2024.

[Code 8] M. Breden. Matlab code for the introduction of "Computer-assisted proofs for differential equations and dynamical systems". https://github.com/MaximeBreden/HDR, 2025.

[Code 9] M. Breden, J. Gonzalez. Julia code for "Validated enclosure of renormalization fixed points via Chebyshev series and the DFT". https://github.com/joluigonza/renor, 2024.

[Code 10] H. Chu. Julia code for "Constructive proofs for some semilinear PDEs on $H^2(e^{|x|^2/4}, \mathbb{R}^d)$". https://github.com/Huggzz/Hermite-Laguerre_proofs, 2024.

[Code 11] H. Chu. Julia code for "Rigorous enclosure of Lyapunov exponents of stochastic flows". https://github.com/Huggzz/Enclosure-of-Lyapunov-exponents, 2024.

[Code 12] M. Payan. Matlab code for "Computer-assisted proofs for the many steady states of a chemotaxis model with local sensing". https://github.com/MaximePayan/NonLinearCrossDiffusion/tree/main, 2023.

Chapter 0

Notations and conventions

We collect here for the convenience of the reader a few conventions and notations. These will be used consistently throughout the manuscript, but we warn the reader that other less important notations may be defined independently in each chapter or section, i.e., a given symbol might mean different things in different chapters or sections.

- **Natural numbers:** $\mathbb{N}$ denotes the set $\{0, 1, 2, \dots\}$ of natural numbers *including* 0. For any integer $n \geq 1$, we write $\mathbb{N}_{\geq n}$ the set $\{n, n+1, n+2, \dots\}$ of natural numbers starting from n.

- **Torus:** $\mathbb{T}$ denotes the one-dimensional torus, of length 2π unless specified otherwise, i.e., $\mathbb{T} = \mathbb{R}/(2\pi\mathbb{Z})$.

- **Norms on Banach spaces and linear operators:** Given Banach spaces[1] $\mathcal{X}$ and $\mathcal{Y}$, we denote by $\|x\|_{\mathcal{X}}$ the norm of an element x of $\mathcal{X}$ (resp. by $\|y\|_{\mathcal{Y}}$ the norm of an element y of $\mathcal{Y}$), and by $\|\mathcal{L}\|_{\mathcal{B}(\mathcal{X},\mathcal{Y})}$ the operator norm of a bounded linear operator $\mathcal{L} : \mathcal{X} \to \mathcal{Y}$. However, when the spaces are clear from context, we might lighten the notation and simply use $\|\cdot\|$ for both the norm on a Banach space and the associated operator norm. Finally, given $x \in \mathcal{X}$ and $r \geq 0$, we denote by $B_r(x)$ the *closed* ball of center x and radius r in $\mathcal{X}$.

- **Weighted ℓ^1 spaces:** Given a Banach space $\mathcal{X}$ and $\nu \geq 1$, we introduce two sequences spaces that play a central role in our analysis:

$$\ell^1_\nu(\mathbb{Z}, \mathcal{X}) = \left\{ u = (u_n)_{n\in\mathbb{Z}} \in \mathcal{X}^{\mathbb{Z}},\ \|u\|_{\ell^1_\nu(\mathbb{Z},\mathcal{X})} := \sum_{n\in\mathbb{Z}} \|u_n\|_{\mathcal{X}}\, \nu^{|n|} < \infty \right\},$$

  and

$$\ell^1_\nu(\mathbb{N}, \mathcal{X}) = \left\{ u = (u_n)_{n\in\mathbb{N}} \in \mathcal{X}^{\mathbb{N}},\ \|u\|_{\ell^1_\nu(\mathbb{N},\mathcal{X})} := \|u_0\|_{\mathcal{X}} + 2\sum_{n\geq 1} \|u_n\|_{\mathcal{X}}\, \nu^{n} < \infty \right\}.$$

  In most cases, $\mathcal{X}$ will simply be $\mathbb{R}$ or $\mathbb{C}$. If the space $\mathcal{X}$ is unimportant or clear from context, we may lighten the notation to $\ell^1_\nu(\mathbb{Z})$ and $\ell^1_\nu(\mathbb{N})$, or even to ℓ^1_ν when the range of indices is unimportant or clear from context.

- **Connection (and abuse of notation) between $\ell^1_\nu(\mathbb{Z})$ and Fourier series:** Elements in $\ell^1_\nu(\mathbb{Z}, \mathcal{X})$ are typically associated with absolutely convergent Fourier series. Indeed,

[1] Many of the definitions given here also make sense for normed vector spaces, but we are only using Banach spaces in this manuscript, hence the restricted definitions.

given a sequence $u \in \ell^1_\nu(\mathbb{Z}, \mathcal{X})$, we can consider the 2π-periodic continuous function with values in $\mathcal{X}$:

$$u : \theta \mapsto \sum_{n\in\mathbb{Z}} u_n e^{in\theta}, \qquad \theta \in [0, 2\pi].$$

Reciprocally, a smooth enough 2π-periodic function u with values in $\mathcal{X}$ can be represented uniquely by it's sequence of Fourier coefficients $(u_n)_{n\in\mathbb{Z}}$, belonging to $\ell^1_\nu(\mathbb{Z}, \mathcal{X})$ for some $\nu \geq 1$ depending on the domain of analyticity of the function. In order to not overburden the notation, we typically use the same symbol (here u), to denote both a function and its sequence of Fourier coefficients.

For the readers who may not be familiar which such ℓ^1_ν spaces, we recall that, if $u \in \ell^1_\nu$, then the function u extends analytically to the complex strip $\{z \in \mathbb{C},\ |\Im(z)| < \ln(\nu)\}$ and remains bounded on its closure. Reciprocally, if a 2π-periodic function u extends analytically to a complex strip $\{z \in \mathbb{C},\ |\Im(z)| < \ln(\nu)\}$ for some $\nu > 1$, then its Fourier sequence belongs to $\ell^1_{\nu'}$ for all $\nu' < \nu$.

- **Connection (and abuse of notation) between $\ell^1_\nu(\mathbb{N})$ and cosines or Chebyshev series:** The above discussion regarding $\ell^1_\nu(\mathbb{Z}, \mathcal{X})$ also applies to $\ell^1_\nu(\mathbb{N}, \mathcal{X})$, but this time with cosines series. That is, $u \in \ell^1_\nu(\mathbb{N}, \mathcal{X})$ is identified with the function

$$u : \theta \mapsto u_0 + 2\sum_{n\geq 1} u_n \cos(n\theta) = \sum_{n\in\mathbb{Z}} u_{|n|} e^{in\theta}, \qquad \theta \in [0, 2\pi],$$

where the link with exponential series explains the factor 2 in the norm on $\ell^1_\nu(\mathbb{N}, \mathcal{X})$.

Because of the connection $T_n(\cos\theta) = \cos(n\theta)$ between Chebyshev polynomials of the first kind T_n and cosines, we also sometimes make use of $\ell^1_\nu(\mathbb{N}, \mathcal{X})$ to represent Chebyshev series. That is, $u \in \ell^1_\nu(\mathbb{N}, \mathcal{X})$ can also be identified with the function

$$u : t \mapsto u_0 + 2\sum_{n\geq 1} u_n T_n(t), \qquad t \in [-1, 1].$$

For Chebyshev series, the connection between ℓ^1_ν spaces and domains of analyticity is expressed in terms of Berstein ellipses (see Section 3.2.3 and the references therein).

- **Projections:** For any $N \in \mathbb{N}$, we define the projection operators $\Pi^{\leq N}$ and $\Pi^{>N}$ on $\ell^1_\nu(\mathbb{Z})$ by

$$\left(\Pi^{\leq N} u\right)_n = \begin{cases} u_n, & |n| \leq N \\ 0, & |n| > N \end{cases} \qquad \text{and} \qquad \left(\Pi^{>N} u\right)_n = \begin{cases} 0, & |n| \leq N \\ u_n, & |n| > N. \end{cases}$$

We use the same notation on $\ell^1_\nu(\mathbb{N})$, where

$$\left(\Pi^{\leq N} u\right)_n = \begin{cases} u_n, & 0 \leq n \leq N \\ 0, & n > N \end{cases} \qquad \text{and} \qquad \left(\Pi^{>N} u\right)_n = \begin{cases} 0, & 0 \leq n \leq N \\ u_n, & n > N. \end{cases}$$

We often identify elements in $\Pi^{\leq N}\ell^1_\nu(\mathbb{Z}, \mathcal{X})$ with vectors in $\mathcal{X}^{2N+1}$, and linear operators on $\Pi^{\leq N}\ell^1_\nu(\mathbb{Z}, \mathcal{X})$ with $(2N+1)\times(2N+1)$ matrices whose coefficients are linear operators on $\mathcal{X}$. The same hold for $\Pi^{\leq N}\ell^1_\nu(\mathbb{N}, \mathcal{X})$, this times with vectors of size $N+1$ and matrices of size $(N+1)\times(N+1)$. Finally, we often refer to elements in $\Pi^{\leq N}\ell^1_\nu(\mathbb{Z}, \mathcal{X})$ as *finite* Fourier series.

- **Multiplication operators:** If the Banach space $\mathcal{X}$ possesses a multiplication operator which makes it a Banach algebra, then $\ell^1_\nu(\mathbb{Z},\mathcal{X})$ is itself a Banach algebra, with the discrete convolution product $*$ defined as follows: for any $u, v \in \ell^1_\nu(\mathbb{Z},\mathcal{X})$,

$$(u*v)_n = \sum_{k\in\mathbb{Z}} u_k v_{n-k}, \qquad \text{for all } n \in \mathbb{Z}.$$

  The same is true for $\ell^1_\nu(\mathbb{N},\mathcal{X})$, where this time, for any $u, v \in \ell^1_\nu(\mathbb{N},\mathcal{X})$,

$$(u*v)_n = \sum_{k\in\mathbb{Z}} u_{|k|} v_{|n-k|}, \qquad \text{for all } n \in \mathbb{N}.$$

  Thanks to this algebra structure, any element $u \in \ell^1_\nu$ defines a multiplication operator on ℓ^1_ν, which we denote $\mathcal{M}(u)$. That is, for all $v \in \ell^1_\nu$,

$$\mathcal{M}(u)v = u * v.$$

  Note that, thanks to the Banach algebra property of the ℓ^1_ν norm,

$$\|\mathcal{M}(u)\|_{\mathcal{B}(\ell^1_\nu,\ell^1_\nu)} = \|u\|_{\ell^1_\nu}.$$

- **Linear operators as infinite matrices.** Given a linear operator $\mathcal{L}$ on $\ell^1_\nu(\mathbb{Z},\mathcal{X})$, we frequently represent $\mathcal{L}$ as the *infinite matrix*, associated with the canonical Schauder basis of $\ell^1_\nu(\mathbb{Z},\mathcal{X})$. That is, we write $\mathcal{L} = (\mathcal{L}_{i,j})_{i,j\in\mathbb{Z}}$, where the coefficients $\mathcal{L}_{i,j}$ are the linear operators on $\mathcal{X}$ (i.e., simply numbers if $\mathcal{X}$ is $\mathbb{R}$ or $\mathbb{C}$) such that

$$(\mathcal{L}u)_i = \sum_{j\in\mathbb{Z}} \mathcal{L}_{i,j} u_j \qquad \text{for all } u \in \ell^1_\nu(\mathbb{Z},\mathcal{X}) \text{ and } i \in \mathbb{Z}.$$

  We do the same, but with all indices ranging over $\mathbb{N}$, for linear operators on $\ell^1_\nu(\mathbb{N},\mathcal{X})$.

Chapter 1

Introduction

1.1 Computer-assisted proofs, within this manuscript and beyond

What is a *computer-assisted proof*? The obvious answer: "it is a proof which uses the computer", is correct but also still rather vague. Even within the mathematical community, there are different notions of proof, and the computer could be involved in many distinct ways.

In this manuscript, we discuss computer-assisted proofs for the analysis of differential equations and dynamical systems. By *proofs*, we mean the usual type of proofs (sometimes called *informal proofs* in proof theory) contained in a typical mathematical paper on PDEs or dynamical systems, as opposed to *formal proofs* using proofs assistants like Rocq, Lean or Isabelle, which are also often referred to as computer-assisted proofs but are not the focus of this manuscript. In our proofs, the computer is crucial for two different steps.

- **Step 1:** Finding a suitable approximate solution.
- **Step 2:** Proving the existence of a true solution nearby.

In a nutshell, we are going to establish the existence of a solution by using a local fixed-point argument, in a neighborhood of an approximate solution. This is in fact a common strategy in pen-and-paper nonlinear analysis, especially in *perturbative settings*, for instance a system with a small nonlinearity for which the linear case is understood, or a system with an arbitrary small or large parameter for which the limit is understood. However, the computer can make this strategy much more broadly applicable, by using numerical simulations to obtain highly nontrivial approximate solutions even outside of a perturbative setting. Once an approximate solution is at hand, one has to do analysis to prove that a suitable operator indeed has a nearby fixed point corresponding to a solution of our problem. Having to deal with highly nontrivial approximate solutions may complicate this analysis, which then often also requires computer assistance. Typically, one derives by hand a finite set of sufficient conditions ensuring the existence of a fixed point, and then uses the computer to rigorously check whether these conditions hold.

Step 1 might be a formidable task for some problems (e.g., finding an accurate approximate blowup profile for the Navier–Stokes equations), but is not the focus of this manuscript. Indeed, we are only going to consider situations where approximate solutions can be obtained by existing numerical methods (typically Newton's method and numerical bifurcation/continuation techniques for invariant sets, and standard integration schemes for initial value problems), and instead discuss how to get existence theorems with guaranteed error bounds out of these approximate solutions.

This second step is outlined more precisely in Section 1.2, and then further detailed in various situations in the different chapters of this document, but let us already mention two main ingredients that will be required.

- **Control of discretization errors.** The solutions that we seek typically live in infinite dimensional function spaces, whereas the computer can only handle finite (but potentially high) dimensional objects. This is where most of the mathematical challenges lie, which will be addressed with a combination of tools from approximation theory and functional analysis.

- **Control of rounding errors.** Our proofs are completely agnostic to the way the approximate solution is actually obtained, and in particular the fact that rounding errors occur in whatever algorithm is used for Step 1 is not an issue.[1] However, when using the computer in Step 2 to check that the sufficient conditions are satisfied, then we have to control rounding errors. This will be accomplished using interval arithmetic.

1.1.1 A succinct description of interval arithmetic

Computer-assisted proofs in analysis are sometimes unfairly summarized as *simply doing numerics, but with interval arithmetic*. This is obviously inaccurate (discretization errors also have to be controlled as soon as the problem is not inherently finite dimensional), but also misleading. Indeed, in most cases, the hard part in a computer-assisted proof consists in fact in reducing the problem to a finite (and not too dramatically large) set of conditions, while checking those using interval arithmetic is then rather routine, even if sometimes computationally expensive. Nonetheless, interval arithmetic is a very useful tool, which we briefly describe here for the sake of keeping this introductory chapter self-contained. For a more in-depth presentation, and examples of pitfalls to avoid, we refer to [232, 259, 283, 254] and to the references therein.

Let $\mathbb{F}$ bet the set of representable numbers, that is, the (finite!) set of real numbers that the computer can represent with a given precision, and $\bigtriangledown, \bigtriangleup : \mathbb{R} \to \mathbb{F}$ the corresponding round-down and round-up operators. That is, for every $x \in \mathbb{R}$,[2]

$$\bigtriangledown(x) = \max\{y \in \mathbb{F},\ y \leq x\} \qquad \text{and} \qquad \bigtriangleup(x) = \min\{y \in \mathbb{F},\ y \geq x\}.$$

Note that $\bigtriangledown(x) \leq x \leq \bigtriangleup(x)$ with equality if and only if $x \in \mathbb{F}$. When using standard floating-point arithmetic, a real number x is actually replaced by its closest floating point approximation, i.e., either $\bigtriangledown(x)$ or $\bigtriangleup(x)$. With interval arithmetic, we instead work with closed representable intervals, i.e., closed intervals whose endpoints are representable numbers. In particular a real number x is replaced by the interval

$$[x] := [\bigtriangledown(x), \bigtriangleup(x)]\,.$$

This interval has the crucial property that it contains the real number x, even when x is not a representable number. One can then extend the elementary operations $(+, -, \times, \div)$ to intervals, combining the set-theoretic definitions of these operation with the appropriate rounding operator, in such a way that the result always contains the true value. For instance, if $I = [a, b]$ and $J = [c, d]$, with $a, b, c, d \in \mathbb{F}$,

$$I + J := [\bigtriangledown(a + c), \bigtriangleup(b + d)]\,.$$

By construction, $I + J$ contains $\{x + y,\ x \in I, y \in J\}$, and in particular $[x] + [y]$ contains the

[1] As long as the obtained approximate solution is still accurate enough, but this is not something we have to know or prove a priori.

[2] For simplicity, we only consider here real numbers x such that $x \in [\min(\mathbb{F}), \max(\mathbb{F})]$, and assume that the results of all operations under consideration lie in that range. Real numbers outside that range lead to so-called underflow and overflow, which have to be handled separately.

real number $x + y$. Similar definitions can be given for subtraction, multiplication and division:

$$\begin{aligned} I - J &:= [\bigtriangledown (a - d), \bigtriangleup (b - c)] \\ I \times J &:= [\bigtriangledown (\min(ac, ad, bc, bd)), \bigtriangleup (\max(ac, ad, bc, bd))] \\ I \div J &:= I \times \left[\bigtriangledown \left(\frac{1}{d}\right), \bigtriangleup \left(\frac{1}{c}\right)\right] \qquad \text{if } 0 \notin J. \end{aligned}$$

Next, one can obtain similar interval extensions for special functions like sqrt, exp, cos, etc., with the property that, given a function f and a representable interval I, $f(I)$ should be a representable interval containing $\{f(x),\ x \in I\}$. This is less trivial, but it can be done and has been implemented in several libraries, including CAPD [178], IntervalArithmetic.jl [30], Intlab [258], MPFR [123], MPI [255], PROFIL/BIAS [189], XSC [188] and in particular Arb [173], which probably contains the larger list of special functions, including many beyond the few mentioned above.

In summary, interval arithmetic allows us to get guaranteed enclosures for the result of numerical calculations, and in particular to check open conditions.

Example 1.1.1. *Let $f : \mathbb{R} \to \mathbb{R}$ be the function given by*

$$f(x) = \exp(\sin(20x)) + x^4 + \frac{x}{1 + x^2} - \frac{1}{8}, \tag{1.1}$$

represented on Figure 1.1. We have $f(-0.4) < 0$.

Proof. Indeed, using the interval arithmetic library Intlab [258],[3] we can get a guaranteed enclosure[4] for $f(-0.4)$, namely

$$f(-0.4) \in [-0.07241235805\mathbf{90}, -0.07241235805\mathbf{89}],$$

which proves that the claim holds. □

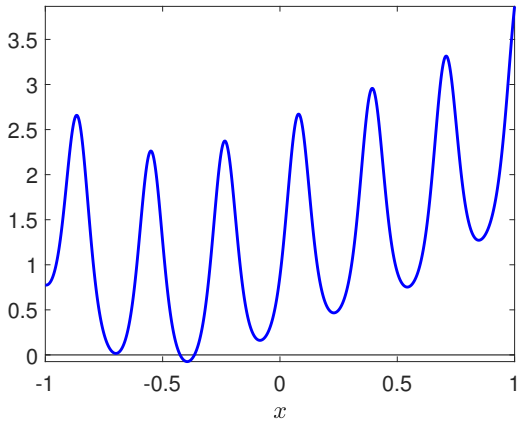

Figure 1.1: Graph of the function f defined in (1.1).

[3] This is the excellent interval arithmetic library used for most of the results discussed in this manuscript, but many others would work just as well for this particular example.

[4] When writing intervals whose endpoints have many digits in common, we bold the parts that differ to make them easier to read.

Remark 1.1.2. *Since we are using interval arithmetic anyway, we can also freely get results that are valid over a whole interval. Indeed, we can consider* $I = [0.25, 0.5]$ *and evaluate* $f(I)$ *using Intlab, which yields*

$$f(I) \subset [0.46221124517227, 3.12637006375317].$$

This enclosure is not extremely sharp, but enough to prove, for instance, that $f(x) > 0$ *for all* $x \in I$*.*

Proving directly that $f(x) = 0$ for a given x might seem more difficult at first glance. Indeed, for any real number x, we will at best get that 0 is contained in $f(x)$, and anyway zeros of f may not be representable numbers. However, as soon as f is continuous one can easily obtain sufficient open conditions for the existence of a zero, using the intermediate value theorem.

Example 1.1.3. *The map* $f : \mathbb{R} \to \mathbb{R}$ *defined in* (1.1) *has at least two distinct zeros, one in* $(-0.45, -0.4)$*, and one in* $(-0.4, -0.35)$*.*

Proof. Using again interval arithmetic we can check that, in addition to having $f(-0.4) < 0$, $f(-0.45) > 0$ and $f(-0.35) > 0$. Indeed

$$f(-0.45) \in [0.2040316808282\mathbf{69}, 0.2040316808282\mathbf{71}]$$
$$f(-0.35) \in [0.0966134050723\mathbf{0}, 0.0966134050723\mathbf{2}],$$

which, since f is continuous, proves that the claim holds. □

Remark 1.1.4. *Using the same strategy, one can in fact get much tighter enclosures of these two zeros: there exists a zero of* f *in the interval*

$$(-0.4254520520117\mathbf{3}, -0.4254520520117\mathbf{2}),$$

and another one in the interval

$$(-0.3645789468128\mathbf{0}, -0.3645789468127\mathbf{9}).$$

For higher (possibly infinite) dimensional problems, topological tools like the intermediate value theorem might become less suitable to study zeros, but the idea that a zero-finding problem can be rephrased using open conditions remains, for instance using the contraction mapping theorem, see Section 1.2.

In this manuscript, we are mostly concerned with local statements like the one from Example 1.1.3. However, with a combination of additional pen-and-paper work and interval arithmetic calculations, one can sometimes also get global results, which we illustrate here with a final example (see [240] for a much more extended discussion related to rigorous global optimization, and [170] for a recent usage of such ideas in infinite dimension).

Example 1.1.5. *The map* $f : \mathbb{R} \to \mathbb{R}$ *defined in* (1.1) *has at exactly two distinct zeros.*

Proof. The proof proceeds in three steps.

1. For all $x \in \mathbb{R}$, we have $\exp(\sin(20x)) \geq \exp(-1)$ and $\frac{x}{1+x^2} \geq -\frac{1}{2}$, hence $f(x) \geq x^4 - 1$. In particular, $f(x) \neq 0$ as soon as $|x| > 1$.

2. Now that we are left with a compact interval to study, we split it into many small pieces, by defining $y_n = -1 + \frac{2n}{N}$ for all $n \in \{0, \dots, N\}$, $N = 256$. We then enclose $f([y_n, y_{n+1}])$ for all $n \in \{0, \dots, N-1\}$ using interval arithmetic, which yields (see Figure 1.2)

$$f([y_n, y_{n+1}]) > 0 \quad \text{for all } n \in \{0, \dots, 72\},$$
$$f([y_n, y_{n+1}]) < 0 \quad \text{for all } n \in \{74, \dots, 80\},$$
$$f([y_n, y_{n+1}]) > 0 \quad \text{for all } n \in \{82, \dots, 255\}.$$

In particular, f can only have zeros in

$$[y_{73}, y_{74}] = [-0.42\mathbf{96875}, -0.42\mathbf{1875}] \quad \text{and in} \quad [y_{81}, y_{82}] = [-0.3\mathbf{671875}. - 0.3\mathbf{59375}],$$

As we have already established in Remark 1.1.4 using the intermediate value theorem, f does have at least one zero in each of these two intervals.

3. Two final interval arithmetic computations yield that

$$f'([y_{73}, y_{74}]) < 0 \quad \text{and} \quad f'([y_{81}, y_{82}]) > 0,$$

therefore f indeed only has a single zero in each of these two intervals.

□

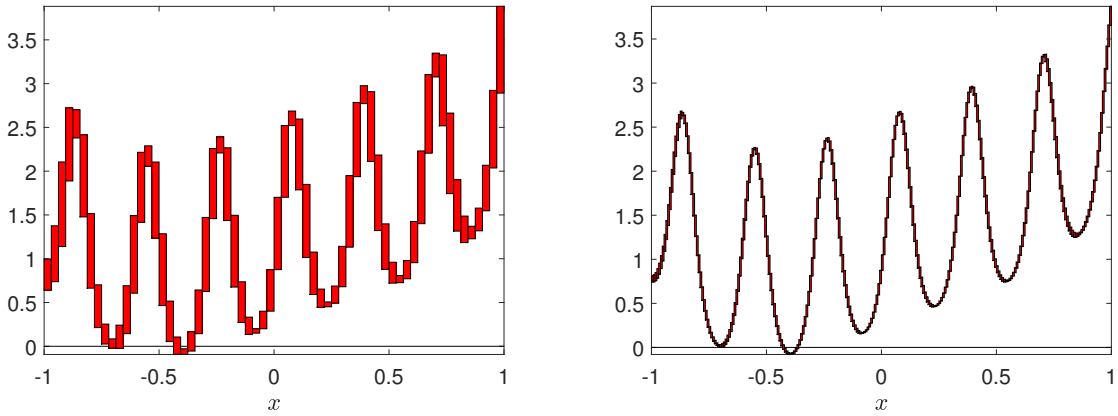

Figure 1.2: Guaranteed enclosures of the function f defined in (1.1), using a uniform subdivision as in Example 1.1.5. On the left, we use $N = 64$, which is too crude and leaves us with intervals that may contain zeros of f but in fact do not. On the right, we use $N = 256$, which gives a fine enough subdivision to only leave two intervals potentially containing zeros of f.

1.1.2 A brief and partial history of computer assisted proofs, and some motivations

Two of the early and most famous computer-assisted results are the proof of the four color theorem [2, 3] and that of the Kepler conjecture on sphere packing [150]. It should be noted that a formal proof checked by a proof assistant has later been provided in both cases [145, 149]. Other notable computer-assisted results in various areas of mathematics include the proof of the Feigenbaum conjectures [195, 109], the uniqueness of Thompson's group and the existence of O'Nan's group [15], the proof of chaos [228, 135] and of the existence of a strange attractor [282] in the Lorenz system, the double bubble generalization of the isoperimetric inequality [155], some rigidity results in 3-manifold theory [129], or the existence of periodic trajectories on obtuse triangular billiards [265]. Some of these problems are already intrinsically finite dimensional, and sometimes even only require integer calculations, therefore one should emphasize that the earlier discussion about discretization and rounding errors is not necessarily relevant for all kinds of computer-assisted proofs. We refer to [91] and the references therein for a broader discussion on computer-assisted proofs in mathematics.

The works presented in this manuscript are computer-assisted proofs in analysis, and more specifically in the study of differential equations and dynamical systems. Computer-assisted proofs have a strong history in this field, in which they can be rather appealing for different

reasons. The first one, which is not specific to this mathematical area, is that computer-assisted proofs provide us with new tools to prove theorems, which are often complementary with existing pen-and-paper techniques, and sometimes allows us to explore new questions or problems that seemed out of reach of standard proofs. For differential equations and other dynamical systems specifically, numerical experiments have long played an important role in helping us discovering and understanding new phenomena. However, there is often a large discrepancy between beautiful, sometimes very deep, theoretical results on one side, which may not apply to the specific system we are interested in, or may not give the full picture, and insightful numerical results on the other side, which give more detailed and quantitative information, but can typically not be proven. Computer-assisted proofs can sometimes bridge the gap between these two worlds. Finally, the type of computer-assisted proofs described in this manuscript, based on first getting an approximate solution and then proving the existence of a nearby exact one, has a lot in common (and takes inspiration from) the more classical study of error estimates in numerical analysis. In particular, these computer-assisted proofs can be seen as a kind of *a posteriori* error analysis, with some specific features related to the fact they are typically used in situations where the existence of the exact solution is not known a priori, and more stringent requirements, as one must get actual bounds on all the involved quantities, whereas some (reasonable but not guaranteed) approximations can be tolerated in classical a posteriori error estimates.

Besides the aforementioned works [228, 135, 282], some of the pioneering works on computer-assisted proofs for ODEs and PDEs are [116, 236, 248, 243, 321, 331, 5, 93], and recent landmarks include the proof of chaos in the Kuramoto–Sivashinsky equation [315, 316] (the first such result for a PDE), and of self-similar blowups in PDEs [44, 74, 103]. More in-depth reviews of the relevant computer-assisted proof literature, with proper regard to more recent works and novel developments, are presented in each of the subsequent chapters of this manuscript. For a broader overview, we refer to the introductory book [283] on rigorous numerics, to the excellent expository article [291] and to the survey [227] on computer-assisted proofs in dynamics, to the survey [143] and the book [238] on computer-assisted proofs in PDEs, and to the next subsection, which describes computer-assisted proofs in differential equations and dynamics with tools or goals that differ from those described in this manuscript.

1.1.3 What this manuscript is NOT about

The field of computer-assisted proofs for differential equations and dynamical systems is relatively young but increasingly active, and there are many remarkable works and directions of research that would at least partially fit the title of this manuscript. We mention below some of the works which, while not being close enough to the focus of this manuscript to be discussed in subsequent chapters, may still be of interest to a reader interested in computer-assisted proofs for differential equations and dynamical systems.

- **Formal proofs.** As already briefly touched upon, there is nothing about formal proofs in this manuscript. Nonetheless, combining the type of computer-assisted proofs described here with proof assistants would be a very valuable direction to explore, and becomes more and more critical with the increase in complexity of some of the codes associated to this type of proofs. The *a posteriori* nature of the computer-assisted proofs described in this manuscript make them rather appealing for proof assistants, as most of the numerical computations can be considered as an oracle and do not have to be certified. Preliminary results in that direction have already been obtained in [41], where polynomial approximations of functions, which is a key step in many of proofs discussed here, is rigorously validated in Rocq, combining a fixed point reformulation similar to the one presented in Section 1.2 with a fully certified implementation of interval arithmetic [222].
- **Linear differential equations.** Most of this manuscript focuses on *nonlinear* equations,

although some linear PDEs will also be considered. When restricting to linear differential equations, and in particular to linear ODEs [40], more detailed studies are sometimes available, and symbolic linear algebra can be used, see [261] and the references therein.

- **Topological/geometrical computer-assisted proofs.** As will be explained in more details later on in this chapter, the computer-assisted proofs described in this manuscript are of *functional analytic* nature, and share many ingredients with more standard PDE analysis proofs. These are by no means the only type of computer-assisted proofs out there. In particular, more *geometric* and *topological* methods based on tools such as the Conley index [229], or covering relations and cone conditions [330, 328, 65] have been very successful. Of particular note is the CAPD library [178], which is one of the most advanced available tool for the rigorous study of dynamical systems, and was recently used in the aforementioned proof of chaos for the Kuramoto–Sivashinsky equation. In a somewhat orthogonal direction, recent computer-assisted proofs based on Morse graphs and Conley index were able to characterize local and global dynamics with rigorous probabilistic guarantees from data only, i.e., without explicit knowledge of the underlying dynamical system [21].

- **Computer-assisted proofs in KAM theory.** An area of dynamics in which computer-assisted proofs have been particularly successful is KAM theory. While some aspects of these proofs are specific to quasi-periodic motions, and to difficulties associated with small divisors, many ideas such as the a posteriori format in which these computer-assisted proofs are formulated, or some of the Fourier analysis, are very similar to those discussed in this manuscript. A thorough overview of this field is far beyond the scope of the present work, but we refer the interested reader to the papers [59, 119], the excellent book [151], and the references therein.

- **Computer-assisted proofs with finite elements methods.** A common feature of all the works presented in this manuscript is that they rely on spectral methods, and the computer-assisted proofs are often obtained in sequence spaces representing, e.g., the Fourier coefficients of a periodic solution. This setting has several advantages which will be presented throughout this manuscript, but also some limitations. In particular, it is not as flexible as finite elements when it comes to complicated geometries. While this manuscript might give the impression that computer-assisted proofs are mostly restricted to spectral methods, nothing could be further from the truth. In fact, some of the earliest computer-assisted proofs in PDEs were done using finite elements [236], and there is a vast literature on the subject, which has mostly been summarized in the book [238]. We stress that, despite differences in presentation and sometimes in viewpoints, computer-assisted proofs based on spectral methods share a lot of ideas and tools with those using finite elements, and that the two are in fact more closely related than the literature sometimes suggests.

- **Computer-assisted proofs for DDEs.** This manuscript deals mainly with computer-assisted proofs for ODEs and PDEs (some of which come from SDEs), but computer-assisted proofs can also be used to study DDEs (delay differential equations), allowing for rigorous integration [270, 201] and computation of Poincaré maps [271], study of Hopf bifurcations, periodic orbits [200, 77] and invariant manifolds [159], sometimes even in presence of state-dependent delay [78, 141]. Most notably, computer-assisted proofs allowed to settle the Jones' and Wright's conjectures [289, 170]. DDE techniques were also used to study famous choreographies in celestial mechanics [58]. Some of these works use the topological computer-assisted proofs mentioned above, but the others are very much of the flavor presented in this manuscript.

1.2 Newton–Kantorovich Theorems

Now that the stage is set, and that we have discussed what this manuscript is not about, it is time to present what this manuscript is actually about and to introduce one of the main ingredients common to many computer-assisted proofs, within and beyond this manuscript. We start with a fixed point theorem, which is a direct consequence of the contraction mapping theorem, but with assumptions reformulated in a way that will prove convenient to check in practice. Henceforth, given a Banach space $\mathcal{X}$, an element x in $\mathcal{X}$ and $r \geq 0$, $B_r(x)$ denotes the *closed* ball of center x and radius r in $\mathcal{X}$.

Theorem 1.2.1. *Let $\mathcal{X}$ be a Banach space, $\bar{x} \in \mathcal{X}$, and $T : \mathcal{X} \to \mathcal{X}$ a C^1 map. Assume there exists $r^* > 0$, and constants $Y, Z_1, Z_2 \geq 0$ such that*

$$\begin{aligned} \|T(\bar{x}) - \bar{x}\| &\leq Y \\ \|DT(\bar{x})\| &\leq Z_1 \\ \|DT(x) - DT(\bar{x})\| &\leq Z_2\|x - \bar{x}\|, \qquad \forall x \in B_{r^*}(\bar{x}). \end{aligned}$$

If there exists $r \in [0, r^*]$ such that

$$Y + Z_1 r + \frac{1}{2} Z_2 r^2 \leq r \tag{1.2}$$

$$Z_1 + Z_2 r < 1, \tag{1.3}$$

then T has a unique fixed point $x^\star$ in $B_r(\bar{x})$.

The proof is elementary, and included here for the sake of making this introductory chapter as self-contained as possible.

Proof. For $r \geq 0$ and $x \in B_r(\bar{x})$, we simply use Taylor's theorem to write

$$\begin{aligned} T(x) - \bar{x} &= T(\bar{x}) - \bar{x} + \int_0^1 DT(\bar{x} + t(x - \bar{x}))(x - \bar{x}) \mathrm{d}t \\ &= T(\bar{x}) - \bar{x} + DT(\bar{x})(x - \bar{x}) + \int_0^1 \left(DT(\bar{x} + t(x - \bar{x})) - DT(\bar{x})\right)(x - \bar{x}) \mathrm{d}t, \end{aligned}$$

which, provided $r \leq r^*$, yields the estimate

$$\begin{aligned} \|T(x) - \bar{x}\| &\leq Y + Z_1\|x - \bar{x}\| + Z_2\|x - \bar{x}\|^2 \int_0^1 t \mathrm{d}t \\ &\leq Y + Z_1 r + \frac{1}{2} Z_2 r^2, \end{aligned}$$

so that (1.2) ensures T maps $B_r(\bar{x})$ into itself. By the triangle inequality, we directly have that, for all $x \in B_r(\bar{x})$,

$$\|DT(x)\| \leq Z_1 + Z_2 r,$$

and (1.3) ensures T is contracting on $B_r(\bar{x})$. The existence and uniqueness of a fixed point of T in $B_r(\bar{x})$ then follows from the Banach fixed-point theorem. □

The reason the above theorem turns out to be relevant for so many different computer-assisted proofs is that we have a generic way of reformulating a non-degenerate zero-finding problem into fixed-point problem that should be a contraction locally: Newton's method or its variants. In order to fix notations, let us consider a C^1 map $F : \mathcal{X} \to \mathcal{Y}$, with $\mathcal{X}$ and $\mathcal{Y}$ Banach spaces, and an element $\bar{x} \in \mathcal{X}$ that should be thought of as an *approximate zero* of F, typically

obtained via a numerical procedure. If F truly has a locally unique zero near $\bar{x}$, then we expect the fixed point map

$$T : x \mapsto x - DF(\bar{x})^{-1}F(x), \tag{1.4}$$

to be a contraction on a small neighborhood of $\bar{x}$.[5] We would like to apply Theorem 1.2.1, in order get explicit conditions in terms of F for the existence (and local uniqueness) of a zero of F near $\bar{x}$. In practice, the main difficulty in doing so is that we then need to control $DF(\bar{x})^{-1}$, which may be a complicated object since $\bar{x}$ is typically a highly nontrivial approximate solution. Note that we usually do not even know a priori that $DF(\bar{x})$ is invertible. Working directly with $DF(\bar{x})^{-1}$ is still sometimes possible, see Section 1.2.2 and also Proposition 2.1.3, but we start by presenting a popular alternative, which is to only work with an approximate inverse A of $DF(\bar{x})$.

1.2.1 Newton–Kantorovich with an approximate inverse

Theorem 1.2.2. *Let $\mathcal{X}, \mathcal{Y}$ be Banach spaces, $\bar{x} \in \mathcal{X}$, $F : \mathcal{X} \to \mathcal{Y}$ a C^1 map, and $A : \mathcal{Y} \to \mathcal{X}$ an injective linear map. Assume there exists $r^* \in (0, \infty]$, and constants $Y, Z_1, Z_2 \geq 0$ such that*

$$\|AF(\bar{x})\|_{\mathcal{X}} \leq Y \tag{1.5}$$

$$\|I - ADF(\bar{x})\|_{\mathcal{B}(\mathcal{X},\mathcal{X})} \leq Z_1 \tag{1.6}$$

$$\|A\left(DF(x) - DF(\bar{x})\right)\|_{\mathcal{B}(\mathcal{X},\mathcal{X})} \leq Z_2 \|x - \bar{x}\|_{\mathcal{X}}, \qquad \forall x \in B_{r^*}(\bar{x}). \tag{1.7}$$

If there exists $r \in [0, r^*]$ such that

$$Y + Z_1 r + \frac{1}{2} Z_2 r^2 \leq r \tag{1.8}$$

$$Z_1 + Z_2 r < 1, \tag{1.9}$$

then F has a unique zero $x^\star$ in $B_r(\bar{x})$.

Proof. We simply apply Theorem 1.2.1 to $T : x \mapsto x - AF(x)$, whose fixed points are in one-to-one correspondence with zeros of F since A is injective. □

Remark 1.2.3. *The conditions on r appear naturally in the form (1.8)-(1.9) in the proof of Theorem 1.2.1, but they could also be equivalently formulated as follows: If*

$$Z_1 < 1 \tag{1.10}$$

$$Y Z_2 < (1 - Z_1)^2, \tag{1.11}$$

let

$$r_{\min} = \frac{1 - Z_1 - \sqrt{(1 - Z_1)^2 - 2Y Z_2}}{Z_2}, \qquad r_{\max} = \max\left(\frac{1 - Z_1}{Z_2}, r^*\right). \tag{1.12}$$

Then, for all $x \in [r_{\min}, r_{\max})$,[6] F has a unique zero $x^\star$ in $B_r(\bar{x})$. That is, $\|x^\star - \bar{x}\| \leq r_{\min}$ is the sharpest error bound we can get out of Theorem 1.2.2, whereas $r_{\max}$ characterizes the largest ball on which we can get the local uniqueness of the zero of F.

Condition (1.10) tells us how good of an approximate inverse of $DF(\bar{x})$ the operator A has to be, and condition (1.11) provides a quantitative criterion telling us how good of an approximate solution we need (how small the bound Y on the residual error has to be in terms of Z_1 and Z_2) in order to be able to guarantee the existence of an exact solution nearby.

[5] The same should also hold for the exact Newton map $x \mapsto x - DF(x)^{-1}F(x)$, but the x dependency in the inverse of the Fréchet derivative makes this operator much harder to study, for little to no gain if $\bar{x}$ is already very close to the exact zero of F.

[6] Even if (1.11)-(1.11) hold, this interval could be empty if r^* is taken too small, leading to to $r_{\max} < r_{\min}$. Moreover, the formula in (1.12) are only valid if $Z_2 > 0$, i.e., if the problem is nonlinear. In the linear case, we simply get $r_{\min} = \frac{Y}{1 - Z_1}$ and $r_{\max} = +\infty$ (because we can then take $r^* = +\infty$).

Remark 1.2.4. *One crucial aspect of Theorem 1.2.2 it that is enable us to turn the search for a zero of F into having to satisfy the* open *conditions* (1.10)-(1.11).

The derivation of the estimates Y, Z_1 and Z_2 is usually done by hand, but the obtained formula are typically complicated, if only because they necessarily involve the approximate solution $\bar{x}$, and are therefore evaluated with the computer and interval arithmetic. As already highlighted in Section 1.1.1, the fact that conditions (1.10)-(1.11) *are open means we can hope to check them with the computer and appropriate control of rounding errors (in our case interval arithmetic), even if the formula for Y, Z_1 and Z_2 are very involved.*

Another important byproduct of this openness is that the locally unique solution provided by Theorem 1.2.2 is robust. Indeed, conditions (1.10)-(1.11) *will continue to hold for arbitrary small perturbations of the map F (or of the norm used on $\mathcal{X}$), provided the estimates Y, Z_1 and Z_2 depend continuously on these perturbations.*

On the other hand, this means we have to be somewhat careful in how we design our zero-finding problem F, which must have isolated and robust zeros if we are to successfully apply Theorem 1.2.2. In particular, translation invariance and other degeneracies leading to continuum of zeros must be factored out with an appropriate choice of the map F and/or of the space $\mathcal{X}$.

In practice, when trying to apply Theorem 1.2.2 to a given problem, the potentially challenging steps are:

- Reformulate the problem as a zero finding problem $F(x) = 0$, on a well chosen Banach space $\mathcal{X}$. There can be many $F = 0$ reformulations that are mathematically equivalent but lead to more or less complicated estimates, and, as is common in PDE analysis, the choice of function space and norm is often crucial.

- Find a suitable approximate inverse (or preconditioner) A, which should be simple enough so that one can derive explicit estimates Y, Z_1, Z_2 satisfying (1.5)-(1.7), but accurate enough so that we can still get $Z_1 < 1$.

- Actually derive computable estimates Y, Z_1, Z_2 satisfying (1.5)-(1.7).

Before giving a somewhat simple (but still non-trivial) example in Section 1.3.1, where all the details will be described, we start with a very basic application of Theorem 1.2.2.

Example 1.2.5. *Let us try to compute an accurate and guaranteed approximation of $\sqrt{2}$, using Theorem 1.2.2. We first consider the map $F : \mathbb{R} \to \mathbb{R}$, $F(x) = x^2 - 2$, compute a positive approximate zero $\bar{x}$ of F using Newton's method, and define $A = \frac{1}{2\bar{x}}$ (since this problem is finite dimensional, and of low dimension, we can easily take for A the exact inverse of $DF(\bar{x})$, of course things will not be so simple later on).*

We then compute $|AF(\bar{x})|$ using interval arithmetic, and take for Y the upper-bound of the obtained interval, which therefore satisfies (1.5). *Since $A = DF(\bar{x})^{-1}$, $Z_1 = 0$ satisfies* (1.6). *Finally, since F is merely quadratic, we can then take $r^* = \infty$ and $Z_2 = |AD^2F(\bar{x})| = 2|A| = \frac{1}{|\bar{x}|}$ satisfies* (1.7). *Again, in practice we actually compute $\frac{1}{|\bar{x}|}$ using interval arithmetic, and take the upper bound for Z_2. Finally, we check that* (1.10)-(1.11) *hold, which implies that $|\bar{x} - \sqrt{2}| \leq r_{\min}$, with $r_{\min}$ as in* (1.12).

Running the actual calculations yields

$$\bar{x} \approx 1.414213562373095,$$

and, only now using interval arithmetic

$$Y = 1.570093 \times 10^{-16}, \qquad Z_2 = 0.7071068, \qquad r_{\min} = 3.14018 \times 10^{-16}.$$

Note that the obtained error bounds $r_{\min}$ is of the order of machine precision, hence as sharp as one can hope for. The simple Matlab code associated with this example is available at [Code 8].

1.2.2 Newton–Kantorovich without approximate inverse

We now go back to the original fixed point reformulation (1.4), and provide sufficient conditions for the existence of a locally unique zero without introducing an approximate inverse.

Theorem 1.2.6. *Let $\mathcal{X}, \mathcal{Y}$ be Banach spaces, $\bar{x} \in \mathcal{X}$ and $F : \mathcal{X} \to \mathcal{Y}$ a C^1 map such that $DF(\bar{x})$ is a Fredholm operator of index 0. Assume there exists $r^* \in (0, \infty]$, and constants $\delta, L \geq 0$ and $\kappa > 0$ such that*

$$\|F(\bar{x})\|_{\mathcal{Y}} \leq \delta \tag{1.13}$$

$$\|x\|_{\mathcal{X}} \leq \kappa \|DF(\bar{x})x\|_{\mathcal{Y}} \qquad \forall x \in \mathcal{X} \tag{1.14}$$

$$\|DF(x) - DF(\bar{x})\|_{\mathcal{B}(\mathcal{X},\mathcal{Y})} \leq L \|x - \bar{x}\|_{\mathcal{X}}, \qquad \forall x \in B_{r^*}(\bar{x}). \tag{1.15}$$

If there exists $r \in [0, r^*]$ such that

$$\kappa\delta + \frac{1}{2}\kappa L r^2 \leq r \tag{1.16}$$

$$\kappa L < r, \tag{1.17}$$

then F has a unique zero $x^\star$ in $B_r(\bar{x})$.

Proof. Assumption (1.14) ensures that $DF(\bar{x})$ is injective, and therefore invertible since it is Fredholm of index 0. The operator $T : \mathcal{X} \to \mathcal{X}$ from (1.4) is therefore well defined. Estimating

$$\left\|DF(\bar{x})^{-1}F(\bar{x})\right\|_{\mathcal{X}} \leq \left\|DF(\bar{x})^{-1}\right\|_{\mathcal{B}(\mathcal{Y},\mathcal{X})} \|F(\bar{x})\|_{\mathcal{Y}} \leq \kappa\delta,$$

and similarly

$$\left\|DF(\bar{x})^{-1}\left(DF(x) - DF(\bar{x})\right)\right\|_{\mathcal{B}(\mathcal{X},\mathcal{X})} \leq \kappa L \|x - \bar{x}\|_{\mathcal{X}},$$

we can take $Y = \kappa\delta$, $Z_1 = 0$, $Z_2 = \kappa L$ and apply Theorem 1.2.1 to T. Conditions (1.16)-(1.17) are equivalent to (1.2)-(1.3). □

Similarly to what we have done following Theorem 1.2.2, the conditions on r in Theorem 1.2.6 can be reformulated as

$$2\kappa^2\delta L < 1,$$

and Remarks 1.2.3 and 1.2.4 also apply here. For slightly more general versions of Theorem 1.2.6, we refer to [238, Section 6.1].

Compared to Theorem 1.2.2, the main difference with Theorem 1.2.6 is that, instead of having to find a suitable approximate inverse (and then to prove that it indeed satisfies (1.6) with $Z_1 < 1$), we have to find an explicit constant κ satisfying (1.14), which essentially corresponds to controlling $\left\|DF(\bar{x})^{-1}\right\|_{\mathcal{B}(\mathcal{Y},\mathcal{X})}$. This might be a formidable task in general, but there exist rather general techniques to obtain such an estimate if we are working with Hilbert spaces instead of general Banach spaces.[7] Indeed, if $DF(\bar{x})$ is self-adjoint, a suitable estimate κ satisfying condition (1.14) can then be obtained from the smallest (in modulus) element in the spectrum of $DF(\bar{x})$. If $DF(\bar{x})$ is not self-adjoint, one has to instead consider the spectrum of $DF(\bar{x})^*DF(\bar{x})$.

This approach hinges on being able to rigorously enclose eigenvalues[8] of self-adjoint operators, which is an entire topic of its own within the field of computer-assisted proofs, as eigenvalue bounds are not only useful to apply Theorem 1.2.6, but are also of natural interest for various problems. In particular, computer-assisted proofs have been used recently to study

[7] One could also try to control $\left\|DF(\bar{x})^{-1}\right\|_{\mathcal{B}(\mathcal{Y},\mathcal{X})}$ by introducing an approximate inverse A of $DF(\bar{x})$ and estimating (1.6), but if this is possible one might as well use Theorem 1.2.2 directly.

[8] If there is continuous spectrum, it has to be controlled as well.

several problems in spectral geometry, including Schiffer's conjecture [242], Payne's nodal line conjecture [89], Polya's conjecture for Euclidian balls [120], or the Polya-Szego conjecture [35].

For a comprehensive overview on rigorous eigenvalue bounds, we refer to the excellent [238, Chapter 10] as well as to [208], and to the references therein. Guaranteed eigenvalue together with eigenvector bounds can also be found in [62, 63]. We give a detailed example of eigenvalue bounds in Section 1.3.2, and make further use of this approach in Chapter 6.

1.2.3 History and further variants

Variations of Theorem 1.2.1, Theorem 1.2.2 and Theorem 1.2.6 can be found in numerous computer-assisted proofs in nonlinear analysis, and the idea of combining this approach with the computer seems to have been independently rediscovered multiple times.

One of the first well-known example is probably Lansford's proof of the Feigenbaum conjectures [195], which uses a variant of Theorem 1.2.2 (although the theorem itself is not stated as such), with a very simple approximate inverse A: essentially the identity, with only the first entry modified. However, similar ideas can in fact already be found in the paper [285] on the rigorous approximation of periodic solutions in ODEs, which dates from 1965!

At around the same time, but restricted to finite dimensional problems, the so-called interval Newton-method and Krawczyk operator were introduced (see [231] and the references therein), also with the goal of, quoting the abstract of [231], providing "computationally verifiable sufficient conditions (...) for the existence of a solution to a system of nonlinear equations". In some sense, Theorem 1.2.2 or Theorem 1.2.6 can therefore be seen as infinite dimensional generalizations of the Krawczyk method. We emphasize that, as shown by the simple proof of Theorem 1.2.1, the difficulty in going to infinite dimension does not lie in proving the theorem for a possibly infinite dimensional Banach space, but rather in actually verifying its assumptions in that case.

All these different approaches can essentially be traced back to the Newton–Kantorovich Theorem [177] (see [245] for a reference in English and a simplified proof) which provides sufficient conditions on the initial data of Newton's method to guarantee its convergence, and whose name is nowadays commonly used to refer to Theorems like 1.2.2 or 1.2.6, or even — somewhat abusively — to Theorem 1.2.1. However, we emphasize that the original Newton–Kantorovich Theorem gives an *a priori* convergence statement, whereas in modern computer-assisted proofs it is used as a mean of validating an approximate solution *a posteriori*. That is, one should not think of $\bar{x}$ as the initial condition for Newton's method, but really as the final iteration of Newton's method (or of any suitable numerical method used to find an approximate solution).

1.3 First illustration: the Swift–Hohenberg equation

We now use the Swift–Hohenberg equation as an example to illustrate how both Theorem 1.2.2 and Theorem 1.2.6 can be used to produce computer-assisted proofs. As already highlighted earlier, the challenging steps are the choice of a proper setup, and then the actual derivation of estimates satisfying the assumptions of these theorems. The Swift–Hohenberg equation was in fact already used as an example in the expository article [286] also illustrating Theorem 1.2.2, in a slightly more complicated setting involving a fixed energy level.

The main interest of this section does not lie in the results themselves. Instead, our goal is to use this rather simple example to provide a detailed treatment of both the approximate inverse (Theorem 1.2.2) and the eigenvalue bound (Theorem 1.2.6) approaches, which should hopefully be intelligible even for people having no previous experience with computer-assisted proofs. At the same time, this section provides us with a reference point for the following chapters of this manuscript, where similar ideas are going to be used in potentially much more technically involved situations.

We focus here on the 1-dimensional Swift–Hohenberg equation

$$\partial_t u = -(1+\Delta)^2 u + \rho u - u^3, \tag{1.18}$$

on the bounded domain $[0,\pi]$ and with Neumann boundary conditions, which in 1D simply write

$$u'(0) = u'(\pi) = u'''(0) = u'''(\pi) = 0. \tag{1.19}$$

Our goal is to showcase how computer-assisted proofs can be used to obtain the existence and a precise description of some nontrivial steady states of (1.18)-(1.19).

The boundary conditions make it natural to use cosine series for this problem. That is, we consider a cosine series Ansatz

$$u(x) = u_0 + 2\sum_{n\geq 1} u_n \cos(nx), \qquad x \in [0,\pi], \tag{1.20}$$

and plug it into the steady state equation

$$-(1+\Delta)^2 u + \rho u - u^3 = 0,$$

in order to get a zero-finding problem in terms of the Fourier coefficients. This zero-finding problem can at the very least be used for getting an accurate numerical solution of the problem, but maybe also for proving the existence of an exact solution nearby.

We first need to specify in which space we want to solve the steady state problem, and this is where the approaches based on approximate inverse and eigenvalue bound start to diverge. Indeed, for the eigenvalue bound approach we must use a Hilbert space (typically some H^k space), whereas weighted ℓ^1 spaces on the cosines coefficients prove way more convenient for the approximate inverse approach (although more classical H^k Sobolev spaces could also be used here [262]). We therefore present them in two separate subsections.

1.3.1 Using an approximate inverse

1.3.1.1 Spaces and the zero finding problem

For the approach using the approximate inverse, we make use of the weighted ℓ^1 spaces

$$\ell^1_\nu = \left\{ u = (u_n)_{n\in\mathbb{N}} \in \mathbb{R}^{\mathbb{N}},\ \|u\|_{\ell^1_\nu} := |u_0| + 2\sum_{n\geq 1} |u_n|\,\nu^n < \infty \right\}, \qquad \nu \geq 1,$$

introduced in a more general setting in Chapter 0, and whose elements we identify with functions of the form (1.20). A specific value of ν will be fixed for the actual proof, but everything that is said below applies to any $\nu \geq 1$.

Note that by using cosine series, we have incorporated the boundary conditions (1.19) in the space. Our zero-finding problem is then simply the map

$$F(u) = -(1+\Delta)^2 u + \rho u - u^3,$$

defined on ℓ^1_ν, where, for $u \in \ell^1_\nu$, Δu is the sequence defined as

$$(\Delta u)_n = -n^2 u_n \qquad \text{for all } n \in \mathbb{N},$$

and $u^3 = u * u * u$, where $*$ is the discrete convolution product:

$$(u * v)_n = \sum_{k\in\mathbb{Z}} u_{|k|} v_{|n-k|} \qquad \text{for all } u, v \in \ell^1_\nu \text{ and } n \in \mathbb{N}.$$

We recall that ℓ^1_ν is a Banach algebra for this discrete convolution product: for all $u, v \in \ell^1_\nu$, $u * v \in \ell^1_\nu$ and

$$\|u * v\|_{\ell^1_\nu} \leq \|u\|_{\ell^1_\nu} \|v\|_{\ell^1_\nu} . \tag{1.21}$$

This property, which is straightforward to obtain, makes the analysis of multiplication operators and nonlinear terms remarkably simple in ℓ^1 spaces.

Remark 1.3.1. *The map F does not send ℓ^1_ν into itself. That is not an issue, as Theorem 1.2.2 allows for F to be defined from a given space $\mathcal{X}$ to a potentially different one $\mathcal{Y}$. Here, $\mathcal{X} = \ell^1_\nu$ for some given $\nu \geq 1$, and we could for instance take*

$$\mathcal{Y} = \left\{ u = (u_n)_{n\in\mathbb{N}} \in \mathbb{R}^{\mathbb{N}},\ |u_0| + 2\sum_{n\geq 1} |u_n|\, n^{-4}\nu^n < \infty \right\}.$$

However, we emphasize that the space $\mathcal{Y}$ typically plays no role whatsoever in the estimates: the only thing that matters is that AF maps $\mathcal{X}$ into itself, and indeed all the bounds in Theorem 1.2.2 only involve elements in $\mathcal{X}$ or linear operators from $\mathcal{X}$ to itself. For those reasons, the space $\mathcal{Y}$ is sometimes not even specified.

From now on, we fix some $N \in \mathbb{N}$, and assume that an approximate zero $\bar{u}$ of F has been obtained numerically, with $\bar{u} \in \Pi^{\leq N}\ell^1_\nu$. This simply means that $\bar{u}$ is a finite cosine series with potentially non-zero modes only for $n \leq N$, see Chapter 0.

1.3.1.2 Construction of the approximate inverse

Our next task is to define a suitable approximate inverse A of $DF(\bar{u})$. Note that

$$DF(\bar{u}) = -(I+\Delta)^2 + \rho I - 3\mathcal{M}(\bar{u}^2), \tag{1.22}$$

where I is the identity operator, and we recall (see Chapter 0) that $\mathcal{M}(\bar{u}^2)$ is the multiplication operator by $\bar{u}^2$. One object that we can easily get our hands on is the finite dimensional projection $\Pi^{\leq N} DF(\bar{u})\Pi^{\leq N}$ of the derivative, which can be computed numerically as an $(N+1)\times(N+1)$ matrix. Provided N is not excessively large, we can therefore use the computer to obtain an approximate[9] inverse denoted $A^{\leq N}$ of $\Pi^{\leq N} DF(\bar{u})\Pi^{\leq N}$. Identifying the matrix $A^{\leq N}$ with an operator on $\Pi^{\leq N}\ell^1_\nu$, and then with its canonical injection as an operator on ℓ^1_ν, we define the operator A as[10]

$$A = A^{\leq N} + \Pi^{>N}\left(-(I+\Delta)^2\right)^{-1}\Pi^{>N}. \tag{1.23}$$

If we consider the decomposition of the spaces associated with the complementary projections $\Pi^{\leq N}$ and $\Pi^{>N}$, A can be represented as a 2×2 block-diagonal matrix:

$$A = \left(\begin{array}{c|c} A^{\leq N} & 0 \\ \hline 0 & \Pi^{>N}\left(-(I+\Delta)^2\right)^{-1}\Pi^{>N} \end{array}\right), \tag{1.24}$$

[9] The word approximate is used here to emphasize that this inverse does not have to be computed rigorously with interval arithmetic. In practice, we do in fact compute this inverse "exactly" up to rounding errors, but one could argue that this is in fact a waste of computational resources, as our approximate inverse is going to be way less accurate on the high modes anyway.

[10] For any $u \in \ell^1_\nu$ and $n \in \mathbb{N}$, $\left(-(I+\Delta)^2 u\right)_n = -(1-n^2)^2 u_n$ and therefore the inverse of $-(I+\Delta)^2$ is not defined on the $n=1$ mode. This does not matter, as $\left(-(I+\Delta)^2\right)^{-1}$ only acts on the $\Pi^{>N}\ell^1_\nu$ subspace here, and we are always going to take $N \geq 1$.

where the bottom-right block is itself diagonal. In the sequel, we often refer to the top-left block of A as *the finite part*, and to the bottom-right block as *the tail part*, or simple *the tail*.

Remark 1.3.2. *The only unbounded factor in F is $(I+\Delta)^2$. By having its inverse in A, at least in the tail, we make sure AF maps ℓ^1_ν back into itself. Equivalently, A is bounded from the space $\mathcal{Y}$ defined in Remark 1.3.1 into ℓ^1_ν.*

Remark 1.3.3. *We used here projections of the same dimension N for the approximate solution $\bar{u}$ and for defining A. This simplifies the presentation by preventing us from having to introduce too many different N's, but we note that one can (and, for hard enough problems, should) take projections of possibly different dimensions for the approximate solution and for the definition of the approximate inverse.*

In a moment, we are going to derive a Z_1 estimate controlling $\|I - ADF(\bar{u})\|$, which is going to be proportional to N^{-4}, thereby justifying rigorously that our choice of A provides a good approximate inverse of $DF(\bar{u})$, at least if N is taken large enough. However, let us first explain heuristically why this construction of A is adequate, and discuss how it can be generalized to different problems.

The operator $-(I+\Delta)^2$ is the *dominant* one in $DF(\bar{u})$, i.e., the differential operator with the highest order derivatives,[11] therefore it makes sense to build the inverse of $DF(\bar{u})$ using $\left(-(I+\Delta)^2\right)^{-1}$. More specifically, $DF(\bar{u}) - \left(-(I+\Delta)^2\right)$ is relatively compact with respect to $-(I+\Delta)^2$, which is why we can obtain an arbitrarily accurate approximate inverse of $DF(\bar{u})$ by a finite rank perturbation of $\left(-(I+\Delta)^2\right)^{-1}$ of sufficiently large dimension.

In the estimates to come, the fact that $-(I+\Delta)^2$ (and therefore it inverse) is diagonal in the Fourier basis is going to prove convenient, but one should not over-emphasize this point too much. Indeed, as will be shown in Chapter 3, if we can write

$$F(u) = \mathcal{L}u + K(u),$$

with $\mathcal{L}$ an invertible operator, $DK(u)$ relatively compact with respect to $\mathcal{L}$, and if we can provide an (exact or approximate) inverse of $\mathcal{L}$ that is "simple enough" to work with (but which does not at all have to be diagonal), then we can still construct an approximate inverse A and proceed with the estimates. As another example, many of the finite-element-based computer-assisted proofs for elliptic problems discussed in [238, Part I] use a similar construction of the approximate inverse, even though Δ is not diagonal on a finite element basis. In that case, it may be convenient to first reformulate the problem, and instead look for a zero of

$$\tilde{F}(u) = u + \mathcal{L}^{-1}K(u).$$

In that case, the dominant term in $D\tilde{F}(\bar{u})$ is the identity operator, which is diagonal in any basis, and one can therefore replicate the block-diagonal construction of the approximate inverse described above. In order to derive suitable Z_1 estimates controlling the quality of this approximate inverse, we need to be able to explicitly control quantities like $\Pi^{>N}\mathcal{L}^{-1}$ and $\mathcal{L}^{-1}\Pi^{>N}$, which is what we meant earlier when we asked for the inverse of $\mathcal{L}$ to be "simple enough". We now translate this rather abstract discussion into concrete estimates.

1.3.1.3 The bounds Y, Z_1 and Z_2 satisfying (1.5)-(1.7)

We start with the Y bound. First note that since $\bar{u}$ belongs to $\Pi^{\leq N}\ell^1_\nu$ and the only nonlinear term in F is cubic, $F(\bar{u})$ lies in $\Pi^{\leq 3N}\ell^1_\nu$. In particular, $F(\bar{u})$ only has finitely many nonzero coefficients, and can therefore be computed exactly using a computer.[12]

[11] $-(I+\Delta)^2$ happens to be the only differential operator in $DF(\bar{u})$, but the same reasoning would still apply if $DF(\bar{u})$ contained additional differential operators of lower order, for instance a $\Delta\bar{u}^2$ term.

[12] This generalizes straightforwardly to polynomial nonlinearities of arbitrary order. The case of non-polynomial nonlinearities is discussed in Section 3.2.

Remark 1.3.4. *Here and in what follows, we make a slight abuse of language when we write that a quantity can be* computed *exactly. What we precisely mean is that this quantity can be expressed with finitely many operations and applications of special functions, and that the output can therefore be* enclosed *rigorously using interval arithmetic.*

Recalling that the operator $\Pi^{>N}\left(-(I+\Delta)^2\right)^{-1}\Pi^{>N}$ is diagonal, and that A is defined as in (1.23) (or equivalently as in (1.24)), we get that $AF(\bar{u})$ also belongs to $\Pi^{\leq 3N}\ell^1_\nu$, and can also be computed exactly. We can therefore define

$$Y = \|AF(\bar{u})\|_{\ell^1_\nu},$$

which is computable and satisfies assumption (1.5) of Theorem 1.2.2.

Remark 1.3.5. *This is again a slight abuse of language, that will also be repeatedly used. What we precisely mean is that we compute a rigorous interval enclosure of $\|AF(\bar{u})\|_{\ell^1_\nu}$ using interval arithmetic, and define Y as the upper-bound of that enclosure.*

We now turn our attention to the Z_1 bound, which requires us to estimate an operator norm. Thanks to our choice of an ℓ^1 space, and to the specific structure of A, we are going to be able to get a very sharp estimate. We first recall the following lemma, which is a straightforward generalization of a well-known property for the ℓ^1 operator norm of finite matrices.

Lemma 1.3.6. *Let $\mathcal{L} : \ell^1_\nu \to \ell^1_\nu$ be a bounded linear operator. Using the infinite matrix representation introduced in Chapter 0, and the weights*

$$\xi_j = \begin{cases} 1, & \text{if } j = 0 \\ 2\nu^j, & \text{if } j \geq 1, \end{cases}$$

we have

$$\|\mathcal{L}\|_{\mathcal{B}(\ell^1_\nu,\ell^1_\nu)} = \sup_{j\in\mathbb{N}} \frac{1}{\xi_j} \sum_{i\in\mathbb{N}} |\mathcal{L}_{i,j}|\,\xi_j.$$

Notice that $\sum_{i\in\mathbb{N}} |\mathcal{L}_{i,j}|\,\xi_j$ is nothing but the ℓ^1_ν norm of the i-th column of $\mathcal{L}$. Therefore, as in the finite dimensional case, the ℓ^1_ν operator norm is obtained as the (weighted) supremum of the norm of the columns.

In order to obtain a Z_1 bound, we therefore have to estimate the norm of all the columns of $I - ADF(\bar{u})$. Ignoring the identity for the moment, note that the i-th column of $ADF(\bar{u})$ is simply obtained by taking the i-th column of $DF(\bar{u})$ and multiplying it by A. In order to better understand the structure of $DF(\bar{u})$, we have the following observations:

$$\begin{aligned} \text{for all } K \in \mathbb{N} \text{ and } v \in \Pi^{\leq K}\ell^1_\nu, \quad & \bar{u}^2 * v \in \Pi^{\leq K+2N}\ell^1_\nu, \\ \text{for all } K \in \mathbb{N}_{\geq 2N} \text{ and } v \in \Pi^{>K}\ell^1_\nu, \quad & \bar{u}^2 * v \in \Pi^{>K-2N}\ell^1_\nu. \end{aligned}$$

These imply that the infinite matrix $\mathcal{M}(\bar{u}^2)$ has a finite bandwidth of $2N$ (with the convention that a bandwith of 0 corresponds to a diagonal matrix). This can also be seen by looking directly at the coefficients of general multiplication matrices, which can be easily derived from the formula of the discrete convolution product. Namely, for any $u \in \ell^1_\nu$, $\mathcal{M}(u)$ can be written as follows in terms of a Toeplitz matrix and of a Hankel matrix (with an erased column)[13]

$$\mathcal{M}(u) = \begin{pmatrix} u_0 & u_1 & u_2 & u_3 & \dots \\ u_1 & u_0 & u_1 & u_2 & \ddots \\ u_2 & u_1 & u_0 & u_1 & \ddots \\ u_3 & u_2 & u_1 & u_0 & \ddots \\ \vdots & \ddots & \ddots & \ddots & \ddots \end{pmatrix} + \begin{pmatrix} 0 & u_1 & u_2 & u_3 & \dots \\ 0 & u_2 & u_3 & u_4 & \iddots \\ 0 & u_3 & u_4 & u_5 & \iddots \\ 0 & u_4 & u_5 & u_6 & \iddots \\ \vdots & \iddots & \iddots & \iddots & \iddots \end{pmatrix},$$

[13] If we were working with $\ell^1_\nu(\mathbb{Z})$ instead of $\ell^1_\nu(\mathbb{N})$, we would simply have a (bi-infinite) Toeplitz matrix instead.

and in particular, since $\bar{u}^2 \in \Pi^{\leq 2N}\ell^1_\nu$ then $\mathcal{M}(\bar{u}^2)$ indeed has bandwidth $2N$.

Recalling the formula (1.22) for $DF(\bar{u})$, this has two very helpful consequences. First, every single column of $DF(\bar{u})$ only has finitely many nonzero terms, therefore we can exactly compute any column of $I - ADF(\bar{u})$, and its corresponding norm. Second, for all $i \leq N$ and $j > 3N$, $(DF(\bar{u}))_{i,j} = 0$. That is, columns of $DF(\bar{u})$ of index $j > 3N$ have zeros on all the rows of index $i \leq N$, and in particular, when these columns get multiplied by A, they only "see" the tail part of A, and not $A^{\leq N}$. Equivalently, but written more algebraically, for all u in $\Pi^{>3N}\ell^1_\nu$, $DF(\bar{u})u$ belongs to $\Pi^{>N}\ell^1_\nu$, and therefore

$$ADF(\bar{u})u = \Pi^{>N}\left(-(I+\Delta)^2\right)^{-1}\Pi^{>N}DF(\bar{u})u. \tag{1.25}$$

Since this expression no longer involves the matrix $A^{\leq N}$ it will be easier to control it by hand.

Denoting $B = I - ADF(\bar{u})$, the above discussion motivates the following splitting

$$\|B\|_{\mathcal{B}(\ell^1_\nu,\ell^1_\nu)} = \max\left(\max_{0\leq j\leq 3N}\frac{1}{\xi_j}\sum_{i\in\mathbb{N}}|B_{i,j}|\,\xi_j,\ \sup_{j>3N}\frac{1}{\xi_j}\sum_{i\in\mathbb{N}}B_{i,j}\xi_j\right),$$

or equivalently

$$\|B\|_{\mathcal{B}(\ell^1_\nu,\ell^1_\nu)} = \max\left(\max_{0\leq j\leq 3N}\frac{1}{\xi_j}\sum_{i\in\mathbb{N}}|B_{i,j}|\,\xi_j,\ \sup_{\substack{u\in\Pi^{>3N}\ell^1_\nu\\ u\neq 0}}\frac{\|Bu\|_{\ell^1_\nu}}{\|u\|_{\ell^1_\nu}}\right).$$

The first term in the maximum can be computed exactly with the computer, because these finitely many columns of B are all finite, and we are going to estimate by hand the remaining supremum. Indeed, according to (1.25), for any u in $\Pi^{>3N}\ell^1_\nu$ we have

$$\begin{aligned} Bu &= u - \left(-(I+\Delta)^2\right)^{-1}\left(-(I+\Delta)^2u + \rho u - 3\bar{u}^2 * u\right)\\ &= \left((I+\Delta)^2\right)^{-1}\left((\rho - 3\bar{u}^2) * u\right). \end{aligned}$$

Recalling that $(\rho - 3\bar{u}^2) * u$ belongs to $\Pi^{>N}\ell^1_\nu$, and using the Banach algebra property (1.21), we get

$$\begin{aligned} \|Bu\|_{\ell^1_\nu} &\leq \frac{1}{((N+1)^2-1)^2}\left\|(\rho - 3\bar{u}^2) * u\right\|_{\ell^1_\nu}\\ &\leq \frac{1}{((N+1)^2-1)^2}\left\|\rho - 3\bar{u}^2\right\|_{\ell^1_\nu}\|u\|_{\ell^1_\nu}. \end{aligned}$$

In conclusion, we can define

$$Z_1 = \max\left(\max_{0\leq j\leq 3N}\frac{1}{\xi_j}\sum_{i\in\mathbb{N}}|B_{i,j}|\,\xi_j,\ \frac{1}{((N+1)^2-1)^2}\left\|\rho - 3\bar{u}^2\right\|_{\ell^1_\nu}\right),$$

which is computable and satisfies assumption (1.6) of Theorem 1.2.2.

The remaining bound Z_2 is much simpler to obtain. Indeed, for all $u \in B_{r^*}(\bar{u})$ and $v \in \ell^1_\nu$, we have

$$A\left(DF(\bar{u}) - DF(u)\right)v = -3A\left((\bar{u}^2 - u^2) * v\right),$$

and using once more the Banach algebra property we get

$$\begin{aligned} \|A\left(DF(\bar{u}) - DF(u)\right)v\|_{\ell^1_\nu} &\leq 3\|A\|_{\mathcal{B}(\ell^1_\nu,\ell^1_\nu)}\|\bar{u} - u\|_{\ell^1_\nu}\|\bar{u} + u\|_{\ell^1_\nu}\|v\|_{\ell^1_\nu}\\ &\leq 3\|A\|_{\mathcal{B}(\ell^1_\nu,\ell^1_\nu)}\left(2\|\bar{u}\|_{\ell^1_\nu} + r^*\right)\|\bar{u} - u\|_{\ell^1_\nu}\|v\|_{\ell^1_\nu}, \end{aligned}$$

which means that

$$Z_2 = 3\,\|A\|_{\mathcal{B}(\ell^1_\nu,\ell^1_\nu)}\left(2\,\|\bar{u}\|_{\ell^1_\nu} + r^*\right)$$

satisfies assumption (1.7) of Theorem 1.2.2. Finally, recalling (1.24) and Lemma 1.3.6, note that

$$\|A\|_{\mathcal{B}(\ell^1_\nu,\ell^1_\nu)} = \max\left(\left\|A^{\leq N}\right\|_{\mathcal{B}(\ell^1_\nu,\ell^1_\nu)}, \frac{1}{((N+1)^2-1)^2}\right),$$

and is computable since $A^{\leq N}$ is merely a finite matrix, therefore the whole Z_2 bound is computable, and we are done.

1.3.1.4 An example of result

Putting all the estimates together, and applying Theorem 1.2.2, we obtain the following result.

Theorem 1.3.7. *Let $\rho = 500$, and $\bar{u}$ be the approximate steady state of the Swift–Hohenberg equation (1.18)-(1.19) depicted on Figure 1.3, which is cosine series of order $N = 50$ whose exact coefficients can be found at [Code 8]. There exists an exact steady state u of (1.18)-(1.19) such that*

$$\|u - \bar{u}\|_{\ell^1_1} \leq 1.72847 \times 10^{-12}.$$

Proof. We (somewhat arbitrarily) fix $r^* = 10^{-5}$ and $\nu = 1$, consider the bounds Y, Z_1 and Z_2 derived in Section 1.3.1.3, and evaluate them using interval arithmetic. We obtain

$$Y = 1.728 \times 10^{-12}, \qquad Z_1 = 3.401 \times 10^{-4}, \qquad Z_2 = 3.9502,$$

and check that the conditions (1.8)-(1.9) of Theorem 1.2.2 hold with $r = 1.72847 \times 10^{-12}$. These calculations can be reproduced by running the code available at [Code 8]. □

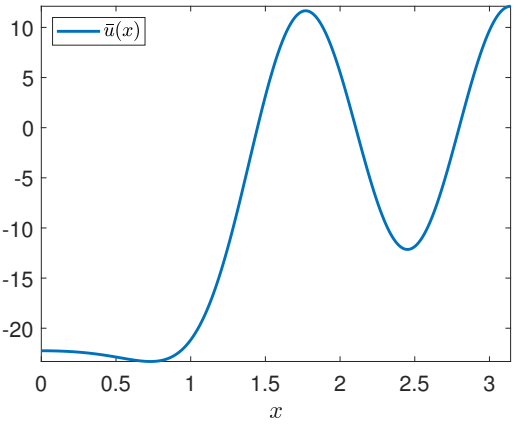

Figure 1.3: The approximate steady state $\bar{u}$ of the Swift–Hohenberg equation (1.18)-(1.19), with $\rho = 500$, validated in Theorem 1.3.7 and Theorem 1.3.18.

Remark 1.3.8. *The ℓ^1_ν norm controls the C^0 norm for any $\nu \geq 1$, hence by taking $\nu = 1$ in Theorem 1.3.7 we obtain the sharpest possible C^0 estimate. However, we could as easily have taken a larger ν. For instance, the proof is also successful with $\nu = 1.5$, and yields*

$$\|u - \bar{u}\|_{\ell^1_{1.5}} \leq 7.02791 \times 10^{-8}.$$

This shows that the obtained steady state of the Swift–Hohenberg equation is in fact analytic and bounded at least on the strip $\{z \in \mathbb{C},\ |\Im(z)| < \ln(1.5)\}$.

Remark 1.3.9. *In this entire manuscript, we mostly use ℓ^1_ν spaces since the solutions we deal with happen to be analytic. However, larger sequence spaces corresponding more or less to $\mathcal{C}^k$ regularities can also be considered if need be, one simply has to replace the geometric weight $\nu^{|n|}$ by an algebraic one like $(1+|n|)^k$, see, e.g., [202].*[14]

1.3.2 Using eigenvalue bounds

We are now going to validate again the same approximate steady state $\bar{u}$ of the Swift–Hohenberg equation as in Theorem 1.3.7, but this time using Theorem 1.2.6 and eigenvalue bounds to control $\left\|DF(\bar{u})^{-1}\right\|_{\mathcal{B}(\mathcal{Y},\mathcal{X})}$.

1.3.2.1 Spaces and the zero finding problem

In order to use eigenvalue bounds, we need to work in Hilbert spaces. We therefore consider

$$\mathcal{X} = \left\{u \in H^4((0,\pi)),\, u'(0) = u'(\pi) = u'''(0) = u'''(\pi) = 0\right\}, \qquad \mathcal{Y} = L^2((0,\pi)),$$

and the same map

$$F(u) = -(1+\Delta)^2 u + \rho u - u^3,$$

as in Section 1.3.1, but this time defined from $\mathcal{X}$ to $\mathcal{Y}$.

Remark 1.3.10. *Alternative and more flexible choices are possible, in particular using the weak form of the equation, but we stick with the strong formulation here in order to stay as close as possible to the setting of Section 1.3.1, and refer to [238, Part II] for a much more general presentation.*

It is mostly in the space $\mathcal{Y}$ that the Hilbertian structure will be leveraged. The scalar product $\langle\cdot,\cdot\rangle_{\mathcal{Y}}$ is taken as the usual (normalized) L^2 scalar product:

$$\langle u, v\rangle_{\mathcal{Y}} = \frac{1}{\pi}\int_0^\pi u(x)v(x)\mathrm{d}x,$$

which we sometimes simply denote $\langle\cdot,\cdot\rangle$. On $\mathcal{X}$, we consider the norm given by

$$\|u\|_{\mathcal{X}} = \sqrt{\|\Delta^2 u\|_{\mathcal{Y}}^2 + \|u\|_{\mathcal{Y}}^2}.$$

Using the boundary conditions incorporated in $\mathcal{X}$, it is straightforward to check that this norm is equivalent to the standard norm on H^4, hence $\mathcal{X}$ is indeed complete.

1.3.2.2 Reducing the problem to an eigenvalue bound

Our goal is to apply Theorem 1.2.6 with the map F, the approximate solution $\bar{u}$ depicted in Figure 1.3 (denoted $\bar{x}$ in Theorem 1.2.6) and the spaces $\mathcal{X}$ and $\mathcal{Y}$ described just above. We must therefore derive estimates δ, κ and L satisfying assumptions (1.13)-(1.15). We will come back to δ and L in the next subsection, but first focus on the most challenging bound, namely κ.

For all the calculations to come, we introduce $c = \rho - 1 - 3\bar{u}^2$, so that, for all u in $\mathcal{X}$,

$$DF(\bar{u})u = -\Delta^2 u - 2\Delta u + cu.$$

Recall that $\kappa > 0$ must satisfy

$$\|u\|_{\mathcal{X}} \le \kappa \left\|DF(\bar{u})u\right\|_{\mathcal{Y}} \qquad \forall u \in \mathcal{X}. \tag{1.26}$$

[14] Note that [202] in fact uses weighted ℓ^∞ spaces, which are slightly more cumbersome to manipulate than weighted ℓ^1 spaces, and have mostly fallen out of use in this context.

The most challenging part will be to obtain $\kappa_0 > 0$ such that

$$\|u\|_{\mathcal{Y}} \leq \kappa_0 \|DF(\bar{u})u\|_{\mathcal{Y}} \qquad \forall u \in \mathcal{X}, \tag{1.27}$$

i.e., to control $\left\|DF(\bar{u})^{-1}\right\|_{\mathcal{B}(\mathcal{Y},\mathcal{Y})}$, the norm of the inverse of $DF(\bar{u})$ from the space $\mathcal{Y}$ into itself. Indeed, once such a κ_0 is obtained, it is rather straightforward to obtain an explicit κ_1 (depending on κ_0) such that

$$\left\|\Delta^2 u\right\|_{\mathcal{Y}} \leq \kappa_1 \|DF(\bar{u})u\|_{\mathcal{Y}} \qquad \forall u \in \mathcal{X}, \tag{1.28}$$

and then (1.26) holds with $\kappa = \sqrt{\kappa_0^2 + \kappa_1^2}$.

Lemma 1.3.11. *Assume there exists $\kappa_0 > 0$ such that (1.27) is satisfied. Then, for all $\eta_1, \eta_2, \eta_3, \eta_4 > 0$ such that $2\eta_1 + \eta_2 + \frac{\eta_4}{2}\left(\frac{2}{\eta_1} + 2\eta_3\right) < 1$, the estimate (1.28) holds with*

$$\kappa_1 = \sqrt{\frac{1 + \kappa_0^2\left(\|c\|_\infty^2\left(\frac{1}{\eta_2} + \frac{1}{2\eta_3}\right) + \frac{1}{2\eta_4}\left(\frac{2}{\eta_1} + 2\eta_3\right)\right)}{1 - \left(2\eta_1 + \eta_2 + \frac{\eta_4}{2}\left(\frac{2}{\eta_1} + 2\eta_3\right)\right)}}.$$

Proof. Expanding

$$\|DF(\bar{u})u\|_{\mathcal{Y}}^2 = \left\langle -\Delta^2 u - 2\Delta u + cu, -\Delta^2 u - 2\Delta u + cu \right\rangle,$$

yields

$$\begin{aligned}\left\|\Delta^2 u\right\|_{\mathcal{Y}}^2 &= \|DF(\bar{u})u\|_{\mathcal{Y}}^2 - 4\left\langle \Delta^2 u, \Delta u\right\rangle - 4\left\langle \Delta u, \Delta u\right\rangle + 2\left\langle \Delta^2 u, cu\right\rangle - 4\left\langle \Delta u, cu\right\rangle - \left\langle cu, cu\right\rangle \\ &\leq \|DF(\bar{u})u\|_{\mathcal{Y}}^2 - 4\left\langle \Delta^2 u, \Delta u\right\rangle + 2\left\langle \Delta^2 u, cu\right\rangle - 4\left\langle \Delta u, cu\right\rangle,\end{aligned}$$

and we simply have to estimate the right hand side, only in terms of $\left\|\Delta^2 u\right\|_{\mathcal{Y}}^2$ and $\|u\|_{\mathcal{Y}}^2$. Applying several times Young's inequality $ab \leq \frac{\eta}{2}a^2 + \frac{1}{2\eta}b^2$, $\eta > 0$, and the elementary interpolation inequality $\|\Delta u\|_{\mathcal{Y}} \leq \|u\|_{\mathcal{Y}}^{\frac{1}{2}} \left\|\Delta^2 u\right\|_{\mathcal{Y}}^{\frac{1}{2}}$, a tedious but straightforward computation shows that, for all $\eta_1, \eta_2, \eta_3, \eta_4 > 0$,

$$\begin{aligned}\left\|\Delta^2 u\right\|_{\mathcal{Y}}^2 \leq \|DF(\bar{u})u\|_{\mathcal{Y}}^2 &+ \left(2\eta_1 + \eta_2 + \frac{\eta_4}{2}\left(\frac{2}{\eta_1} + 2\eta_3\right)\right)\left\|\Delta^2 u\right\|_{\mathcal{Y}}^2 \\ &+ \left(\|c\|_\infty^2\left(\frac{1}{\eta_2} + \frac{1}{2\eta_3}\right) + \frac{1}{2\eta_4}\left(\frac{2}{\eta_1} + 2\eta_3\right)\right)\|u\|_{\mathcal{Y}}^2.\end{aligned}$$

Under the additional assumption $2\eta_1 + \eta_2 + \frac{\eta_4}{2}\left(\frac{2}{\eta_1} + 2\eta_3\right) < 1$, and using (1.27) to control $\|u\|_{\mathcal{Y}}$, we finally get

$$\left\|\Delta^2 u\right\|_{\mathcal{Y}}^2 \leq \frac{1 + \kappa_0^2\left(\|c\|_\infty^2\left(\frac{1}{\eta_2} + \frac{1}{2\eta_3}\right) + \frac{1}{2\eta_4}\left(\frac{2}{\eta_1} + 2\eta_3\right)\right)}{1 - \left(2\eta_1 + \eta_2 + \frac{\eta_4}{2}\left(\frac{2}{\eta_1} + 2\eta_3\right)\right)}\|DF(\bar{u})u\|_{\mathcal{Y}}^2. \qquad \square$$

Choosing, somewhat arbitrarily, $\eta_1 = \frac{1}{16}$, $\eta_2 = \frac{1}{8}$, $\eta_3 = 16$ and $\eta_4 = \frac{1}{128}$ yields

$$\kappa_1 = \sqrt{2 + \kappa_0^2\left(\|c\|_\infty^2\left(16 + \frac{1}{16}\right) + 8192\right)}.$$

In practice, once κ_0 and $\|c\|_\infty$ are explicitly known, one can numerically optimize to find values of $\eta_1, \eta_2, \eta_3, \eta_4$ giving a smaller constant κ_1.

The last missing piece in order to get κ is to find a positive and explicit κ_0 satisfying (1.27). This is where the Hilbert space structure really comes into play. Indeed, note that the unbounded operator $DF(\bar{u}) : \mathcal{X} \subset \mathcal{Y} \to \mathcal{Y}$ is self-adjoint, and has compact resolvant, hence its spectrum $\sigma(DF(\bar{u}))$ is purely discrete, and any u in $\mathcal{X}$ can be written as a converging sum of $\mathcal{Y}$-orthogonal eigenfunctions, which yields

$$\|DF(\bar{u})u\|_{\mathcal{Y}} \geq \inf_{\lambda \in \sigma(DF(\bar{u}))} |\lambda| \, \|u\|_{\mathcal{Y}} .$$

Therefore, assuming 0 is not in the spectrum of $DF(\bar{u})$, any κ_0 such that

$$0 < \kappa_0^{-1} \leq \inf_{\lambda \in \sigma(DF(\bar{u}))} \tag{1.29}$$

satisfies (1.27). In other words, if we can get rigorous and sharp enough enclosures of the eigenvalues of $DF(\bar{u})$ that are the closest to 0, we will be able to obtain κ_0.

We now slightly reformulate the problem by flipping the spectrum of $DF(\bar{u})$, in preparation for the eigenvalue enclosure procedure to come. That is, we consider the operator $\mathcal{L} : \mathcal{X} \subset \mathcal{Y} \to \mathcal{Y}$ defined as $\mathcal{L} = -DF(\bar{u})$, and denote by

$$\tilde{\lambda}_1 \leq \tilde{\lambda}_2 \leq \ldots \leq \tilde{\lambda}_m \leq \ldots$$

the eigenvalues of $\mathcal{L}$, counting multiplicity and arranged in increasing order. Note that the eigenvalues of $DF(\bar{u})$ are simply given by $\left(-\tilde{\lambda}_m\right)_{m \geq 1}$. In particular, if we can find an integer m and sharp enough enclosures of the eigenvalues of $\mathcal{L}$ to prove that

$$\tilde{\lambda}_{m-1} < 0 < \tilde{\lambda}_m, \tag{1.30}$$

then

$$\kappa_0 := \frac{1}{\min\left(|\tilde{\lambda}_{m-1}|, |\tilde{\lambda}_m|\right)} = \frac{1}{\inf_{\tilde{\lambda} \in \sigma(DF(\bar{u}))}}$$

satisfies (1.29), and therefore (1.27).

1.3.2.3 Eigenvalue enclosures using the homotopy method

We now present a very versatile method allowing to rigorously enclose the M first eigenvalues of a self-adjoint operator which is bounded below.[15] The entire procedure we are about to describe was introduced in [247], and is now often referred to as *the homotopy method*. It is in fact made of three main ingredients, the last one being where a homotopy plays a crucial role.

In this subsection, we place ourselves in a slightly more general context than that of the example discussed in Section 1.3.2: we consider an arbitrary separable Hilbert space $\mathcal{H}$, whose scalar product is still denoted $\langle \cdot, \cdot \rangle$, and a densely defined self-adjoint operator $S : D(S) \subset \mathcal{H} \to \mathcal{H}$, with domain $D(S)$. Nonetheless, our aim is to present the main ideas as clearly as possible rather than to state each result in the most general context possible, and we instead refer to [238, Chapter 10] for a much broader exposition. In particular, for the sake of simplifying the presentation, we assume that the spectrum of S only consists of eigenvalues, which accumulate only at $+\infty$, and denote by

$$\lambda_1 \leq \lambda_2 \leq \ldots \leq \lambda_m \leq \ldots$$

the eigenvalues of S, counting multiplicity and arranged in increasing order.

The first ingredient of the homotopy method is the well-known Rayleigh-Ritz method, which can in fact produce rigorous and very sharp upper-bounds of the M first eigenvalues of S. The statement below is essentially [238, Theorem 10.12].

[15] In full generality, this approach only allows to enclose the eigenvalues that are below the essential spectrum, but we do not need to worry about this for our specific example, since $\mathcal{L}$ has compact resolvent and therefore only discrete spectrum.

Theorem 1.3.12. *Let $M \in \mathbb{N}_{\geq 1}$ and $u_1, \ldots, u_M \in D(S)$ be linearly independent. Define the matrices*

$$A_0 = (\langle u_i, u_j \rangle)_{1 \leq i,j \leq M} \qquad \text{and} \qquad A_1 = (\langle Su_i, u_j \rangle)_{1 \leq i,j \leq M},$$

and let

$$\overline{\lambda}_1 \leq \ldots \leq \overline{\lambda}_M,$$

be the eigenvalues of the generalized eigenvalue problem

$$A_1 v = \overline{\lambda} A_0 v. \tag{1.31}$$

Then, for all $1 \leq m \leq M$

$$\lambda_m \leq \overline{\lambda}_m.$$

Remark 1.3.13. *This result is nothing but a generalization to more than one eigenvalue of the basic estimate*

$$\langle Su, u \rangle \geq \lambda_1 \langle u, u \rangle \qquad \text{for all } u \in D(S),$$

which provides an upper-bound for λ_1 for any fixed $u \neq 0$. The quality of the upper-bounds produced by Theorem 1.3.12 depends on the choice of the elements u_i. If we take them to be accurate approximations of the M first eigenfunctions of S, we get sharp upper-bounds.

Provided the entries of the matrices A_0 and A_1 are computed with interval arithmetic, and the finite-dimensional *eigenvalue problem (1.31) is also solved rigorously (there are standard techniques for this, see, e.g., [258]), the $\overline{\lambda}_m$ are computable and rigorous upper-bounds for the eigenvalues λ_m.*

Finally, let us emphasize that Theorem 1.3.12 requires approximate eigenvectors u_i that exactly belong to the domain of S. For our Swift–Hohenberg example of Section 1.3 this is trivial, because we natural use finite cosine series for the numerics, and these all belong to $H^4((0,\pi))$ and satisfy the boundary conditions. However, for situations where this would be a troublesome requirement, we point out the existence of an elegant workaround: the so-called Goerisch extension [29] (see also [238, Section 10.2.3]).

The second ingredient of the homotopy method is the Lehmann-Maehly method, which can produce rigorous and very sharp lower-bounds of the M first eigenvalues of S, provided some a priori knowledge on the next eigenvalue λ_{M+1} is available. The statement below is essentially [238, Theorem 10.14].

Theorem 1.3.14. *Repeat the assumptions of Theorem 1.3.12. Assume further that there exists $\nu \in \mathbb{R}$ such that*

$$\overline{\lambda}_M < \nu \leq \lambda_{M+1}, \tag{1.32}$$

define the matrices

$$A_2 = (\langle Su_i, Su_j \rangle)_{1 \leq i,j \leq M}, \qquad B_1 = A_1 - \nu A_0 \quad \text{and} \quad B_2 = A_2 - 2\nu A_1 + \nu^2 A_0,$$

let

$$\mu_1 \leq \ldots \leq \mu_M$$

be the eigenvalues of the generalized eigenvalue problem

$$B_1 v = \mu B_2 v, \tag{1.33}$$

and assume that $\mu_M < 0$. Then, for all $1 \leq m \leq M$

$$\underline{\lambda}_m \leq \lambda_m,$$

where

$$\underline{\lambda}_m := \nu + \frac{1}{\mu_{M+1-m}}.$$

Remark 1.3.15. *Again, in the case $M = 1$, this is nothing but the estimate*

$$\langle (S-\nu)^{-1}u, u\rangle \geq (\lambda_1 - \nu)^{-1}\langle u, u\rangle,$$

which, taking $u = (S-\nu)v$, yields

$$\langle (S-\nu)v, v\rangle \geq (\lambda_1 - \nu)^{-1}\langle (S-\nu)v, (S-\nu)v\rangle$$

The remainder of Remark 1.3.13 also applies here.

Taken together, Theorem 1.3.12 and Theorem 1.3.14 allow to get rigorous and sharp enclosures of the M first eigenvalues of S, but the lower bounds hinge on assumption (1.32), which can be very challenging to check. The third and final ingredient of the homotopy-method is a robust way of satisfying this assumption, using a well chosen homotopy between S and a so-called base problem.

Definition 1.3.16. *A self-adjoint operator $S^{(0)} : D(S)$[16] $\subset \mathcal{H} \to \mathcal{H}$ whose spectrum only consists of eigenvalues*

$$\lambda_1^{(0)} \leq \lambda_2^{(0)} \leq \ldots \leq \lambda_m^{(0)} \leq \ldots$$

is a suitable base problem for S if:

1. *We know, by pen-and-paper calculations or by a previous computer-assisted argument, explicit lower bounds on the eigenvalues of $S^{(0)}$;*
2. *$\langle S^{(0)}u, u\rangle \leq \langle Su, u\rangle$ for all $u \in D(S)$.*

In the simplest cases, like for our Swift–Hohenberg example, the base problem is a linear operator with constant coefficients, whose spectrum can be computer by hand using Fourier analysis, but much more involved situations are also possible, see [238, Section 10.2.5].

A critical consequence of point 2. in Definition 1.3.16 is that, by Poincaré's min-max principle,

$$\lambda_m^{(0)} \leq \lambda_m \qquad \text{for all } m \geq 1.$$

In particular, $\lambda_{M+1}^{(0)} \leq \lambda_{M+1}$, and we know $\lambda_{M+1}^{(0)}$ explicitly (or at least a lower bound for it). Therefore, one can first apply Theorem 1.3.12 to get rigorous upper-bounds on the first M eigenvalues of S, and then check whether $\overline{\lambda}_M < \lambda_{M+1}^{(0)}$. If this inequality holds, then any $\nu \in (\overline{\lambda}_M, \lambda_{M+1}^{(0)})$ satisfies assumption (1.32), and we can apply Theorem 1.3.14 to get rigorous lower bounds on the first M eigenvalues of S as well. However, we cannot expect the inequality $\overline{\lambda}_M < \lambda_{M+1}^{(0)}$ to hold in general (unless the operator S is already very close to a base problem).

A more robust strategy is to consider a simple homotopy between $S^{(0)}$ and S, given by

$$S^{(s)} := S^{(0)} + s(S - S^{(0)}) \qquad \text{for all } s \in [0,1].$$

The crucial property of this homotopy is that eigenvalues behave monotonically with respect to s. Indeed, denoting the eigenvalues of $S^{(s)}$ by

$$\lambda_1^{(s)} \leq \lambda_2^{(s)} \leq \ldots \leq \lambda_m^{(s)} \leq \ldots$$

we have thanks to point 2. of Definition 1.3.16 that

$$\lambda_m^{(s)} \leq \lambda_m^{(t)} \qquad \text{for all } 0 \leq s \leq t \leq 1 \text{ and } m \geq 1.$$

In order to rigorously enclose the first M eigenvalues of S, we can then use the following iterative procedure.

[16] The assumption that $S^{(0)}$ has the same domain as S is made here for simplicity, but is in fact not needed, see [238, Section 10.1.4], and also [B16, Section 3.3.2] for a specific example.

1. Numerically compute the M first eigenvalues of S, and pick $K > M$ such that $\lambda_K^{(0)}$ is larger than the approximate M-th eigenvalue of S. By assumption on the base problem, we have an explicit lower bound $\underline{\lambda}_K^{(0)}$ on the K-th eigenvalue of $S^{(0)}$.

2. Fix a tolerance $\varepsilon \ll 1$ and numerically compute eigenvalues of $S^{(s)}$ in order to find, non-rigorously, the largest possible $s_1 \in [0,1]$ such that $\lambda_{K-1}^{(s_1)} \leq \underline{\lambda}_K^{(0)} - \varepsilon$.

3. For the s_1 obtained in the previous step, apply Theorem 1.3.12 to get rigorous upper-bounds $\overline{\lambda}_m^{(s_1)}$ on the $K-1$ first eigenvalues of $S^{(s_1)}$, and check that $\overline{\lambda}_{K-1}^{(s_1)} < \underline{\lambda}_K^{(0)}$. If not, take s_1 slightly smaller and repeat this step.

4. Once $\overline{\lambda}_{K-1}^{(s_1)} < \underline{\lambda}_K^{(0)}$, by monotonicity of the homotopy we have $\overline{\lambda}_{K-1}^{(s_1)} < \lambda_K^{(s)}$ and can therefore use Theorem 1.3.14 to get rigorous lower-bounds $\underline{\lambda}_m^{(s_1)}$ on the $K-1$ first eigenvalues of $S^{(s_1)}$, and in particular $\underline{\lambda}_{K-1}^{(s_1)}$.

5. Now that we have an explicit lower bound $\underline{\lambda}_{K-1}^{(s_1)}$ for the $K-1$-th eigenvalue of $S^{(s_1)}$, we can go forward in s, and repeat steps 2-4 with one less eigenvalue. That is, find the largest possible $s_2 \in [s_1, 1]$ such that $\lambda_{K-2}^{(s_2)} \leq \underline{\lambda}_{K-1}^{(s_1)} - \varepsilon$, and then compute rigorous upper- and lower-bounds on the first $K-2$ eigenvalues of $S^{(s_2)}$ using Theorem 1.3.12 and Theorem 1.3.14. We keep repeating these steps until, either s reaches 1, or we have done too many steps and ran out of eigenvalues. If we reach $s = 1$ with still at least M eigenvalues we are done, otherwise we should start again with a larger number K of eigenvalues for the base problem (and/or a smaller tolerance ε).

For a slightly more efficient procedure, where we do not compute all the lower bounds but only that of the last eigenvalue at each intermediate step, see [B16, Proposition 3.13]. We now apply this whole procedure to our operator $\mathcal{L} = -DF(\bar{u})$, in order to find an M such that (1.30) holds, and again refer to [238, Chapter 10] for a broader discussion on the homotopy method.

1.3.2.4 Application of the homotopy method

In Section 1.3.2.2, we studied how to find an explicit constant κ satisfying assumption (1.14) of Theorem 1.2.6, for our $F(u) = 0$ steady state problem in the Swift–Hohenberg equation. We first reduced the problem to that of finding κ_0 satisfying (1.27), for which we need rigorous enclosures of the eigenvalues of the self-adjoint operator $\mathcal{L} = -DF(\bar{u})$.

In order to apply the homotopy method to $\mathcal{L}$, we derive a suitable base problem $\mathcal{L}^{(0)}$. Recall that

$$\mathcal{L}u = \Delta^2 u + 2\Delta u - cu,$$

where $c = \rho - 1 - 3\bar{u}^2$. We therefore pick a constant $\overline{c} \geq \max_{x\in[0,\pi]} c(x)$ (such a rigorous upper bound for c can easily be obtained using interval arithmetic, given that $\bar{u}$ is a known trigonometric polynomial) and define

$$\mathcal{L}^{(0)}u = \Delta^2 u + 2\Delta u - \overline{c}u,$$

for which we have

$$\langle \mathcal{L}^{(0)}u, u\rangle \leq \langle \mathcal{L}u, u\rangle \qquad \text{for all } u \in \mathcal{X}.$$

Moreover, we have explicit formulas for the eigenvalues of $\mathcal{L}^{(0)}$, which are given by

$$m^4 - 2m^2 - \overline{c}, \qquad m \geq 0,$$

therefore $\mathcal{L}^{(0)}$ is a suitable base problem for $\mathcal{L}$.

1.3.2.5 Remaining estimates

Let us finally discuss the derivation of bounds δ and L for Theorem 1.2.6. As already explained in Section 1.3.1.3, $F(\bar{u})$ is merely a finite cosine series, whose coefficients can all be computed exactly, and $\|F(\bar{u})\|_{\mathcal{Y}}$ can therefore also be computed exactly.[17] We therefore define

$$\delta = \|F(\bar{u})\|_{\mathcal{Y}},$$

which is computable and satisfies assumption (1.13) of Theorem 1.2.6.

Regarding the local Lipschitz constant L on DF, we have to work slightly more than for the corresponding Z_2 bound in Section 1.3.1.3, because we no longer have the Banach algebra property to deal with nonlinearities. We instead rely on Sobolev embeddings, and the additional work comes from the fact that we need explicit constants. Note however that, at least for H^1 and H^2 spaces, many explicit embedding constants are already readily available in the literature, see for instance [238, Section 6.2.6] and the references therein.

For any $u \in B_{r^*}(\bar{u})$ and any $v \in \mathcal{X}$, we have

$$\begin{aligned}\|(DF(u) - DF(\bar{u}))\, v\|_{\mathcal{Y}} &= 3\, \|(u+\bar{u})(u-\bar{u})v\|_{\mathcal{Y}} \\ &\leq 3\left(2\,\|\bar{u}\|_{\mathcal{Y}} + \|u-\bar{u}\|_{\mathcal{Y}}\right) \|(u-\bar{u})\|_{\infty}\, \|v\|_{\infty} \\ &\leq 6\left(\pi^4 + \frac{\pi^2}{2}\right)^2 \left(2\,\|\bar{u}\|_{\mathcal{Y}} + r^*\right) \|(u-\bar{u})\|_{\mathcal{X}}\, \|v\|_{\mathcal{X}},\end{aligned}$$

where we used Lemma 1.3.17 to explicitly control the embedding $\mathcal{X} \to \mathcal{C}([0,\pi])$, with admittedly no effort to obtain a sharp constant. We therefore define

$$L = 6\left(\pi^4 + \frac{\pi^2}{2}\right)^2 \left(2\,\|\bar{u}\|_{\mathcal{Y}} + r^*\right),$$

which is computable and satisfies assumption (1.15) of Theorem 1.2.6.

Lemma 1.3.17. *For all $u \in \mathcal{X}$,*

$$\|u\|_{\infty} \leq \sqrt{2}\left(\pi^4 + \frac{\pi^2}{2}\right) \|u\|_{\mathcal{X}}.$$

Proof. For any u in $\mathcal{X}$, successive applications of the fundamental theorem of calculus, together with the boundary conditions in $\mathcal{X}$, yield

$$u(x_1) = u(x_2) + \int_{x_1}^{x_2}\int_{0}^{x_3}\left(u''(x_5) + \int_{x_4}^{x_5}\int_{0}^{x_6} u''''(x_7)\mathrm{d}x_7\mathrm{d}x_6\right)\mathrm{d}x_4\mathrm{d}x_3,$$

for all $x_1, x_2, x_5 \in [0,\pi]$. A couple of brutal estimates, followed by Cauchy-Schwarz inequality, then give

$$\begin{aligned}|u(x_1)| &\leq |u(x_2)| + \int_0^{\pi}\int_0^{\pi}\left(|u''(x_5)| + \int_0^{\pi}\int_0^{\pi} |u''''(x_7)|\,\mathrm{d}x_7\mathrm{d}x_6\right)\mathrm{d}x_4\mathrm{d}x_3 \\ &\leq |u(x_2)| + \pi^2\left(|u''(x_5)| + \pi^2\,\|u''''\|_{\mathcal{Y}}\right).\end{aligned}$$

We then average with respect to x_2 and x_5, and again using Cauchy-Schwarz inequality, which yields

$$|u(x_1)| \leq \|u\|_{\mathcal{Y}} + \pi^2\,\|u''\|_{\mathcal{Y}} + \pi^4\,\|u''''\|_{\mathcal{Y}}.$$

[17] Here the integral involved in the definition of the norm can indeed be computed exactly by hand in terms of the Fourier coefficients of $F(\bar{u})$, but more generally one can use quadrature rules with computable error bounds to rigorously enclose such integrals.

Finally, integrating by part and using Cauchy-Schwarz and Young's inequalities, we get

$$\|u''\|_{\mathcal{Y}} \leq \|u\|_{\mathcal{Y}}^{\frac{1}{2}} \|u''''\|_{\mathcal{Y}}^{\frac{1}{2}} \leq \frac{1}{2}\left(\|u\|_{\mathcal{Y}} + \|u''''\|_{\mathcal{Y}}\right),$$

hence

$$\begin{aligned} |u(x_1)| &\leq \left(1 + \frac{\pi^2}{2}\right)\|u\|_{\mathcal{Y}} + \left(\pi^4 + \frac{\pi^2}{2}\right)\|u''''\|_{\mathcal{Y}} \\ &\leq \sqrt{2}\left(\pi^4 + \frac{\pi^2}{2}\right)\|u\|_{\mathcal{X}}. \end{aligned}$$

□

1.3.2.6 An example of result

Putting all the estimates together, and applying Theorem 1.2.6, we obtain the following result.

Theorem 1.3.18. *Let $\rho = 500$, and $\bar{u}$ be the approximate steady state of the Swift–Hohenberg equation (1.18)-(1.19) depicted on Figure 1.3, which is cosine series of order $N = 50$ whose exact coefficients can be found at [Code 8]. There exists an exact steady state u of (1.18)-(1.19) such that*

$$\|u - \bar{u}\|_{\mathcal{X}} \leq 6.00732 \times 10^{-9}.$$

Proof. We (somewhat arbitrarily) fix $r^* = 10^{-5}$ and consider the bounds δ, κ and L derived in Section 1.3.2, and evaluate them using interval arithmetic. We obtain

$$\delta = 2.182 \times 10^{-10}, \qquad \kappa = 22.7, \qquad L = 1.9049 \times 10^{6},$$

and check that the conditions (1.16)-(1.17) of Theorem 1.2.2 hold with $r = 6.00732 \times 10^{-9}$. These calculations can be reproduced by running the code available at [Code 8]. □

Remark 1.3.19. *Even though it is somewhat hard to precisely compare the error bounds obtained in Theorem 1.3.7 and 1.3.18, as they are in different norms, we expect the one obtained in Theorem 1.3.7 to be slightly sharper, for two reasons. The first one is intrinsic to the fact that, with Theorem 1.2.2 we directly compute $\|AF(\bar{u})\|$, whereas the corresponding quantity within Theorem 1.2.6, namely $\left\|DF(\bar{u})^{-1}F(\bar{u})\right\|$ is only estimated via $\left\|DF(\bar{u})^{-1}\right\|\|F(\bar{u})\|$. This can have a noticeable impact, and indeed for this specific example $\|AF(\bar{u})\|_{\ell^1_1}$ ends up being one order of magnitude smaller than $\|A\|_{\ell^1_1}\|F(\bar{u})\|_{\ell^1_1}$. However, the second reason is that we made little effort to optimize some of the analytic computations involved in deriving the estimates κ_1 and L, that could probably be significantly improved.*

Chapter 2

Two specific examples

In this chapter, we study some specific solutions of two different PDEs, namely periodic orbits of the Navier–Stokes equation in Section 2.1, and traveling waves of the so-called DPCM: a free boundary problem composed of coupled drift-diffusion equations and a Poisson equation, in Section 2.2. In both cases, the proof is heavily computer-assisted and relies on the Newton–Kantorovich Theorem 1.2.2. These proofs are technically much more involved than the basic example given in Section 1.3.1, but several of the main ideas were already presented there, therefore we mainly focus in this chapter on the aspects where significant changes or different approaches are needed. Overall, we believe that the main interest of this chapter does not lie in the computer-assisted techniques employed, most of which could by now be considered standard, but rather in the results that are obtained, which provide good examples of interesting problems that are very challenging to study by hand, but for which computer-assisted proofs can bring answers.

2.1 Spontaneous periodic solutions of the Navier–Stokes equations

2.1.1 Motivations

The Navier–Stokes equations govern the dynamics of viscous fluids and are widely studied and used, both in the mathematical community and for numerous real-life applications. These equations describe the velocity field u and pressure p of a fluid:

$$\begin{cases} \partial_t u + (u \cdot \nabla)u - \nu \Delta u + \nabla p = f \\ \nabla \cdot u = 0, \end{cases} \tag{2.1}$$

where ν is the kinematic viscosity, and f is an external forcing term. These equations can be considered on bounded or unbounded domains, complemented by suitable boundary and initial conditions.

The Navier–Stokes equations are famous in part because they are featured in one of the Millenium prize problems, which consists in proving whether these equations are globally well-posed or exhibit a blowup in three spatial dimensions. However, there are many other interesting open questions regarding the dynamics of fluids, often related to real observations, experiments, or numerical simulations.

When trying the understand the dynamics of any given nonlinear dynamical system, a first step one can take is study its invariant sets, some of the simplest ones being steady states and periodic orbits. The fact that fluids can exhibit (sometimes intricate) periodic motions has been noticed experimentally more than a century ago, the most famous example being the so-called von Karman vortex street observed in the wake of an obstacle. Starting with the work of Serrin [266], most of the literature on the existence of periodic solutions of the

Navier–Stokes equations deals with the case where the fluid is under some external influence which is itself periodic in time, i.e., time periodic forcing terms or boundary conditions, or periodically moving boundaries, see [176, 276, 215, 191, 322, 134] for a far from exhaustive list of references covering the different cases mentioned above, both on bounded and unbounded domains. However, many examples, including the aforementioned von Karman vortex street, do not fall within that category: There is no external periodic influence, and the periodic motion of the fluid is then a genuine consequence of the nonlinearity of the equations. In this setting, actually proving the existence of periodic orbits is much harder, and the few existing results predating [B3] fall into the *perturbative* category. Indeed, they only establish the existence of small amplitude periodic perturbations of a steady state, also only for small perturbations of a given parameter in the model (for instance the viscosity), essentially by establishing the existence of a Hopf bifurcation [168, 166, 174, 220, 133]. These are by no mean easy results, as proving the existence of a Hopf bifurcation in infinite dimension can be very challenging, yet they can only be applied for very specific parameter values, and fail to capture the periodic motions typically observed in experiments whose amplitude is not arbitrarily small. On the other hand, many numerical simulations have been conducted to study periodic motions away from bifurcation points, see, e.g., [181] for branches of periodic orbits in Couette flow that do not stem from Hopf bifurcations, or [83, 300] for different geometries and forcing mechanisms.

By using computer-assisted proofs, we managed in [B3] to bridge the gap between the rigorous perturbative results and the non-perturbative simulations, for periodic motions in the Navier–Stokes equations without external periodic influence. This is the first computer-assisted proof for a time-dependent solution of the Navier–Stokes equations, but we note that earlier works successfully used computer-assisted techniques to study non-trivial stationary solutions of the Navier–Stokes equations [311, 186, 308, 309], with more recent papers dealing with whole branches and bifurcations of stationary solutions [4], stationary solutions on an unbounded strip with an obstacle [318], and 3D stationary solutions for general bounded domains [209]. More broadly speaking, computer-assisted proofs have become increasingly useful for establishing new results about fluid dynamics, e.g., global uniqueness of extreme Stokes waves [190], instability of the Poiseuille flow [310], global smooth solutions for the inviscid SQG equation [67], cusped periodic waves and solitary waves in the Whitham equation [110, 51], self-similar blowups in the 2D Boussinesq and the 3D Euler equations [74] as well as in the 3D compressible Euler and Navier–Stokes equations [44], non-convex uniformly rotating vortex patches of the incompressible 2D Euler equations [68], or chaos in high order Galerkin truncations of the stochastic 2D Navier–Stokes equations [28].

2.1.2 A computer-assisted framework for periodic solutions of the Navier–Stokes equations on the torus

In [B3], we develop a general framework to study, with computer-assistance, periodic solutions of the incompressible Navier–Stokes equations (2.1) on the 3-dimensional torus, with a time independent forcing f.

As already hinted at in Chapter 1, a crucial first step is the choice of a suitable reformulation of the problem, and of a good function space. It turns out that using the vorticity formulation of the Navier–Stokes equations

$$\partial_t \omega - ((\Delta^{-1}\nabla \times \omega) \cdot \nabla)\omega + (\omega \cdot \nabla)\,(\Delta^{-1}\nabla \times \omega) - \nu\Delta\omega = g, \tag{2.2}$$

with $\omega = \nabla \times u$ and $g = \nabla \times f$, is a convenient way of getting rid of the pressure. The fact that we work on the torus and are looking for periodic solutions in time makes Fourier series a very natural choice, both for discretizing the problem and for choosing a function space. Also, the somewhat nasty-looking terms $((\Delta^{-1}\nabla \times \omega) \cdot \nabla)\omega$ and $(\omega \cdot \nabla)\,(\Delta^{-1}\nabla \times \omega)$ become rather straightforward in Fourier space, where all the involved differential operators are diagonal. That

is, our $F = 0$ problem is obtained by plugging a space-time Fourier series Ansatz

$$\omega(t,x) = \sum_{n\in\mathbb{Z}^4} \omega_n e^{i(n_1x_1+n_2x_2+n_3x_3+n_4\Omega t)},$$

into the Navier–Stokes equations in vorticity form (2.2), the unknown then being the sequence of Fourier coefficients $\omega = (\omega_n)_{n\in\mathbb{Z}^4}$,[1] and the frequency Ω of the solution, which also has to be solved for. This yields a zero-finding problem of the form

$$F_n(\omega,\Omega) = \left(\nu(n_1^2+n_2^2+n_3^3) + i\Omega n_4\right)\omega_n + \text{nonlinear terms} - g_n.$$

Since the forcing f is assumed to be time independent, periodic solutions of (2.1) or (2.2) are in fact not isolated: if $\omega = \omega(t,x)$ is a periodic solution of (2.2), so is $\omega(t+\tau,x)$ for any $\tau\in\mathbb{R}$. In order to recover locally unique solutions, which is essential if we hope to prove the existence of solutions using the Newton–Kantorovich Theorem 1.2.2, we simply add a phase condition to the zero-finding problem.

Let us now discuss the function space in which we are going to conduct our Newton–Kantorovich argument. Although an arbitrary solution of the Navier–Stokes initial value problem may or may not be very regular, we expect periodic solutions, when they exist, to have better smoothness properties (this is more generally the case for solutions lying on the global attractor [252]). We note that we do not need to prove a priori that the solutions we are looking for have any regularity: once we select a function space and successfully apply the Newton–Kantorovich strategy, we will have proven a posteriori that the solution we obtain has the regularity encoded in that function space. In this work, we use a norm based on the weighted ℓ^1_ν norm introduced in Chapter 0, and already used in Section 1.3.1, meaning that the periodic solutions of the Navier–Stokes equation we obtain are proven to be analytic in space and time. More precisely, we take

$$\|(\omega,\Omega)\| := |\Omega| + \sum_{j=1}^{3}\sum_{n\in\mathbb{Z}^4} \left|\omega_n^{(j)}\right| \nu^{|n|_1},$$

where $\nu > 1$, $|n|_1 = \sum_{k=1}^4 |n_k|$, and $\omega^{(j)}$, $j = 1,2,3$, are the three components of ω. In particular, we get error estimates between the approximate solution and the one proven to exist in a norm which control the C^0 norm. Also, even though the Newton–Kantorovich argument is used to obtain a periodic solution of the vorticity equation (2.2), once such a solution is obtained our error estimates give us enough control to recover error estimates on the velocity and the pressure as well. Below is an example of the kind of results that can be obtained with our approach.

Theorem 2.1.1. *Consider the incompressible Navier–Stokes equations (2.1) defined on the three-torus $\mathbb{T}^3$ (with size length $L = 2\pi$), with the so-called Taylor-Green forcing*

$$f = f(x) = \begin{pmatrix} 2\sin x_1 \cos x_2 \\ -2\cos x_1 \sin x_2 \\ 0 \end{pmatrix}. \tag{2.3}$$

Let $\nu = 0.265$ and $(\bar u, \bar p)$ be the approximate solution whose vorticity $\bar\omega$ is represented in Figure 2.1, and whose Fourier coefficients and time frequency $\bar\Omega$ are given in the file `dataorbit2.mat` *available at [Code 1]. Let $r^\Omega = 2.2491\cdot 10^{-6}$, $r^u = 2.2491\cdot 10^{-6}$, and $r^p = 5.6486\cdot 10^{-5}$. There exists a smooth $\frac{2\pi}{\Omega}$-periodic solution (u,p) of (2.1) with $|\Omega - \bar\Omega| \le r^\Omega$ and such that*

$$\sup_{(t,x)\in\mathbb{R}\times\mathbb{T}^3} \|u(t,x) - \bar u(t\theta,x)\| \le r^u \quad \text{and} \quad \sup_{(t,x)\in\mathbb{R}\times\mathbb{T}^3} |p(t,x) - \bar p(t\theta,x)| \le r^p, \qquad \text{with } \theta = \frac{\Omega}{\bar\Omega}.$$

[1] As explained in Chapter 0, we abuse notations and use the same symbol for the function ω and for its sequence of Fourier coefficients.

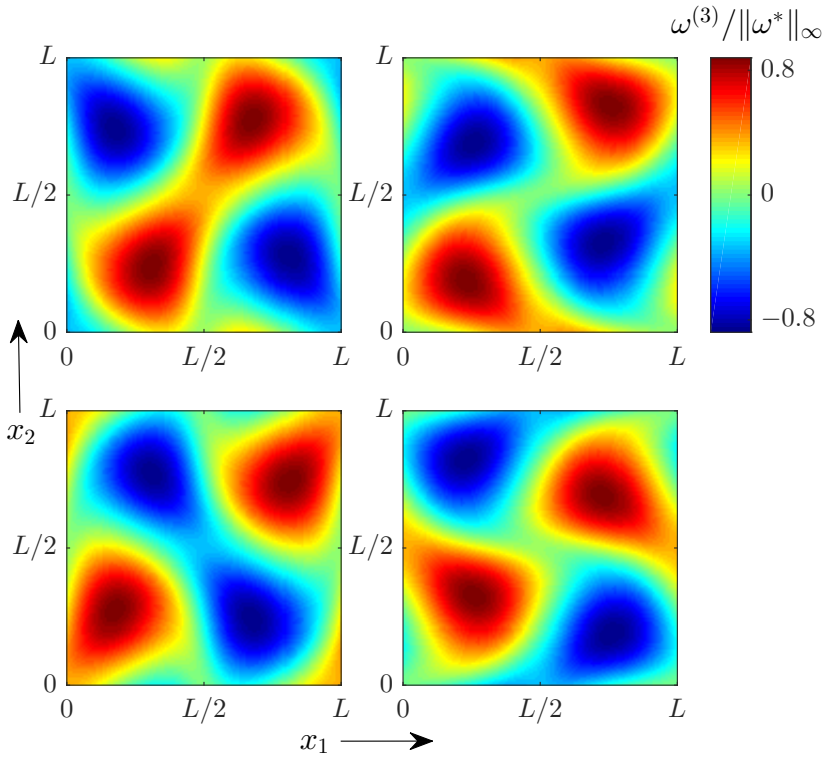

Figure 2.1: The third component of the vorticity $\bar{\omega} = \nabla \times \bar{u}$ of the spontaneous periodic flow obtained in Theorem 2.1.1, normalized by the amplitude of the equilibrium solution. Snapshots are depicted at times 0, $\frac{\pi}{2\Omega}$, $\frac{\pi}{\Omega}$ and $\frac{3\pi}{2\Omega}$.

Remark 2.1.2. *The Navier–Stokes equations on the three-torus with the Taylor–Green [278] forcing term (2.3) provide a favorable setting for closely studying the transition to turbulence in fluids. Indeed, it is convenient for numerical experiments because the geometry allows for Fourier series, but we also have a theoretical starting point, as there exists a steady state given in closed form:*

$$u^*(x) = \frac{1}{2\nu} f(x), \qquad p^*(x) = \frac{1}{4\nu^2} \left(\cos 2x_1 + \cos 2x_2\right).$$

This equilibrium is stable when the viscosity ν is large enough, and our computer-assisted proofs provide a way to rigorously analyze some of the periodic orbits that appear when the viscosity is decreased and the equilibrium looses its stability.

2.1.3 Some notable features of the proof

Because the heat operator $\partial_t - \nu\Delta$, which is the dominant differential operator in the Navier–Stokes equations (also in vorticity form 2.2), acts diagonally on Fourier modes, the construction of the approximate inverse A to be used in the Newton–Kantorovich Theorem 1.2.2 is conceptually straightforward, and very similar to the one presented in the example of Section 1.3.1.2. Moreover, the Banach algebra property of ℓ^1_ν then facilitates the derivation of sharp bounds Y, Z_1 and Z_2 for Theorem 1.2.2. That being said, the interplay between temporal and spatial derivatives, and the fact that the nonlinear terms in the Navier–Stokes equations contain first order derivatives in space (this is apparent in (2.1) but still also true in the vorticity formulation (2.2)) lead to compactness estimates which are much weaker than in the Swift–Hohenberg example of Section 1.3.1.

That is, if we consider the eigenvalues $\lambda_n := \nu(n_1^2 + n_2^2 + n_3^2) + i\bar{\Omega}n_4$ of the heat operator, some threshold $N > 0$, and build the finite part $A^{\leq N}$ of A with all the modes $n \in \mathbb{Z}^4$ such that $|\lambda_n| \leq N$, then the Z_1 estimate we get for the quality of the approximate inverse behaves, at first order, like

$$\left\| I - ADF\left(\bar{\Omega}, \bar{\omega}\right) \right\| \approx \frac{\|\bar{\omega}\|}{\sqrt{\nu N}}.$$

This has practical consequences, because we need such estimate to be less than 1 for the Newton–Kantorovich argument to be successful. Also note that, compared to the Swift–Hohenberg example which was only in one dimension, the number of modes n such that $|\lambda_n| \leq N$ grows much quicker with N in the Navier–Stokes case. In [B3], we were able to fight off the curse of dimensionality by leveraging the many symmetries that are present in the periodic orbits whose existence we were trying to prove, following a strategy laid out in [298]. Since the Navier–Stokes equations themselves, and therefore also our $F = 0$ problem, are equivariant under these symmetries, meaning that $F \circ S = S \circ F$ for each symmetry S, we were able to incorporate the symmetries directly into the zero finding problem, and to work only with a much reduced set of Fourier coefficients. It should also be emphasized that, although the theoretical estimates derived in [B3] are valid in two and three spatial dimensions, we took advantage of the fact that the periodic orbit obtained in Theorem 2.1.1 did not depend on the spatial variable x_3 to further reduce the number of Fourier mode we actually work with.

Another remarkable feature of the proof of Theorem 2.1.1 is related to the incompressiblity condition in (2.1), but the way we handled it is in fact rather general, and can be of interest whenever one tries to use the Newton–Kantorovich approach to study a problem with some sort of invariance. Indeed, once we get the existence of a periodic solution of the Navier–Stokes equation in vorticity form (2.2), we also need to know that this solution is divergence free in order to recover a solution of the incompressible Navier–Stokes equations (2.1). As soon as ω is divergence free, so is $F(\omega)$, so in principle one might also incorporate the divergence free constraint directly into the zero finding problem, but this would be very cumbersome in practice, especially once we go to the symmetry-reduced variables. A much easier alternative is to prove a posteriori that the obtained solution is divergence free, which can be done under the (natural) assumption that the approximate solution itself is divergence free. The argument can be summarized in a rather general way in the following statement, which is proved in a specific case in [B3, Theorem 2.15].

Proposition 2.1.3. *Consider the setting and assumptions of the Newton–Kantorovich Theorem 1.2.2. Assume further there exist closed subspaces $\mathcal{X}_s \subset \mathcal{X}$ and $\mathcal{Y}_s \subset \mathcal{Y}$ such that*

- $\bar{x} \in \mathcal{X}_s$,
- $F(\mathcal{X}_s) \subset \mathcal{Y}_s$,
- $DF(\bar{x}) : \mathcal{X}_s \to \mathcal{Y}_s$ *is a Fredholm operator of index 0.*

Then, the zero x of F proven to exist in Theorem 1.2.2 in fact belongs to $\mathcal{X}_s$.

This result is essentially based on the following observation. Although the proof of Theorem 1.2.2 usually consists in proving that

$$T_{\text{approx}} : x \mapsto x - AF(x),$$

is a contraction on the ball $B_r(\bar{x})$ in $\mathcal{X}$, the assumptions of Theorem 1.2.2 in fact also imply that

$$T : x \mapsto x - DF(\bar{x})^{-1}F(x),$$

is well defined and a contraction on the same ball. The crucial difference is that, under the assumptions of Proposition 2.1.3, $T(\mathcal{X}_s) \subset \mathcal{X}_s$, which immediately yields that the fixed point must in fact be in $\mathcal{X}_s$. In order to instead have $T_{\text{approx}}(\mathcal{X}_s) \subset \mathcal{X}_s$, one would have to make sure that the approximate inverse A exactly maps $\mathcal{Y}_s$ into $\mathcal{X}_s$, which in theory is possible, but can be very daunting in practice, even more so in the context of symmetry reduced variables as in [B3].

2.2 Traveling waves in the DPCM

2.2.1 Motivations

The Diffusion Poisson Coupled Model (DPCM) describes the corrosion processes that arise at the surface of carbon steel canisters which are in contact with a claystone formation. It has been proposed in [19] and is part of a broader study of the long-term safety of the geological repository of nuclear wastes.

The model focuses on the development of a dense oxide layer in the region of contact between the metal and the claystone. From a mathematical point of view, this model is a free boundary problem composed by a system of drift-diffusion equations for the transport of charge carriers (electrons, ferric cations and oxygen vacancies, whose densities are denoted N, P and C) coupled via an electric potential ψ solving a Poisson equation. One of the main mathematical difficulties in studying this model stems from the realistic boundary conditions that are rather involved and highly nonlinear: they describe the electrochemical reactions and the potential drops at the boundaries of the oxide layer with the claystone and with the metal. The system also includes moving boundary equations, and the total length ℓ of the domain, representing the width of the oxide layer, can therefore vary.

Before the work [B10], no rigorous existence results were known on the DPCM, although simplified models were successfully studied in [70, 71]. On the other hand, extensive numerical experiments were conducted [20], leading to the development of the code CALIPSO used at ANDRA (the French national agency for the management of radioactive wastes), and the model was also validated against real-life experiments [19, 20].

The typical long-time behavior that is predicted by numerical simulations is the formation of a kind of traveling wave solution, where both interfaces move at a constant speed c, and the densities of the charge carrier and the electric potential between the interfaces becomes fixed in the frame moving at speed c. The value of c dictates how fast the corrosion layer progresses within the steel canister, and is therefore of paramount importance for evaluating the long term safety of these nuclear wastes repositories. However, one key aspect is that this speed c cannot be predetermined, but is instead one of the outputs of the simulations. This is a typical example of a situation where, provided we trust the model under consideration, we would really like to have as strong as possible guarantees and a posteriori error bounds on the output of the numerical simulations.

2.2.2 Computer-assisted proofs for boundary value problems using Chebyshev series

In [B10], we did not try to study the general time evolution of the DPCM, but instead directly focused on establishing the existence of these traveling wave solutions that had been observed numerically. A similar attempt had previously been made in [69], but only succeeded in treating a simplified version of the DPCM, where electroneutrality in the oxide layer is assumed.

Successfully proving the existence of traveling wave solutions for the full model was accomplished in [B10] thanks to computer-assisted proofs. As a significant byproduct of using such techniques, we were able to provided a tight and guaranteed enclosure of the speed c at which the corrosion layer advances.

In order to directly study traveling wave solutions, we apply the classical strategy of using a traveling wave Ansatz, e.g., for the electric potential ψ, we look for a solution of the form $\psi(t,x) = \psi(x - ct)$, while also prescribing that the boundaries move at constant speed c. This leads to finding profiles for the charge carriers and the electric potential, together with a constant c, that solve a coupled system of boundary value problems, still featuring the complicated boundary conditions mentioned earlier. The full set of equations is somewhat cumbersome to write down, if only because even after rescaling the system it still involves *a lot* of physically relevant parameters, therefore we do not include them in this document, but the adventurous reader can consult [B10].

Compared to the situation described in the previous section of this chapter regarding periodic solutions of the Navier–Stokes equations on the torus, there are three main changes here. First, the problem for traveling wave profiles in the DPCM is one dimensional only, so the computational cost associated to the proof is much lower, even without any kind of symmetry. Second, because of the intricate boundary conditions in the DPCM, we can no longer use Fourier series to accurately represent the solutions. However, one can use Chebyshev series instead, i.e. series expansions of the form

$$\psi(x) = \sum_{n=0}^{\infty} \psi_n T_n(x), \qquad x \in [-1,1],$$

where T_n are the Cheybyshev polynomials of the first kind, after having rescaled the problem to the interval $[-1,1]$. Thanks to the identity $T_n(\cos\theta) = \cos(n\theta)$, Chebyshev expansions enjoy very similar properties to Fourier series. In particular, finite Chebyshev series provide excellent approximations to smooth functions defined on a bounded interval [280], and they allow for efficient computer-assisted proofs [204, 40], especially in weighted ℓ^1 spaces as in the Fourier case [296]. Third, because the components of the system represent very disparate quantities (density of electrons, of ferric cations, of oxygen vacancies, and electric potential), there are vastly different scales in the problem. In particular, when choosing a norm on the full system, simply taking the maximum or the sum of the norms of each component proves highly inefficient: even if the problem is only one-dimensional, one has to keep so many modes in the finite part of A for the assumptions of the Newton–Kantorovich Theorem 1.2.2 to hold that the proof becomes impractical. In [B10], we overcome this issue by considering, for the norm on the full system, a weighted sum of the norms of each component, and by optimizing for the weights. A similar approach, but which provides a better understanding of the underlying phenomena and is easier to use in practice, is presented in Section 4.2.4.

Of course, the precise equations of the DPCM are rather different from the Swift–Hohenberg or the Navier–Stokes ones, which leads to technical variations at the level of the estimates, but overall the Newton–Kantorovich strategy based on Theorem 1.2.2 can then be applied in exactly the same way, and leads to the following result.

Theorem 2.2.1. *Fix all the parameters of the DPCM as in [B10, Appendix A]. There exist analytic profiles $\psi, C, N, P : [-1,1] \to \mathbb{R}$ and a speed $c > 0$ and length $\ell > 0$ such that (ψ, C, N, P, c, ℓ) is a traveling wave solution of the DPCM. Besides, this solution satisfies*

$$\sup_{[-1,1]} |\psi - \bar{\psi}| \leq 1.3 \times 10^{-9},$$

$$\sup_{[-1,1]} |C - \bar{C}| \leq 1.1 \times 10^{-10}, \quad \sup_{[-1,1]} |N - \bar{N}| \leq 4.9 \times 10^{-10}, \quad \sup_{[-1,1]} |P - \bar{P}| \leq 1.4 \times 10^{-10},$$

where $\bar{\psi}$, $\bar{C}$, $\bar{N}$ and $\bar{P}$ are the approximate solutions represented in Figure 2.2, whose precise description in terms of Chebyshev coefficients can be found at [Code 3], and c and ℓ fulfill

$$c \in [33.4947256\mathbf{0}, 33.4947256\mathbf{4}], \quad \ell \in [1.703352535\mathbf{2}, 1.703352535\mathbf{6}].$$

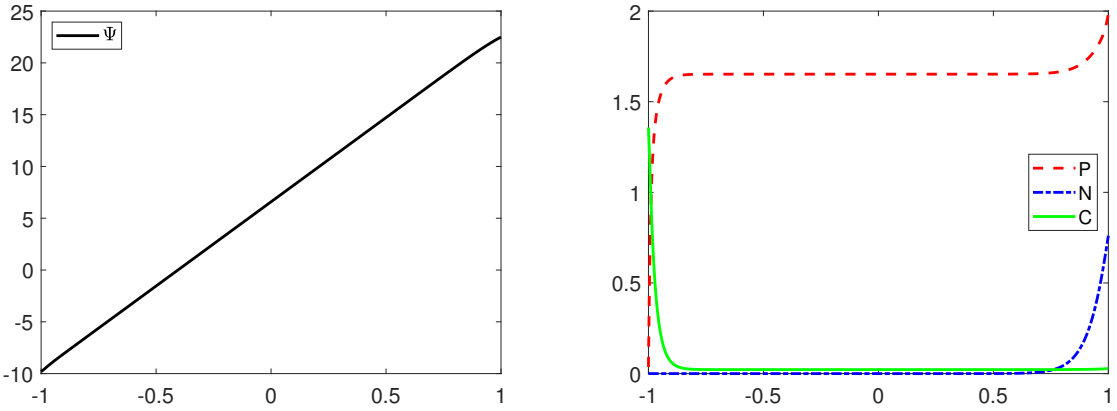

Figure 2.2: An approximate traveling wave profile $(\bar{\psi}, \bar{C}, \bar{N}, \bar{P})$ of the DPCM.

Remark 2.2.2. *As previously discussed, not only is this the only available* existence *result for traveling wave solutions in the DPCM, but it also provides a guaranteed enclosure of the speed c at which the corrosion layer deteriorates the steel canisters. The value of c provided in Theorem 2.2.1 is dimensionless, but the appropriate rescaling to physical units can be found in [B10].*

2.3 Perspectives

- **Improving the DPCM.** One of the appealing features of computer-assisted proofs is that they can provide quantitative results like the enclosure of the speed c in Theorem 2.2.1, that are mathematically guaranteed. Indeed, for the practical application of the DPCM, namely ensuring the safe long term storage of nuclear wastes, having a very high level of confidence in the predictions obtained using numerical simulations is crucial. However, one can only trust these results as much as one trusts the model that was solved using computer-assisted proofs. For the DPCM, this is a legitimate concern. Indeed, even though some aspects of the DPCM were tested against real-life experiments [19, 20], the model was mostly derived empirically, and recently observed to not be fully thermodynamically consistent. Attempts (to which I am not part of) are currently being made to slightly modify the model in order to make it consistent with thermodynamics and its second principle, with partial results already obtained in [61]. Once a new and more trustworthy version of the full DPCM is available, one should again precisely study its traveling wave solutions, possibly using computer-assisted proofs. One of the advantages of computer-assisted proofs are their inherent robustness: even if the new version of the DPCM has slightly different nonlinearities or boundary conditions, this should only amount to a couple of small changes in the Z_1 and Z_2 estimates, and the overall strategy will not be affected.

- **Stability of traveling wave solutions in the DPCM.** The proof of existence of a traveling wave solution in the DPCM is only the first step in order to understand the global dynamics. This solution seems particularly relevant because numerical simulations suggest it is the global attractor of the system, and therefore accurately describes the long term evolution of these oxide layers. However, from a mathematical point of view, proving that the obtained traveling wave solution is stable is a challenging question, even if we first only consider linear stability. After using a traveling wave Ansatz, the equations to solve for finding the solution described in Theorem 2.2.1 are essentially steady states equations of a coupled parabolic-elliptic system on a bounded domain (whose length is also an unknown). Let us ignore the elliptic part for the sake of simplifying the discussion,

and simply think about a general parabolic problem $\partial_t u = F(u)$ on a bounded domain. Suppose we are able to directly study the steady state problem $F(u) = 0$ using a Newton–Kantorovich argument with an approximate inverse like Theorem 1.2.2, and to obtain the existence of a steady state $u^\star$. Then, as a byproduct of the proof we get a lot of control on $DF(u^\star)$ (or on its inverse), which can often be leveraged to get precise information on the spectrum of $DF(u^\star)$, and therefore to conclude as to the linear stability or instability of the steady state $u^\star$. However, in the case of Theorem 2.2.1 we did not directly consider the problem $F(u) = 0$, but instead an equivalent problem akin to $\Delta^{-1}F(u) = 0$, basically because differentiation do not have a nice structure in the Chebyshev basis, whereas anti-differentiation does. This means we only get information on the spectrum of $\Delta^{-1}DF(u^\star)$, which does not easily relate to the spectrum of $DF(u^\star)$. Overcoming these difficulties is the subject of a current joint work with Antoine Zurek and Matthieu Cadiot.

- **Truly three-dimensional periodic orbits of the Navier–Stokes equations.** Although all of the theoretical estimates derived in [B3] are valid in two and three spatial dimensions, the periodic orbit obtained in Theorem 2.1.1 is essentially two-dimensional, as it does not depend on the third variable x_3. We did find (many) fully three-dimensional periodic orbits numerically, but validating them proved very challenging in terms of computational costs (especially in terms of memory requirement). It would be of great interest to improve the validation procedure, both the actual implementation and the mathematical construction, so as to be able to validate three dimensional periodic orbits. One of the potential avenues of improvement lies in the way we construct the finite part of the approximate inverse A. Currently, this is done by numerically inverting a finite dimensional projection of $DF(\bar{u})$, without trying to take advantage of any of the mathematical structures $DF(\bar{u})$ can have.

- **Towards chaos in the Navier–Stokes equations.** One of the long-term goals related to this project is to rigorously prove that the Navier–Stokes equations are chaotic. Indeed, many simulations and real-life experiments showcase that fluids can behave in complex and sometimes even unpredictable ways, with very sensitive dependence on initial conditions. General mechanisms trying to explain the apparition of turbulent behavior in fluids have been proposed [257], and numerical simulations suggest that a homoclinic tangle could be at the origin of some turbulent flows [301]. This opens a potential avenue towards rigorously proving the existence of chaotic dynamics for the Navier- Stokes equations, by proving the existence of a transverse homoclinic orbit to a hyperbolic periodic orbit. The work we conducted in [B3] constitutes the first step of this program, in which I am only one of the many contributors, and another step (namely rigorous time integration required to study connecting orbits) will be discussed in Chapter 4.

Chapter 3

Noncanonical structures: beyond the "easy" framework of bounded domain, diagonal linear operator and polynomial nonlinearities

In the Swift–Hohenberg example of Section 1.3.1, there are three features of the problem that make the computer-assisted proof rather straightforward:

- The problem is posed on a bounded domain,
- There is an explicit basis in which the dominant differential operator is diagonal (or at least asymptotically diagonally dominant),
- The nonlinearity is polynomial.

The two examples discussed in Chapter 2 are more involved, and therefore each first requires problem-specific work in order to devise the right framework in which to conduct a computer-assisted proof. However, once this is done, the procedure for applying the Newton–Kantorovich argument to those problems can by now be described as being, perhaps not straightforward, but at least routine, precisely because these problems also exhibit the three aforementioned features.

In the last twenty years or so, there has been a lot of work devoted to studying and reformulating very different problems so that they in the end have these three features, and can then be attacked with computer-assisted proofs. When some of these features are lacking, using computer-assisted proofs becomes more challenging. In this chapter, we present our contributions to broadening the framework of applications of computer-assisted proofs, and discuss new techniques allowing to specifically deal with: some non diagonal dominant operators in Section 3.1, some non-polynomial nonlinearities in Section 3.2, and some PDEs on unbounded domains in Section 3.3.

3.1 Nonlinear diffusion

3.1.1 Motivations

In this section, we tackle a class of PDEs for which the dominant linear operator is generically not diagonal nor asymptotically diagonally dominant in Fourier space. These equations belong to the class of *quasilinear* PDEs, whereas most of the computer-assisted proof literature only deals with *semilinear* ones. Computer-assisted proofs for semilinear elliptic PDEs were introduced in the pioneering works [236, 248], and where then further developed and popularized in many

papers, including [243, 321, 331, 5, 93, 274, 297, 307]. For a broader description of computer-assisted proofs for PDEs, we refer to the survey [143] and the book [238], and to the references therein.

In the particular case of computer-assisted proofs using sequences spaces, it should be emphasized that previous approaches were almost always relying on the fact that the dominant linear operator is diagonal. Before the publication of the works described in this section, the only exception we are aware of is the work [B15] from my PhD thesis, in which the specific case of dominant tridiagonal operators was studied (still under some weak diagonal dominance assumption).

However, there are many simple, well-known, and extensively studied equations, for which a diagonal dominance assumption clearly does not hold. If we look for instance at elliptic operators on the torus, where the Laplacian is the canonical example of a diagonal operator in Fourier space, a simple operator like $\mathcal{L} : u \mapsto \Delta(a(x)u)$, where a is some smooth positive function on the torus, is not necessarily diagonally dominant in Fourier space. Yet, such nonhomogenous elliptic operators directly appear in many models, or as linearizations of problems with nonlinear diffusion, i.e., for problems with terms of the form $\Delta(\Phi(u))$ for some nonlinear map Φ. A famous example is the porous medium equation

$$\partial_t u = \Delta(u^m).$$

Nonlinear diffusion terms are maybe even more prevalent for systems. In many situations, including (but not limited to) biological systems, coupling at the level of the diffusion terms are critical modeling assumptions, and often refer to as *cross-diffusion*. Here are two specific examples.

The SKT system. This system of PDEs was introduced in the seminal work [268], and is used to model the evolution of two competing species u_1 and u_2. It writes

$$\begin{cases} \partial_t u_1 = \Delta\left(\left(d_1 + d_{11}u_1 + d_{12}u_2\right)u_1\right) + \left(r_1 - a_1u_1 - b_1u_2\right)u_1 = 0 & \text{in } \Omega, \\ \partial_t u_2 = \Delta\left(\left(d_2 + d_{21}u_1 + d_{22}u_2\right)u_2\right) + \left(r_2 - b_2u_1 - a_2u_2\right)u_2 = 0 & \text{in } \Omega, \\ \partial_n\left(\left(d_1 + d_{11}u_1 + d_{12}u_2\right)u_1\right) = \partial_n\left(\left(d_2 + d_{21}u_1 + d_{22}u_2\right)u_2\right) = 0 & \text{on } \partial\Omega. \end{cases} \tag{3.1}$$

The reactions terms are standard Lotka-Volterra terms with signs indicating intra-specific and inter-specific competition. The key feature of this model is the presence of nonlinear diffusion terms: the diffusion rate of each species depends on the local density of both species. These nonlinear diffusion terms can give rise to a repulsive effect which leads to *spatial segregation*: the two species co-exist but mostly concentrate in different regions of the domain Ω. Mathematically, this corresponds to the existence of non-homogeneous steady states of (3.1) exhibiting this type of patterns. It should be noted that the nonlinear cross-diffusion terms are instrumental in generating these patterns: if $d_{11} = d_{12} = d_{21} = d_{22} = 0$, the system cannot have stable non-homogeneous steady states, at least on a convex domain [187]. In other words, without cross-diffusion there cannot be any kind of Turing instability which could produce nontrivial steady states.

When the cross-diffusion terms are included, the existence and stability of nontrivial steady states has been studied extensively, through a wide variety of techniques such as bifurcation theory, singular perturbation theory or fixed point index theory, see e.g. [224, 225, 213, 260], which provide a qualitative understanding on the conditions required on the many parameters of (3.1) for non-homogeneous steady states to exist. Some asymptotic parameter regimes have also been scrutinized, especially when one or both of the cross-diffusion coefficients d_{12} and d_{21} become very large, and in such cases additional information about the shape of the obtained solutions is also available, see e.g. [241, 214]. However, numerical studies like [165, 169] show that the steady states of (3.1) can be very diverse, already in the one dimensional case, and

that many of them can co-exists for a given set of parameter values. Proving the existence, and characterizing the shape, of all these different steady states seems very hard by purely analytic means, but computer-assisted techniques provide a valuable tool to attack such questions. For a more in-depth discussion about the literature around patterns in (3.1), we refer to the introduction of [B20] and to the references therein.

A *local sensing* version of the Keller-Segel model. Chemotaxis describes the movement of small organisms, typically bacteria or cells, in response to chemical stimulus. Keller-Segel systems [183, 184] are among the most studied equations in the mathematical literature which model such phenomena, in the particular case where the attracting chemical is produced by the organisms themselves. There are many versions of the Keller-Segel system, but we focus on a specific one here, which writes

$$\begin{cases} \partial_t u_1 = \Delta\left(\gamma(u_2)u_1\right) + \sigma u_1(1-u_1) & \text{in } \Omega, \\ \partial_t u_2 = d\Delta u_2 + u_1 - u_2 & \text{in } \Omega, \\ \partial_n\left(\gamma(u_2)u_1\right) = \partial_n u_2 = 0 & \text{on } \partial\Omega, \end{cases} \tag{3.2}$$

with a decreasing function γ, which essentially models that u_1 diffuses less when there is a lot of u_2 around. This specific system was already included in the orginial work by Keller and Segel [184] (up to the logistic reaction term), and was also reintroduced later in [125], as an attempt to explain the stripe patterns observed in [207]. The main distinctive feature of (3.2) is that it models *local sensing*, i.e., the fact that bacteria u_1 are sensitive to the actual concentration of u_2, whereas most variants of the Keller-Segel model assume *gradient sensing*, i.e., that bacteria instead measure gradients of u_2. For more details on these modeling interpretations, we refer to [96] and the references therein.

System (3.2) also exhibits a wide variety of nontrivial steady states, and the situation is somewhat similar to that of the SKT system, in that pen-and paper results only cover part of what can be observed numerically.

Before focusing more specifically on computer-assisted proofs for steady-states of (3.1) and (3.2), we mention that the global well-posedness of these systems is also extensively studied. For the SKT system, the existence of local solutions mostly relies on the general work [1] on quasilinear systems, although a simpler approach has been proposed recently [136]. Proving that these solutions are in fact global is very challenging, and was made possible thanks to an entropy structure (see [75, 97] as well as the book [175] for a broader overview), which allowed to establish the existence of global weak solutions. Regarding the existence of global strong solutions, see, e.g., [163, 148] and the references therein.

For the Keller-Segel system (3.2) the situation is slightly different, and in particular blowups might be expected if $\sigma = 0$, because of the similarities with the minimal Keller-Segel model for which blowups are known to occur and are well understood [160]. It turns out that the situation is rather delicate and depends on the motility function γ. For $\gamma(v) = e^{-v}$, it has been proven that blowup can occur if the initial mass is large enough [172], although only in infinite time [46, 126], whereas solutions are globally bounded if γ decays only algebraically and is of the form $\gamma(v) = \frac{a}{v^k}$, at least if a is small enough [324]. When $\sigma > 0$, global existence results can be found in [171, 210, 305].

3.1.2 A nondiagonal approximate inverse

The main challenge in using the Newton–Kantorovich Theorem 1.2.2 for studying steady states of nonlinear diffusion problems lies in the construction of a suitable approximate inverse. Consider first a scalar steady state problem

$$\Delta\left(\Phi(u)\right) + R(u) = 0 \qquad \text{in } \Omega, \tag{3.3}$$

together with some boundary conditions, where Φ and R are smooth maps from an open set $U \subset \mathbb{R}$ into $\mathbb{R}$. The argument to follow works exactly the same for systems (i.e., when $u = (u_1, \dots, u_d)$ and Φ, R are smooth maps from an open set $U \subset \mathbb{R}^d$ into $\mathbb{R}^d$), but we first restrict ourselves to the scalar case, in order to make the notation lighter and to simplify the exposition. Assume one can look for solutions as Fourier series, for instance because Ω is a torus, or a (hyper-) rectangle with suitable boundary conditions and symmetries in the equation allowing for a cosine or sine expansion. Let $F(u) := \Delta(\Phi(u)) + R(u)$ be the zero-finding problem, defined on ℓ^1_ν, and assume that $\bar{u}$ is an approximate solution, non-degenerate in the sense that $D\Phi(\bar{u}(x))$ is invertible for all $x \in \Omega$ (in the scalar case, this simply means that $\Phi'(\bar{u}(x)) \neq 0$ for all $x \in \Omega$).

The Fréchet derivative of F at $\bar{u}$ writes

$$DF(\bar{u}) : u \mapsto \Delta\left(\Phi'(\bar{u}) * u\right) + R'(\bar{u}) * u = \Delta\left(\mathcal{M}(\Phi'(\bar{u}))u\right) + \mathcal{M}(R'(\bar{u}))u,$$

where $\mathcal{M}(\Phi'(\bar{u}))$ denotes the multiplication operator introduced in Chapter 0. The main observation from [B7], which in hindsight is almost embarrassingly simple, is that, although the dominant part of the linearized operator $DF(\bar{u})$, namely $\Delta(\mathcal{M}(\Phi'(\bar{u}))\cdot)$, is not diagonally dominant in Fourier space, its inverse is still in some sense very "simple". Indeed, the operator $\mathcal{M}(\Phi'(\bar{u}))^{-1}\Delta^{-1}\cdot$ is just the composition of the inverse Laplacian with a multiplication operator, and this structure can be used to build a suitable approximate inverse A for this problem.

First, since we only look for an approximate inverse, we do not need to invert $\mathcal{M}(\Phi'(\bar{u}))$ exactly. Let us therefore consider a finite Fourier series $\bar{\omega}$ such that $\mathcal{M}(\bar{\omega}) \approx \mathcal{M}(\Phi'(\bar{u}))^{-1}$, i.e., $\bar{\omega}$ should be an approximate inverse of $\Phi'(\bar{u})$ in ℓ^1_ν. Next, we consider an $N \times N$ matrix $A^{\leq N}$, obtained as a numerically computed approximation of $\Pi^{\leq N}\left(DF(\bar{u})^{-1}\right)\Pi^{\leq N}$. Identifying $A^{\leq N}$ with an operator on $\Pi^{\leq N}\ell^1_\nu$, we define the crucial operator A as follows:

$$A = A^{\leq N} + \left(\mathcal{M}(\bar{\omega})\Delta^{-1} - \Pi^{\leq N}\left(\mathcal{M}(\bar{\omega})\Delta^{-1}\right)\Pi^{\leq N}\right). \tag{3.4}$$

In order to better understand this operator, one might think of it as an *infinite matrix*, which writes

$$\left(\begin{array}{ccccc|cccc}
 & & & & & 0 & 0 & 0 & \dots \\
 & & & & & \frac{-\bar{\omega}_N}{((N+1)\pi)^2} & 0 & 0 & \\
 & & A^{\leq N} & & & \vdots & \frac{-\bar{\omega}_N}{((N+2)\pi)^2} & 0 & \ddots \\
 & & & & & \frac{-\bar{\omega}_2}{((N+1)\pi)^2} & \vdots & \frac{-\bar{\omega}_N}{((N+3)\pi)^2} & \ddots \\
 & & & & & \frac{-\bar{\omega}_1}{((N+1)\pi)^2} & \frac{-\bar{\omega}_2}{((N+2)\pi)^2} & \vdots & \ddots \\
\hline
0 & \frac{-\bar{\omega}_N}{\pi^2} & \dots & \frac{-\bar{\omega}_2}{((N-1)\pi)^2} & \frac{-\bar{\omega}_1}{(N\pi)^2} & \frac{-\bar{\omega}_0}{((N+1)\pi)^2} & \frac{-\bar{\omega}_1}{((N+2)\pi)^2} & \frac{-\bar{\omega}_2}{((N+3)\pi)^2} & \\
0 & 0 & \frac{-\bar{\omega}_N}{(2\pi)^2} & \dots & \frac{-\bar{\omega}_2}{(N\pi)^2} & \frac{-\bar{\omega}_1}{((N+1)\pi)^2} & \frac{-\bar{\omega}_0}{((N+2)\pi)^2} & \frac{-\bar{\omega}_1}{((N+3)\pi)^2} & \ddots \\
0 & 0 & 0 & \frac{-\bar{\omega}_N}{(3\pi)^2} & \dots & \frac{-\bar{\omega}_2}{((N+1)\pi)^2} & \frac{-\bar{\omega}_1}{((N+2)\pi)^2} & \frac{-\bar{\omega}_0}{((N+3)\pi)^2} & \ddots \\
\vdots & & \ddots & \ddots & \ddots & & \ddots & \ddots & \ddots
\end{array}\right),$$

or in a more compact form,

$$A = \begin{pmatrix} A^{\leq N} & \\ & \mathcal{M}(\bar{\omega})\Delta^{-1} \end{pmatrix}.$$

In particular, even if the *tail* of A is no longer diagonal as in the examples of Chapter 1 or Chapter 2, the multiplication operator $\mathcal{M}(\bar{\omega})$ can still be represented with finite data, hence one should be able to estimate a posteriori the quality of this approximate inverse in a very similar manner to what was presented in Section 1.3.1. Indeed, denoting again $B = I - ADF(\bar{u})$, we have the following estimate (compare with the Z_1 estimate obtained in Section 1.3.1.3).

Lemma 3.1.1. *Assume for simplicity that Φ and R are quadratic polynomials, that the domain Ω is equal to $(0, \pi)$, and that the nonlinear diffusion equation (3.3) is complemented with homogeneous Neumann boundary conditions. Then,*

$$\sup_{\substack{u \in \Pi^{>2N} \ell^1_\nu \\ u \neq 0}} \frac{\|Bu\|_{\ell^1_\nu}}{\|u\|_{\ell^1_\nu}} \leq \left\|1 - \bar{\omega} * \Phi'(\bar{u})\right\|_{\ell^1_\nu} + \frac{1}{(N+1)^2} \left\|\bar{\omega} * R'(\bar{u})\right\|_{\ell^1_\nu}.$$

The second term in the right hand side is comparable to the one obtained in Section 1.3.1.3 for the Swift–Hohenberg equation (with an additional multiplication by $\bar{\omega}$ since this has been added to the tail of A), whereas the first one should be very small, because we chose $\bar{\omega}$ so that $\bar{\omega} * \Phi'(\bar{u}) \approx 1$. For the finite part of the Z_1 estimate, as well as for the Y and Z_2 estimate, the unusual structure of A makes essentially no difference: we only have to consider an additional multiplication by $\bar{\omega}$, which is harmless both numerically and theoretically.

For systems, the above construction of A generalizes in a completely straightforward way. Indeed, the operator $D\Phi(\bar{u})$ can now be seen as a $d \times d$ matrix of multiplication operators, whose inverse can also be represented by a $d \times d$ matrix of multiplication operators. This can be rigorously justified a priori by instead interpreting $D\Phi(\bar{u})$ as a $d \times d$ matrix with entries in the commutative Banach algebra ℓ^1_ν (this viewpoint will be elaborated upon in Chapter 5), but, as usual with such computer-assisted proofs, we in fact do not *need* any a priori justification, as we will check a posteriori that our choice of approximate inverse is suitable.

Consequently, we are in principle able to use Theorem 1.2.2 to rigorously validate any non-trivial steady state of the SKT system (3.1) that are found numerically, and similarly for the Keller-Segel model (3.2), at least on hyperrectangular domains, and provided we are not exactly at a bifurcation point.

3.1.3 New steady states for cross-diffusion systems

In this section, we illustrate our ability to rigorously validate non-trivial steady states of the SKT system (3.1) and the Keller-Segel system (3.2).

We emphasize that most of the non-trivial equilibria of the SKT system presented here, and validated in [B7], were in fact first found numerically in [B20]. In that work, a relatively straightforward but exhaustive pen-and-paper linearized analysis allowed to better understand how the many parameters of the SKT model collectively influence the appearance or disappearance of patterns close to homogeneous steady states. Numerical explorations using the continuation software pde2path [284] then shed some more light on global behavior far away from bifurcations, and unveiled new parameter regimes in which non-trivial steady states seemed to exist, which was then validated in [B7] using computer-assisted proofs.

Theorem 3.1.2. *Take $\Omega = (0,1)$ and fix the parameters in the SKT system (3.1) as*

$$d_1 = 0.05,\ d_2 = 0.05,\ d_{12} = 3,\ d_{21} = 0,\ d_{11} = 0,\ d_{22} = 0,$$

$$r_1 = 15,\ r_2 = 5,\ a_1 = 1,\ a_2 = 1,\ b_1 = 0.5,\ b_2 = 3.$$

For each of the couples (u_1, u_2) represented in Figure 3.1, and whose precise description in terms of Fourier coefficients can be found at [Code 5], there exists a smooth steady state of the SKT system (3.1), at a distance of at most 9×10^{-11} in $\mathcal{C}^0$ norm.

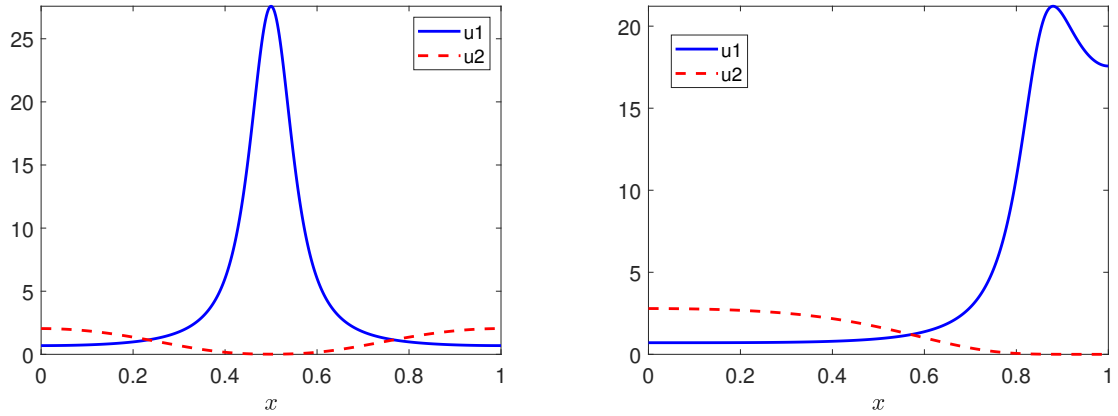

Figure 3.1: The two approximate steady states of the SKT system (3.1), which have been validated in Theorem 3.1.2.

In order to understand the interest of Theorem 3.1.2, it is helpful to briefly consider the homogeneous case of the SKT system, i.e., the system of ODEs obtained by keeping only the reaction terms in (3.1), for which one can easily identify three different parameter regimes with different dynamics, see, e.g., [213].

- **Case 1 (weak competition):**

$$\frac{b_1}{a_2} < \frac{r_1}{r_2} < \frac{a_1}{b_2}.$$

Here, any solution $(u_1(t), u_2(t))$ with positive initial data converges to the co-existence steady state given by

$$\left(\frac{r_1 a_2 - r_2 b_1}{a_2 a_1 - b_2 b_1}, \frac{r_2 a_1 - r_1 b_2}{a_2 a_1 - b_2 b_1} \right). \tag{3.5}$$

- **Case 2 (strong competition):**

$$\frac{a_1}{b_2} < \frac{r_1}{r_2} < \frac{b_1}{a_2}.$$

Here, the above co-existence steady state (3.5) is still positive, but it is unstable, and generically a solution with positive initial data converges to one of the two extinction states

$$\left(\frac{r_1}{a_1}, 0 \right) \qquad \text{or} \qquad \left(0, \frac{r_2}{a_2} \right), \tag{3.6}$$

depending on the initial condition.

- **Case 3:** everything else (except the case $b_1/a_2 = r_1/r_2 = a_1/b_2$ which is degenerate). Here, any solution with positive initial data also converges to one of the two extinction states (3.6), but all solutions converge to the same one, and the one being selected depends on the parameter values, not on the initial data.

The aim of introducing a spatial dimension to the model, and more precisely nonlinear diffusion as in (3.1), is to obtain more interesting and realistic solutions, and in particular non-homogeneous positive steady states. However, it is striking that in the literature on the SKT system, the existence of non-homogeneous steady states is usually studied in cases 1 and 2 only. This might be related to the fact that the analysis in case 3 can be more difficult, because there is no positive trivial steady state that can be used as a kind of starting point: the co-existence steady states (3.5) still exists (except if $a_1a_2 = b_1b_2$), but it is no longer positive in case 3.

However, recent numerical experiments suggested that positive non-homogeneous steady states do also exist in case 3 [B20]. In Theorem 3.1.2, the selected parameter values correspond to this case, and we have therefore rigorously established the existence of the new steady states that were found numerically in [B20].

Below is another example of steady states of the SKT system that can be obtained with computer-assisted proofs.

Theorem 3.1.3. *Take $\Omega = (0,1)$ and fix the parameters in the SKT system (3.1) as*

$$d_1 = -0.007,\ d_2 = -0.007,\ d_{12} = 3,\ d_{21} = 0.002,\ d_{11} = 0.05,\ d_{22} = 0.05,$$

$$r_1 = 5,\ r_2 = 2,\ a_1 = 3,\ a_2 = 3,\ b_1 = 1,\ b_2 = 1.$$

For each of the couples (u_1, u_2) represented in Figure 3.2, and whose precise description in terms of Fourier coefficients can be found at [Code 5], there exists a smooth steady state of the SKT system (3.1), at a distance of at most 9×10^{-9} in $\mathcal{C}^0$ norm.

The interest of Theorem 3.1.3 is twofold. First, it showcases that our approach is not restricted to the so-called *triangular* SKT system, for which $d_{21} = d_{11} = d_{22} = 0$. This specific case has received a lot of attention in the literature, because the triangular structure means the equation on u_2 is only coupled via the reaction terms, which simplifies the analysis of the system. In particular, earlier computer-assisted proofs for this specific case were already obtained in [B9]. Second, note that the linear diffusion coefficients d_1 and d_2 are negative in Theorem 3.1.3. Therefore, the SKT system (3.1) is non longer well-posed, even locally in time, for arbitrary positive initial data. Thanks to the nonlinear diffusion terms, the diffusion matrix $D\Phi(u)$ could still be non-degenerate, but this depends on the values taken by (u_1, u_2) and is therefore difficult to control a priori. However, is long as the diffusion matrix $D\Phi(u)$ happens to be non-degenerate at a steady state u, our computer-assisted proofs can in principle work, and show a posteriori that the diffusion matrix was in fact not degenerate.

We now turn out attention to some non-trivial steady states of the Keller-Segel system (3.2).

Theorem 3.1.4. *Take $\Omega = (0, 3\pi)$, $\gamma(x) = \frac{1}{1+x^9}$, and fix the parameters in the Keller-Segel system (3.2) as $\sigma = 0.053$, $d = 1$.*

There exists a smooth steady state of the Keller-Segel system (3.2), at a distance of at most 3×10^{-8} in $\mathcal{C}^0$ norm of the approximate steady state represented in Figure 3.3, whose precise description in terms of Fourier coefficients can be found at [Code 12].

Theorem 3.1.5. *Take $\Omega = (0, 9\pi)$, $\gamma(x) = \frac{1}{1+e^{9(x-1)}}$, and fix the parameters in the Keller-Segel system (3.2) as $\sigma = 0.6$, $d = 1$.*

There exists a smooth steady state of the Keller-Segel system (3.2), at a distance of at most 2×10^{-12} in $\mathcal{C}^0$ norm of the approximate steady state represented in Figure 3.4, whose precise description in terms of Fourier coefficients can be found at [Code 12].

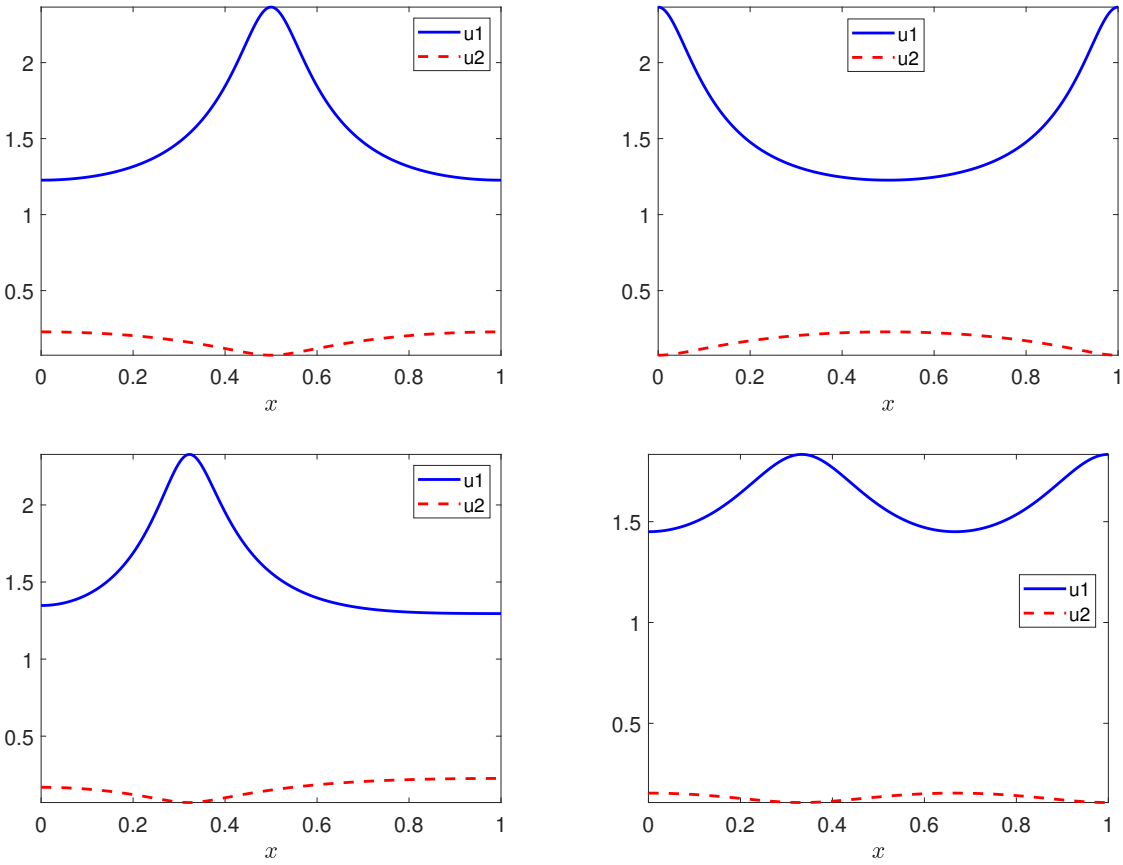

Figure 3.2: The four approximate steady states of the SKT system (3.1) which have been validated in Theorem 3.1.3.

Beyond the fact that quantitative theoretical results on the steady states of (3.2) are sparse, one interesting feature of Theorem 3.1.4 and Theorem 3.1.5 is the fact that the function γ is non polynomial, which will be discussed further in Section 3.2.

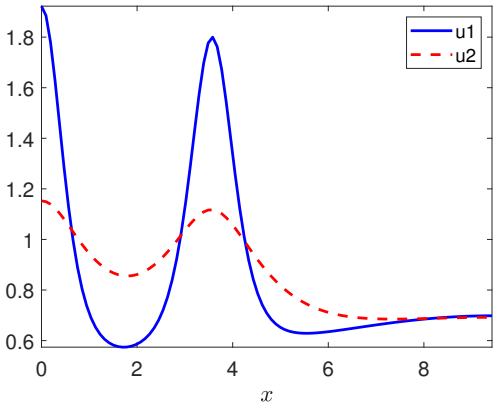

Figure 3.3: The approximate steady state of the Keller-Segel system (3.2) which has been validated in Theorem 3.1.4.

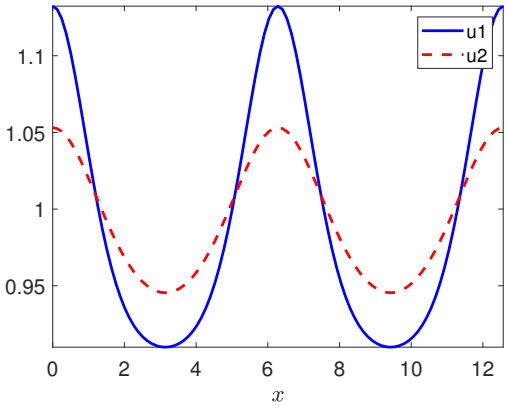

Figure 3.4: The approximate steady state of the Keller-Segel system (3.2) which has been validated in Theorem 3.1.5.

3.2 Non-polynomial nonlinearities

In this section, we discuss how to deal with non-polynomial nonlinearities, in the context of computer-assisted proofs using ℓ^1_ν spaces. To make things concrete, we often consider a finite Fourier series $\bar{u}$ and nonlinear functions applied to it, but the whole discussion also applies if $\bar{u}$ is a finite Chebyshev or Taylor series.

3.2.1 Polynomial embedding

As highlighted in Section 1.3.1, having polynomial nonlinearities makes some of the analysis required for computer-assisted proofs using sequence spaces, and in particular ℓ^1_ν spaces, rather direct, and allows for sharp estimates. When facing a non-polynomial nonlinearity, say g, two additional difficulties emerge:

1. Even if $\bar{u}$ is a finite Fourier series, determining the Fourier expansion of $g(\bar{u})$ is no longer straightforward, and the expansion is now infinite,
2. On has to make sense of $g(u)$, and explicitly control $\|g(u)\|_{\ell^1_\nu}$, for all u in a neighborhood of $\bar{u}$ in the space ℓ^1_ν.

In order to avoid these difficulties, many works then resort to the so-called *polynomial embedding* strategy related to automatic differentiation, which consists in reformulating the problem into a system with more equations and unknowns, but having only polynomial nonlinearities [203, 158]. Although we advocate for different strategies in this manuscript, we still showcase on a simple example below how polynomial embedding works, as this idea can prove useful in many contexts.

Example 3.2.1. *Consider the ODE*

$$\begin{cases} u' = \dfrac{u}{1+u^2} \\ u(0) = u_0, \end{cases} \tag{3.7}$$

and assume that, for whatever reason, we would only like to deal with polynomial vector fields. One can then for instance introduce the extra variable $v = \frac{1}{1+u^2}$*, and look for a differential equation satisfied by* v*:*

$$v' = \frac{-2u'}{(1+u^2)^2} = \frac{-2u}{(1+u^2)^3} = -2uv^3.$$

Hence, the non-polynomial ODE (3.7) is in fact equivalent to the polynomial system of ODEs

$$\begin{cases} u' = uv \\ v' = -2uv^3 \\ u(0) = u_0 \\ v(0) = \dfrac{1}{1+u_0^2}, \end{cases} \tag{3.8}$$

thanks to the specific choice of the initial condition on v*.*

Although the way we reformulated the above example into a polynomial system might seem somewhat ad hoc, this strategy can in fact be applied to a broad class of analytic nonlinearities, including many special functions, because these are typically solutions of differential equations, see the examples and discussions in [203, 158].

Remark 3.2.2. *It should be emphasized that this obsession with polynomial nonlinearities is at least partially tied with working in sequences spaces, and, to a lesser degree, in weighted ℓ^1 Banach algebras. Indeed, for computer-assisted proofs using finite elements, having non-polynomial nonlinearities makes much less of a difference (see, e.g., [250]), in part because in that context one cannot so easily exploit the polynomial nonlinearities anyway compared to the sequence space setting.*

As already emphasized, the polynomial embedding strategy can prove very useful, but it is not without disadvantages:

- It often forces to go back to first order systems, which can be detrimental for the quality of the bounds in the computer-assisted validation. For instance, if instead of the first order ODE (3.7), one considers the second order ODE

$$\begin{cases} u'' = \dfrac{u}{1+u^2} \\ u(0) = u_0 \\ u'(0) = u_1, \end{cases}$$

  then one has to first go back to a system of first order equations in order to use the polynomial embedding presented above.

- Polynomial embedding leads to larger systems, with more equations and unknowns than the original one. For instance, in [185], polynomial embedding was used for the equilateral planar circular restricted four body problem. The initial system is made of two second order ODEs, with non-polynomial nonlinearities describing gravitational interactions, but polynomial embedding leads to a system of seven first order ODEs, with nonlinearities which are polynomial but of degree up to nine. The larger number of equations and relatively high polynomial degree of the polynomial embedding do not create any fundamental difficulty for applying computer-assisted techniques, and indeed it did not prevent the authors of [185] from establishing very impressive results about this system, namely the existence of transverse homoclinic orbits leading to chaotic dynamics, but it does make all the pen-and-paper estimates more painful, and the computational parts of the proof more costly.

- Finally, this polynomial embedding strategy does not seem straightforward to generalize to PDEs, say to $-\Delta u = \frac{u}{1+u^2}$ in more than one dimension, at least not in a way that would lead to a zero-finding problem with a convenient structure for computer-assisted proofs.

3.2.2 Some alternatives to polynomial embedding

In this section, we discuss several alternate ways of dealing with some non-polynomial nonlinearities.

Using Taylor series and the Banach algebra property. Assume that the non-polynomial nonlinearity g is analytic, and that it has a known Taylor expansion around some x_0, with a radius of convergence R:

$$g(x) = \sum_{k=0}^{\infty} g_k (x - x_0)^k, \qquad \text{for all } |x - x_0| < R.$$

Then, given a finite Fourier series $\bar{u}$, one can approximate $g(\bar{u})$ by the polynomial expression $\sum_{k=0}^{K} g_k(\bar{u} - x_0)^k$, and, provided $\|\bar{u} - x_0\|_{\ell^1_\nu} < R$, use the Banach algebra property of ℓ^1_ν to

control the error:

$$\left\| g(\bar{u}) - \sum_{k=0}^{K} g_k (\bar{u} - x_0)^k \right\|_{\ell^1_\nu} \leq \sum_{k=K+1}^{\infty} |g_k| \|\bar{u} - x_0\|^k_{\ell^1_\nu}.$$

Controlling $g(u)$ for all u in a neighborhood of $\bar{u}$ can then for instance easily be achieved using the mean value inequality. Indeed, for all $u \in B_r(\bar{u})$,

$$\|g(u) - g(\bar{u})\|_{\ell^1_\nu} \leq \sup_{v \in B_x(\bar{u})} \left\|g'(\bar{u} + v)\right\|_{\ell^1_\nu} \|u - \bar{u}\|_{\ell^1_\nu} \leq \left(\sum_{k=0}^{\infty} k|g_k| \left(\|\bar{u} - x_0\|_{\ell^1_\nu} + r \right)^k \right) \|u - \bar{u}\|_{\ell^1_\nu}, \tag{3.9}$$

which is finite provided $\|\bar{u} - x_0\|_{\ell^1_\nu} + r < R$.

This simple approach has been successfully used for the exponential function [B24, 299],[1] but it also has several shortcomings. First, if g is analytic but not entire, there may not exist a good choice of x_0 such that $\|\bar{u} - x_0\|_{\ell^1_\nu}$ is below the radius of convergence. Second, even when g is entire, one might need to keep a lot of terms in the finite series approximation (i.e. take K large), which can lead to practical difficulties with precision, as already noticed in [299].

Adding extra equations and unknowns but NOT differentiating. Let us go back to the example (3.7), whose nonlinearity is a rational function, and once again consider the extra variable $v = \frac{1}{1+u^2}$. The paradigm of polynomial embedding has always been to differentiate these new relations, in order to obtain differential equations satisfied by the new variables. However, in this case we could in fact stick with this algebraic equation, and rewrite it as a polynomial one, leading to a *differential-algebraic system of equations* (DAE) which is also equivalent to (3.7)

$$\begin{cases} u' = uv \\ (1 + u^2)v - 1 = 0 \\ u(0) = u_0. \end{cases} \tag{3.10}$$

For computer-assisted proofs in Banach algebras, algebraic equations are in fact especially easy to deal with (see Chapter 5 for more details), and so is coupling them with differential equations, as showcased in [B7]. Compared to the traditional polynomial embedding presented in Section 3.2.1, this approach can sometimes better preserve the strucutre of the original problem. For instance, if we start with a second order differential equation, we can retain this property in the differential part of the DAE, and then leverage it in the computer-assisted proof [B7]. This approach can also be used if g contains a square root, or any kind of algebraic nonlinearity, but in contrast to the traditional polynomial embedding technique it cannot deal with transcendental nonlinearities.

NOT adding any new equation. Beyond the limitation to algebraic nonlinearities, another drawback of the DAE approach presented in the above paragraph is that one still has to add extra equations and unknowns, as is also the case for the polynomial embedding technique, which increases the cost of the proofs. However, as put forward in [B24], one in fact does not have to solve for the new unknowns and the original ones simultaneously. Instead, each non-polynomial term can be dealt with independently, in some sense in a black box fashion, using either Taylor series and the Banach algebra property, or the Newton–Kantorovich approach for algebraic nonlinearities (see, e.g., [41], and also Section 5.3.1), which also relies on Banach algebra properties. In each case, given a specific nonlinearity g, a finite Fourier series $\bar{u}$, and

[1] With some improvements over the basic estimate (3.9), which for the exponential function would lead to very crude overestimations of the form $\|e^v\|_{\ell^1_\nu} \leq e^{\|v\|_{\ell^1_\nu}}$.

some $\delta_u > 0$, we would like to obtain another finite Fourier series $\bar{v}$ and $\delta_v > 0$ (depending on $\bar{u}$, g and δ_u) such that

$$\|g(u) - \bar{v}\|_{\ell^1_\nu} \leq \delta_v, \qquad \text{for all } u \text{ such that } \|u - \bar{u}\|_{\ell^1_\nu} \leq \delta_u.$$

In [B24], we provide such construction for $g(x) = \exp(x)$ and $g(x) = 1/x$. Of course such construction is also readily available whenever g is a polynomial. Once these black boxes are in place, one can then compose them as needed, which is how we deal with the nonlinearities $\gamma(x) = \frac{1}{1+x^9}$ and $\gamma(x) = \frac{1}{1+e^{9(x-1)}}$ in Theorem 3.1.4 and Theorem 3.1.5, without having to consider a larger system with extra unknowns. Note part of this procedure has in fact already been implemented using the proof assistant Rocq, see [41].

3.2.3 The case of renormalization operators

A different context in which non-polynomial nonlinearities appear, in an arguably more intricate manner, is the study of the Feigenbaum-Cvitanovic renormalization operators:

$$R_m(f)(x) = \frac{1}{f^m(0)} f^m\left(f^m(0)x\right), \qquad x \in [-1, 1]. \tag{3.11}$$

Here f is a function defined on $[-1, 1]$, $m \geq 2$ is an integer, and f^m denotes the function f composed m times with itself. For $m = 2$, the existence of a hyperbolic fixed point of R_2 is intimately related to the universality of period-doubling cascades conjectured by Feigenbaum, Coullet and Tresser [117, 281], which we briefly recall below.

Consider the quadratic family $f_\mu(x) = 1 - \mu x^2$. For any $\mu \in [0, 2]$, f_μ maps the interval $[-1, 1]$ into itself, and one can consider the discrete dynamical system

$$\begin{cases} x_{n+1} = f_\mu(x_n) \\ x_0 = 0. \end{cases}$$

For μ close to zero, the orbit (x_n) converges to a globally attracting fixed point, but at some threshold value μ_1 the fixed point become instable, and an attracting period 2 orbit emerges. At some larger value μ_2, the period 2 orbit becomes unstable and leaves way to an attracting period 4 orbit, and this keeps repeating: There is a converging sequence of parameter values μ_k at which the system switches from period 2^{k-1} to period 2^k (see Figure 3.5). The convergence of the sequence μ_k is geometric, and one has

$$\frac{\mu_k - \mu_{k-1}}{\mu_{k+1} - \mu_k} \underset{k\to\infty}{\longrightarrow} \delta \approx 4.6692...$$

The truly amazing fact is that this behavior, and in particular the limiting ratio δ, which is called the (first) Feigenbaum constant, is universal. Indeed, let us consider another one-parameter family of even unimodal functions $\tilde{f}_\mu$ mapping $[-1, 1]$ into itself, and also having a period doubling cascade at a sequence of parameters $\tilde{\mu}_k$. Then, under a mild non-degenracy assumption (namely, that $\tilde{f}_\mu$ behaves quadratically around 0), the ratio $\frac{\tilde{\mu}_k - \tilde{\mu}_{k-1}}{\tilde{\mu}_{k+1} - \tilde{\mu}_k}$ converges to the same limit δ.

This universal behavior was first observed empirically, and then explained geometrically [79], showing that this universality is a consequence of the following statement, which essentially constitutes the Feigenbaum conjectures: There exists an even unimodal analytic map $f^\star : [-1, 1] \to [-1, 1]$, which is a hyperbolic fixed point of the renormalization operator R_2 having a single unstable eigenvalue δ (which is the universal constant), and whose unstable manifold intersect transversally the set Σ of even unimodal functions such that $f^2(0) = 0$. These conjectures were

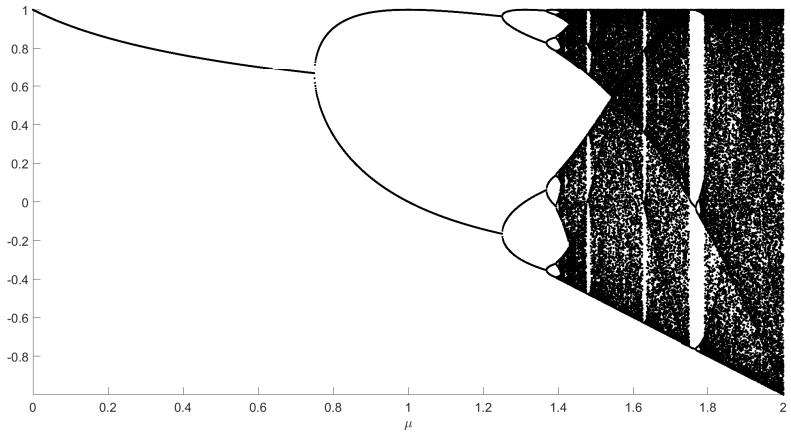

Figure 3.5: Accumulations points of the sequence $x_{n+1} = 1 - \mu x_n^2$, for different values of μ.

established in [195, 109], using computer-assisted proofs already containing several of the ideas that are at the core of this manuscript.[2]

Similarly, period tripling cascades are related to fixed points of R_3, and more generally period m-tupling cascades to fixed points of the renormalization operator R_m [95]. In a somewhat orthogonal direction, for each $m \in \mathbb{N}_{\geq 2}$ there are different fixed points and different corresponding universal behavior if, instead of looking at maps which behaves quadratically around 0, one focuses on even unimodal maps from $[-1, 1] \to [-1, 1]$ whose Taylor expansion at zero writes

$$f(x) = 1 - \alpha x^{2d} + o(x^{2d}),$$

for an integer $d \geq 2$ (the nondegenerate case discussed up to now corresponds to $d = 1$). As soon as $m \geq 3$ or $d \geq 2$, very few rigorous quantitative results are known about renormalization fixed points and their universal constants. Some pertubative results are available when $d = 1$ and m is large enough [107], or when $m = 2$ and d is large enough [108], as well as a computer-assisted proof for $m = 2$ and $d = 2$ [45].

In [B17], we develop general and flexible computer-assisted tools to study fixed points of R_m and their universal constants, and obtain the following results.

Theorem 3.2.3. *For each $m \in \{2, 3, \dots, 10\}$ there exists a fixed point $f_m^\star$ of R_m, which is at most 10^{-17} away in $\mathcal{C}^0$ norm from the approximate fixed point represented in Figure 3.6, whose precise description in terms of Chebyshev coefficients can be found at [Code 9]. All these fixed points correspond to the $d = 1$ case, i.e., they behave quadratically near the origin. For each fixed point, the associated universal constant (the unstable eigenvalue of $DR_m(f_m^\star)$) is at most 10^{-17} away from the value given in Table 3.1.*

All the renormalization fixed point obtained in Theorem 3.2.3 are in the most studied setting of $d = 1$, but our technique also allows to deal with fixed points with larger values of d.

Theorem 3.2.4. *For each $m \in \{2, 3\}$ there exists a fixed point of R_m, which is at most 10^{-40} away in $\mathcal{C}^0$ norm from the approximate fixed point represented in Figure 3.7, whose precise description in terms of Chebyshev coefficients can be found at [Code 9]. All these fixed point correspond to the $d = 2$ case, i.e., they behave quartically near the origin. For each fixed point, the associated universal constant (the unstable eigenvalue of $DR_m(f_m^\star)$) is at most 10^{-40} away from the value given in Table 3.2.*

[2] Later, computer-free proofs were also obtained [212, 16].

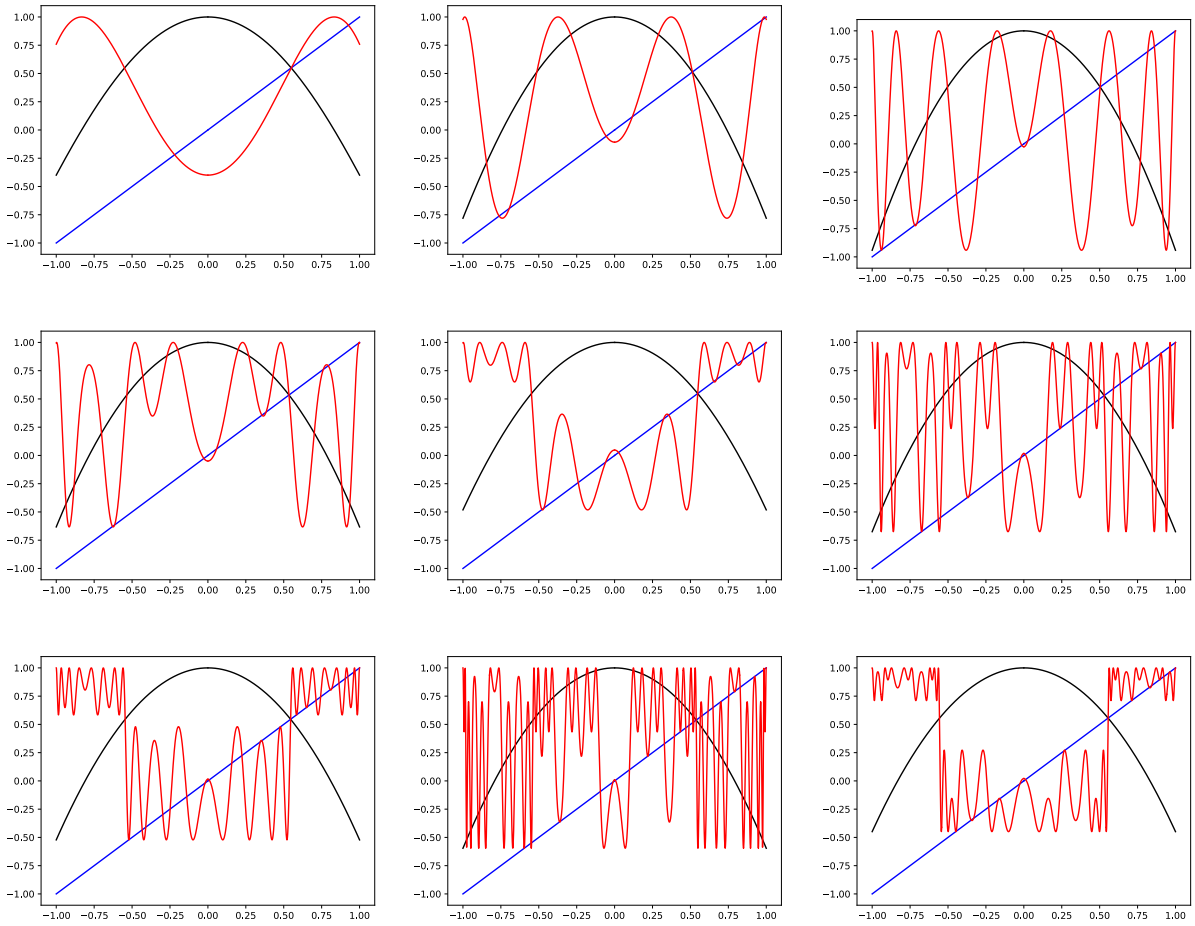

Figure 3.6: The approximate fixed point of R_m validated in Theorem 3.2.3. The sub-figures are arranged in increasing order with respect to m: the approximate fixed point for $m = 2$ is depicted in the top left, and the one for $m = 10$ in the bottom right. In each frame the black line is the graph of the approximate fixed point $\bar{f}$, and the red curve illustrates the composition of $\bar{f}$ with itself m times (but without rescaling and dividing by $\bar{f}^m(0)$, so the result is not fixed). For reference, the blue line $y = x$ is added to each picture.

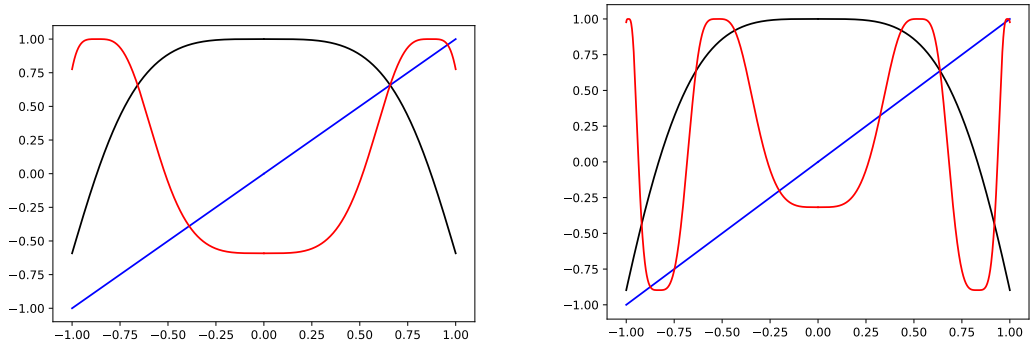

Figure 3.7: The approximate fixed point of R_m validated in Theorem 3.2.4, for $m = 2$ to the left and $m = 3$ to the right. The color code is the same as in Figure 3.6.

m	Approximate universal constant
2	4.6692016091029906
3	55.247026588671997372
4	981.594976534071427646
5	255.545253865903316209
6	218.41179514049496309
7	2253.792576403832804223
8	2304.557844448592270375
9	7918.223563171202619286
10	1110.537874176532781602

Table 3.1: For each m, the exact universal constant associated with the renormalization fixed point $f_m^\star$ obtained in Theorem 3.2.3, i.e., the unstable eigenvalue of $DR_m(f_m^\star)$, is at most 10^{-17} away from the approximate value given here.

m	Approximate universal constant
2	7.284686217073343364308930567995553069478 04
3	85.791629091356048744085122184129388676804896 9103

Table 3.2: For each m, the exact universal constant associated with the renormalization fixed point $f_m^\star$ obtained in Theorem 3.2.4, i.e., the unstable eigenvalue of $DR_m(f_m^\star)$, is at most 10^{-40} away from the approximate value given here.

Remark 3.2.5. *The fact that the error bounds are smaller in Theorem 3.2.4 than in Theorem 3.2.3 should not be seen as an indication that the second proof is easier than the first. In fact, from the theoretical side the proof is exactly the same for both theorems, but in practice the proof is computationally more involved for Theorem 3.2.4, and the smaller error bounds only reflect the fact that we had to use a higher precision in that case.*

The proof that the fixed points obtained in Theorem 3.2.4 are indeed quartic at the origin can be easily obtained using Proposition 2.1.3.

Finally, while all these fixed points are locally unique by construction, we emphasize that, even fixing $d = 1$, R_m can have multiple fixed points, which can all be validated separately in the same fashion (see [B17] for some examples, and the references therein for a broader discussion about the relationship between these different fixed points and the concept of kneading sequence). Hence, each universal constant is not simply associated with a value of m and d, but really to a renormalization fixed point.

Compared to the existing computer-assisted proofs for renormalization fixed points, the main difference in our approach is that we use a Chebyshev expansion of f instead of a Taylor expansion. One major disadvantage of Taylor expansions for this problem is this that, although renormalization fixed points are real analytic [60], there is no guarantee that their domain of analyticity contains the unit disk, which is necessary for being able to be describe them on the entire interval $[-1, 1]$ with a single Taylor expansion at 0. This happens to be true for $m = 2$ and $d = 1$, which made the early computer-assisted proofs in [195, 109] using Taylor series possible, as well as for $m = 2$ and $d = 2$ [45]. However, theoretical and numerical investigations indicate that the domain of analyticity of renormalization fixed points are rather complicated [113, 239], and shrink to $\mathbb{R} \cup i\mathbb{R}$ when d increases [108], which then prevents the Taylor expansion at 0 to be convergent on $[-1, 1]$.

On the other hand, Chebyshev expansions are less sensitive to these poles. Indeed, any function f which is Lispchtiz continuous on $[-1, 1]$ has a converging Chebyshev expansion, and

the convergence is geometrical with rate ρ as soon as the function extends analytically on the Bernstein ellipse $\mathcal{E}_\rho$, where

$$\mathcal{E}_\rho = \left\{ \frac{1}{2}\left(z + z^{-1}\right),\ z \in \mathbb{C},\ 1 \leq |z| \leq \rho \right\}.$$

Since Bernstein ellipses limit to the segment $[-1, 1]$ as ρ goes to 1 (see Figure 3.8), one can get a geometrically convergent Chebyshev series even if the function under consideration has poles close to the segment $[-1, 1]$. We refer to [280] for more background on Chebyshev expansions, and to [216, 230] for numerical computations of renormalization fixed point using Chebyshev series, for $m = 2$.

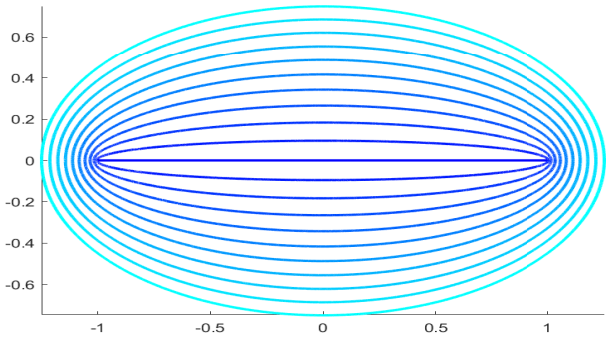

Figure 3.8: Boundaries of Bernstein ellipses, for $\rho \in \{1, 1.1, 1.2, \ldots, 2\}$. Darker blue corresponds to smaller values of ρ (note that $\mathcal{E}_1$ is simply the segment $[-1, 1]$).

Theorem 3.2.3 and Theorem 3.2.4 are obtained by applying a Newton–Kantorovich argument similar to Theorem 1.2.2 to the zero-finding problem $F(f) = f - R_m(f)$, which requires dealing with the non-polynomial nonlinearities appearing in $R_m(f)$, when f is expressed as a Chebyshev series. Even when $\bar{f}$ is a finite Chebyshev series, i.e., a polynomial, rigorously computing $\bar{f} \circ \bar{f}$ (or more generally $\bar{f}^m$ with $m \geq 3$) using discrete convolutions becomes impractical, especially since we use Chebyshev series instead of Taylor series. Instead, we directly obtain a finite Chebyshev series approximation of $\bar{f} \circ \bar{f}$ by computing an interpolation polynomial of $\bar{f} \circ \bar{f}$ (in the Chebyshev basis), and then rigorously bound the interpolation error, using geometrically decaying error estimates based on bounding $\bar{f} \circ \bar{f}$ on some Bernstein ellipses. We also need to control $R_m(f)$ for all f in a ball centered at $\bar{f}$ in ℓ^1_ν. Interpolation error estimates are again involved in this step, but we also take advantage of the rescaling properties of R_m. More precisely, we pick a $\rho > 1$ such that $\bar{f}$ is analytic on $\mathcal{E}_\rho$ and $\bar{f}^{m-1}(\bar{f}^m(0)\mathcal{E}_\rho)$ is compactly included in $\mathcal{E}_\rho$, which provides us with some margin allowing to control $R_m(f)$ for all f in a sufficiently small neighborhood of $\bar{f}$. We mention that a somewhat similar strategy was used in [119] in a different context, namely KAM theory, where this margin is obtained by slightly changing the regularity at each step.

For each fixed point in Theorem 3.2.3 and Theorem 3.2.4, the rigorous enclosure of the unstable eigenvalue (which is known to be unique by [16]) is also obtained by applying a Newton-Kantorovich argument, this time to the eigenvalue-eigenfunction problem.

3.3 Unbounded domains

3.3.1 Computer-assisted proofs on unbounded domains

In the last section of this chapter, we discuss computer-assisted proofs for some elliptic PDEs on $\mathbb{R}^d$. In that context, computer-assisted proofs have been notoriously harder to employ than on

bounded domains. One main reason is the lack of compactness, e.g., of the $H^2(\mathbb{R}^d)$ to $L^2(\mathbb{R}^d)$ embedding. When it comes to spectral approaches, another difficulty lies in the selection of a suitable basis.

Until recently, the only approach that could handle a variety of problems on unbounded domains Ω was the one developed by Michael Plum, where Theorem 1.2.6 is applied with $\mathcal{X} = H^1_0(\Omega)$ and $\mathcal{Y} = H^{-1}(\Omega)$, and $DF(\bar{x})^{-1}$ is controlled thanks to the homotopy method presented (in a simpler setting) in Section 1.3.2.3. We refer to [238, Part II] for a more general presentation, and to [318] for a recent example. Lately, other general computer-assisted methodologies were developed for (systems of) PDEs on unbounded domains, first specifically for radial solutions [287, 288], and then for more general solutions in [55, 56, 51, 52]. In these recent approaches, one goes back to a problem on a bounded domain, either by compactifying the domain, or by dealing separately with the solutions at infinity, or by introducing a periodized problem whose solutions approximate those of the original problem. Such techniques are well-suited to study localised solutions of equations having only bounded coefficients. We also mention the works [234, 235], where specific spectral problems on unbounded domains are studied using computer-assisted proofs.

In [B11], we study elliptic PDEs of the form

$$-\Delta u - \frac{x}{2} \cdot \nabla u = f(x, u, \nabla u), \quad x \in \mathbb{R}^d, \tag{3.12}$$

and develop new computer-assisted tools for such equations. Equations of the form (3.12) have already been studied extensively, as they naturally appear in several context, for instance when studying self-similar solutions of the nonlinear heat equation [43, 246, 312, 114, 323] or the Navier–Stokes equations [39]. Using the change of variable $u(x) = e^{-|x|^2/8}\varphi(x)$, equations of the form (3.12) are also connected to Schrödinger equations [180], as

$$-\Delta u - \frac{x}{2} \cdot \nabla u = e^{-\frac{|x|^2}{8}} \left(-\Delta \varphi + \left(\frac{|x|^2}{16} + \frac{d}{4} \right) \varphi \right).$$

3.3.2 A new setting

Our approach relies on developing a framework for computer-assisted proofs tailored to the operator $\mathcal{L} := -\left(\Delta + \frac{x}{2} \cdot \nabla\right)$ on $\mathbb{R}^d$, which in fact allows us to retrieve many of the convenient properties of computer-assisted proofs on bounded domains based on spectral expansions. We summarize below the main features of this new approach.

Appropriate spaces. We work with weighted Sobolev spaces, namely $H^2(\mu)$ and $L^2(\mu)$, where $\mu(x) = \frac{\Gamma(d/2)}{(2\sqrt{\pi})^d} e^{|x|^2/4}$. These are in some sense the natural spaces for $\mathcal{L}$, which are also typically used in pen-and-paper studies of, e.g., self-similar solutions of the nonlinear heat equation [179]. Indeed, $\mathcal{L}$ is self-adjoint on $L^2(\mu)$, $\mathcal{L}$ is an isomorphism between $H^2(\mu)$ and $L^2(\mu)$, and the embedding from $H^2(\mu)$ into $L^2(\mu)$ is compact (see Lemma 3.3.2 for a quantitative statement).

An eigenbasis of $\mathcal{L}$. We use a single spectral expansion to represent the solutions on the entire space $\mathbb{R}^d$. This is in contrast with [288], where a Taylor expansion is used around the origin, a Chebyshev one in the intermediate range, and some pen-and-paper analysis is used at infinity, and with [55] and subsequent works, which use a Fourier expansion on a bounded subdomain and then also control the behavior at infinity separately. Our spectral expansion is based on eigenfunctions of $\mathcal{L}$. Previous theoretical [114] and numerical [128] studies related to the operator $\mathcal{L}$ made use of multivariate Hermite functions, i.e., cartesian products on one-

dimensional bases:

$$\mathcal{L}\Psi_\beta = \frac{d+|\beta|}{2}\Psi_\beta, \quad \text{where} \quad \Psi_\beta(x) = e^{-\frac{|x|^2}{4}} \prod_{i=1}^{d-1} H_{\beta_i}\left(\frac{x_i}{2}\right), \quad \beta \in \mathbb{N}^d,$$

where H_n denotes the Hermite polynomial of degree n. However, in [B11] we advocate for the usage of a spherical coordinate basis, which better takes advantage of the radial symmetry of the operator $\mathcal{L}$, and seems to have better approximation properties even for non radially symmetric solutions. That is, for $d = 2$, we use as basis functions

$$\psi_{k,m}(r,\theta) = e^{-\frac{r^2}{4}} \left(\frac{r}{2}\right)^{|k|} L_m^{(|k|)}\left(\frac{r^2}{4}\right) \times \begin{cases} \cos(k\theta) & k \geq 0, \\ \sin(k\theta) & k < 0, \end{cases} \qquad m \in \mathbb{N},\ r \geq 0,\ \theta \in \mathbb{S}^1,$$

where $L_m^{(\alpha)}$ are generalized Laguerre polynomials, and for which we have

$$\mathcal{L}\psi_{k,m} = \left(\frac{2+|k|}{2} + m\right)\psi_{k,m}.$$

Similar formula can be obtained for any d, using hyperspherical functions, see [B11].

Remark 3.3.1. *In some sense, the usage of these bases for computer-assisted proofs can be seen as the generalization, to higher dimensions and to unbounded domains, of computer-assisted proofs on the disk introduced in [8].*

Since we have a diagonal basis for $\mathcal{L}$, and $\mathcal{L}^{-1} : L^2(\mu) \to L^2(\mu)$ is compact, we are in fact a similar situation to that of the Swift–Hohenberg equation on a bounded domain discussed in Chapter 1. We consider the zero-finding problem

$$F(u) = u - \mathcal{L}^{-1} f(x, u, \nabla u),$$

and, given an approximate solution $\bar{u}$, construct an approximate inverse A of $DF(\bar{u})$ as in Section 1.3.1.2. One then easily recovers compactness estimates similar to those typically used for controlling the quality of the approximate inverse when doing computer-assisted proofs using Fourier series. Let $\|u\|_{H^2(\mu)} := \|Lu\|_{L^2(\mu)}$, and, for any $N > 0$, define $\pi^{\leq N}$ as the orthogonal projection in $L^2(\mu)$ onto the finite dimensional subspace spanned by all the eigenfunctions of $\mathcal{L}$ having an eigenvalue λ such that $|\lambda| \leq N$.

Lemma 3.3.2. *For any $u \in H^2(\mu)$,*

$$\left\|u - \pi^{\leq N} u\right\|_{L^2(\mu)} \leq \frac{1}{N}\left\|u - \pi^{\leq N} u\right\|_{H^2(\mu)}.$$

Using this estimate, we can get suitable Z_1 bounds for this problem, which will have a $\frac{1}{N}$ decay.

Handling nonlinearities. Although we have an eigenbasis of $\mathcal{L}$ at our disposal for efficiently decomposing functions, the corresponding ℓ^1 space does not have as nice properties as in the Fourier case, and in particular is not a Banach algebra for the product corresponding to pointwise multiplication of functions. In that context, we therefore work instead with weighted Sobolev spaces, whose norms can be represented as ℓ^2 norms at the level of the coefficients in the eigenbasis of $\mathcal{L}$. In particular, even if the nonlinearities in f are only polynomial, more work is required to handle them compared to the Fourier case on bounded domains. This is achieved thanks to a combination of Sobolev embeddings, for which explicit constants for the weighted spaces used here are derived in [B11], and quadrature formulas which we discuss below.

As an example, let us assume we want to compute $\bar{u}^p$, for some $p \in \mathbb{N}_{\geq 2}$, where $\bar{u} \in \pi^{\leq N} H^2(\mu)$. A major difference with the case of Fourier series is that $\bar{u}^p$ does not have a finite expansion in our basis, because basis functions are not merely polynomials or trigononometric polynomials, but contain an $e^{-r^2/4}$ term. Nonetheless, we are able to exactly compute $\langle \bar{u}^p, \psi_n \rangle$ for any given basis function ψ_n, as well as $\|\bar{u}^p\|_{L^2(\mu)}$. What is needed is being able to compute integrals of the form

$$\int_{\mathbb{R}^d} \left(\prod_{j=1}^{J} \psi_j(x) \right) \mu(x) \mathrm{d}x = C \int_0^\infty \int_{\mathbb{S}^{d-1}} \left(\prod_{j=1}^{J} \psi_j(r, \theta) \right) r^{d-1} e^{\frac{r^2}{4}} \mathrm{d}r \mathrm{d}\theta, \quad J \geq 2,$$

where the ψ_j are basis functions described in the above paragraph. Focusing on the radial component which is where all the difficulties lie, the problem boils down to evaluating integrals of the form

$$\int_0^\infty P\left(\frac{r^2}{4}\right) r^\alpha e^{-\beta \frac{r^2}{4}} \mathrm{d}r,$$

where P is polynomial and $\beta > 0$, because there is an $e^{-r^2/4}$ term in each basis function ψ_j. Using the change of variable $z = r^2/4$, we end up with integrals of the form

$$\int_0^\infty P(z) z^{\frac{\alpha-1}{2}} e^{-\beta z} \mathrm{d}z.$$

Since P is a polynomial, such integral can in principle be computed from finitely many evaluations of P, using the exactness of Gauss quadrature. For this to be effective, one has to be able to rigorously evaluate the nodes and weights of the corresponding Gauss quadrature rule. Densities of the form $\omega(z) = z^\alpha e^{-\beta z}$, with $\alpha \in \mathbb{R}$ and $\beta > 0$, correspond to so-called generalized Gauss-Laguerre quadratures, for which explicit formulas for the nodes and weights are available, in terms of the Γ function and of roots of generalized Laguerre polynomials. See [B11] for details, and [Code 10] for a Julia code, written by Hugo Chu, allowing to compute these roots rigorously.

Going back to non-polynomial nonlinearities. For some nonlinear heat equations (see Theorem 3.3.6), it is natural to consider nonlinearities of the form u^p with a noninteger power p, because rapidly decaying self-similar solutions do not exist for integer powers. If p is a fraction, we are back into the case of algebraic nonlinearities discussed in Section 3.2.2. However, since we cannot rely on Banach algebra properties here, the techniques presented in Section 3.2.2 do not directly apply. In [B11], we therefore introduce a different approach, which relies on an ad hoc construction of the approximate solution. Suppose we want to compute $\bar{u}^{5/3}$, where $\bar{u}$ is an approximate solution defined with finitely many basis functions. We get around the issue of having to rigorously compute fractional powers by first finding numerically another function $\bar{v}$, also defined in terms of finitely many basis functions, such that $\bar{v} \approx \bar{u}^{1/3}$, and by then defining $\bar{u} := \bar{v}^3$. Then, $\bar{u}^{5/3}$ is exactly equal to $\bar{v}^5$, and we are back to computing polynomial nonlinearities.

3.3.3 Results

Below are some examples of results that can be obtained with this approach. We focus here only on the nonlinear heat equation

$$\partial_t v = \Delta v - \epsilon |v|^{p-1} v, \qquad \epsilon = \pm 1, \tag{3.13}$$

posed on $\mathbb{R}^d$, and more specifically on self-similar solutions of the form $v(t,x) = t^{-1/(p-1)}u(x/\sqrt{t})$, for which the profile u satisfies

$$\mathcal{L}u = \frac{u}{p-1} - \epsilon|u|^{p-1}u. \tag{3.14}$$

However, we emphasize that [B11] also contains similar results for some self-similar solutions of the critical nonlinear Schrodinger equation

$$i\partial_t v + \Delta v + \epsilon|v|^{4/d}v = 0,$$

in dimension $d = 2$, as well as for a generalized viscous Burgers equation

$$\partial_t v + v^2\partial_x v = \partial_{xx} v,$$

in dimension $d = 1$.

Theorem 3.3.3. *Let $d = 3$, $p = 2$, $\epsilon = -1$ and $\bar{u} : \mathbb{R}^3 \to \mathbb{R}$ be the radial function whose radial profile restricted to the interval $[0, 4]$ is represented in Figure 3.9, and whose precise description is available at [Code 10]. There exists a positive radial solution $u^\star \in H^2(\mu)$ to (3.14) such that*

$$\|u^\star - \bar{u}\|_{H^2(\mu)} \leq 1.5 \times 10^{-21}.$$

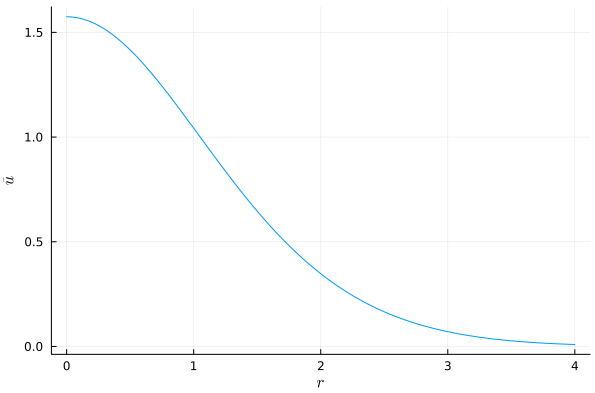

Figure 3.9: Radial component of an approximate self-similar profile $\bar{u}$ of the nonlinear equation (3.13) in dimension 3, with $p = 2$ and $\epsilon = -1$, rigorously validated in Theorem 3.3.3.

Remark 3.3.4. *Proving positivity is often easy a posteriori with computer-assisted proofs, because we have an accurate description of the solution, but is slightly non-trivial here since the exact solution goes to 0 at infinity, so L^∞ bounds will not be good enough. Therefore, we only check the positivity of $u^\star$ using L^∞ bounds on a large enough compact set, and use a maximum principle argument to conclude that the solution must then be positive everywhere.*

While many existence results for such radial self-similar profiles of the nonlinear heat equation were already available in the literature, using for instance variational methods or shooting methods [43, 246, 312], our results also provide a very precise description of these solutions. Furthermore, our methods can also deal with non-radial solutions, without relying on a perturbation argument. The only other work we are aware of where non-radial solutions are found is [114, Remark 3.11], which relies on local bifurcation theory and therefore only holds for p close to specific values.

Theorem 3.3.5. *Let $d = 2$, $p = 3$, $\epsilon = -1$ and $\bar{u} : \mathbb{R}^2 \to \mathbb{R}$ be the function whose restriction to the disk $\{(x, y) \mid x^2 + y^2 \leq 4^2\}$ is represented in Figure 3.10, and whose precise description is available at [Code 10]. There exists a solution $u^\star \in H^2(\mu)$ to (3.14) such that*

$$\|u^\star - \bar{u}\|_{H^2(\mu)} \leq 1.6 \times 10^{-3}.$$

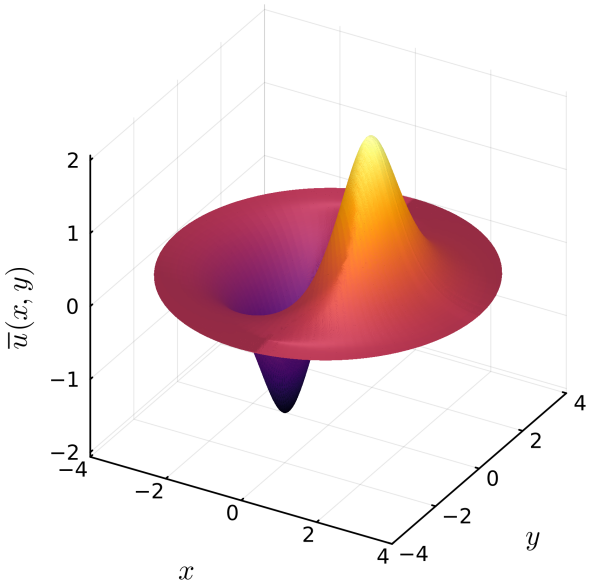

Figure 3.10: A non-radially symmetric approximate self-similar profile $\bar{u}$ of the nonlinear equation (3.13) in dimension 2, with $p = 3$ and $\epsilon = -1$, rigorously validated in Theorem 3.3.5.

Finally, let us turn to the case $\epsilon = 1$ in (3.13), for which rapidly decaying self-similar solutions only exist for $p < 1 + 2/d$ [43, 114], and therefore integer exponents are excluded as soon as $d > 1$. We use the approach described at the end of Section 3.3.2 in order to deal with fractional exponents.

Theorem 3.3.6. *Let $d = 2$, $p = 5/3$, $\epsilon = 1$ and $\bar{u} : \mathbb{R}^2 \to \mathbb{R}$ be the radial function whose radial profile restricted to the interval $[0, 4]$ is represented in Figure 3.11, and whose precise description is available at [Code 10]. There exists a positive radial solution $u^\star \in H^2(\mu)$ to (3.14) such that*

$$\|u^\star - \bar{u}\|_{H^2(\mu)} \leq 1.6 \times 10^{-23}.$$

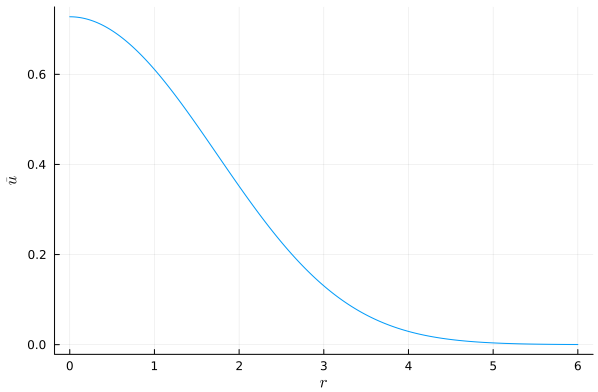

Figure 3.11: Radial component of an approximate self-similar profile $\bar{u}$ of the nonlinear equation (3.13) in dimension 2, with $p = 5/3$ and $\epsilon = 1$, rigorously validated in Theorem 3.3.6.

3.4 Perspectives

- **Stability of nontrivial steady states of cross-diffusion systems.** Similarly to the discussion regarding the DPCM at the end of Chapter 2, the steady states of the cross-diffusion models obtained in Section 3.1.3 are only a first step in understanding the global

dynamics. Once again, establishing the stability of some of the obtained steady states is an interesting problem, because for these systems there can be many co-existing steady states, and only a few of them seem to be stable. However, this is also a challenging question which requires new tools, this time because of the non-diagonal structure. Indeed, the multiplication by (a good approximation of) $\mathcal{M}(\Phi'(\bar{u}))$, which saved the day for the study of the steady states, turns the eigenvalue problem into a generalized one, and once again we are in a situation where the linear operator on which we have a good control is not the right one for studying linear stability. In the upcoming PhD thesis of Maxime Payan, in collaboration with Olivier Hénot and Antoine Zurek, we propose a new approach for proving the stability of these steady states, which is based on the construction of a Lyapunov functional adapted to the cross-diffusion structure, and also allows to prove local nonlinear stability.

- **Using a similar approximate inverse for FEM-based computer-assisted proofs.** The new construction of an approximate inverse adapted to cross-diffusion systems described in Section 3.1.2 was up to now only used for spectral methods, but it may also prove useful for computer-assisted proofs based on finite-elements, allowing to treat cross-diffusion problems on more complicated geometries.

- **A more general and unified treatment of non-polynomial nonlinearities.** The strategies for analytic but non-polynomial nonlinearities proposed in Section 3.2 are still not fully satisfying, especially for nonlinearities having poles and branch-cuts, for which none of the proposed methods is guaranteed to work, but also because of the lack of unified treatment. In collaboration with Jan Bouwe van den Berg, Jean-Philippe Lessard and Jason Mireles James, we are working on a more systematic way of handling general analytic nonlinearities, based on approximations using (trigonometric) interpolation polynomials as in Section 3.2.3, but with the additional difficulty that there will not be a rescaling granting "free" extra domain of analyticity.

- **Connecting orbits for renormalization operators.** Now that we have a robust and flexible setup for rigorously studying fixed point of the renormalization operator R_m (3.11), many new questions can be asked. In particular, in collaboration with Jorge Gonzalez and Jason Mireles James, we plan to rigorously study connecting orbits between different renormalization fixed points, and to therefore provide concrete applications of the PACSE theory laid out in [94].

- **More computer-assisted proofs on unbounded domains.** The setup introduced in Section 3.3 for dealing with operators of the form $\mathcal{L} = -\left(\Delta \cdot + \frac{x}{2}\nabla\cdot\right)$ in a fashion compatible with computed assisted proofs opens new possibilities. An interesting one would be to develop rigorous time-integrators allowing to study time-dependent problems on unbounded domain, extending what is presented in Chapter 4 for bounded domains only. Another one, which will be the subject of further investigations in collaboration with Hugo Chu, is the computer-assisted study of self-similar solutions in some Keller-Segel models. One of the main difficulty there is that the two equations in the system have different scales, i.e., one would have to deal with operators of the form $\mathcal{L}_\alpha = -\left(\Delta \cdot + \frac{\alpha x}{2}\nabla\cdot\right)$ with different values of α for the two components, which means different function spaces may have to be used for each component of the system, and leads to many new questions.

- **Computer-assisted proofs on unbounded domains with different potentials.** The operator $\mathcal{L} = -\left(\Delta \cdot + \frac{x}{2}\nabla\cdot\right)$ is only a special case in the family of operators of the form $\mathcal{L} = -\left(\Delta \cdot + V'(x)\nabla\cdot\right)$, which appear naturally in many contexts, and in particular in connection with stochastic differential equations of the form

$$\mathrm{d}x_t = -V(x_t)\mathrm{d}t + \sqrt{2}\mathrm{d}B_t,$$

leading to invariant probability densities of the form e^{-V} as soon as V is a confining potential. Quadratic potentials like $V(x) = |x|^2$ are the simplest ones among those, but more complicated potentials are also of interest. Unfortunately, the quadratic case is the only one in which $\mathcal{L}$ can be diagonal with respect to the basis of orthogonal polynomials associated with the invariant density. For polynomial potentials of higher degree, we propose in an upcoming work with Hugo Chu a new construction of so-called Sobolev orthogonal polynomials, which provides a natural framework in which the operator $\mathcal{L}$ becomes tridiagonal, and can then be dealt with using, among other things, the tools introduced in [B15].

Chapter 4

Time-integration

4.1 Literature review

Going back to the pioneering works [236, 248], many computer-assisted proofs techniques have been developed for elliptic PDEs, see for instance [243, 321, 331, 5, 93, 274, 307, 298, 55], as well as the book [238] and the references therein for a broader overview. Other types of specific solutions have also been studied with computer-assistance, such as traveling waves [7, 42, B2, 295, B10], periodic solutions [327, 6, 137, 118, B3], even for some ill-posed problems [66], or more recently self-similar solutions [44, 73, B11, 88]. For other types of specific solutions we refer to the survey [143]. Although these are time-dependent solutions, in many cases the problem is reformulated as an elliptic one after using a suitable Ansatz.

A different approach is needed in order to study generic initial value problems for parabolic PDEs. Within the computer-assisted proof community, techniques allowing to rigorously solve such problems are often described as *rigorous PDE integrators*. One main motivation for developing rigorous integrators is to then be able to study boundary value problems in time, in conjunction with rigorous enclosures for local stable and unstable manifolds that have been developed recently [253, 290], in order to obtain connecting orbits in parabolic PDEs. Rigorous PDE integrators can also be used to rigorously compute Poincaré maps, see [178] and the references therein.

One class of rigorous PDE integrators, which uses completely different techniques compared to the ones discussed in this manuscript, is the one developed in [327, 329]. It is not centered around a fixed point argument, but rather based on the validated integration of a finite dimensional system of ODEs using Lohner-type algorithms developed in [326], and on the notion of self-consisted bounds introduced in [331]. This methodology was further developed in [84], and has been used to rigorously study, among other things, globally attracting solutions in the one dimensional Burgers equation [87], heteroclinic connections in the one-dimensional Ohta-Kawasaki model [86] and recently to prove chaos in the Kuramoto–Sivashinky equation [315, 316].

A second family of rigorous PDE integrators, to which the approach described in this chapter belongs, is based on a fixed point reformulation which allows to prove, a posteriori, that a true solution exists in a small neighborhood of a numerically computed approximation. While these reformulations could in principle be expressed within the Newton–Kantorovich framework, this is an instance where the structure of the problem naturally leads to fixed-point reformulations without first going via a zero-finding problem. In other words, we may use Theorem 1.2.1 directly, rather than Theorem 1.2.2.

In order to first better present the different existing approaches, and then explain the main features of the one proposed in this chapter, let us fix a framework and some notations. We

consider scalar parabolic PDEs of the form

$$\begin{cases} \dfrac{\partial u}{\partial t} = (-1)^{J+1}\dfrac{\partial^{2J} u}{\partial x^{2J}} + \displaystyle\sum_{j=0}^{2J-1} \frac{\partial^j g^{(j)}(u)}{\partial x^j}, & t \in (0,\tau],\ x \in \mathbb{T}, \\ u(0,x) = u^{in}(x), & x \in \mathbb{T}, \end{cases} \tag{4.1}$$

where $J \in \mathbb{N}_{\geq 1}$ is a positive integer, $\tau > 0$ determines the integration time, $g^{(j)} : \mathbb{R} \to \mathbb{R}$ are given polynomial functions for $j = 0, \dots, 2J-1$, and $u^{in} : \mathbb{T} \to \mathbb{R}$ is a smooth function. Many of these assumptions can in fact be relaxed, and the strategy we are going to present generalizes in a straightforward manner to a broader class of problems, including:

- Systems of parabolic PDEs,
- Higher dimensional torus, or rectangular spatial domains with boundary conditions allowing for smooth Fourier series representations,
- Non polynomial nonlinearities like those handled in Section 3.2,
- Non constants coefficients in the lower order terms, that is, anywhere except in the $\dfrac{\partial u}{\partial t} - (-1)^{J+1}\dfrac{\partial^{2J} u}{\partial x^{2J}}$ part.

However, the fact that the highest order term $(-1)^{J+1}\dfrac{\partial^{2J} u}{\partial x^{2J}}$ is dissipative is crucial and will be heavily used. Besides that, the specific structure of the equation does no matter so much at this stage, and for the remainder of the preliminary discussion we introduce

$$F(u) = (-1)^{J+1}\frac{\partial^{2J} u}{\partial x^{2J}} + \sum_{j=0}^{2J-1} \frac{\partial^j g^{(j)}(u)}{\partial x^j},$$

so that the evolution equation simply writes $\partial_t u = F(u)$. We assume that we have at our disposal an approximate solution $\bar{u}$ of (4.1).

In order to rewrite the initial value problem as a fixed point problem, one typically starts by choosing a splitting

$$F(u) = \mathcal{L}u + G(u), \tag{4.2}$$

where $\mathcal{L}$ is a linear operator which may or may not depend on time. If $\mathcal{L}$ is time-independent, a solution of (4.1) can (at least formally) be rewritten as a fixed point of the operator $\tilde{T}$ defined by

$$\tilde{T}(u)(t) = e^{t\mathcal{L}}u^{in} + \int_0^t e^{(t-s)\mathcal{L}} G(u(s))\mathrm{d}s, \qquad t \in [0,\tau]. \tag{4.3}$$

If $\mathcal{L}$ depends on time, more care has to be taken, but a similar reformulation of (4.1) as a fixed point is possible:

$$\tilde{T}(u)(t) = U(t,0)u^{in} + \int_0^t U(t,s)G(s,u(s))\mathrm{d}s, \tag{4.4}$$

where $U(t,s)$ is the evolution operator associated to $\mathcal{L}$, i.e. $U(t,s)\varphi$ is the solution at time t of

$$\begin{cases} \partial_t u = \mathcal{L}(t)u & \text{on } (s,\tau] \times \mathbb{T} \\ u(s,\cdot) = \varphi & \text{on } \mathbb{T}. \end{cases}$$

Among the rigorous integrators based on fixed point reformulations, one of the earliest ones can be found in [6], where numerical solutions are validated using a fixed point operator similar to $\tilde{T}$ in (4.3), and where $\mathcal{L}$ is in some sense chosen to be as simple as possible, namely $\mathcal{L} = DF(0)$.[1] This choice for $\mathcal{L}$ is enticing for making it easier to control the associated semigroup, which is needed when trying to prove that $\tilde{T}$ is a contraction. This is especially true if the domain and the boundary conditions allow for an explicit diagonalization of such an $\mathcal{L}$, as is the case for the problem considered in [6] and in the current chapter. However, while this choice of $\mathcal{L}$ simplifies the analysis of $\tilde{T}$, it also comes at the cost of making the operator $\tilde{T}$ potentially *less contracting* ($DG(\bar{u})$ has no reason to be small), and $\tilde{T}$ can generally only be contracting for relatively small values of the integration time τ. A similar approach, at least at the level of choosing the fixed point reformulation, is used in [85].[2]

On the other end of the spectrum, at least with regards to $\mathcal{L}$, are the techniques introduced in [275, 273, 104]. There, in the splitting (4.2), $\mathcal{L}$ is chosen as a very accurate time dependent approximation of $DF(\bar{u})$. By allowing $\mathcal{L}$ to depend on time, one can in principle make $DG(\bar{u}) = DF(\bar{u}) - \mathcal{L}$ arbitrarily small, hence ensuring that the fixed point operator $\tilde{T}$ in (4.4) is contracting in a neighborhood of $\bar{u}$ without restricting to a small integration time τ. Nevertheless, when actually having to prove that $\tilde{T}$ is a contraction in this setting, one then has to explicitly control the evolution operator $U(t, s)$, which can be much more challenging and resource consuming than only having to control the semigroup associated to a time *independent* $\mathcal{L}$. Nonetheless, this approach can be quite powerful, and recently led to rigorous integration of PDEs in three dimensions [104].

Yet another approach, which starts with a different viewpoint but for which the fixed point reformulation ends up being very similar, is the one in [154], see also [238, Chapter 5]. In the context of (4.1), assuming $J = 1$, the approach in [154] can be interpreted as taking $\mathcal{L}$ to be exactly equal to $DF(\bar{u})$, and the validation is then based on applying Schauder's fixed point theorem to the operator (4.4), where now $U(t, s)$ is the evolution operator associated to $DF(\bar{u})$. This choice of $\mathcal{L}$ leads to $DG(\bar{u}) = 0$, hence one should be able to find a small neighborhood of $\bar{u}$ being mapped into itself by $\tilde{T}$, but doing so now requires controlling the evolution operator associated to $\mathcal{L} = DF(\bar{u})$. In the end, this is accomplished by introducing some approximation of $DF(\bar{u})$, see, e.g., [153] for the details. We point out that some of the ideas in this approach, but also in all the other ones, can be traced back to the early work [237], in which $\mathcal{L}$ was simply taken to be the Laplacian.

All these works share some similarities regarding the fixed point operator used for the validation, or, at the very least, they can all be reformulated into this common framework. However, we emphasize that they then differ significantly when it comes to how this fixed point operator is analyzed, which is in particular impacted by the spatial domains that are considered and the corresponding discretization choices that are made. Fourier series and associated sequences spaces are used in [6, 273, 104], whereas results using finite elements and Sobolev spaces allowing in principle for more complex geometries can be found in [154, 238]. Regarding the time variable, most of the existing works make use of low order piece-wise constant or linear approximations, the notable exception being [85], where a setup allowing for a spectral approach in both space and time is introduced.

4.2 A new rigorous integrator

[1] To be more precise, the operator $\mathcal{L}$ used in [6] is sometimes slightly modified, the parts that would contribute to eigenvalues with positive real part being moved to G.

[2] This approach also suffers from a severe limitation regarding the integration time τ, but this limitation is currently being removed [54].

4.2.1 Our choice of $\mathcal{L}$

The setup proposed in [B4], and simplified in [B1], can be seen as a judicious compromise between the different approaches just mentioned. Indeed, we try to take for $\mathcal{L}$ an approximation of $DF(\bar{u})$ which is *as good as we can while remaining time independent*, thereby avoiding the problem of having to deal with the solution operator of a non-autonomous system, while still improving the contractiveness of $\tilde{T}$ in (4.3). Of course, this can only work well if the solution does not change too drastically on the time interval $[0, \tau]$, or equivalently, if τ is not too large, otherwise a time independent approximation of $DF(\bar{u})$ cannot be a reasonable approximation. We resolve this issue by using a domain decomposition strategy, which amounts to taking $\mathcal{L}$ piece-wise constant in time when τ is large. We give some more details on this domain decomposition strategy in Section 4.2.3, but first describe the construction of $\mathcal{L}$ in the case of a single domain here.

Given an approximate solution $\bar{u}$ to the initial value problem (4.1), we first define the functions $\bar{v}^{(j)} = \bar{v}^{(j)}(x)$, $j = 1, \dots, 2J-1$, by

$$\bar{v}^{(j)} = \frac{1}{\tau} \int_0^\tau \left(g^{(j)}\right)' (\bar{u}(t, \cdot)) \mathrm{d}t.$$

As usual, these functions can be interpreted as elements of ℓ^1_ν. Introducing the Fourier transform $\mathcal{D}$ of $\dfrac{\partial}{\partial x}$, i.e.,

$$(\mathcal{D}u)_n = inu_n,$$

the Fréchet derivative $DF(\bar{u})$ writes, in Fourier space,

$$DF(\bar{u}) = (-1)^{J+1}\mathcal{D}^{2J} + \sum_{j=0}^{2J-1} \mathcal{D}^j \mathcal{M}\left(\left(g^{(j)}\right)' (\bar{u}(t, .))\right),$$

where we recall that $\mathcal{M}$ is the notation for multiplication operators on sequence spaces introduced in Chapter 0. We then consider the time independent approximation of $DF(\bar{u})$ given by

$$\tilde{\mathcal{L}} = (-1)^{J+1}\mathcal{D}^{2J} + \sum_{j=0}^{2J-1} \mathcal{D}^j \mathcal{M}\left(\bar{v}^{(j)}\right).$$

In order to more easily deal with the semi-group $e^{t\mathcal{L}}$, we make a final simplification, by taking advantage of the fact that $\tilde{\mathcal{L}}$ is asymptotically diagonally dominant. We therefore fix a threshold N and define

$$\mathcal{L} = \Pi^{\leq N} \tilde{\mathcal{L}} \Pi^{\leq N} + \Pi^{>N} \operatorname{diag}(\tilde{\mathcal{L}}) \Pi^{>N}.$$

We have explicit formula for the diagonal terms in the tail, namely

$$\lambda_n := \mathcal{L}_{n,n} = -n^{2J} + \sum_{j=0}^{2J-1} (in)^j \bar{v}_0^{(j)}, \qquad |n| > N,$$

and we can diagonalize the finite part $\Pi^{\leq N} \tilde{\mathcal{L}} \Pi^{\leq N}$ in order to explicitly obtain $e^{t\mathcal{L}}$.

4.2.2 Proving the contraction

Once $\mathcal{L}$ has been defined, we are left with trying to prove that $\tilde{T}$ defined in (4.3) is a contraction on a small neighborhood of $\bar{u}$, by using Theorem 1.2.1. As usual, one has to select a function space and a norm.

We use the Banach space $\mathcal{X}_\nu$ of continuous functions u on $[0, \tau]$ with values in ℓ^1_ν such that

$$\|u\|_{\mathcal{X}_\nu} = \sum_{n \in \mathbb{Z}} \sup_{t \in [0,\tau]} |u_n(t)| \, \nu^{|n|} < \infty. \tag{4.5}$$

We note that a slightly different norm, namely

$$\sup_{t\in[0,\tau]} \sum_{n\in\mathbb{Z}} |u_n(t)|\, \nu^{|n|},$$

is used in [273, 104], but that (4.5) seems to be more convenient to obtain semi-group estimates allowing to control lower order derivatives, i.e., when there is a $g^{(j)}$ which is non-zero in (4.1) for $j \geq 1$. We then consider $\tilde{T}$ defined in (4.3), with $\mathcal{L}$ as in Section 4.2.1, and derive estimates Y, Z_1 and Z_2 satisfying the assumptions of Theorem 1.2.1, see [B4] for the details.

Whether $\tilde{T}$ is contracting or not (i.e., whether we manage to get $Z_1 < 1$ or not) essentially only depends on the truncation level N used for defining $\mathcal{L}$, and on the final time τ. On the other hand, provided $\tilde{T}$ is contracting, whether a small ball around $\bar{u}$ actually gets mapped into itself by $\tilde{T}$ or not (i.e., whether Y is small enough on not) mostly depends on whether $\bar{u}$ is an accurate enough approximate solution of the initial value problem (4.1). It is for this specific step, and only for this one, that on top of taking enough Fourier modes, it is helpful to have an accurate discretization in time of the problem. We accomplish this by using a polynomial representation of potentially high order in time, obtained using interpolation at Chebyshev nodes.

Remark 4.2.1. *In [B4], we did not directly try to prove that $\tilde{T}$ from (4.3) is a contraction. Instead, we first turned this fixed point problem into a zero finding problem $\tilde{F}(u) = u - \tilde{T}(u)$, and then went back to a fixed point problem via the Newton–Kantorovich approach, using an approximate inverse of $D\tilde{F}(\bar{u})$. However, we later realized [B1] that one should in fact directly work with $\tilde{T}$ as indicated above (or equivalently, take the identity for the approximate inverse in the Newton–Kantorovich reformulation), for several reasons.*

In order to use a non-trivial approximate inverse, one needs a finite dimensional projection, i.e., to not only truncate Fourier modes but also to choose a projection in time. We need such a projection anyway to find the approximate solution, so this is the one we used: the finite dimensional projection in time is defined as taking an interpolation polynomial at Chebyshev nodes. However, once this projection is used for defining the approximate inverse, it also has to be incorporated in the norm, which has to be split between a finite part in time and a tail part in time.[3] *This splitting leads to more involved estimates, which also turn out to be less sharp than if one could first simply take the C^0 norm in time, and then do precise estimates in space using the ℓ^1 structure.*

More importantly, the computational costs associated to the construction and storage of the approximate inverse A are often the practical bottleneck of such computer-assisted proofs. Therefore, getting rid of the approximate inverse significantly increases the applicability of the method. In many situations this is not possible, because the approximate inverse is the only reason why the fixed point operator we study should be contracting. However, for initial value problems specifically, we can build contracting fixed point operators without using a large approximate inverse, as was also noticed in [104].

4.2.3 Increasing the maximal integration time using domain decomposition

As explained in Section 4.2.1, taking $\mathcal{L}$ time independent has the advantage of leading to a simple semi-group $e^{t\mathcal{L}}$ in the fixed point operator $\tilde{T}$ defined in (4.3). However, this also means we can approximate $DF(\bar{u})$ by $\mathcal{L}$ relatively well, and therefore expect $\tilde{T}$ to be contracting, only if the total integration time τ is not too large. One option to integrate over longer times is to iterate this procedure:

1. Starting from a given initial condition, rigorously integrate over a not so large time τ,
2. Extract a rigorous enclosure of the solution at the final time,

[3] Avoiding this is one of the motivations for developing a fully spectral method, also in time, as in [85, 54].

3. Use this as an (interval) initial condition for the next step, and start again.

This is definitely a valid option, which we implemented in [B4], and which is used in a much more refined fashion in the CAPD library [178]. However, beyond the propagation and amplification of errors which is sometimes hard to avoid with this approach, another drawback of this iterative procedure is that it cannot be used to solve boundary value problems, at least not directly.

We therefore consider a different approach to deal with potentially large integration times, namely a domain decomposition (in time) technique, which has already proven successful for rigorously integrating ODEs [296]. We start by taking a subdivision $0 = \tau_0 < \tau_1 < \ldots < \tau_M = \tau$ of the interval $[0, \tau]$. Then, for each $m = 1, \ldots, M$, we consider $DF(\bar{u})$ on the time subinterval $[\tau_{m-1}, \tau_m]$, and define a time independent approximation $\mathcal{L}_m$. The construction is exactly the same as in Section 4.2.1, except the $v^{(j)}$ now depend on the selected subinterval:

$$\bar{v}_m^{(j)} = \frac{1}{\tau_m - \tau_{m-1}} \int_{\tau_{m-1}}^{\tau_m} \left(g^{(j)}\right)' (\bar{u}(t, \cdot)) \mathrm{d}t.$$

A piece-wise defined fixed point reformulation of (4.1) is then given by

$$\tilde{T}(u)(t) = e^{(t-\tau_{m-1})\mathcal{L}_m} \theta_{m-1}(u) + \int_{\tau_{m-1}}^{t} e^{(t-s)\mathcal{L}_m} G_m(u(s)) \mathrm{d}s, \qquad t \in [\tau_{m-1}, \tau_m], \tag{4.6}$$

where

$$\theta_0(u) = u^{in}, \qquad \theta_m(u) = e^{(\tau_m - \tau_{m-1})\mathcal{L}_m} \theta_{m-1}(u) + \int_{\tau_{m-1}}^{\tau_m} e^{(\tau_m - s)\mathcal{L}_m} G_m(u(s)) \mathrm{d}s, \qquad m \geq 1,$$

and $G_m := F - \mathcal{L}_m$.

Remark 4.2.2. *This piece-wise definition of the fixed point operator $\tilde{T}$ in (4.6) will prove convenient in a moment, when trying to select a suitable norm in order to prove that this $\tilde{T}$ is a contraction, but is also a necessity. Indeed, what we did here simply corresponds to choosing an operator $\mathcal{L}$ which is no longer constant but merely piece-wise constant , and equal to $\mathcal{L}_m$ on $[\tau_{m-1}, \tau_m]$. Therefore, the corresponding evolution operator no longer simply writes $e^{(t-s)\mathcal{L}}$, but it can still be written down explicitly, if we describe it piece-wise as in (4.6).*

The idea is then again to prove that this new $\tilde{T}$ is a contraction on a neighborhood of $\bar{u}$, hence validating the entire solution over the interval $[0, \tau]$ at once. Since $\tilde{T}$ in (4.6) is obtained by taking $\mathcal{L}$ piece-wise constant, instead of constant in the single domain version (4.3), the piece-wise constant $\mathcal{L}$ should be able to better approximate $DF(\bar{u})$, and hence $\tilde{T}$ in (4.6) should be more contracting than $\tilde{T}$ in (4.3). In order to prove this quantitatively, it is helpful to consider a product space corresponding to the subdivision of the time interval, together with a well chosen norm.[4] That is, we consider for each $m \in \{1, \ldots, M\}$ the Banach space $\mathcal{X}_\nu^m$ of continuous functions $u^{(m)}$ on $[\tau_{m-1}, \tau_m]$ with values in ℓ_ν^1 such that

$$\left\| u^{(m)} \right\|_{\mathcal{X}_\nu^m} = \sum_{n \in \mathbb{Z}} \sup_{t \in [\tau_{m-1}, \tau_m]} \left| u_n^{(m)}(t) \right| \nu^{|n|} < \infty, \tag{4.7}$$

and the product space $\mathcal{X}_\nu^{\mathrm{prod}} = \prod_{m=1}^M \mathcal{X}_\nu^m$. The domain decomposition fixed point operator $\tilde{T}$ from (4.6) can naturally be written as an operator from $\mathcal{X}_\nu^{\mathrm{prod}}$ to itself: Given $u = (u^{(1)}, \ldots, u^{(M)}) \in \mathcal{X}_\nu^{\mathrm{prod}}$, we can write $\tilde{T}(u) = (\tilde{T}^{(1)}(u), \ldots, \tilde{T}^{(M)}(u))$, where

$$\tilde{T}^{(m)}(u)(t) = e^{(t-\tau_{m-1})\mathcal{L}_m} \theta_{m-1}(u) + \int_{\tau_{m-1}}^{t} e^{(t-s)\mathcal{L}_m} G_m(u^{(m)}(s)) \mathrm{d}s, \qquad t \in [\tau_{m-1}, \tau_m], \tag{4.8}$$

[4] On a conceptual level, the more straightforward way to think about this is that we would like a norm on $C([0, \tau], \ell_\nu^1)$ which is similar to (4.5), but with a weighted C^0 norm in time. However, choosing a suitable weight a priori is difficult, and one would rather optimize for the weight a posteriori. Our weighted product space in fact essentially corresponds to taking (4.5) with a time-dependent weight which is piece-wise constant, which makes the optimization problem finite dimensional.

with

$$\theta_0(u) = u^{in}, \qquad \theta_m(u) = e^{(\tau_m - \tau_{m-1})\mathcal{L}_m}\theta_{m-1}(u) + \int_{\tau_{m-1}}^{\tau_m} e^{(\tau_m - s)\mathcal{L}_m} G_m(u^{(m)}(s))\mathrm{d}s, \qquad m \geq 1.$$

With respect to the product space decomposition, a key feature of $\tilde{T}$, which comes from the fact that we are looking at an initial value problem, is that it is lower triangular: $\tilde{T}^{(m)}(u)$ only depends on $u^{(1)}, \dots, u^{(m)}$. Moreover, the terms θ_m which couple the different subdomains are strictly lower triangular, whereas the $\int_{\tau_{m-1}}^{t} e^{(t-s)\mathcal{L}_m} G_m(u^{(m)}(s))\mathrm{d}s$ terms are diagonal.

Looking back at the operator (4.3) without domain decomposition, whether or not it is contracting near $\bar{u}$ depends on τ and on how small $DG(\bar{u}) = DF(\bar{u}) - \mathcal{L}$ is, i.e., on how well the time independent operator $\mathcal{L}$ approximates $DF(\bar{u})$. In comparison, each $DG_m(\bar{u}^{(m)}) = DF(\bar{u}^{(m)}) - \mathcal{L}_m$ term should be significantly smaller, because each one only approximates $DF(\bar{u})$ on a fraction of the whole time interval. Furthermore, each of the integrals is now only over a subinterval $[\tau_{m-1}, \tau_m]$ rather than on the whole interval $[0, \tau]$. In other words, we expect the norm of the partial Fréchet derivatives of the domain decomposition operator (4.8), i.e.,

$$\left\| \frac{\partial \tilde{T}^{(m)}(u)}{\partial u^{(m)}} \right\|_{\mathcal{X}_\nu^{(m)}},$$

to be much smaller than the norm of the Fréchet derivative of the original fixed point operator (4.3). While those are only the diagonal elements of the full Fréchet derivative, if they are all smaller than 1 then we can find a weighted norm on the product space such that the norm of the full Fréchet derivative is smaller than 1, because of the lower triangular structure. This is where the choice of the norm on the product space $\mathcal{X}_\nu^{\mathrm{prod}}$ comes in. We present the argument in a more general setting in the next subsection, as it is of independent interest and can be extremely useful whenever one tries to apply the fixed point Theorem 1.2.1 (or its corollary Theorem 1.2.2) to systems.

4.2.4 Newton–Kantorovich on a product space

Let $(\mathcal{X}_m, \|\cdot\|_{\mathcal{X}_m})$ be Banach spaces for $m \in \{1, \dots, M\}$, $\mathcal{X} = \Pi_{m=1}^M \mathcal{X}_m$ the product space, and $\bar{x} = (\bar{x}_1, \dots, \bar{x}_M) \in \mathcal{X}$. If we have a zero finding problem or a fixed point problem defined on $\mathcal{X}$, and we want to directly apply the Newton–Kantorovich Theorem 1.2.2 or the fixed point Theorem 1.2.1, we need to define a norm on $\mathcal{X}$. There are a few canonical choices, like

$$\|x\|_{\mathcal{X}} = \max_{1 \leq m \leq M} \|x_m\|_{\mathcal{X}_m}, \quad \|x\|_{\mathcal{X}} = \sum_{m=1}^{M} \|x_m\|_{\mathcal{X}_m}, \quad \text{or} \quad \|x\|_{\mathcal{X}} = \sqrt{\sum_{m=1}^{M} \|x_m\|_{\mathcal{X}_m}^2}.$$

However, one could have a contraction for one norm but for in the others, or for none of these three norms but for some other norm. In fact, in order to apply the contraction mapping theorem we need two different ingredients: a closed subset of $\mathcal{X}$ that is mapped into itself, and a norm for which the fixed point operator is contracting on that set. For convenience, that set is usually defined as a ball for the norm which one uses to measure the contractivity, but this is not at all necessary.

We present here a more general approach introduced in [B4], which is the culmination of earlier attempts in that direction [297, 286, B18]. We emphasize that this approach uses exactly the same bounds as the ones that are typically derived we trying to use a Newton–Kantorovich or fixed point argument, they are just post-processed in a more optimized way. Getting these bounds is usually where most of the work lies (both in terms of pen-and-paper calculations and of computational cost), so once we have them we should definitely try to squeeze the most out of them, which is what we do here.

We start with a bit more notation. Let $\pi_m : \mathcal{X} \to \mathcal{X}_m$ the projections onto the components of $\mathcal{X}$ and $r^* = (r_1^*, \dots, r_m^*) \in \mathbb{R}^M_{>0}$. For $r \in \mathbb{R}^M_{>0}$, we define

$$\mathrm{Box}(\bar{x}, r) = \{x \in \mathcal{X} : \|\pi_m(x - \bar{x})\|_{\mathcal{X}_m} \leq r_m \text{ for } 1 \leq m \leq M\}.$$

Note that this set $\mathrm{Box}(\bar{x}, r)$ could be interpreted as a unit ball for a weighted ℓ^∞ norm on the product space $\mathcal{X}$, but we do not want to chose a norm yet, and it turns out we will use a different norm to study contractivity.

We consider a map $T \in C^1(\mathrm{Box}(\bar{x}, r), \mathcal{X})$. Finally, we denote partial Fréchet derivatives by D_i and, for any two vectors $r, r^* \in \mathbb{R}^M_{>0}$, we say that $r \leq r^*$ if $r_m \leq r_m^*$ for all $m \in \{1, \dots, M\}$.

Theorem 4.2.3. *Assume that $Y_m \geq 0$, $Z^1_{m,i} \geq 0$, $Z^2_{m,i,j} \geq 0$ for $1 \leq i, j, m \leq M$ satisfy*

$$\|\pi_m(T(\bar{x}) - \bar{x})\|_{\mathcal{X}_m} \leq Y_m, \tag{4.9}$$

$$\|\pi_m D_i T(\bar{x})\|_{B(\mathcal{X}_i, \mathcal{X}_m)} \leq Z^1_{m,i}, \tag{4.10}$$

$$\|\pi_m(D_i T(x) - D_i T(\bar{x}))\|_{B(\mathcal{X}_i, \mathcal{X}_m)} \leq \sum_{j=1}^M Z^2_{m,i,j} \|\pi_j(x - \bar{x})\|_{\mathcal{X}_j} \quad \text{for all } x \in \mathrm{Box}(\bar{x}, r^*). \tag{4.11}$$

If $r, \eta \in \mathbb{R}^M_{>0}$ with $r \leq r^*$ satisfy

$$Y_m + \sum_{i=1}^M Z^1_{m,i} r_i + \frac{1}{2} \sum_{i,j=1}^M Z^2_{m,i,j} r_i r_j \leq r_m \tag{4.12}$$

$$\sum_{i=1}^M Z^1_{m,i} \eta_i + \sum_{i,j=1}^M Z^2_{m,i,j} \eta_i r_j < \eta_m \tag{4.13}$$

for all $1 \leq m \leq M$, then T has a unique fixed point in $\mathrm{Box}(\bar{x}, r)$.

Proof. Writing

$$T(x) - \bar{x} = T(\bar{x}) - \bar{x} + DT(\bar{x})(x - \bar{x}) + \int_0^1 \left[DT\left(\bar{x} + s(x - \bar{x})\right) - DT\left(\bar{x}\right)\right](x - \bar{x}) \mathrm{d}s,$$

the inequalities (4.12) imply that T maps $\mathrm{Box}(\bar{x}, r)$ into itself. Then, writing

$$DT(x) = DT(\bar{x}) + \left[DT\left(x\right) - DT\left(\bar{x}\right)\right],$$

and considering the weighted maximum norm

$$\|x\|_{\mathcal{X}} = \max_{1 \leq m \leq M} \frac{\|\pi_m x\|_{\mathcal{X}_m}}{\eta_m}, \tag{4.14}$$

we get, for all x in $\mathrm{Box}(\bar{x}, r^*)$,

$$\|DT(x)\|_{B(X,X)} \leq \max_{1 \leq m \leq M} \frac{1}{\eta_m} \sum_{i=1}^M \left(Z^1_{m,i} + \sum_{j=1}^M Z^2_{m,i,j} r_j \right) \eta_i,$$

and (4.13) yields that T is a contraction on $\mathrm{Box}(\bar{x}, r) \subset \mathcal{X}$, which is a closed set for $\|\cdot\|_{\mathcal{X}}$. □

This theorem can be directly applied to study any fixed point problem, or, as shown in Section 1.2.1, used to derive a Newton–Kantorovich Theorem by studying a specific quasi-Newton fixed point associated to a zero finding problem. As mentioned earlier, the bounds Y_m, $Z^1_{m,i}$, and $Z^2_{m,i,j}$ are the ones that one has to estimate anyway, and Theorem 4.2.3 is just about combining them a posteriori in a somewhat optimal way to obtain a contraction.

Remark 4.2.4. *Since Theorem 4.2.3 decouples the choice of the set and the choice of the norm, one can first solve for the set only, i.e. try to find r satisfying (4.12), and then solve for the norm, i.e. try to find η satisfying (4.13).*

If there exists an open set of $r \in \mathbb{R}^M_{>0}$ satisfying (4.12), then by convexity the smallest one can be found by simply solving for the equality case with Newton's method, starting from $r = 0$. Once an r satisfying (4.12) is selected, note that (4.13) is equivalent to finding a vector $\eta \in \mathbb{R}^M_{>0}$ such that $Z\eta < \eta$, where the matrix Z has nonnegative entries $Z_{m,i} := Z^1_{m,i} + \sum_{j=1}^M Z^2_{m,i,j} r_j$. Assuming for simplicity that all the $Z_{m,i}$ are in fact positive, by the Perron-Frobenuis theorem there exists $\eta \in \mathbb{R}^M_{>0}$ satisfying (4.13) if and only if the spectral radius $\rho(Z) < 1$, in which case the positive Perron-Frobenuis eigenvector provides a suitable η.

Finally, let us note that we typically do not even need an explicit η, as the error bound between $\bar{x}$ and the fixed point of T provided by Theorem 4.2.3, namely

$$\|x_m - \bar{x}_m\|_{\mathcal{X}_m} \leq r_m \qquad \text{for all } 1 \leq m \leq M,$$

only depends on r.

4.2.5 Results

Using the domain decomposition approach introduced in Section 4.2.3, together with the fixed point theorem 4.2.3, we can rigorously integrate various parabolic PDEs. In all the examples below, $\mathbb{T}_L$ denotes the one dimensional torus of length L, i.e., $\mathbb{R}/(L\mathbb{Z})$.

Theorem 4.2.5. *Consider the Swift–Hohenberg equation*

$$\begin{cases} \dfrac{\partial u}{\partial t} = -\left(\dfrac{\partial^2}{\partial x^2} + 1\right)^2 u + \rho u - u^3, & t \in (0,\tau],\ x \in \mathbb{T}_L, \\ u(0,x) = u^{in}(x), & x \in \mathbb{T}_L, \end{cases} \tag{4.15}$$

with $\rho = 5$, $L = 6\pi$, $\tau = 3/2$, and $u^{in}(x) = 0.4\cos\left(\frac{2\pi x}{L}\right) - 0.3\cos\left(\frac{4\pi x}{L}\right)$. Let $\bar{u} = \bar{u}(t,x)$ be the function represented in Figure 4.1, and whose precise description in terms of Fourier-Chebyshev coefficients can be downloaded at [Code 2]. Then, there exists a smooth solution u of (4.15) such that

$$\sup_{t\in[0,\tau]} \sup_{x\in\mathbb{T}_L} |u(t,x) - \bar{u}(t,x)| \leq 4 \times 10^{-8}.$$

Theorem 4.2.6. *Consider the Kuramoto–Sivashinsky equation*

$$\begin{cases} \dfrac{\partial u}{\partial t} = -\dfrac{\partial^4 u}{\partial x^4} - \dfrac{\partial^2 u}{\partial x^2} - \dfrac{1}{2}\dfrac{\partial}{\partial x} u^2, & t \in (0,\tau],\ x \in \mathbb{T}_L, \\ u(0,x) = u^{in}(x), & x \in \mathbb{T}_L, \end{cases} \tag{4.16}$$

with $L = 5\pi$, $\tau = 12$, and $u^{in}(x) = -\sin\left(\frac{2\pi x}{L}\right)$. Let $\bar{u} = \bar{u}(t,x)$ be the function represented in Figure 4.2, and whose precise description in terms of Fourier-Chebyshev coefficients can be downloaded at [Code 2]. Then, there exists a smooth solution u of (4.16) such that

$$\sup_{t\in[0,\tau]} \sup_{x\in\mathbb{T}_L} |u(t,x) - \bar{u}(t,x)| \leq 4 \times 10^{-7}.$$

Theorem 4.2.7. *Consider the Ohta-Kawasaki equation*

$$\begin{cases} \dfrac{\partial u}{\partial t} = -\dfrac{1}{\gamma^2}\dfrac{\partial^4 u}{\partial x^4} - \dfrac{\partial^2}{\partial x^2}(u - u^3) - \sigma(u - m), & t \in (0,\tau],\ x \in \mathbb{T}_L, \\ u(0,x) = u^{in}(x), & x \in \mathbb{T}_L, \end{cases} \tag{4.17}$$

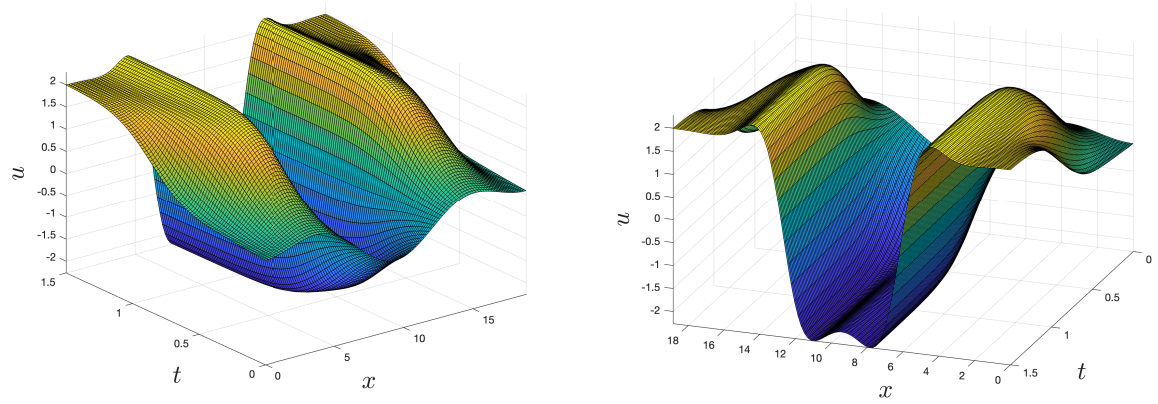

Figure 4.1: The approximate solution $\bar{u}$ of (4.15), which has been validated in Theorem 4.2.5, depicted twice with different views.

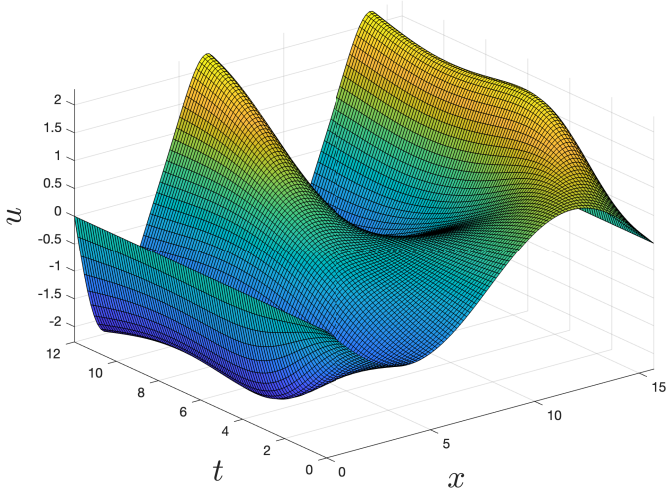

Figure 4.2: The approximate solution $\bar{u}$ of (4.16), which has been validated in Theorem 4.2.6.

with $\gamma = \sqrt{8}$, $\sigma = 1/5$, $m = 1/10$, $L = 2\pi$, $\tau = 5$, *and* $u^{in}(x) = m + \frac{1}{10}\cos\left(\frac{2\pi x}{L}\right)$. *Let* $\bar{u} = \bar{u}(t,x)$ *be the function represented in Figure 4.3, and whose precise description in terms of Fourier-Chebyshev coefficients can be downloaded at [Code 2]. Then, there exists a smooth solution* u *of* (4.17) *such that*

$$\sup_{t\in[0,\tau]} \sup_{x\in\mathbb{T}_L} |u(t,x) - \bar{u}(t,x)| \leq 3 \times 10^{-3}.$$

As these theorems were first obtained in [B4], their proof in fact uses a setup which is more complicated than the one presented in Section 4.2, as we still used an approximate inverse (see Remark 4.2.1). For instance, this means the proof of Theorem 4.2.7 required computing and storing a matrix of size approximately $50,000 \times 50,000$. However, as explained in Remark 4.2.1, we later realized that such approximate inverse could be removed, which means Theorem 4.2.7 can now easily be proved on a laptop.

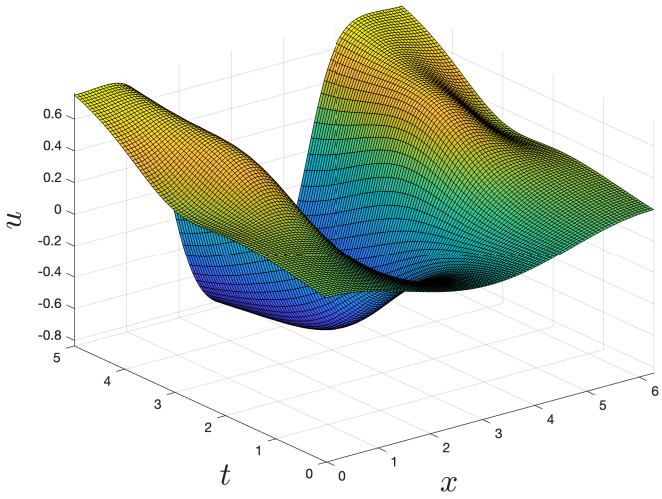

Figure 4.3: The approximate solution $\bar{u}$ of (4.17), which has been validated in Theorem 4.2.7.

4.3 Perspectives

- **Computer-assisted proofs for connecting orbits in parabolic PDEs.** As mentioned earlier, the main motivation for the development of this rigorous integrator is to then be able to obtain computer-assisted proofs of connecting orbits in parabolic PDEs. This is the subject of ongoing works with Jan Bouwe van den Berg, Matthieu Cadiot, Jonathan Jaquette, Jean-Philippe Lessard, Jason Mireles James and Akitoshi Takayasu. Beyond having to connect this integrator or others with the works [253, 290], where computer-assisted proofs for local stable and unstable manifolds are provided, one of the challenges is to understand how one can retain the feature of having a contracting fixed point without a heavy numerical approximate inverse, even though the coupling between the integrator and the manifolds results in a much more involved structure.

- **Links with previous chapters.** Extensions and further objectives that were already mentioned in previous chapters include: extending the ideas developed in this chapter and combining them with those of Section 3.3 in order to rigorously integrate PDEs of the form

$$\partial_t u = \partial_{xx} u + V(x)\partial_x u + g(u),$$

  posed on the whole space $\mathbb{R}^d$, and proving the existence of a homoclinic orbit to a periodic orbit in the Navier–Stokes equations, which is a long term goal still requiring many new developments.

- **A rigorous integrator for cross-diffusion systems.** Another extension of interest would be to rigorously integrate cross-diffusion systems like the SKT model (3.1), and in particular to study its connecting orbits, in order to better describe the intricate global dynamics generated by the presence of many co-existing steady states. Compared to the equations of the form (4.1) studied in this chapter, the nonlinear diffusion structure generates severe additional difficulties, and the strategy proposed in Section 3.1 to study the steady state problem does not seem adequate for dealing with the time evolution: new ideas are required here.

Chapter 5

Rigorous continuation

5.1 Context

Understanding the influence of parameters is crucial when studying the global dynamics of ODEs, PDEs, or other dynamical systems. Even for fixed parameters, fully characterizing the global dynamics of a given nonlinear system is usually very challenging. As a first step, one can study simple invariant sets such as steady states, periodic orbits, invariant manifold attached to them, connecting orbits between them, etc, as these specific solutions often act as *building blocks* for the global dynamics. Once such solutions are found for fixed parameters, one can try to study how they evolve with respect to (some of) the parameters.

This question can be investigated numerically, as there exists many powerful softwares allowing to do numerical continuation and bifurcation analysis for ODEs [102, 99, 90], PDEs [284] and even DDEs [112]. Using these tools, one can obtain very informative bifurcation diagrams, displaying bifurcations and branches of invariant sets. Regarding rigorous results, while the mathematical theory of continuation and bifurcation is well established [193, 147], and is at the heart of the aforementioned softwares, applying it rigorously to a given nonlinear differential equation can be difficult, especially when trying to continue or to bifurcate from a nontrivial solution, whose existence might already be challenging to establish by pen-and-paper techniques.

In this chapter, we discuss how computer-assisted proofs can be extended to handle continuation problems. This is by no mean the first work on that question, and we in fact build upon many previous results [249, 92, 5, 292, B23, 138, 307].

In order to make the discussion more precise, let us consider a compact parameter space $\Lambda \subset \mathbb{R}^d$, two Banach spaces $\mathcal{X}$ and $\mathcal{Y}$, and a smooth map $F : \Lambda \times \mathcal{X} \to \mathcal{Y}$ defining a continuation problem of the form

$$F(\lambda, x) = 0. \tag{5.1}$$

Assume we are given an approximate branch of solutions $\lambda \mapsto \bar{x}(\lambda)$ (or a higher dimensional manifold of solutions if $d > 1$), obtained for instance using some numerical continuation software. The goal of these computer-assisted techniques is to prove a posteriori that there exists a genuine branch of solutions, i.e., a map $\lambda \mapsto x(\lambda)$ such that $F(\lambda, x(\lambda)) = 0$, in a small and explicit neighborhood of the branch of approximate solutions $\bar{x}$. In the sequel, we refer to such methods as *rigorous continuation techniques*. Among the benefit of these techniques, let us mention that they provide local uniqueness of the solution along the branch, hence they can be used to prove that there is no bifurcation[1] along a given branch, which can never be completely ruled out when using purely numerical continuation tools.

[1] To be precise, what one can prove is that there is no bifurcation with the same type of solutions. That is, if we rigorously validate a branch of steady states for a given problem, it proves that each steady state is locally unique, hence there cannot be a transcritical or pitchfork bifurcation on that branch, but this does not prevent the existence of a Hopf bifurcation leading to a branch of periodic orbits.

Rigorous continuation techniques were already used successfully in many contexts, yielding for instance a complete description of the attractor of the Swift–Hohenberg equation [92], uniqueness results for a parameter-dependent family of semilinear elliptic equations [218, 219], an exhaustive description of a bifurcation diagram in the Kuramoto–Sivashinsky equation [5], the resolution of conjectures about the existence of slowly oscillating periodic solutions in a DDE [200, 289, 170] and progress about another conjecture concerning existence of traveling waves in a fourth order PDE [B2], or the rigorous computation of a bifurcation diagram delimiting energy minimizers for diblock copolymers [297]. The above list is by no mean exhaustive, but hopefully helps emphasize that rigorous continuation techniques are important and useful.

We now review some of the main features shared by most existing rigorous continuation techniques until very recently. For the sake of simplifying the discussion, we assume first that $d = 1$. For a fixed parameter value $\lambda_0 \in \mathbb{R}$, suppose we have an approximate zero $\bar{x}_0$ of $F(\lambda_0, \cdot)$, and we have proven the existence of a nearby exact zero by successfully applying the Newton–Kantorovich Theorem 1.2.2. Since F is continuous with respect to λ, the estimates Y, Z_1 and Z_2 typically also are continuous with respect to λ. Therefore, since the conditions (1.5)-(1.7) hold for $\lambda = \lambda_0$ and $\bar{x} = \bar{x}_0$, they also holds for all λ in neighborhood of λ_0, hence we can replace the contraction mapping theorem by the *uniform* contraction mapping theorem, and immediately get the existence of a curve of solutions $\lambda \mapsto x(\lambda)$ close to the constant approximate solution curve $\lambda \mapsto \bar{x}_0$. In practice, this can be accomplished very simply by replacing the floating point number λ_0 by an interval λ, as evaluating the bounds with interval arithmetic then takes care of the rest. Of course, this approach is rather crude, and is only likely to succeed if the interval λ is taken small. In order to get slightly larger chunks of solution curve, what is typically done in the literature on rigorous continuation techniques is to take two nearby parameters λ_0 and λ_1, two corresponding approximate solutions $\bar{x}_0$ and $\bar{x}_1$, and to interpolate linearly between the two: $\bar{x}(\lambda) := \bar{x}_0 + \frac{\lambda-\lambda_0}{\lambda_1-\lambda_0}(\bar{x}_1 - \bar{x}_0)$, in order to have an approximate solution that is hopefully more accurate for all λ in $[\lambda_0, \lambda_1]$.[2] In most cases, the approximate inverse A is still taken constant for λ in $[\lambda_0, \lambda_1]$, but linear interpolation for A has also been used [294]. One then has to carefully track by hand λ dependencies in all the estimates, in order to derive uniform Y, Z_1 and Z_2 bounds for λ in $[\lambda_0, \lambda_1]$. In practice, this still leads to relatively small portions of solution curves, and what is then done is to repeat the argument over many small intervals, and to additionally check that all the small pieces glue together. That is, the global solution branch is obtained using a piece-wise linear approximation and a combination of local proofs. This approach can and has been extended to two-dimensional manifolds of solutions (i.e., to continuation with respect to two parameters), but the required adaptations are rather technically involved, and in practice the validation procedure is computationally expensive [138, 77].

5.2 A higher order rigorous continuation approach

Recently, an alternative approach for conducting rigorous continuation was independently proposed in [4, B8]. In contrast to the previous literature, these two works use a global, high order approximation of the solution curve, based on Taylor expansions in [4], and on Chebyshev expansions in [B8]. This new approach allows for several significant improvements over the existing low-order and local rigorous continuation techniques. We first give a high level description of some of the main features of this new approach below, before giving a more concrete and precise presentation in Section 5.3.

- The seemingly natural space in which to derive continuation estimates is $C^0(\Lambda, \mathcal{X})$, the space of continuous functions over Λ with values in $\mathcal{X}$, as we want to apply the uniform contraction mapping theorem on $\mathcal{X}$. However, going from punctual estimates in $\mathcal{X}$ (for a

[2] Alternatively, one can also use a single approximate solution and an approximate tangent vector in order to define an approximate solution for nearby values of λ [307].

fixed λ) to estimates in $C^0(\Lambda, \mathcal{X})$ typically requires rather straightforward but painstaking calculations. On the other hand, the high order approximations based on series expansions suggest to instead derive the continuation estimates in $\ell^1_\eta(\mathcal{X})$, a subspace of $\mathcal{X}^{\mathbb{N}}$ introduced in Chapter 0, with a weighted ℓ^1 norm which is stronger than the C^0 norm. In this setting, the continuation estimates can be obtained as very straightforward generalizations of the punctual estimates, in particular because operator norms on $\ell^1_\eta(\mathcal{X})$ are easy to control.

- For punctual computer-assisted proofs, a crucial role is often played by a finite dimensional subspace, say of dimension N, used to represent the approximate solution and to build the finite part $A^{\leq N}$ of the approximate inverse A,[3] see for instance Section 1.3.1.2. In that context, the practical bottleneck of the computer-assisted proof is often related to how large N must be, as one then has to manipulate matrices with N^2 entries. When using a series expansion in the λ variable, one has to introduce another finite dimensional subspace, say of dimension K, corresponding to finite series that will be manipulated by the computer, and combining the two in a naive way leads to matrices of size N^2K^2. However, with Chebyshev (or Taylor) series, we can use the FFT for computing many operations such as multiplication, evaluation or interpolation of Chebyshev series. By leveraging these properties in a systematic way, we construct rigorous continuations algorithms which only deal with matrices of size at most N^2K instead of N^2K^2.

- If F is smooth enough, one can in principle use the implicit function theorem to control derivatives of $\lambda \mapsto x(\lambda)$. However, starting from the C^0 control provided by the rigorous continuation procedure and getting *explicit* estimates on derivatives of x this way requires extra work [5], especially if several derivatives are required. Doing rigorous continuation in $\ell^1_\eta(\mathcal{X})$ directly provides us with analytic regularity for $\lambda \mapsto x(\lambda)$, from which the obtention of explicit estimates for any derivative becomes straightforward.

- Last but not least, rigorous continuation in $\ell^1_\eta(\mathcal{X})$ generalizes trivially to multi-parameter continuation [B8], yielding an approach which is both simpler and more efficient than the two-parameters setting from [138]. The latter might seem more flexible at first glance, as it is based on a fine triangulation of the surface of solutions together with local validation on each triangle, and can therefore deal with parameter spaces of arbitrary shapes. Although multivariate Chebyshev series are naturally defined on (hyper-)rectangles, we will showcase that one can in fact embed those into arbitrary shapes without difficulty.

- Our approach can also be seen as a generalization of previous first order rigorous continuation techniques. Indeed, we develop a framework for performing continuation with a Chebyshev expansion of arbitrary order K in the parameter, and the case $K = 1$ in fact corresponds to what was done in these earlier works, but even in that case our new framework allows for a simpler presentation.

5.3 Chebyshev continuation

We now describe the new rigorous continuation framework proposed in [B8]. As a pedagogical example, we first study an algebraic equation, which can be seen as a continuation problem of the form (5.1) where $\mathcal{X}$ is simply $\mathbb{R}$, before moving on the the more involved case where $\mathcal{X}$ is infinite dimensional.

Remark 5.3.1. *In the more involved examples to come of Section 5.3.2, we will have several weighted ℓ^1 spaces of rather different nature:*

[3] In principle, one could use two subspaces of different dimension for the approximate solution and for constructing A, but in order to simplify the discussion we ignore this possibility here.

1. *The ℓ^1 spaces corresponding to functions of the space variable x. In our case, these will be cosine series solutions respecting homogeneous Neumann boundary conditions, but in other contexts one could also have general Fourier series, Taylor series (e.g., for local (un)stable manifolds) or Chebyshev series.*

2. *The ℓ^1 spaces corresponding to functions of the continuation parameter λ, represented as Chebyshev series.*

In order to easily distinguish between the two without overburdening the notation too much, we make the convention of always using a weight called ν, i.e., ℓ^1_ν spaces, when dealing with functions of the space variable, and a weight called η, i.e., ℓ^1_η spaces, when dealing with functions of the parameter. Similarly, indices n and N are always related to expansions in space, whereas k and K are related to expansions in the parameter.

5.3.1 Solving algebraic equations using Chebyshev series

Let us focus here on a simple problem: finding a polynomial approximation, together with guaranteed error bounds, for the positive solution $x = x(\lambda)$ of

$$x^2 = \lambda, \qquad \lambda \in [1, 3].$$

We have already seen in Example 1.2.5 how to rigorously enclose the solution x to this problem for a fixed λ, and we now show how this can be extended, in a relatively straightforward way, to deal with functions of λ.

As we are going to use Chebyshev series, let us first rescale the problem, and consider

$$x(\lambda)^2 - (2 + \lambda) = 0, \quad \lambda \in [-1, 1]. \tag{5.2}$$

We are going to look for the solution $x = x(\lambda)$ to this problem as a Chebyshev series, in the space ℓ^1_η for some $\eta \geq 1$. Given an element x in ℓ^1_η, which, as explained in Chapter 0, we view either as a function or as a sequence of coefficients, we define the zero-finding problem

$$F(x) = x * x - g, \tag{5.3}$$

where $g = g(\lambda) = 2 + \lambda$, or equivalently $g = (2, 1/2, 0, 0, \ldots) \in \ell^1_\eta$. Our goal is to obtain a zero of F in ℓ^1_η, which will give us a function $x : [-1, 1] \to \mathbb{R}$ satisfying (5.2), by using the Newton Kantorovich Theorem 1.2.2, with F as in (5.3) and $\mathcal{X} = \ell^1_\eta$.

Our first task is to define an approximate zero $\bar{x} \in \ell^1_\eta$ of F. For $K \in \mathbb{N}_{\geq 1}$, we recall that the Chebyshev nodes (of the second kind) are given by

$$\lambda_k = \cos\left(\frac{k\pi}{K}\right), \quad k \in \{0, \ldots, K\}.$$

We consider for each k an approximate zero $\tilde{x}(\lambda_k) \in \mathbb{R}_{>0}$ of (5.2) with $\lambda = \lambda_k$, and construct $\bar{x}$ as the Lagrange interpolation polynomial of all the $\tilde{x}(\lambda_k)$'s. That is, $\bar{x}$ is a polynomial of degree at most K such that $\bar{x}(\lambda_k) = \tilde{x}(\lambda_k)$ for all $k \in \{0, \ldots, K\}$. In practice, we represent $\bar{x}$ in the Chebyshev basis, or equivalently, as a finite Chebyshev series

$$\bar{x}(\lambda) = \bar{x}_0 + 2\sum_{k=1}^{K} \bar{x}_k T_k(\lambda),$$

and its Chebyshev coefficients $(\bar{x}_k)_{0 \leq k \leq K}$ can then efficiently be obtained from the interpolation values $\tilde{x}(\lambda_k)$ by simply using the FFT. Note that $\bar{x}$ is just an approximate solution anyway, so this construction can be done with floating point arithmetic, as in general we do not need $\bar{x}$ to be the exact interpolation polynomial.

Now that we have an approximate zero $\bar{x}$, we need to construct an approximate inverse A to the linear operator $DF(\bar{x})$. However, $DF(\bar{x})$ is merely the multiplication operator $\mathcal{M}(2\bar{x})$. We can therefore easily get a very accurate approximation of $DF(\bar{x})^{-1}$, by considering $A = \mathcal{M}(\bar{y})$ where $\bar{y}$ is a finite Chebyshev series such that $\bar{y} \approx (2\bar{x})^{-1}$.[4] Such an $\bar{y}$ can again easily be obtained as a polynomial in the Chebyshev basis by interpolating the function $\lambda \mapsto (2\bar{x}(\lambda))^{-1}$ at Chebyshev nodes.

We are now reading to compute, this time rigorously

$$\begin{aligned} Y &= \|AF(\bar{x})\|_{\ell^1_\eta} = \left\|\bar{y} * (\bar{x}^2 - g)\right\|_{\ell^1_\eta} \\ Z_1 &= \|I - ADF(\bar{x})\|_{B(\ell^1_\eta,\ell^1_\eta)} = \|I - \mathcal{M}(\bar{y})\mathcal{M}(2\bar{x})\|_{B(\ell^1_\eta,\ell^1_\eta)} = \|1 - \bar{y} * (2\bar{x})\|_{\ell^1_\eta} \\ Z_2 &= 2\,\|A\|_{B(\ell^1_\eta,\ell^1_\eta)} = 2\,\|\bar{y}\|_{\ell^1_\eta}\,, \end{aligned}$$

in order to apply the Newton–Kantorovich Theorem 1.2.2 to F from (5.3). Note the similarities with the estimates for fixed λ derived in Example 1.2.5. Except for the fact that $\bar{y} * (2\bar{x})$ is not *exactly* equal to 1, the estimates are essentially the same, with products between real numbers and absolute values in Example 1.2.5 replaced by convolutions between elements of ℓ^1_η and ℓ^1_η-norms here.

Also, note that the quantities appearing in the bounds, like $\bar{y} * (\bar{x}^2 - g)$, can again be computed by combining calculations for fixed λ and interpolation. Indeed, assuming that both $\bar{x}$ and $\bar{y}$ are in $\Pi^{\leq K}\ell^1_\eta$, we know that $\bar{y} * (\bar{x}^2 - g)$ will be in $\Pi^{\leq 3K}\ell^1_\eta$, hence we can compute it by rigorously evaluating $\bar{y}(\lambda)(\bar{x}(\lambda)^2 - g(\lambda))$ for all λ on a Chebyshev grid of size $3K$ and then interpolating back (this time rigorously), to obtain the Chebyshev coefficients of $\bar{y} * (\bar{x}^2 - g)$, and finally compute its ℓ^1_η norm.

Example 5.3.2. *Approximating the square root function on* $[1, 3]$ *by its interpolation polynomial using* $K + 1$ *Chebyshev nodes (up to the numerical errors involved in the computation of* $\bar{x}$*, this is in fact what* $\bar{x}$ *is) should yield a very good approximation, already with moderate values of* K*. This is indeed confirmed when we execute the procedure described above, evaluate the bounds* Y*,* Z_1 *and* Z_2*, and compute the corresponding* $r_{\min}$ *in Theorem 1.2.2. With* $K = 2$*, and* $\eta = 1$*, we already have that* $\|\bar{x} - x\|_{\ell^1_\eta} \leq 9 \times 10^{-3}$*, and with* $K = 20$ *we get* $\|\bar{x} - x\|_{\ell^1_\eta} \leq 7 \times 10^{-13}$*. The entire procedure can be reproduced by running the code available at [Code 8].*

We emphasize that the whole procedure (obtaining the approximate solution $\bar{x}$, constructing A, and evaluating the bounds) only requires repeated punctual calculations, i.e., calculations for fixed values of the parameter λ, and interpolation to combine them together. In particular, if we do know how to deal with the punctual problem, then we have all we need to handle the continuation problem, and the cost of the continuation only scales linearly with the order K used for the expansion in λ in terms of memory requirement, and like $K \ln K$ in terms of numbers of operations (provided we use the FFT for evaluation and interpolation at Chebyshev nodes).

5.3.2 Back to infinite dimensional problems

We now showcase that the procedure described in the previous subsection is very robust, and can also easily be applied to situations where the punctual problem is already infinite dimensional. Indeed, let us revisit the example of the Swift–Hohenberg eqation, and in particular the proof of a solution for a fixed parameter that was presented in Section 1.3.1. We now try to validate entire branches of steady states. We again start by normalizing the parameter: Given an interval $[\rho_{\min}, \rho_{\max}]$ within which we want to let ρ vary, we write $\rho = \frac{\rho_{\min}+\rho_{\max}}{2} + \frac{\rho_{\max}-\rho_{\min}}{2}\lambda$, where $\lambda \in [-1, 1]$ is the normalized parameter.

[4] If $x \in \ell^1_\eta$ and $x(\lambda) \neq 0$ for all $\lambda \in [-1, 1]$, we know by Wiener's $1/f$ theorem that x is indeed invertible in ℓ^1_η, provided $\eta \geq 1$ is small enough so that x does not vanish on the Bernstein ellipse $\mathcal{E}_\eta$.

For a fixed ρ, we described in Section 1.3.1 steady states as elements u of $\ell^1_\nu(\mathbb{R})$ representing cosine series, where we emphasize in the notation that each Fourier coefficient u_n of u belongs to the field $\mathbb{R}$. If we now let ρ (or equivalently λ) vary, each coefficient u_n of the steady state becomes a function $u_n = u_n(\lambda)$. As suggested in the previous subsection, we will look for such functions in an $\ell^1_\eta(\mathbb{R})$ space representing Chebyshev series. That is, we look for a branch of steady states in the space $\ell^1_\nu(\ell^1_\eta(\mathbb{R}))$ of Fourier series u whose Fourier coefficients u_n are themselves Chebyshev series, i.e., $u_n = (u_{n,k})_{k\in\mathbb{N}}$ and such that

$$\|u\|_{\ell^1_\nu(\ell^1_\eta)} := \|u_0\|_{\ell^1_\eta} + 2\sum_{n\geq 1} \|u_n\|_{\ell^1_\eta}\, \nu^n < \infty,$$

where, for all $n \in \mathbb{N}$,

$$\|u_n\|_{\ell^1_\eta} = |u_{n,0}| + 2\sum_{k=1}^{\infty} |u_{n,k}|\, \eta^k.$$

Remark 5.3.3. *At an abstract level, the reason the estimates for validating the whole branch are going to be very similar to those for validating a single steady state is that, for the validation of a single steady state, we in fact never crucially used that the $\mathbb{R}$ in $\ell^1_\nu(\mathbb{R})$ was a field, but only that it was a commutative Banach algebra.*[5] *The same estimates can therefore be reproduced almost verbatim when $\mathbb{R}$ is replaced by any commutative Banach algebra, and in particular by $\ell^1_\eta(\mathbb{R})$.*

Note that the space $\ell^1_\nu(\ell^1_\eta(\mathbb{R}))$ can be identified with the space $\ell^1_\eta(\ell^1_\nu(\mathbb{R}))$ (they are isometrically isomorphic), which brings us back to the viewpoint presented in Section 5.2: we try to solve the continuation problem in $\ell^1_\eta(\mathcal{X})$, where $\mathcal{X}$ is the space in which we solved the problem for a fixed parameter value.

We now proceed as in Section 5.3.1 in order to validate an entire branch of steady states of (1.18)-(1.19). We consider the space $\mathcal{X} = \ell^1_\nu(\ell^1_\eta(\mathbb{R}))$ and the map

$$F(u) = -(1+\Delta)^2 u + \rho u - u^3,$$

defined on that space. We then construct an approximate branch of steady states $\bar{u}$ belonging to $\Pi^{\leq N}\ell^1_\nu\left(\Pi^{\leq K}\ell^1_\eta\right)$ by interpolating between approximate steady states $\tilde{u}(\lambda_k)$ in $\Pi^{\leq N}\ell^1_\nu(\mathbb{R})$, obtained for fixed values λ_k of λ. For each λ_k, we also compute the finite part of an approximate inverse, i.e. an $(N+1)\times(N+1)$ matrix $\tilde{A}^{\leq N}(\lambda_k)$ with real entries. We then interpolate between those, which yields a $(N+1)\times(N+1)$ matrix denoted $A^{\leq N}$, where each entry is a vector of $K+1$ real numbers, representing an element of $\Pi^{\leq K}\ell^1_\eta$: For each $i,j \in \{0,1\ldots,N\}$, $\left(A^{\leq N}\right)_{i,j} \in \ell^1_\eta$. This matrix $A^{\leq N}$ can then be interpreted as a linear operator on $\Pi^{\leq N}\ell^1_\nu\left(\ell^1_\eta\right)$, by considering for each $\left(A^{\leq N}\right)_{i,j} \in \ell^1_\eta$ the associated multiplication operator on ℓ^1_η.

Remark 5.3.4. *We emphasize that we never need to actually build all these multiplications operators in practice, because we can always go via evaluation and interpolation, as in Section 5.3.1. For instance, suppose we have to compute $A^{\leq N}\bar{v}$, where $\bar{v}$ belongs to $\Pi^{\leq N}\ell^1_\nu(\Pi^{\leq K}\ell^1_\eta)$. For all λ on a Chebyshev grid of size $2K$, we first evaluate $A^{\leq N}(\lambda)$ (which, for fixed λ, is again an $(N+1)\times(N+1)$ matrix with real entries) and $\bar{v}(\lambda)$ (a vector of size $N+1$), and compute the product $A^{\leq N}(\lambda)\bar{v}(\lambda)$. We then interpolate between all the taken λ's in order to recover the Chebyshev coefficients of $A^{\leq N}\bar{v}$.*

For the tail part of A, we keep the same definition as in Section 1.3.1.2, which does not depend on ρ. We are now ready to derive estimates Y, Z_1 and Z_2, for the above map F

[5] The fact that at least some elements are invertible, although not explicitly needed, is still important because it explains why we can expect to build a suitable approximate inverse A

defined on $\mathcal{X} = \ell^1_\nu(\ell^1_\eta(\mathbb{R}))$. We can replicate almost verbatim the estimates from Section 1.3.1.3, thanks to the fact that, as was $\ell^1_\nu(\mathbb{R})$, $\ell^1_\nu(\ell^1_\eta(\mathbb{R}))$ is still a Banach algebra. Denoting once more $B = I - ADF(\bar{u})$, we end up with

$$Y = \|AF(\bar{u})\|_{\ell^1_\nu(\ell^1_\eta)},$$

$$Z_1 = \max\left(\max_{0\le j\le 3N}\frac{1}{\xi_j}\sum_{i\in\mathbb{N}}\|B_{i,j}\|_{\mathcal{B}(\ell^1_\eta,\ell^1_\eta)}\,\xi_j,\ \frac{1}{((N+1)^2-1)^2}\left\|\rho-3\bar{u}^2\right\|_{\ell^1_\nu(\ell^1_\eta)}\right),$$

$$Z_2 = 3\,\|A\|_{\mathcal{B}\left(\ell^1_\nu(\ell^1_\eta),\ell^1_\nu(\ell^1_\eta)\right)}\left(2\,\|\bar{u}\|_{\ell^1_\nu(\ell^1_\eta)} + r^*\right).$$

As already shown on the simple example of Section 5.3.1, and further illustrated in Remark 5.3.4, all these estimates can in fact be evaluated by doing repeated computations for different values of λ and then interpolating. Here is an example of the type of results that can be obtained with this approach.

Theorem 5.3.5. *Consider $[\rho_{\min},\rho_{\max}] = [1.3, 4.5]$, and the branch of approximate steady states $\bar{u}$ represented in blue in Figure 5.1, whose precise description in terms of Cosine×Chebyshev coefficients can be downloaded at [Code 6]. Take also $\nu = \eta = 1$.*

There exists a zero u of F in $\mathcal{X} = \ell^1_\nu(\ell^1_\eta(\mathbb{R}))$, i.e., an isolated curve of steady states of the Swift–Hohenberg equation (1.18)-(1.19) for $\rho \in [1.3, 4.5]$, such that $\|\bar{u} - u\|_{\mathcal{X}} \le 3.8\times 10^{-4}$.

Remark 5.3.6. *Only 15 Chebyshev interpolation nodes, i.e. $K = 14$, were needed in order to validate the entire branch, and a smaller error bound could easily have been obtained by taking K larger.*

As already highlighted earlier, one of the strength of rigorous continuations methods is that they guarantee that each solution along the branch is locally unique: hence, we have a proof that there is no bifurcation of steady states along the validated portion of the branch.

Everything that we discussed in this chapter using Chebyshev series could also be accomplished using Taylor series, which is what is done in [4]. However, because Chebyshev series have better global approximating properties than Taylor series, the validation is typically cheaper using Chebyshev series. For the branch validated in Theorem 5.3.5, in order to at least get a successful proof using Taylor series, one would need to use $K = 46$, and even $K = 71$ in order to get a similar error bounds, compared to $K = 14$ with Chebyshev series. Further examples and comparisons, leading to the same conclusions, can be found in [B8].

We took $\eta = 1$ in the proof of Theorem 5.3.5 because we only cared about a $\mathcal{C}^0$ enclosure of the branch here, but another advantage of this new rigorous continuation approach is that we can take $\eta > 1$ and then get an analtyic enclosure of the branch, and in particular explicitly control any number of derivatives with respect to the parameter. Here are some examples of explicit bounds, which were obtained and used in [B5, Section 5.2].

Lemma 5.3.7. *Let $\eta > 1$, and $u \in \ell^1_\eta(\mathbb{N},\mathbb{R})$, identified with the map*

$$u : \lambda \mapsto u_0 + 2\sum_{k=1}^{\infty} u_k T_k(\lambda), \qquad \lambda \in [-1, 1].$$

For all $x \in [0, 1]$, let

$$\delta[x,\eta] = \begin{cases} \frac{\eta+\eta^{-1}}{2} - x & x > \frac{2}{\eta+\eta^{-1}}, \\ \frac{\eta-\eta^{-1}}{2}\sqrt{1-x^2} & \text{otherwise.} \end{cases}$$

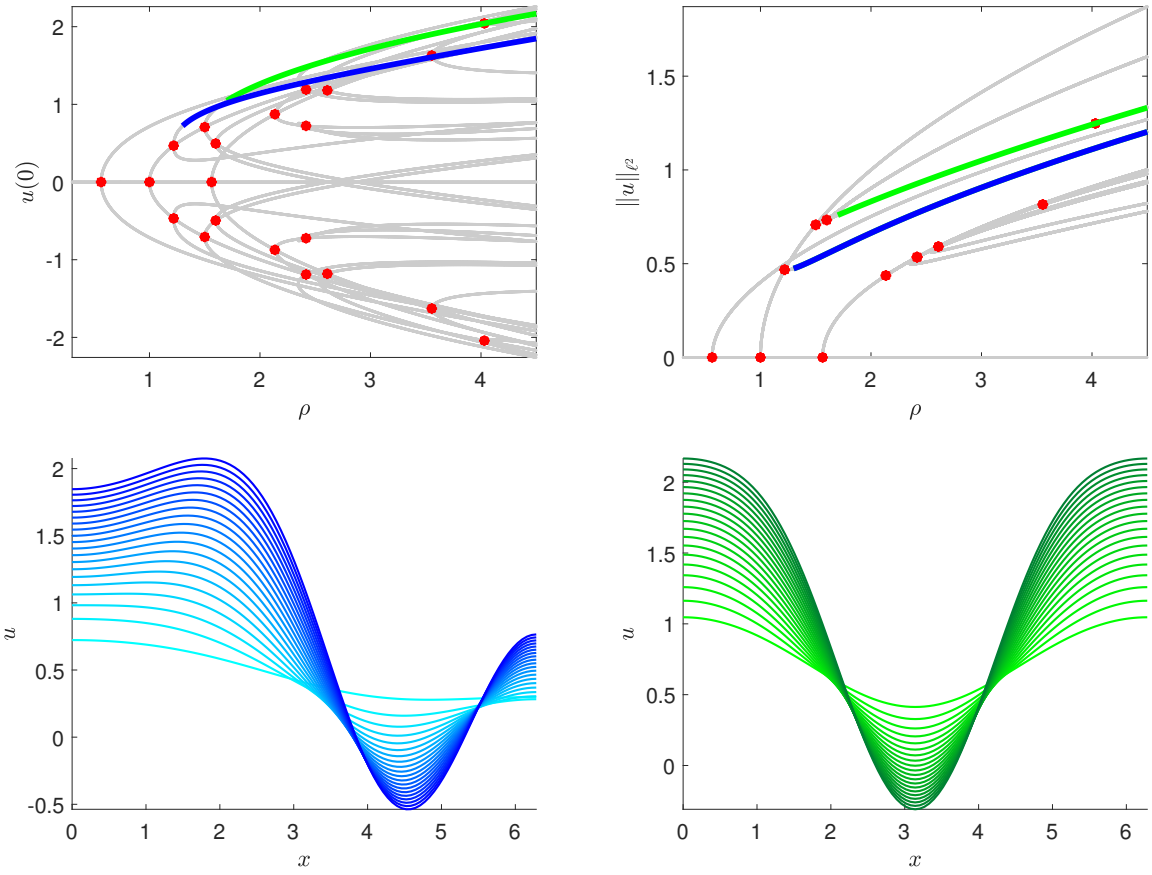

Figure 5.1: At the top is a numerical bifurcation diagram of steady states of the Swift–Hohenberg equation (1.18)-(1.19), displayed with two different projections: the value of u at 0 on the left, and the ℓ^2 norm of u on the right. Two specific portions of branches are highlighted in blue and green on the bifurcation diagrams, and several solutions along these branches are represented at the bottom (left for the blue branch and right for the green one). Regarding the solutions at the bottom, the lighter the color the smaller the corresponding value of ρ. The whole blue branch has been validated in Theorem 5.3.5. The validation of green branch failed, which is coherent with the fact that numerics suggest the presence of a bifurcation across that branch.

For all $\lambda_1, \lambda_2 \in [-1,1]$, $\lambda_1 \leq \lambda_2$, define

$$C^1_\eta(\lambda_1,\lambda_2) = \min\left(\max_{\substack{k\in\mathbb{N}\\ 1\leq k\leq \frac{2}{\ln\eta}}} \frac{k^2}{\eta^k},\ \frac{1}{\delta[\max(|\lambda_1|,|\lambda_2|),\eta]}\right),$$

$$C^2_\eta(\lambda_1,\lambda_2) = \min\left(\max_{\substack{k\in\mathbb{N}\\ 2\leq k\leq \frac{4}{\ln\eta}}} \frac{k^2(k^2-1)}{3\eta^k},\ \frac{2}{(\delta[\max(|\lambda_1|,|\lambda_2|),\eta])^2}\right).$$

Then, the map u is twice differentiable, and

$$\sup_{\lambda\in[\lambda_1,\lambda_2]} \left|u'(\lambda)\right| \leq C^1_\eta(\lambda_1,\lambda_2)\,\|u\|_{\ell^1_\eta}, \qquad \sup_{\lambda\in[\lambda_1,\lambda_2]} \left|u''(\lambda)\right| \leq C^2_\eta(\lambda_1,\lambda_2)\,\|u\|_{\ell^1_\eta}.$$

5.3.3 Multi-parameter continuation

The last aspect which makes this new setup for rigorous continuation so appealing is that multi-parameter continuation becomes completely straightforward, at least regarding the estimates, and mostly also implementation-wise (of course, if the dimension of the parameter space becomes too large, then the computational cost can still be an issue). Indeed, if we want to vary, say, two parameters, we simply consider a Chebyshev expansion in each of them, and the associated sequence space $\ell^1_\eta\left(\mathbb{N}, \ell^1_\eta(\mathbb{N},\mathbb{R})\right) \simeq \ell^1_\eta\left(\mathbb{N}^2,\mathbb{R}\right)$, and similarly for an arbitrary number d of parameters. Since this space is still a Banach algebra, all the estimates are then exactly the same as in the one-parameter case, except we have a different norm. As an example, let us add an extra parameter to the Swift–Hohenberg equation, and consider

$$\partial_t u = -(1+\Delta)^2 u + \rho u - \beta u^3, \tag{5.4}$$

still with homogeneous Neumann boundary conditions.

Theorem 5.3.8. *Consider* $[\rho_{\min},\rho_{\max}] = [2,4]$, $[\beta_{\min},\beta_{\max}] = [0.25,1.75]$, *and the surface of approximate steady states* $\bar{u}$ *represented in Figure 5.2, whose precise description in terms of Cosine×Chebyshev×Chebyshev coefficients can be downloaded at [Code 6]. Take also* $\nu = \eta = 1$.

There exists a zero u *of* F *in* $\mathcal{X} = \ell^1_\nu(\ell^1_\eta(\ell^1_\eta(\mathbb{R}))$, *i.e., an isolated surface of steady states of the Swift–Hohenberg equation (5.4)-(1.19) for* $(\rho,\beta) \in [2,4]\times[0.25,1.75]$, *such that* $\|\bar{u}-u\|_{\mathcal{X}} \leq 5\times 10^{-3}$.

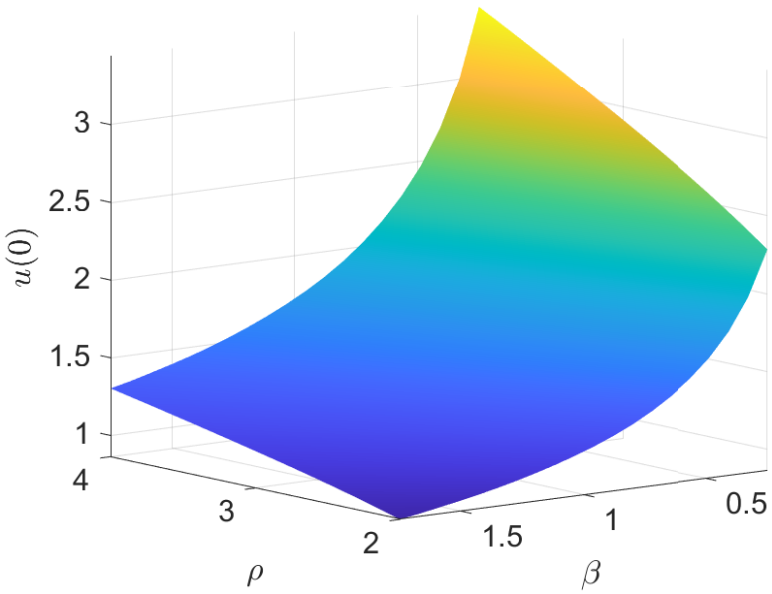

Figure 5.2: A 2-dimensional manifold of approximate steady states of Swift–Hohenberg equation (5.4)-(1.19), displayed using the $u(0)$ projection, and validated in Theorem 5.3.8.

5.4 Perspectives

- **Rigorous pseudo-arclength continuation.** One important aspect which was left unexplored in [B8] is that of pseudo-arclength continuation. The techniques presented in this chapter can clearly be used in the context of pseudo-arclength continuation, but there is no longer a canonical way to pick the interpolation points, and this raises interesting questions regarding how to optimize this choice. For a single parameter this might not be such

an important issue, but for multi-parameter continuation, and highly non-flat manifolds of solutions, the choice of how to parametrize these manifold from the (hyper-)rectangles where the Chebyshev nodes naturally lie may have a significant impact on the cost of the validation. Some of these questions are currently being investigated in collaboration with Oliver Hénot, Jean-Philippe Lessard and Alessandro Pugliese.

- **Combining Chebyshev continuation with FEM-based computer-assisted proofs.** In principle, the rigorous continuation approach proposed in this chapter can be used as soon as computer-assisted proofs based on the Newton–Kantorovich Theorem 1.2.2 can be done for fixed parameter values. When these punctual proofs rely on sequence spaces that are Banach algebras, which is the case we focused on here, we have extra structural properties which simplify (both theoretically and practically) the continuation setup. It would be interesting to investigate whether such high order rigorous continuation based on Chebyshev expansion could also be efficiently used in combination with punctual computer-assisted proofs based on finite elements.

- **Rigorous study of the bifurcation points.** As highlighted with the example described in Figure 5.1, the rigorous continuation techniques discussed here can only apply to branches (or to higher dimensional manifolds) of solutions that do not contain bifurcations. Nonetheless, studying these bifurcations is also of great interest, and computer-assisted proofs can also be helpful for that, especially when the bifurcation occurs at a non-trivial solution. One existing approach which could be rather directly connected to the techniques of this chapter consists in desingularizing or blowing up the bifurcation in order to recover locally unique curves (see, e.g., [293, 4] and the references therein). Another option is to set up a so-called *extended zero-finding problem*, whose solutions are bifurcation points of a certain type (see, e.g., [205, 256] and the references therein). Both approaches require having a good enough understanding of the underlying bifurcation, in order to choose a suitable desingularization, or to introduce an appropriate extended zero-finding problem. In collaboration with Evelyn Sander and Thomas Wanner, we are currently developing a general framework for a large class of transcritial and symmetry breaking bifurcations occurring in the SKT system (3.1), with the long term goal of providing a complete and fully rigorous description of the intricate bifurcation diagrams obtained numerically for this system, in the spirit of what was accomplished in [5] for the Kuramoto–Sivashinsky equation.

Chapter 6

Stochastic problems

In the last chapter of this manuscript, we discuss computer-assisted proofs related to stochastic systems, and in particular to stochastic differential equations (SDEs). The very quantitative and precise nature of the computer-assisted results discussed up to now might at first seem incompatible with the randomness and fluctuations inherent to stochastic systems. One way to resolve this apparent contradiction is to leverage some well-known connections between SDEs and *deterministic* objects, using for instance large deviation theory in the small noise limit, or more generally Fokker–Planck equations associated with SDEs, which are deterministic PDEs describing the evolution of probability densities (for stochastic maps, transfer operators play a similar role). One can then use computer-assisted proofs to study these deterministic objects, and in turn get rigorous information on some properties or behavior of the original stochastic system. A specific example where this general strategy can prove very powerful is the study of Lyapunov exponents associated to SDEs, which, under generic ergodicity assumptions, are deterministic quantities of interest to better understand the global dynamics of SDEs. In particular, a negative (first) Lyapunov exponent often implies *synchronization* of trajectories [22, 121], whereas a positive Lyapunov exponent can lead to *chaotic dynamics* [198, 194]. See also [9, 325, 303] for a broader introduction to Lyapunov exponents and random dynamical systems. However, rigorously establishing the positivity of a Lyapunov exponent is a notoriously difficult question, even for relatively simple and low dimensional SDEs. We present below some significant progress obtained recently on this question, thanks to novel computer-assisted proofs.

Computer-assisted proofs for stochastic systems are relatively new, and apart from the works [B18, B19, B8, B16, B5, B12] discussed below, most of the existing literature deals with discrete random dynamical systems, i.e., stochastic maps. Early works on (piece-wise) expanding maps can be found in [182, 211]. Some of these ideas were picked up again a decade later [167, 17, 132], leading in particular to a general procedure for the rigorous computation of linear response[1] [18], and to a computer-assisted proof of noise-induced order [130], i.e., a transition from a positive Lyapunov exponent to a negative one as the noise intensity *increases*. One of the main ingredients in these works is a finite dimensional approximation of the transfer operator, with a controlled error based on compactness estimates, which shares many similarities with the construction and usage of an approximate inverse for the Newton–Kantorovich Theorem 1.2.2. Most of the works mentioned above use the so-called Ulam-method, i.e., a piece-wise constant approximation of the functions on which the transfer operator acts, but higher order approximations have later been introduced [317]. For a broader overview and recent developments, we refer to [131] and the references therein.

Coming back to differential equations, the works presented in this chapter are split into three parts. We start in Section 6.1 with the study of *random differential equations*, i.e., differential equations in which the randomness does not come from a stochastic forcing, but from random coefficients. In this setting, which is very natural for applications, we rigorously study some

[1] That is, of the derivative of the invariant measure with respect to some parameter.

random invariant sets, using polynomial chaos expansions and ideas very close to those already presented in Chapter 5. In the subsequent two sections, we then turn to proper SDEs with a stochastic forcing. In Section 6.2, we discuss the rigorous computation of *minimum energy paths*, which describe, in the small noise limit, noise-induced transitions between local minima in metastable gradient systems. Finally, in Section 6.3 we consider SDEs with noise that does not have to be small, and study the associated Lyapunov exponents, first in the context of *conditioned* Lyapunov exponents, and then in the more classical setting. In particular, we present in Section 6.3.3 a new computer-assisted method which significantly enlarges the class of systems for which one can prove that there is a positive Lyapunov exponent.

6.1 Polynomial chaos expansions for the rigorous computation of random invariant sets

6.1.1 Context

Many of the mathematical models that are used nowadays to try and describe the world we live in, or at least some very specific region or aspect of it, include some stochastic component. This randomness can have various sources: sometimes we do not fully know or understand the mechanisms underlying the phenomenon we are trying to describe, sometimes we need to account for the influence of events occurring at much smaller scales than that of the full system, for which we cannot afford to solve too accurately, and sometimes our model contains crucial parameters whose value can only be known up to some uncertainty level.

A common mathematical framework to study this last situation is the one of random differential equations, say a random ODE described by a nonlinear vector field f

$$x' = f(x, p), \tag{6.1}$$

or more generally a random PDE, where p denotes a parameter whose value is not known precisely, and is therefore represented by a random variable. We assume here that the probability distribution of p is known, for instance through some preliminary statistical inference. In this situation, one would like to understand and quantify as precisely as possible how the uncertainty in p affects the outputs of the system [269].

If we want to study the global behavior of (6.1), one option is to use a Monte-Carlo type approach: sample p according to its known distribution, and study for each sampled value p_i the deterministic system $x' = f(x, p_i)$. Of course, even in the deterministic case, understanding the global dynamics of a system of nonlinear ODEs can already be a daunting task. Numerical simulations can then be of great help to get some insights, in particular in order to study invariant sets (equilibria, periodic orbits, invariant manifolds, connecting orbits, etc), which typically act as building blocks of the global dynamics.

Another option to study problems with random parameters like (6.1), which has risen in popularity in the last decades, is the usage of generalized polynomial chaos (gPC) expansions [314, 140, 320]. The main idea is to expand the random quantity of interest as a series with a well chosen basis, namely polynomials in p which are orthogonal with respect to the probability distribution of p. One is then left with computing the (deterministic!) coefficients of this series expansion, which can often be done using existing solvers for deterministic problems. Once a (truncated) gPC expansion has been computed, it readily gives us access to the (approximate) mean and variance of the quantity of interest, but one can also then cheaply compute higher order moments and perform Monte-Carlo simulations, as "solving" the system for a given p now simply means evaluation the basis of orthogonal polynomials at this value of p.

This strategy has proven very effective in various contexts, see, e.g., [196, 319] and the reference therein, but has mostly been used to study initial value problems, and elliptic PDEs, i.e., equilibria of parabolic PDEs. Eigenvalue problems [139] and periodic orbits [197, 264] have

also been considered, but with mixed success in the latter case. In [B19], we showed that a larger class of invariant sets could be efficiently approximated using gPC expansions.

Polynomial chaos expansions have proven to be very useful tools, especially in the field of uncertainty quantification. This is somewhat ironic, because in practice one always uses a truncated expansion, typically of rather low order, which in facts adds a layer of uncertainty to the obtained results. Granted, it is known a priori that the truncation error decays quickly (spectral convergence) when the quantity of interest depends smoothly on p [64, 127], and some tight convergence results were even obtained recently in a non-smooth case [36]. However, when the quantity of interest is not known a priori, these estimates cannot give any quantitative information about the truncation error. A posteriori error estimators for gPC expansions have also been developed, especially in the context of random linear elliptic PDEs, but also for more general random PDEs [47, 217, 223]. Yet again, for nonlinear problems these estimators typically still contain some approximations and cannot provide fully rigorous error bounds between the approximate solution and the exact one, if only because the existence of an exact solution is not always readily available. In [B8], we showed that the setup introduced in [B19] allows to validate truncated gPC expansions a posteriori using computer-assisted proofs based on Theorem 1.2.2, and therefore to obtain explicit and guaranteed error bounds.

6.1.2 Generalized polynomial chaos expansions

6.1.2.1 The usual gPC setting

We briefly recall here some basic definitions and known properties regarding gPC expansions. Let $\rho : \mathbb{R} \to \mathbb{R}$ be a probability density function having finite moments of all orders. We recall that there exists a unique (up to sign) family of orthonormal polynomials $(\phi_k)_{k\in\mathbb{N}}$ associated to the weight ρ, i.e., satisfying

$$\langle \phi_k, \phi_l \rangle_\rho := \int_{\mathbb{R}} \phi_k(t)\phi_l(t)\rho(t)\mathrm{d}t = \delta_{k,l}, \qquad \text{for all } k, l \in \mathbb{N}.$$

Moreover, if ρ has compact support or decays at least exponentially at fast infinity, then $(\phi_k)_{k\in\mathbb{N}}$ is a Hilbert basis of the weighted space $L^2(\rho)$ with scalar product $\langle \cdot, \cdot \rangle_\rho$.

We now consider a quantity $X(p)$, depending (typically in a nonlinear and non-explicit manner) on a random variable p having a density function ρ. This could for instance be a steady state of (6.1), and more involved examples will be given in Section 6.1.3. The paradigm of polynomial chaos is that one should approximate the random function $X(p)$ by a truncated series expansion in p, in the basis $(\phi_k)_{k\in\mathbb{N}}$. Indeed, writing

$$X(p) = \sum_{k\in\mathbb{N}} X_k \phi_k(p),$$

so that, for fixed $K \in \mathbb{N}$,

$$\pi^{\leq K} X(p) := \sum_{k=0}^{K} X_k \phi_k(p),$$

one has by orthogonality that

$$\mathbb{E}\left(\left|X(p) - \pi^{\leq K} X(p)\right|^2\right) = \inf_{\substack{Q \text{ polynomial} \\ \deg Q \leq K}} \mathbb{E}\left(\left|X(p) - Q(p)\right|^2\right).$$

Therefore, using the truncated series expansion in the basis ϕ_k naturally provides the minimal quadratic mean error, which is a natural metric for random quantities.

Remark 6.1.1. *For the sake of simplicity, we restricted the presentation to the case of a single random parameter p, but the generalization to multiple random parameters is straightforward: one just has to take tensor products of the orthogonal polynomials associated with each parameter.*

6.1.2.2 An ℓ^1 Banach algebra setting

Among the classical orthogonal polynomials and associated gPC expansions, we focus on the Jacobi polynomials, which are the orthogonal polynomials $P_n^{\alpha,\beta}$, $\alpha, \beta > -1$, associated with the density $\rho(t) = \mathbb{1}_{(-1,1)}(t)\frac{(1-t)^\alpha(1+t)^\beta}{2^{\alpha+\beta+1}B(\alpha+1,\beta+1)}$, where $B(x,y) = \frac{\Gamma(x)\Gamma(y)}{\Gamma(x+y)}$ is the Euler beta function. The family of Jacobi polynomials contains many well know cases, including

- The Legendre polynomials, for $\alpha = \beta = 0$.
- The Chebyshev polynomials of the first kind, for $\alpha = \beta = -1/2$.
- The Chebyshev polynomials of the second kind, for $\alpha = \beta = 1/2$.
- More generally, the Gegenbauer or ultraspherical polynomials, for $\alpha = \beta = \mu$, $\mu \geq -1/2$.

For a more complete description of possible gPC choices and their relations to the Askey scheme, see [320].

While $L^2(\rho)$ spaces are natural to define gPC expansions in a probabilistic setting, in many cases we expect the quantity $X(p)$ to be smooth with respect to p, for instance if the vector field f in (6.1) is itself smooth, and there is no bifurcation over the range of values that can be taken by p. Moreover, L^2 spaces are not necessarily the most convenient to use if we want to analyze and control nonlinearities, which is needed in order to obtain computer-assisted proofs for gPC expansions by using Theorem 1.2.2. The following statement shows that, once again, weighted ℓ^1 spaces are well suited to control nonlinearities.

Theorem 6.1.2. *Let $\mu \geq -1/2$ and $(\phi_k)_{k\in\mathbb{N}}$ be the family of Gegenbauer polynomials, renormalized so that $\phi_k(1) = 1$ for all $k \in \mathbb{N}$. Then, there exists a generalized discrete convolution product, of the form*

$$(x * y)_k = \sum_{\substack{l_1,l_2\geq 0\\ l_1+l_2\leq k}} \alpha_k^{l_1,l_2} x_{l_2} y_{l_2},$$

such that:

1. *For any $\eta \geq 1$, ℓ^1_η with this generalized discrete convolution product is a Banach algebra;*
2. *If the sequences x and y in ℓ^1_η are associated to Gegenbauer expansions, i.e.,*

$$x(p) = \sum_{k\in\mathbb{N}} x_k\phi_k(p) \qquad \text{and} \qquad y(p) = \sum_{k\in\mathbb{N}} y_k\phi_k(p),$$

then $(x * y)$ is the Gegenbauer expansions of the function $p \mapsto x(p)y(p)$.

The proof is given in [B8], but is merely a compilation of previously known results, and is in fact valid for a larger class of Jacobi polynomials. In particular, we refer to [272] for a broader discussion about Banach algebra structures associated to orthogonal polynomials.

Also, we point out that there are explicit formulas (in terms of special functions) for the so-called *linearization coefficients* $\alpha_k^{l_1,l_2}$, see [B19, Appendix] or [244], which can therefore be used to compute such generalized convolution products in practice. Alternatively, even if in general there is no simple equivalent of the FFT for computing these generalized convolution products, one could still proceed as in Chapter 5 and compute products by first evaluating, then doing point-wise multiplications, and finally interpolation again. This procedure is not the one used in [B19, B8], where we simply used the linearization coefficients, but it might be more flexible and convenient to use in many cases, and is detailed in the context of rigorous numerics in [53].

6.1.3 Nested series expansions for random invariant sets

Let us for a moment go back to the situation where the parameters in the ODE (6.1), or in a more general dynamical system, are fixed. In this manuscript, we have seen several instances of steady states of PDEs being described using Fourier or Chebyshev series, and of periodic orbits also being represented using Fourier series. Another example of invariant set where Fourier series naturally come into play is invariant tori, see, e.g., the recent [152]. In the same vein, Taylor expansions are often used to described local (un)stable manifolds of equilibria or periodic orbits, using the so-called *parameterization method* [48, 49, 50, 151]. This approach has many appealing features, one of them being that it lends itself well to computer-assisted proofs using the Newton–Kantorovich approach, see [226] and the references therein. Connecting orbits are another type of invariant set that can also be represented using series expansions, namely by coupling a Taylor description of local invariant manifolds together with a resolution of the boundary problem between the manifolds using Chebyshev series [226, 295].

In all these examples, series expansions are not only an efficient and natural way of doing numerics, but they also provide a convenient framework for conducting computer-assisted proofs based on the Newton–Kantorovich Theorem 1.2.2. Therefore, as already explained in Chapter 5, one can in a straightforward way extend these proofs to incorporate gPC expansions in the parameters, since these expansions also have a Banach algebra structure (Theorem 6.1.2). The only difference with Chapter 5 is that, as already mentioned in Section 6.1.2.2, one cannot use the FFT to compute nonlinear terms for general Gegenbauer expansions (at least not directly, see [251] for fast numerical algorithms that also apply to the Gegenbauer family), which makes handling nonlinearities a bit slower. We give below some examples of random invariant sets computed using gPC expansions, for the famous Lorenz system

$$\begin{cases} x' = \sigma(y - x) \\ y' = px - y - xz \\ z' = -\beta x + xy, \end{cases} \tag{6.2}$$

where $\sigma = 10$ and $\beta = 8/3$ are fixed, but p is a random variable, having a uniform distribution on some interval $[p_{\min}, p_{\max}]$. Following the paradigm of gPC, we therefore use a Legendre expansion in p.

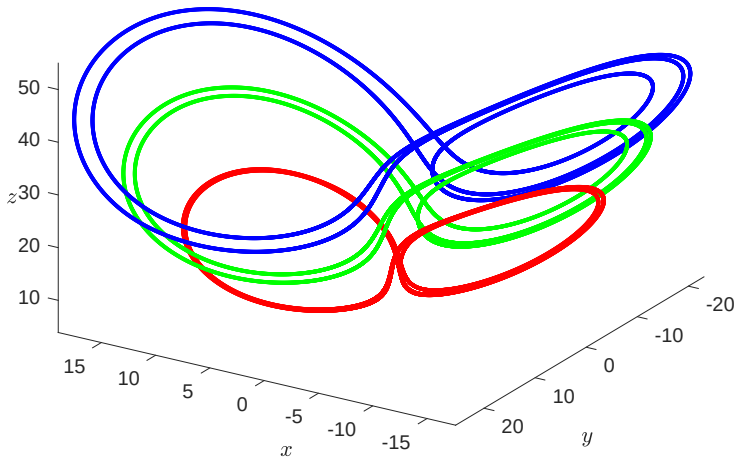

Figure 6.1: Several approximate periodic orbits of the Lorenz system (6.2), for $p = 18$ in red, $p = 28$ in green, and $p = 38$ in blue, all encoded in the Fourier×Legendre expansion $\bar{u}$, and validated in Theorem 6.1.3.

We start with the case of random periodic orbits. Note that not only the Fourier coefficients of x, y and z, but also the frequency Ω (or equivalently the period) of the periodic orbit becomes random, and therefore should be represented using Legendre series. That is, the exact random periodic orbit is described as $u = (\Omega, x, y, z)$ belonging to the space $\mathcal{X} = \ell^1_\eta \times \left(\ell^1_\nu\left(\ell^1_\eta\right)\right)^3$, for some $\eta, \nu \geq 1$. As in Chapter 5, ℓ^1_η represents expansions in the parameter, here Legendre series, whereas ℓ^1_ν represents Fourier series. On the space $\mathcal{X}$, we use the following norm

$$\|(\Omega, x, y, z)\|_{\mathcal{X}} = \|\Omega\|_{\ell^1_\eta} + \|x\|_{\ell^1_\nu(\ell^1_\eta)} + \|y\|_{\ell^1_\nu(\ell^1_\eta)} + \|z\|_{\ell^1_\nu(\ell^1_\eta)}.$$

Theorem 6.1.3. *Take $[p_{\min}, p_{\max}] = [18, 38]$ and consider the finite Fourier×Legendre expansion $\bar{u}$, whose coefficients are available at [Code 6], and for which a couple of orbits are represented in Figure 6.1. There exists $u \in \mathcal{X}$ representing and exact family of periodic orbits of the Lorenz system (6.2), such that $\|u - \bar{u}\|_{\mathcal{X}} \leq 2 \times 10^{-4}$.*

Remark 6.1.4. *We re-emphasize that gPC expansions are entirely deterministic objects, and that the randomness only comes from evaluating them at a p which is a random variable. Therefore, even if we assume that p has a uniform distribution, nothing prevents us from computing the expansion in p over $[p_{\min}, p_{\max}] = [18, 38]$ using for instance Chebyshev series, and then to plug a uniform random variable in the obtained Chebyshev series. The only minor difference is that, when using the orthogonal polynomials associated to the distribution of the random variable (like Legendre polynomials for uniform random variables), the first two moments are directly encoded in the gPC expansions. For instance, from Theorem 6.1.3 we get that $|\Omega_0 - \bar{\Omega}_0| \leq 2 \times 10^{-4}$, which directly shows that the true mean of the frequency of the random periodic orbit, which is simply Ω_0, is at most 2×10^{-4} away from the approximate mean frequency $\bar{\Omega}_0$ given by the finite gPC approximation. If we had used a Chebyshev expansion, while still assuming that p is uniformly distributed, one would have had to make some (easy) post-processing calculations to recover the mean of Ω from its Chebyshev coefficients.*

Let us finally give another example, namely an approximate family of heteroclinic orbits for the Lorenz system, again obtained using a Legendre expansion in p, which is this time assumed to vary in $[p_{\min}, p_{\max}] = [35, 65]$, and represented in Figure 6.2.

Remark 6.1.5. *Even if we choose to present Section 6.1 after Chapter 5 in this manuscript, what happened is actually the opposite: I was trying to better understand gPC in the context of random ODEs, and how one could possibly give guaranteed error bounds on the truncations in those expansions, and only then realized that gPC expansions were in fact nothing but a disguised way of doing deterministic high order continuation, which, especially in the case of Chebyshev series, turned out to be very efficient for doing rigorous continuation.*

Remark 6.1.6. *As already explained in Chapter 5 in the case of Chebyshev expansions, with our techniques we can only hope to validate gPC expansions if the portion of branch that is described does not undergo any bifurcation. However, at least from a numerical perspective, it was recently noticed that gPC expansions could also be used to recover partial information over parameter ranges including bifurcations [144].*

6.2 Minimum energy paths

6.2.1 Context

Consider a smooth confining potential $V : \mathbb{R}^d \to \mathbb{R}$, $d \geq 2$, with several local minima. For the sake of simplifying the discussion, let us simply assume that V has two non-degenerate local minima m_1 and m_2, separated by a hyperbolic saddle point s. If we consider the gradient flow induced by this potential, i.e., the ODE

$$x' = -\nabla V(x), \tag{6.3}$$

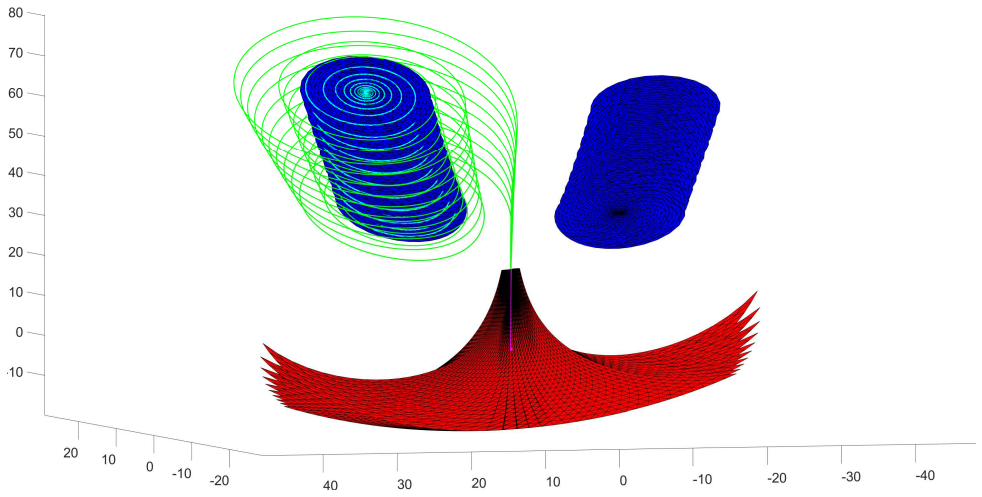

Figure 6.2: Some of the approximate heteroclinic orbits for the Lorenz system (6.2) encoded in a truncated gPC expansion, depicted for ten uniformly spaced values of p between 35 and 65. In red and blue are the local stable manifold of the origin, and the local unstable manifolds of the eyes, computed using Taylor×Legendre expansions. In green are the parts of the heteroclinic orbits that solves the boundary value problem between the two manifolds, computed via piecewise Chebyshev×Legendre expansions. The remaining parts of the heteroclinic orbits (in cyan and magenta), are obtained *for free* via the conjugation properties of the parameterizations, see [B19] for more details.

the dynamics is rather simple: except if the initial condition lies on the stable manifold of s, trajectories converge either to m_1 or to m_2. In particular, there is no solution connecting m_1 to m_2. However, the situation is radically different if one tries to take into account some small fluctuations, under the form of the SDE

$$\mathrm{d}x_t = -V(x_t)\mathrm{d}t + \sigma \mathrm{d}W_t, \tag{6.4}$$

where $0 < \sigma \ll 1$ and W_t is a vector of independent and identically distributed Brownian motions. In that case, noise-induced transitions occur for (6.4): given two small neighborhoods of m_1 and m_2, there exist sample paths $\gamma = \gamma(t)$ solving (6.4) and connecting both neighborhoods in final time. For the gradient system we considered here, it is well-known that the most probable path γ, also called *minimum energy path (MEP)*, passes through the saddle point s. Moreover, the average first passage time is well-understood via the classical Arrhenius-Eyring-Kramers law [14, 115, 192, 37, 38, 32, 199], which states that transition probabilities are exponentially small in the noise level σ as $\sigma \to 0$.

6.2.2 Large deviation theory and MAPs/MEPs

A general framework for studying the small-noise case is provided by *large deviation theory* [302, 124], which can be formulated for more general SDEs such as

$$\mathrm{d}x_t = f(x_t)\ \mathrm{d}t + \sigma \mathrm{d}W_t, \tag{6.5}$$

where f is a sufficiently smooth vector field. Let $\phi : [0, T] \to \mathbb{R}^n$ be an absolutely continuous path over fixed time $T > 0$, and define the *action* (or *action functional*)

$$S_T(\phi) = \frac{1}{2}\int_0^T L(\phi, \phi')\ \mathrm{d}t,$$

where the Lagrangian L is given by

$$L(\phi, \phi') = \|\phi' - f(\phi)\|_2^2. \tag{6.6}$$

We can think of $S_T(\phi)$ as the energy spent following a solution ϕ against the deterministic ($\sigma = 0$) flow for (6.5). Then, Freidlin–Wentzell theory [124] states that the probability of a solution x of (6.5) to stay within a δ-tube around $\phi(t)$ for all $t \in [0, T]$ is given by

$$\mathbb{P}\left(\sup_{t\in[0,T]} \|x_t - \phi(t)\|_2 < \delta\right) \approx \exp\left(-\frac{1}{\sigma^2} S_T(\phi)\right),$$

for sufficiently small σ and δ (see [124, Section. 3, Theorem. 2.3]). More generally, one can just take any measurable set $\mathcal{A}$ of random events and obtain the large deviation principle

$$\lim_{\sigma\to 0} \sigma^2 \ln\left(\mathbb{P}\left(x \in \mathcal{A}\right)\right) = -\inf_{\phi\in\mathcal{A}} S_T(\phi).$$

Note carefully that this formulation has converted a stochastic problem of estimating a probability into a deterministic optimization problem.

If we want to specify the transition problem between two points a and b, we should set

$$\mathcal{A} = \{x_0 = a,\, x_T = b\},$$

and consider

$$\inf_{\substack{\phi\in\mathcal{A}\\ T>0}} S_T(\phi). \tag{6.7}$$

If a minimizer ϕ_* of the action functional exists, one refers to ϕ_* as a minimum action path (MAP). We reserve MEP for the case of a minimizer in gradient systems for a transition between states.

In practice, it is often more important to know the geometrical path described by ϕ_* (i.e. the set $\{\phi_*(t) \,|\, t \in [0, T]\}$) rather than the function ϕ_* itself. One can then consider the *geometric action functional* [161]

$$\tilde{S}_T(\phi) = \int_0^T \Big(\left\|\phi'\right\|_2 \|f(\phi)\|_2 - \langle \phi', f(\phi)\rangle \Big) \mathrm{d}t, \tag{6.8}$$

which is only sensitive to the path described by ϕ, but not to the function ϕ itself. More precisely, for any time reparametrization $\theta : [0, T] \to [0, \tau]$ preserving orientation, one has $\tilde{S}_T(\phi) = \tilde{S}_\tau(\phi \circ \theta)$. Besides, the geometric action functional can also be used to characterize MAPs/MEPs since we have

$$\inf_{\substack{\phi\in\mathcal{A}\\ T>0}} S_T(\phi) = \inf_{\substack{\phi\in\mathcal{A}\\ T>0}} \tilde{S}_T(\phi) = \inf_{\phi\in\mathcal{A}} \tilde{S}_1(\phi).$$

For gradient systems, the geometric action functional also provides another useful characterization of MEPs. Consider for instance the transition between m_1 and s for (6.4), i.e. set

$$\mathcal{A} = \{x_0 = m_1,\, x_T = s\}.$$

We then have

$$\begin{aligned}
\tilde{S}_T(\phi) &= \int_0^T \Big(\left\|\phi'\right\|_2 \|\nabla V(\phi)\|_2 + \langle \phi', \nabla V(\phi)\rangle \Big) \mathrm{d}t \\
&\geq 2 \int_0^T \langle \phi', \nabla V(\phi)\rangle \mathrm{d}t \\
&= 2\left(V(s) - V(m_1)\right),
\end{aligned}$$

where the inequality becomes an equality if $\phi'(t)$ and $\nabla V(\phi(t))$ are positively collinear for all $t \in [0, T]$.

It is usually not possible to calculate MAPs/MEPs analytically due to the need to solve a nonlinear deterministic problem. However, there are many numerical methods, mainly motivated by molecular dynamics applications, and mostly based on the geometric action potential. For MEPs in gradient systems, there is the classical nudged elastic band method [157] as well as the string method [106]. Both methods start with an initial piecewise-linear path in the phase space $\mathbb{R}^d$. Making use of the above characterization, the path is then evolved so that $\phi'(t)$ and $\nabla V(\phi(t))$ align. Both methods show often quite similar performance as just the re-meshing strategies differ [267]. In cases when the final state is not known a priori, the dimer method [156] can be used. Of course, one can also directly discretize the action and try to minimize it, which leads to another natural set of numerical methods [105]. Another option is to look at the Euler-Lagrange equation associated to the geometrical action path [162].

6.2.3 MEPs as connecting orbits

Finally, one can also numerically compute MAPs/MEPs by noticing that in many situations they are (concatenations of) orbits for the deterministic system ($\sigma = 0$). For example, consider again the gradient system ODE (6.3) with the three critical points m_1, s, m_2, and assume we are interested in the transition going from m_1 to m_2. Then the path associated to

$$\phi_* = \{m_1\} \cup \gamma_{s\to m_1} \cup \{s\} \cup \gamma_{s\to m_2} \cup \{m_2\},$$

where $\gamma_{s\to m_1}$ is a heteroclinic orbit from s to m_1 and $\gamma_{s\to m_2}$ is a heteroclinic orbit from s to m_2, i.e.,

$$\lim_{t\to-\infty} \gamma_{s\to m_1}(t) = s, \quad \lim_{t\to+\infty} \gamma_{s\to m_1}(t) = m_1, \quad \lim_{t\to-\infty} \gamma_{s\to m_2}(t) = s, \quad \lim_{t\to+\infty} \gamma_{s\to m_2}(t) = m_2,$$

is a MEP. Of course, the heteroclinic solution going from s to m_1 does not truly describe the transition, as it goes in the wrong direction. However the function $\tilde\gamma_{s\to m_1}$ defined by $\tilde\gamma_{s\to m_1}(t) = \gamma_{s\to m_1}(-t)$ does, as it still satisfies $\tilde\gamma'_{s\to m_1} = \nabla V(\tilde\gamma_{s\to m_1})$ and therefore minimizes the geometric action, while now going from m_1 to s. Since the path associated to $\tilde\gamma_{s\to m_1}$ and $\gamma_{s\to m_1}$ is the same, the path associated to ϕ_* is indeed a MEP. Hence, a MEP algorithm can also be built around calculating minima, saddles and heteroclinic connections between them. More precisely, once approximate minima, saddles and heteroclinic orbits have been located, for instance using one of the algorithms for approximating MEPs described in Section 6.2.2, one can then try to rigorously validate them using computer-assisted proofs.

This strategy was put forward in [B18], where we used it to rigorously compute a MEP for the so-called Müller-Brown potential [233], which is a well-known test case for numerical methods in theoretical chemistry. The corresponding potential $V : \mathbb{R}^2 \to \mathbb{R}$ is represented in Figure 6.3 and given by

$$V(x,y) = \sum_{i=1}^{4} \alpha_i \exp\left(a_i\,(x-\tilde x_i)^2 + b_i\,(x-\tilde x_i)\,(y-\tilde y_i) + c_i\,(y-\tilde y_i)^2\right),$$

where a standard set of parameters is

$$\alpha = (-200,-100,-170,15), \quad \tilde x = (1,0,-0.5,-1), \quad \tilde y = (0,0.5,1.5,1)$$
$$a = (-1,-1,-6.5,0.7), \quad b = (0,0,11,0.6), \quad c = (-10,-10,-6.5,0.7).$$

As already mentioned in Section 6.1, there are by now standard techniques based on the Newton–Kantorovich Theorem 1.2.2 and appropriate series expansions to rigorously compute connecting orbits for ODEs, and we refer again to [226, 296] for details. In the specific case of the Müller-Brown potential, the situation is even simpler, as we do not have any *saddle-to-saddle*

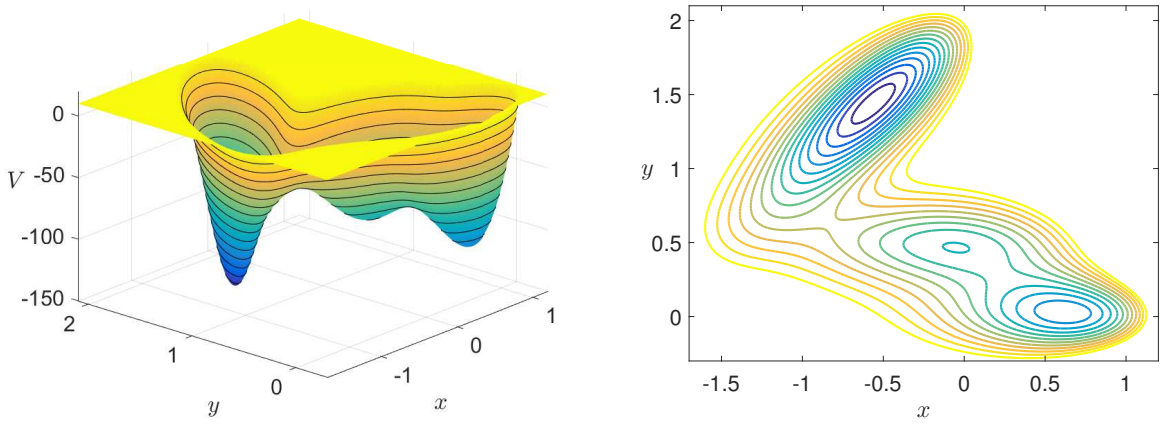

Figure 6.3: The Müller-Brown potential (graph to the left, and level sets to the right). It has three local minima and two saddle points.

connecting orbits to validate, but only *saddle-to-sink* ones. Therefore, one can simply compute small trapping regions around the sinks, as well as the local unstable manifolds of the saddles, and then rigorously integrate from the boundary of these local manifolds until the sinks are reached. The corresponding computer-assisted proof is illustrated in Figure 6.4, and we refer to [B18] for the details. We simply note that this proof is somewhat outdated already, as in [B18] we deal with the non-polynomial terms in V using the polynomial embedding strategy rather than the new alternatives discussed in Section 3.2, and we use weights for the product space selected in a non optimal manner compared to using Theorem 4.2.3.

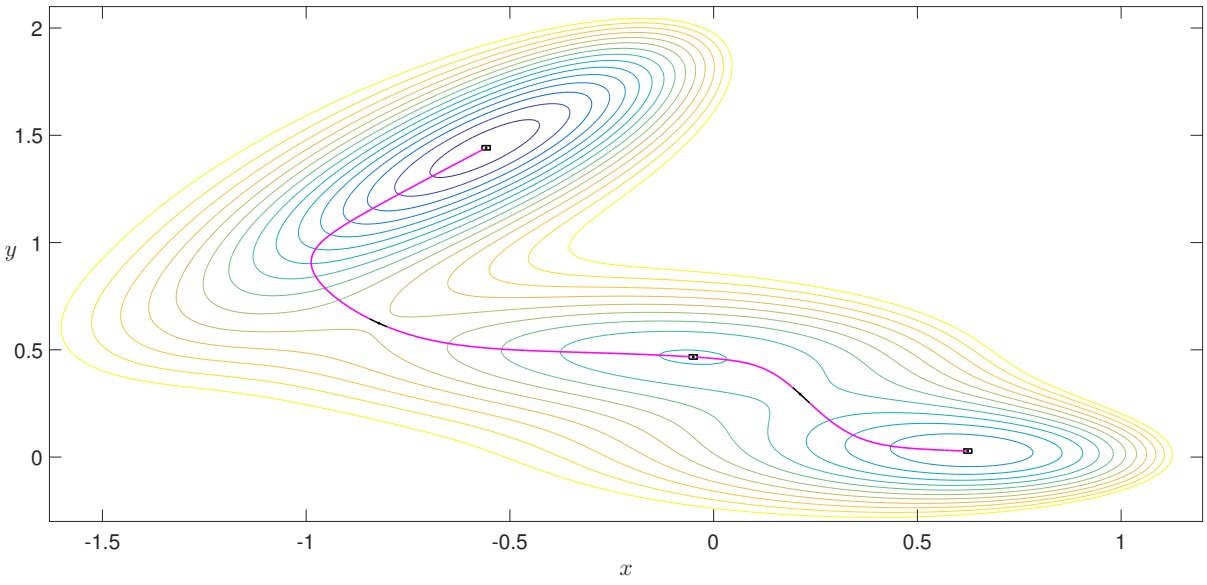

Figure 6.4: A validated MEP for the Müller-Brown potential, represented in the (x, y) phase space, between the minimum at the top and the one at the bottom right. The small black parts of the path near each saddle represent the validated unstable manifolds, whereas the magenta parts corresponds to rigorous integration performed using piece-wise Chebyshev series. The tiny boxes around each local minimum are the validated trapping regions.

6.3 Rigorous computation of Lyapunov exponents for SDEs

In the previous two sections, while we treated some stochastic problems, in hindsight one could argue that we dealt with situations in which the randomness did not really create additional difficulties, at least after suitable reformulations. Indeed, in Section 6.1 we studied ODEs with random coefficients but ended up using rigorous continuation techniques for deterministic ODEs, and in Section 6.2 we considered SDEs but looked at the small noise limit, for which we could again get away with studying only deterministic ODEs. Rigorously solving these deterministic ODE problems might still be challenging with traditional pen-and-paper analysis techniques, but with computer-assisted proofs we now have rather refined tools to study ODEs.

In the final section of this manuscript, we work again with SDEs, but no longer in the small noise limit, and study their Lyapunov exponents. In that case, the stochasticity is more central to the problem, and even if we in the end again use computer-assisted proofs on deterministic problems, this time it will not be merely on ODEs but on PDEs, which showcases that these are intrinsically more difficult questions.

6.3.1 Lyapunov exponents for SDEs

The goal of this subsection is not to provide a detailed and exhaustive introduction to the theory of Lyapunov exponents, but merely to set the stage for what is to come, and to recall how Lyapunov exponents for SDEs can be linked with deterministic PDEs. For a broader discussion, we refer again to [9, 325, 303].

Although we sometimes consider more general situations later on, for the sake of simplifying the discussion we only focus here on the case of additive noise, i.e., we consider SDEs of the form

$$\mathrm{d}x_t = f(x_t)\mathrm{d}t + \sqrt{2}\sigma \mathrm{d}W_t, \tag{6.9}$$

where f is an analytic vector field, W_t is a vector of independent and identically distributed Brownian motions, and σ is a diagonal matrix with nonnegative diagonal entries σ_i, $i \in \{1, \dots, d\}$. We assume here that the state space is simply the torus $\mathbb{T}^d$ or the whole euclidean space $\mathbb{R}^d$, or a cartesian product of these.[2] In order to study the dynamics of SDEs, a key object is the associated variational equation

$$\mathrm{d}v_t = Df(x_t)v_t\mathrm{d}t. \tag{6.10}$$

Note that, at least in the case where there is only additive noise in the original SDE (6.9), there is no longer a stochastic forcing in the variational equation (6.10), but the latter is still stochastic because of the presence of x_t. One can then consider the (top) Lyapunov exponent:

$$\lambda(\omega, x_0, v_0) = \lim_{t\to\infty} \frac{1}{t} \ln \|v_t\| . \tag{6.11}$$

Under some assumptions, which essentially amount to asking that the SDE (6.9) has a unique invariant measure which is ergodic (plus some integrability conditions), by Osdelets multiplicative ergodic theorem [9] the limit in (6.11) exists, and is in fact constant (almost surely), i.e., it is a deterministic quantity, which does not depend on the noise realization ω, nor on the initial conditions x_0 and v_0. In Section 6.3.4, we also consider finite time Lyapunov exponents (FTLEs), namely

$$\lambda_t(\omega, x_0, v_0) = \frac{1}{t} \ln \|v_t\| , \qquad t > 0. \tag{6.12}$$

[2] In principle, one could consider the broader setting of SDEs on Riemannian manifolds, but this more abstract framework will not be needed here.

In contrast to the asymptotic Lyapunov exponent λ, FTLEs λ_t do typically depend on ω, x_0 and v_0, even if we might sometimes simply write λ_t to lighten the notation.

The (asymptotic) Lyapunov exponent λ is an essential tool to characterize stochastic dynamics, and typically plays an important role in the proof of *synchronization when λ is negative* [22, 121] or in the characterization of various forms of *chaotic dynamics when λ is positive* [198, 194]. In particular, since it comes from the variational equation (6.10), it is directly linked to sensitivity to initial conditions, which is a quintessential feature of chaos. Thus, obtaining rigorous bounds on the Lyapunov exponent is crucial to determine the dynamics of the original SDE (6.9).

To that end, let us introduce the polar coordinates $\|v_t\|$ and $s_t := \frac{v_t}{\|v_t\|}$, where s_t solves the equation

$$\mathrm{d}s_t = \left(Df(x_t) - Q(x_t, s_t)\right) s_t \mathrm{d}t, \tag{6.13}$$

with $Q(x, s) := \langle Df(x)s, s\rangle$. Under additional erogdicity assumptions on the so-called projective process (x_t, s_t) given by

$$\begin{cases} \mathrm{d}x_t = f(x_t)\mathrm{d}t + \sqrt{2}\sigma \mathrm{d}W_t \\ \mathrm{d}s_t = h(x_t, s_t)\mathrm{d}t, \end{cases} \tag{6.14}$$

where $h(x, s) = \left(Df(x) - Q(x, s)\right) s$, one can show that the Lyapunov exponent λ can also be obtained as an ergodic average, given by the so-called Furstenberg–Khasminskii formula

$$\lambda = \int Q(x, s)\mathrm{d}\mu, \tag{6.15}$$

where μ is the invariant measure of the projective process (6.14). We refer to [9] for a broader presentation of the Furstenberg–Khasminskii formula, and to [B12, Section 3.1] and [B5, Section 2] for specific discussions related to the examples to come.

Remark 6.3.1. *In practice, checking that the required ergodicity assumptions are satisfied (both for the initial SDE and for the whole projective process) can be very challenging, especially if there is no noise in some of the components of the original SDE (6.9), i.e., if some of the σ_i are equal to zero. However, we do not focus on this aspect in this manuscript. Rather, we assume that these assumptions are satisfied (and work with examples for which we can indeed prove that they hold), and show how one can then use computer-assisted proofs to get quantitative and rigorous information about the Lyapunov exponent using the Furstenberg–Khasminskii formula (6.15). For sufficient conditions ensuring that this formula holds, which can be checked on concrete examples, we refer to [B12, Section 3.2], [B5], and the references therein.*

The Furstenberg–Khasminskii formula (6.15) provides us with a link between the SDE (6.9) and deterministic PDEs. Indeed, denoting w the density of the invariant measure μ of the projective process, we have that w is characterized by the PDE $\mathcal{L}^* w = 0$, where $\mathcal{L}^*$ is the Fokker–Planck operator (also called forward Kolmogorov operator) associated to the projective process (6.14), and, as indicated by the notation, is the adjoint of the operator $\mathcal{L}$, which is the generator of the projective process (also called backward Kolmogorov operator). That is, for $u = u(x, s)$, where x lives in the state space of the original SDE (6.9), and s lives in $\mathbb{S}^{d-1}$,

$$\mathcal{L}u = \sigma^2 \Delta_x u + f(x) \cdot \nabla_x u + h(x, s) \cdot \nabla_s u, \tag{6.16}$$

and

$$\mathcal{L}^* u = \sigma^2 \Delta_x u - \nabla_x \cdot (f(x)u) - \nabla_s \cdot (h(x, s)u). \tag{6.17}$$

This suggests a natural plan to rigorously enclose Lyapunov exponents of SDEs using computer assisted proofs: from the Furstenberg–Khasminskii formula (6.15), in which Q is a known

map, it is sufficient to have rigorous bounds on the density w of μ (in an appropriate topology, for instance L^1 bounds on w are enough if Q is in L^∞) in order to obtain a rigorous enclosure on λ. That is, we "only" need to solve the linear PDE $\mathcal{L}^* w = 0$ quantitatively, using computer-assisted proofs.

However, there is a big issue with that plan: $\mathcal{L}^*$ (and $\mathcal{L}$) are not fully elliptic, as there is only diffusion in the x variable, but not in the s variable. Therefore, this puts the equation $\mathcal{L}^* w = 0$ completely outside of the framework in which we currently know how to apply the computer-assisted techniques presented in Section 1.2 and used in the previous chapters of this manuscript. One day, we will hopefully be able to use computer-assisted proofs not only for elliptic equations but also for hypoelliptic ones, but in the meantime different approaches to the rigorous computation of Lyapunov exponents are needed.

In Section 6.3.2, we present a specific example where uniform ellipticity can in fact be retrieved and for which, using the concept of conditioned Lyapunov exponent, we partially solved a conjecture related to shear-induced chaos in [B16]. In Section 6.3.3, we come back to usual Lyapunov exponents, and present a new and relatively simple but very powerful computer-assisted technique introduced in [B12], which allows us to bypass the resolution of the Fokker–Planck equation $\mathcal{L}^* w = 0$ and still get tight and rigorous enclosures on Lyapunov exponents, even for non-elliptic equations. Finally, in Section 6.3.4 we investigate finer properties of Lyapunov exponents, and in particular some large deviation estimates for finite time Lyapunov exponents and their links with random bifurcations [B5].

Remark 6.3.2. *For each of these three works [B16, B12, B5], we mostly focus here on the aspects related to computer-assisted proofs. These papers also contain results pertaining to probability and ergodic theory, for instance for proving that all the assumptions allowing to use the Furstenberg–Khasminskii formula (6.15) really do hold in [B12], of for providing a suitable framework to derive large deviation estimates of FTLEs when the state space is unbounded in [B5]. However, these results are not discussed much in this manuscript, not because they are not interesting, but rather because I contributed very little to these parts, which are mostly due to the work of my co-authors. Similarly, we do not discuss here the underlying theory of random dynamical systems, and instead refer to [9], as well as to [B16, Appendix] for a more succinct description of some of the aspects of this theory most relevant to the works presented below.*

6.3.2 Conditioned Lyapunov exponents and shear-induced chaos

In this subsection, we focus on the two-dimensional SDE given by the Hopf normal form with additive noise:

$$\mathrm{d}\begin{pmatrix} x_t \\ y_t \end{pmatrix} = \left[\begin{pmatrix} \alpha & -\beta \\ \beta & \alpha \end{pmatrix} \begin{pmatrix} x_t \\ y_t \end{pmatrix} - \begin{pmatrix} a & b \\ -b & a \end{pmatrix} \begin{pmatrix} x_t \\ y_t \end{pmatrix} (x_t^2 + y_t^2) \right] \mathrm{d}t + \sigma \mathrm{d} \begin{pmatrix} W_t^1 \\ W_t^2 \end{pmatrix}. \tag{6.18}$$

6.3.2.1 Description of the problem

The system (6.18) was introduced in the context of random dynamical systems in [98], as a simple perturbation of the deterministic Hopf normal form, but is also related to applications in ocean and laser dynamics [100, 313, 277] . This system has been conjectured [101] to exhibit the *shear-induced chaos* scenario proposed in [206], for which the perturbation of a limit cycle induces a stretch-and-fold mechanism leading to chaos. This conjecture can be quantitatively translated into proving a transition from a negative to positive Lyapunov exponent λ as the shear strength b increases. It had been proven by hand that the Lyapunov exponent for (6.18) is negative when either the noise σ goes to 0 [98], or the shear b is sufficiently small [111] (with an explicit threshold). However, while numerical experiments strongly suggested that large enough shear led to a positive Lyapunov exponent, no proof of a positive Lyapunov exponent had been found before [B16].

Remark 6.3.3. *Note that this shear-induced chaos mechanism relies on the presence of noise (the deterministic ODE version with $\sigma = 0$ is very tame, no matter the value of b), and is only seen* dynamically*: If one only looks at the invariant density of (6.18), there is no apparent transition as b is varied, indeed the density is given (up to a normalization constant) by*

$$\rho(x, y) = \exp\left(\frac{2\alpha(x^2 + y^2) - a(x^2 + y^2)^2}{2\sigma^2}\right),$$

and does not even depend on b.

Following Section 6.3.1, we first consider the projective process associated with (6.18), where in that case (x, y) lives in $\mathbb{R}^2$ and the variable s lives on the circle $\mathbb{S}^1$, and can therefore be described by an angle θ. As discussed in Section 6.3.1, there is no additive noise in the equation on θ (or equivalently s), because we have additive noise in the original SDE (6.18). However, for this specific example there is additional structure that enables us to improve the situation. Indeed, following an approach presented in [98], one can first rewrite the SDE (6.18) on (x_t, y_t) in polar coordinates (r_t, ϕ_t), and then combine the equations on θ_t and ϕ_t, leading to an equivalent projective process which is only two-dimensional and has noise in both components:

$$\begin{cases} \mathrm{d}r_t = \left(\alpha r_t - a r_t^3 + \dfrac{\sigma^2}{2r_t}\right)\mathrm{d}t + \sigma \mathrm{d}W_t^r \\ \mathrm{d}\psi_t = \left(b r_t^2 + \sqrt{a^2 + b^2}\, r_t^2 \cos(2\psi_t)\right)\mathrm{d}t - \dfrac{\sigma}{r_t}\mathrm{d}W_t^\phi, \end{cases}$$

where $\psi_t = \theta_t - \frac{1}{2}\arccos(b/\sqrt{a^2 + b^2}) - \phi_t$, and W_t^r, W_t^ϕ are still independent and identically distributed Brownian motions (see [B12] for more details). Note that this reformulation is the one introduced in [B12], which differs sightly from the previous literature, and in particular from [B16]. The advantage of this reformulation is that the corresponding generator $\mathcal{L}$ can be naturally written in polar coordinates as

$$\mathcal{L} = \frac{\sigma^2}{2}\Delta + (\alpha r - a r^3)\partial_r + \left(b r^2 + \sqrt{a^2 + b^2}\, r^2 \cos 2\psi\right)\partial_\psi,$$

where Δ is the polar coordinate Laplacian

$$\Delta = \frac{1}{r}\partial_r\,(r\partial_r) + \frac{1}{r^2}\partial_{\theta\theta},$$

whereas in [B16] we had a slightly modified operator with an annoying factor 4 in front of the $r^{-2}\partial_{\theta\theta}$ term.

In the coordinates (r, ψ) we get

$$Q(r, \psi) = \alpha - 2a r^2 + \sqrt{a^2 + b^2}\, r^2 \sin 2\psi,$$

and, denoting again w the unique positive function of mass 1 such that $\mathcal{L}^* w = 0$, the (top) Lyapunov exponent associated to (6.18) is then given by the Furstenberg–Khasminskii formula

$$\lambda = \int_{\mathbb{R}_+ \times \mathbb{T}} Q(r, \psi) w(r, \psi) \mathrm{d}r \mathrm{d}\psi.$$

6.3.2.2 Conditioned Lyapunov exponents

Although the algebraic manipulations outlined in Section 6.3.2.1 led to an operator $\mathcal{L}^*$ which is in fact elliptic, providing tight and explicit bounds on the solution w to $\mathcal{L}^* w = 0$ using computer-assisted proofs is very challenging, because the problem is posed on the whole space $\mathbb{R}^2$, and none of the existing techniques for unbounded domains (see Section 3.3) apply to this

equation. At the same time, one could argue that looking at the problem on the whole space is somewhat counter-intuitive, as we are trying to study the effect of noise on a deterministic *local* bifurcation.

For these two reasons, instead of studying (6.18) on the whole plane $\mathbb{R}^2$, we considered in [B16] the same SDE but on an annulus, and looked at trajectories starting inside that annulus and conditioned on the fact that they never reach its boundary. In other words, trajectories are killed as soon as they hit the boundary. This means mass is lost with time, and the notion of stationarity has to be replaced by quasi-stationarity [221, 80]. The notion of Lyapunov exponent also has to be adapted accordingly, leading to so-called *conditioned Lyapunov exponents* [111].

Fixing $0 < R_1 < R_2$, and the annulus $\Omega = \left\{(x, y) \in \mathbb{R}^2, R_1 < \sqrt{x^2 + y^2} < R_2\right\}$, it is shown in [111] that the corresponding conditioned Lyapunov exponent for (6.18) is given by

$$\lambda_{\text{cond}} = \int_{(R_1,R_2)\times\mathbb{T}} Q(r, \psi) w_c(r, \psi) \mathrm{d}r\mathrm{d}\psi,$$

where the quasi-stationary density w_c can be obtained as $w_c(r, \psi) = \eta(r, \psi)\eta^*(r, \psi)$, where η and η^* are the principal eigenfunctions of $\mathcal{L}$ and $\mathcal{L}^*$ on Ω, with homogeneous Dirichlet boundary conditions. That is, the generator $\mathcal{L}$ posed on Ω with homogeneous Dirichlet boundary conditions admits a single eigenvalue $\tilde{\lambda}$ of largest real part, and η and η^* are the unique positive functions on Ω, having mass 1 and such that

$$\begin{cases} \mathcal{L}\eta = \tilde{\lambda}\eta & \text{in } \Omega \\ \eta = 0 & \text{on } \partial\Omega \end{cases} \quad \text{and} \quad \begin{cases} \mathcal{L}^*\eta^* = \tilde{\lambda}\eta^* & \text{in } \Omega \\ \eta^* = 0 & \text{on } \partial\Omega. \end{cases}$$

Note that these problems are now posed on bounded domains, therefore we finally reached a reformulation which can be handled with current computer-assisted proofs. Indeed, an eigenvalue problem for $\mathcal{L}$ (or $\mathcal{L}^*$) can easily be turned into a zero finding problem, for instance by considering, for complex numbers z and functions $v : \Omega \to \mathbb{C}$ satisfying the homogeneous Dirichlet boundary conditions, the map

$$F(z, v) := \begin{pmatrix} \mathcal{L}v - zv \\ N(v) - 1 \end{pmatrix},$$

where N is any normalization condition ensuring that zeros of F are locally unique (for simple eigenvalues). Any simple eigenpair of $\mathcal{L}$ can therefore be rigorously enclosed using the Newton–Kantorovich approach described in Section 1.2. At the time we started to work on this problem, there was no known spectral-based computer-assisted techniques to deal with problems on the disk or on the annulus, therefore in [B16] we made used of Theorem 1.2.6 (i.e., Newton–Kantorovich without an approximate inverse but with eigenvalue bounds) and of the homotopy method described in Section 1.3.2.3 in order to obtain the required eigenvalue bounds on $DF(\bar{z}, \bar{v})DF(\bar{z}, \bar{v})^*$. It now looks likely that one could in fact also have used Theorem 1.2.2 (i.e. Newton–Kantorovich with an approximate inverse), adapting the tools developed in [8, 53] for computer-assisted proofs on disks.

Once an eigenpair (z, v) of $\mathcal{L}$ has been validated, one still has to show that we have the right eigenpair, i.e., that v is indeed equal to η and not to any other eigenfunction of $\mathcal{L}$. To that end, we use the fact that we know a priori [B16, Proposition 3.2.1] that η is the only (up to normalization) eigenfunction of $\mathcal{L}$ that is positive on Ω. We therefore check a posteriori that the obtained eigenfunction for $\mathcal{L}$ is indeed positive on Ω, which guarantees that we have found η. Finally, we obtain an eigenfunction v^* of $\mathcal{L}^*$ using a similar zero-finding problem, and it is enough to check (again a posteriori) that η and v^* are not orthogonal to guarantee that $v^* = \eta^*$. The whole procedure is detailed in [B16] (and implemented in [Code 4]), and leads to the following result.

Theorem 6.3.4. *Consider the Hopf normal form with noise (6.18), with $a = \alpha = \beta = 1$, $b = 3.6$ and $\sigma = 1.3$. On the annulus given by $R_1 = 0.5$ and $R_2 = 1.5$, the conditioned Lyapunov exponent λ_{cond} is positive.*

A numerical computation of λ_{cond} for various values of σ is also provided in Figure 6.5. After

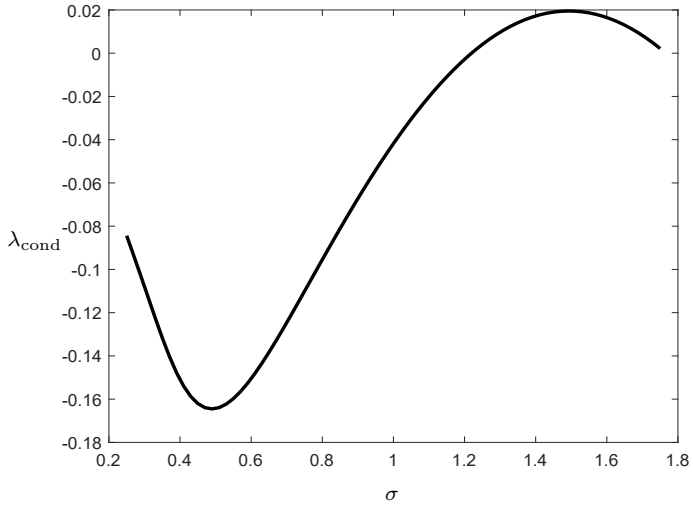

Figure 6.5: Numerical computation of the conditioned Lyapunov exponent λ_{cond} of the SDE (6.18), as a function of σ, all the other parameters being fixed as in Theorem 6.3.4. For $\sigma = 1.3$, the obtained value was validated in Theorem 6.3.4, and proven to be in $[0.00970, 0.00972]$.

we proved Theorem 6.3.4, with computer-assistance, it was established by more traditional techniques in [72, 24] that the (non-conditioned) Lyapunov exponent λ associated to (6.18) becomes positive in the asymptotic regime $b \to \infty$, whereas the actual transition in the non-conditioned case was obtained in [B12], again with computer-assistance, and will be discussed in the next subsection.

6.3.3 A new framework for the rigorous computation of Lyapunov exponents

We now go back to the more general question of rigorously computing (non-conditioned) Lyapunov exponents for SDEs. As explained in Section 6.3.1, the usage of the Furstenberg–Khasminskii formula (6.15) is appealing, but actually solving $\mathcal{L}^* w = 0$ for the invariant density of the projective process (6.14) seems rather daunting because of the lack of ellipticity. Even in specific situations where ellipticity can be recovered, as in Section 6.3.2.2, if the initial SDE is posed on the whole space, the PDE $\mathcal{L}^* w = 0$ might still be too difficult to handle with computer-assisted proofs.

In [B12], we introduce a new computer-assisted strategy allowing to rigorously enclose Lyapunov exponents, which still uses the Furstenberg–Khasminskii formula (6.15) but does not require solving for the invariant measure. This strategy is in fact well known in the pen-and-paper study of Lyapunov exponents, and called the *adjoint method*. It was introduced in [12] and used for instance in [24] in order to estimate the (top) Lyapunov exponent of the Hopf normal form (6.18) in the asymptotic limit $b \to \infty$. However, by combining it with computer-assisted tools, we make it way more versatile and broadly usable. More generally, we note that in some specific cases, for instance in the asymptotic regime where the noise strength σ goes to 0, or for volume-preserving or Hamiltonian systems, some estimates for the Lyapunov exponent can be obtained analytically, see, e.g., [10, 25, 26, 27, 81]. In contrast, the computer-assisted techniques that we present here apply outside of these specific or perturbative regimes.

6.3.3.1 The adjoint method on the computer

Let us now explain the rather simple idea behind the *computer-assisted adjoint method*. Recalling the Furstenberg–Khasminskii formula (6.15), $Q - \lambda$ has μ-mean zero, and should therefore be in the range of $\mathcal{L}$, i.e. there should exist a function u solving

$$\mathcal{L}u = Q - \lambda. \tag{6.19}$$

Solving that equation rigorously using computer-assisted proofs is essentially as hard as solving $\mathcal{L}^* w = 0$, but suppose that we can find numerically an approximate solution of (6.19), i.e., a function $\bar{u}$ and a number $\bar{\lambda}$ such that $\mathcal{L}\bar{u} \approx Q - \bar{\lambda}$. Then, defining $\bar{Q} := \mathcal{L}\bar{u} + \bar{\lambda}$, and integrating with respect to μ, observe that

$$\int \bar{Q} \mathrm{d}\mu = \int \mathcal{L}\bar{u} \mathrm{d}\mu + \bar{\lambda} = \bar{\lambda}. \tag{6.20}$$

Indeed, any function $\mathcal{L}u$ in the range of $\mathcal{L}$ has μ-mean zero, since (denoting $\xi = (x, s)$)

$$\int \mathcal{L}u \mathrm{d}\mu = \int \mathcal{L}u(\xi) w(\xi) \mathrm{d}\xi = \int u(\xi) \mathcal{L}^* w(\xi) \mathrm{d}\xi = 0.$$

Hence, going back to (6.20) and subtracting it from the Furstenberg–Khasminskii formula (6.15), we get

$$\lambda - \bar{\lambda} = \int \left(Q - \bar{Q}\right) \mathrm{d}\mu,$$

and in particular

$$\left|\lambda - \bar{\lambda}\right| \leq \int \left|Q - \bar{Q}\right| \mathrm{d}\mu. \tag{6.21}$$

Recall that our goal is to explicitly and rigorously enclose λ. In (6.21), Q is known, $\bar{\lambda}$ is just a numerical approximation for λ and is therefore known explicitly, and so is $\bar{Q}$, which is defined explicitly in terms of $\bar{\lambda}$ and $\bar{u}$. Hence, assuming for instance that $\left|Q - \bar{Q}\right|$ is bounded in L^∞, we immediately get a rigorous and explicit enclosure for λ, given by

$$\left|\lambda - \bar{\lambda}\right| \leq \left\|Q - \bar{Q}\right\|_{L^\infty}. \tag{6.22}$$

Let us recap, and re-emphasize where the computer has to be used and in what way.

- The most intensive part numerically, but which does not have to be rigorous, is to find approximate solutions $\bar{u}$ and $\bar{\lambda}$ to equation (6.19). In practice we found most efficient to find $\bar{u}$ by numerically solving (a finite dimensional projection of) the least square problem

  $$\operatorname*{argmin}_u \|\pi_0^\perp \left(\mathcal{L}u - Q\right)\|,$$

  where π_0 denotes the orthogonal projection onto the constants, and then taking

  $$\bar{\lambda} = \pi_0 \left(\mathcal{L}\bar{u} - Q\right).$$

  The least square problem can be solved iteratively, and in particular we can leverage any potentially helpful structural properties of $\mathcal{L}$, like sparsity, during that step.

- Once $\bar{u}$ and $\bar{\lambda}$ have been obtained (using the approach described just above, or any other scheme potentially more appropriate for the problem at hand), once has to compute, this time rigorously, $\bar{Q} = \mathcal{L}\bar{u} - \bar{\lambda}$. This part is still using the computer, but one has to apply $\mathcal{L}$ rigorously. If $\bar{u}$ is obtained as a polynomial (or trigonometric polynomial), and the non-constant coefficients in $\mathcal{L}$ also are polynomials, then $\mathcal{L}\bar{u}$ can be evaluated exactly with finitely many operations, and one simply has to use interval arithmetic for that step to be rigorous. Otherwise, some combination of pen-and-paper estimates and interval arithmetic computations might be needed.

- Finally, one has to estimate rigorously $\|Q - \bar{Q}\|_{L^\infty}$. Since Q and $\bar{Q}$ are known explicitly, this is usually not too difficult. One can for instance use crude interval arithmetic calculations, or, depending on the basis which was used to express $\bar{Q}$, apply usual bounds on the L^∞ norm in terms of the coefficients.

Remark 6.3.5. *We stress again that, with the approach described here, we never need to rigorously solve a PDE. In particular, even in situations where one could actually do a computer-assisted proof for $\mathcal{L}^* w = 0$, the adjoint method provides a much cheaper alternative, as it only requires rigorously applying $\mathcal{L}$ once (and also estimating $\|Q - \bar{Q}\|_{L^\infty}$). If $\mathcal{L}$ is sparse, then this sparsity can be used for applying $\mathcal{L}$, whereas it is typically lost when one has to compute an approximate inverse in order to apply the Newton–Kantorovich Theorem 1.2.2.*

Moreover, since we no longer have to solve $\mathcal{L}^* w = 0$, the fact that $\mathcal{L}$ and $\mathcal{L}^*$ may not be elliptic is no longer a real issue, although strong lack of ellipticity typically means that in practice, solving for $\bar{u}$ accurately becomes harder.

Remark 6.3.6. *Estimate (6.22) is in some sense rather crude, as it does not seem to use any information on the invariant measure μ, but this is in fact a strength of this approach. Indeed, as already discussed, obtaining quantitative information on μ (or equivalently on the density w) can be very hard, and being able to rigorously enclose λ without knowing anything about w is part of what makes our method broadly applicable. Of course, if some information on w is available, then it may be leveraged to obtain sharper estimates, but directly using the simple estimate (6.22) can already lead to very precise results.*

Finally, let us discuss a possible generic strategy to employ when an L^∞ bound on $Q - \bar{Q}$ is too much to ask for. For instance, if we work on an unbounded domain and $\bar{Q}$ is obtained as a polynomial, $Q - \bar{Q}$ will typically be unbounded. However, one can then introduce a well-chosen positive weight function W, and estimate (6.21) by

$$|\lambda - \bar{\lambda}| \leq \left\| \frac{Q - \bar{Q}}{W} \right\|_{L^\infty} \int W \mathrm{d}\mu, \tag{6.23}$$

provided $\int W \mathrm{d}\mu$ can be estimated explicitly. In some cases, this can naturally be accomplished using a Lyapunov functional for $\mathcal{L}$, which is often needed anyway in order to prove the ergodicity of the projective process (see, e.g., [B12, Section 5]).

Remark 6.3.7. *We end this section on the computer-assisted adjoint method by noting that the strategy described here has in fact nothing specific to do with Lyapunov exponents, and can be used to rigorously enclose any ergodic average of the form*

$$\int g(x, s) \mathrm{d}\mu,$$

for a sufficiently explicit function g.

6.3.3.2 Some examples

We now give three examples for which a rigorous enclosure of the (top) Lyapunov exponent was obtained thanks to the computer-assisted adjoint method. All of these proofs can be reproduced using the code available at [Code 11].

Theorem 6.3.8. *Consider the cellular flow with sinks generated by the following SDE on $\mathbb{T}^2$*

$$\begin{cases} \mathrm{d}x_t &= (\cos(x_t)/2 - \cos y_t) \sin x_t \mathrm{d}t + \sigma \mathrm{d}W_t^1 \\ \mathrm{d}y_t &= (\cos(y_t)/2 + \cos x_t) \sin y_t \mathrm{d}t + \sigma \mathrm{d}W_t^2. \end{cases} \tag{6.24}$$

Then, for $\sigma = \sqrt{2}$, we have the following bounds for the Lyapunov exponent λ:

$$\lambda \in [0.055845309985\mathbf{6}, 0.055845309985\mathbf{8}].$$

Note that, even if we could and did use the crude-looking estimate (6.21) because we are on the torus, we obtain a 10^{-13} sharp enclosure. The underlying deterministic vector field, as well as a numerical simulation suggesting the appearance of a random attractor, are shown in Figure 6.6.

Remark 6.3.9. *In this example the state space is compact, therefore the positivity of the Lyapunov exponent alone does imply that the system (6.24) displays a random strange attractor [198]. Furthermore, applying the results of [164] also shows the existence of a random weak horseshoe for this system. This is a typical example where computer-assisted proofs are complementary with more traditional tools, as they enable the usage of powerful theoretical results whose assumptions (in that case, the assumption that the system has a positive Lyapunov exponent) are often very challenging to check in practice.*

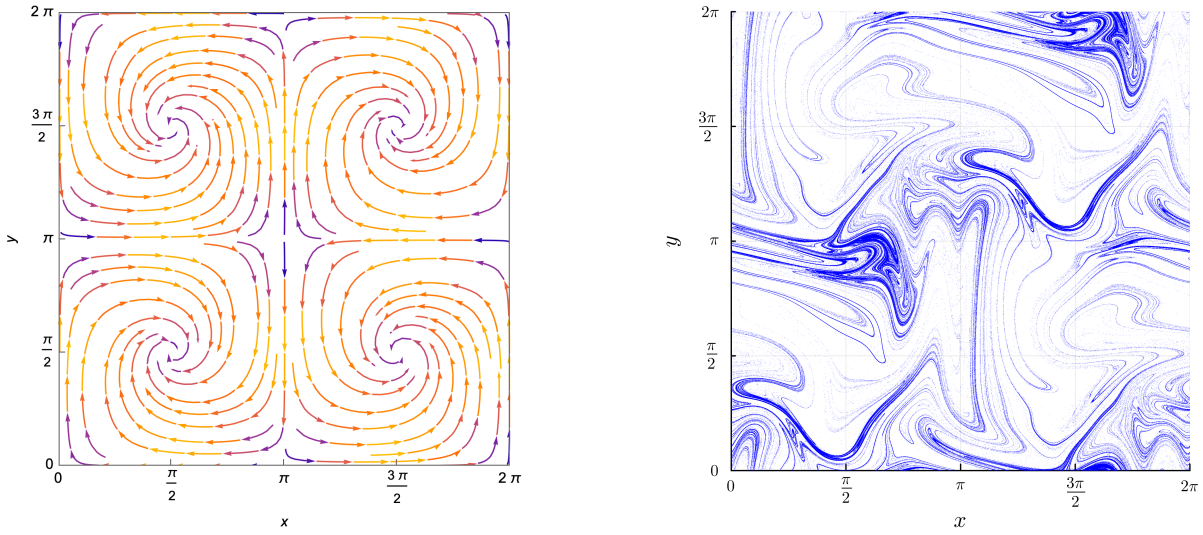

Figure 6.6: Deterministic and random dynamics of (6.24). Phase portrait for $\sigma = 0$ on the left, and numerical chaotic random attractor for $\sigma = \sqrt{2}$ on the right.

We now give a much more challenging example, where the state space of the SDEs is unbounded, and there is no noise in one component.

Theorem 6.3.10. *Consider the "noisy pendulum" given by the following SDE on* $\mathbb{T} \times \mathbb{R}$

$$\begin{cases} \mathrm{d}x_t &= y_t \mathrm{d}t \\ \mathrm{d}y_t &= -(\kappa \sin x_t + \gamma y_t)\mathrm{d}t + \sigma \mathrm{d}W_t. \end{cases} \tag{6.25}$$

Then, for $\kappa = 2/3$, $\gamma = 1/4$ *and* $\sigma = 4$, *we have the following bounds for the Lyapunov exponent* λ*:*

$$\lambda \in [0.00\mathbf{22}, 0.00\mathbf{32}].$$

In that case, the enclosure for the Lyapunov exponent is much less sharp than in Theorem 6.3.8. This is at least partially due to two factors: The phase space is unbounded, and the associated projective process is highly non-elliptic (there is already no noise in the x-direction in (6.25), and also no noise in the variational equation), which both contribute to making the numerical resolution of the equation (6.19) rather challenging in practice. The underlying deterministic vector field associated to the SDE (6.25), as well as a numerical simulation suggesting the appearance of a random attractor, are shown in Figure 6.7. Even if this model might seem rather simple, we emphasize that we know of no other technique that would allow to prove that the Lyapunov exponent is positive, especially since there is no obvious mechanism explaining the appearance of chaotic dynamics here.

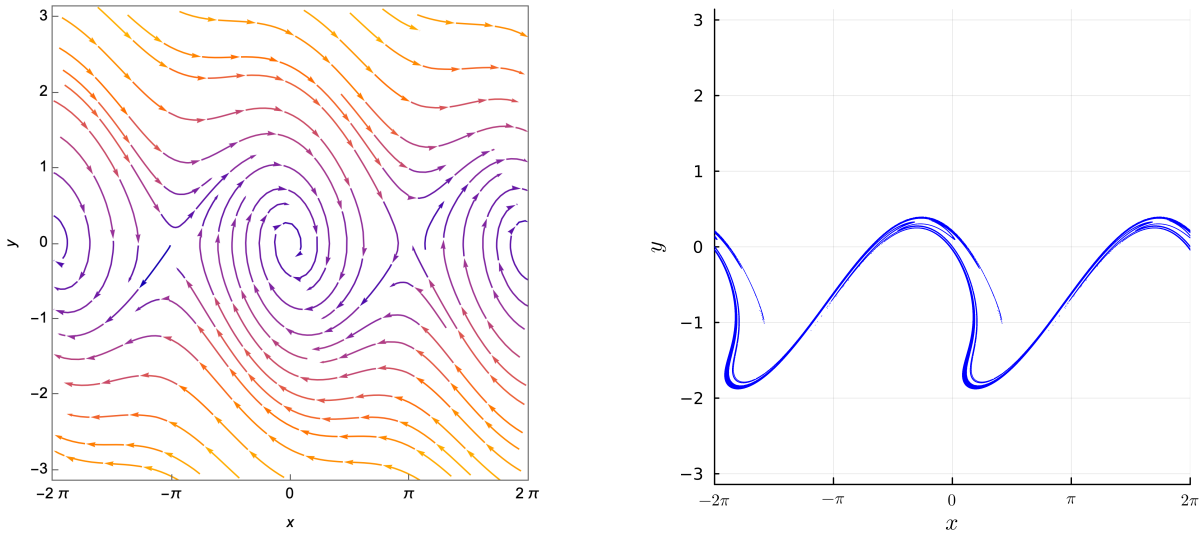

Figure 6.7: Deterministic and random dynamics of (6.25) for $\kappa = 2/3$ and $\gamma = 1/4$. Phase portrait for $\sigma = 0$ on the left, and numerical chaotic random attractor for $\sigma = 4$ on the right.

Finally, we come back to the Hopf bifurcation with noise (6.18), and combine the computer-assisted adjoint method with the rigorous continuation techniques using Chebyshev series described in Chapter 5, in order to obtain a rigorous enclosure of the Lyapunov exponent for all values of the shear parameter b in a relatively large interval, covering the transition from negative to positive Lyapunov exponent.

Theorem 6.3.11. *Consider the Hopf normal form with additive noise* (6.18) *on* $\mathbb{R}^2$*, with* $a = \alpha = \beta = 4$ *and* $\sigma = \sqrt{2}$*. For any* $b \in \mathbb{R}$*, denote* λ_b *the Lyapunov exponent of* (6.18) *with this* b*. For* $b \in [0, 30]$*, let* $b \mapsto \bar{\lambda}_b$ *be the function represented in Figure 6.8, and whose precise description can be found that at [Code 11]. Then, for* all $b \in [0, 30]$

$$|\lambda_b - \bar{\lambda}_b| \leq 3.41 \times 10^{-4}.$$

Corollary 6.3.12. *For* λ_b *as in Theorem 6.3.11, there exists* $b^* \in (21.53\mathbf{22}, 21.53\mathbf{81})$ *such that* $\lambda_{b^*} = 0$*. Furthermore,* $\lambda_b < 0$ *for* $b \in [0, 21.5322]$ *and* $\lambda_b > 0$ *for* $b \in [21.5381, 30]$*.*

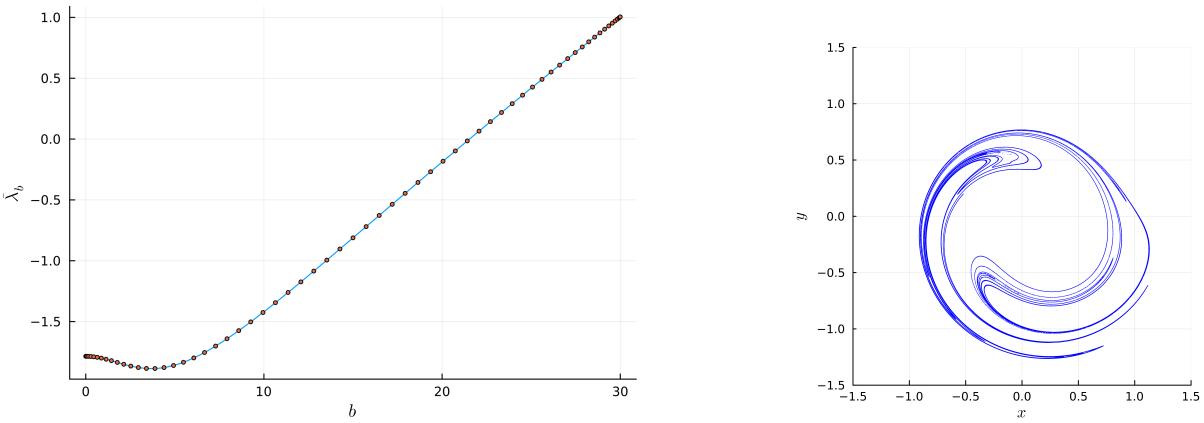

Figure 6.8: Quantitative and qualitative random dynamics induced by (6.18). On the left: graph of the function $b \mapsto \bar{\lambda}_b$ validated in Theorem 6.3.11, the orange points are the values at Chebyshev nodes which are used to construct $\bar{\lambda}_b$. On the right: numerical chaotic random attractor for $a = \alpha = 4$, $\sigma = \sqrt{2}$ and $b = 21.5381$.

Remark 6.3.13. *Finally, we note that while we restricted ourselves to SDEs with additive noise here for the sake of simplifying the presentation, SDEs with multiplicative noise can also be handled with our approach, see [B12, Section 4.2] for an example of the cellular flow (6.24) with a specific multiplicative noise inspired from [23].*

6.3.4 Random bifurcations and moment Lyapunov exponents via rigorous enclosures of large deviations rate functions

In this final section on computer-assisted proofs for SDEs and random dynamical systems, we discuss finite time Lyapunov exponents (FTLEs) (recall (6.12)), and their links with random bifurcations.

6.3.4.1 Motivations

Let us immediately start with an example, namely the normal form of the pitchfork bifurcation with additive noise:

$$\mathrm{d}x_t = (\alpha x_t - x_t^3)\mathrm{d}t + \sigma \mathrm{d}W_t, \qquad x_0 \in \mathbb{R}. \tag{6.26}$$

If there is no noise ($\sigma = 0$), the resulting ODE undergoes a pitchfork bifurcation at $\alpha = 0$, resulting in the creation of a pair of stable equilibria and a change of stability for the equilibrium at 0. When $\sigma > 0$, this bifurcation can also be seen at the level of the invariant density

$$\rho_{\sigma,\alpha}(x) = \frac{1}{Z} \exp\left(\frac{2}{\sigma^2}\left(\frac{1}{2}\alpha x^2 - \frac{1}{4}x^4\right)\right), \tag{6.27}$$

where Z is just a normalization constant. Indeed, $\rho_{\sigma,\alpha}$ is unimodal for $\alpha < 0$ but becomes bimodal for $\alpha > 0$.

However, it was shown in [82] that some features of the pitchfork are *destroyed by additive noise* in the following sense. If φ_t denotes the stochastic flow generated by equation (6.26) for $\sigma > 0$ (the analogue of the solution flow to an ODE) then for all fixed initial conditions $x_0, y_0 \in \mathbb{R}$, one has that

$$|\varphi_t(x_0) - \varphi_t(y_0)| \to 0 \qquad \text{as } t \to \infty, \tag{6.28}$$

with probability 1, irrespective of the value of α. Contrast this to the deterministic case ($\sigma = 0$), where *synchronization* as in (6.28) also occurs unconditionally when $\alpha < 0$, but only if x_0, y_0 are nonzero and share the same sign when $\alpha > 0$. In accordance with the fact that, when $\sigma > 0$, trajectories synchronize no matter the value of α, one has that the Lyapunov exponent $\lambda(\alpha)$ of (6.26) is negative for all $\alpha \in \mathbb{R}$. In particular, the bifurcation is not detected by the Lyapunov exponent.

Nonetheless, it was pointed out in [57] that one can recover some "signature" of the original pitchfork by examining quantitatively the synchronization property (6.28). Their argument is framed around the statistics of FTLEs. When $t \to \infty$, the ergodic theorem implies that the FTLEs $\lambda_t(\alpha; x_0)$ converge, with probability 1 and for all $x_0 \in \mathbb{R}$, to the *asymptotic* Lyapunov exponent $\lambda(\alpha)$, which as recalled above, is always negative. However, the FTLEs themselves undergo a qualitative transition through the bifurcation value $\alpha = 0$, which we can an *FTLE transition*:

- For $\alpha < 0$, $\lambda_t(\alpha; x_0) < 0$ with probability 1, for all $t > 0$ and $x_0 \in \mathbb{R}$;
- for $\alpha > 0$ the event $\{\lambda_t(\alpha; x_0) > 0\}$ has *positive probability* for all $t > 0$ and $x_0 \in \mathbb{R}$.

Viewed another way, for $\alpha > 0$ synchronization as in (6.28) is only true asymptotically, as $t \to \infty$, while transient derivative growth can persist for arbitrarily long times with positive probability, preventing the merging of $\varphi_t(x_0)$ and $\varphi_t(y_0)$. We refer to [57] for additional discussions on the

connection between FTLEs and synchronization, and note that FTLE transitions have already been established in a variety of settings: for discrete dynamical systems [263], for SDEs [101], and even for SPDEs [33, 34]. For a more general overview on stochastic bifurcations, we refer to [13] and [9, Chapter 9].

In [B5], we study quantitatively the statistics of λ_t (for more general SDEs than (6.26)), and the transition from negative FTLEs to positive FTLEs with positive probability. Our results are framed around the *large deviations rate function* tracking the statistics of deviations of the FTLEs from their asymptotic value. For $r > \lambda(\alpha)$, this rate function takes the form

$$\mathcal{I}_\alpha(r) := -\lim_{t\to\infty} \frac{1}{t} \ln \mathbb{P}(\lambda_t(\alpha; x_0) > r) \in (0, \infty]. \tag{6.29}$$

In particular, when $\lambda(\alpha) < 0$, the rate $\mathcal{I}_\alpha(0)$ quanitifies the likelihood of transient nonsynchronization in the sense that

$$\mathbb{P}(\lambda_t(\alpha; x_0) > 0) \approx e^{-t\mathcal{I}_\alpha(0)}, \tag{6.30}$$

for large times t. Moreover, we prove in [B5, Theorem 3.3] that, under some mild conditions that are for instance satisfied by (6.26), an FTLE transition occurs at some $\alpha = \alpha_0$ if and only if, for some $\varepsilon > 0$, $\mathcal{I}_\alpha(0) = \infty$ for all $\alpha \in (\alpha_0 - \varepsilon, \alpha_0)$ and $\mathcal{I}_\alpha(0) < \infty$ for all $\alpha \in (\alpha_0, \alpha_0 + \varepsilon)$.

Motivated by these connections between the rate function $\mathcal{I}_\alpha(0)$ and the probability of having positive FTLEs, we develop in [B5] computer-assisted tools which enable us to obtain precise and quantitative statements about this rate function. In particular, we first observed numerically and then could prove rigorously that $\mathcal{I}_\alpha(0)$ behaves non-monotonically with respect to α, and has a local minimum (see Theorem 6.3.14 for a precise statement, and Figure 6.9 for a more global illustration), which suggests the existence of a specific value of $\alpha > 0$ for which synchronization is the weakest. Heuristically, the existence of this minimum should have to do with the trade-off, between increased expansion near 0, which increases FTLEs, and a shortening of the time spent in the expanding region, which decreases FTLEs. While this heuristic applies to FTLEs as well as to the asymptotic Lyapunov exponent, it is notable that they exhibit their local extrema at distinct values of the parameter α (see Figure 6.9).

Theorem 6.3.14. *Let $\sigma = 1$ in (6.26). The map $\alpha \mapsto \mathcal{I}_\alpha(0)$ has a local minimum at some $\alpha_* \in [1.22\mathbf{5}, 1.22\mathbf{9}]$.*

6.3.4.2 From the rate function to moment Lyapunov exponents and rigorous eigenvalue enclosures

We now explain how we obtained the computer-assisted proof of Theorem 6.3.14, and more generally of the enclosures of the rate function depicted in Figure 6.9. All the following discussion applies to any fixed α, and we therefore no longer keep the α dependency in the notations.

One crucial ingredient is the notion of moment Lyapunov exponents (MLEs), defined, with the notations of Section 6.3.1, as

$$\Lambda(p) = \lim_{t\to\infty} \frac{1}{t} \ln \mathbb{E}\left(\|y_t\|^p\right), \qquad p \in \mathbb{R}. \tag{6.31}$$

This limit indeed exists (and is independent of the initial conditions) for the SDE (6.26), and moreover Λ is an analytic and convex function of p, which satisfies $\Lambda(0) = 0$ and $\Lambda'(0) = \lambda$. Finally, $\Lambda''(0)$ is the asymptotic variance appearing in the central limit theorem governing convergence in distribution of $\sqrt{t}(\lambda_t - \lambda)$ [11]. These properties still hold for a large class of SDEs, and we refer to [B5] and the references therein for sufficient conditions.

The MLEs are directly connected with the rate function $\mathcal{I}$, via the Legendre–Fenchel transform:

$$\mathcal{I}(r) = \sup_{p\in\mathbb{R}} \left(rp - \Lambda(p)\right), \tag{6.32}$$

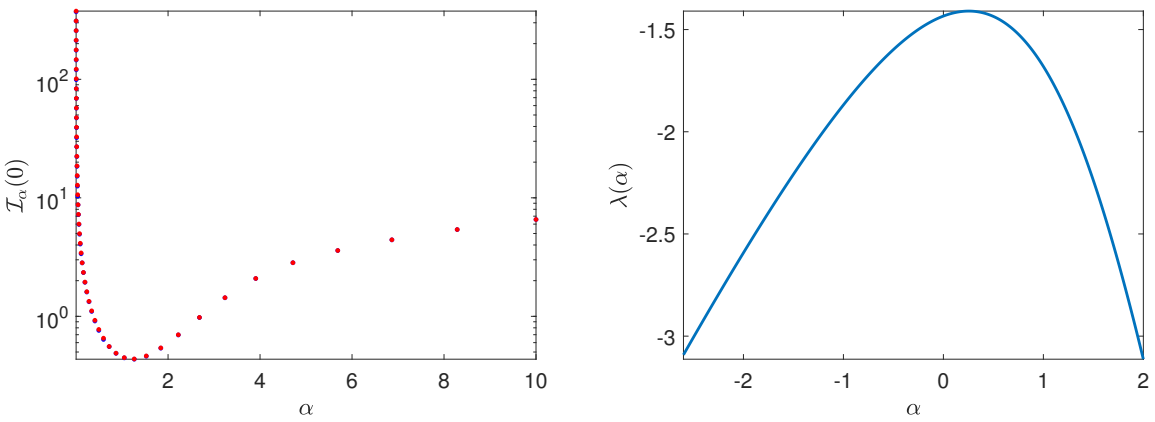

Figure 6.9: A quantitative study of the synchronization for (6.26), with $\sigma = 1$. On the left, we show rigorous enclosures of the rate function $\mathcal{I}_\alpha(0)$, for different values of α. Upper-bounds are shown in red, and lower bounds in blue, but they are close enough to be hard to distinguish. On the right we show a numerical computation of the asymptotic Lyapunov exponent λ_α, highlighting that its maximum is not reached at the same value α at which $\mathcal{I}_\alpha(0)$ reaches its minimum.

and we recall that this rate function characterizes large deviation estimates for FTLEs,[3] see for instance [B5, Theorem 2.4] for explicit statements. According to (6.32), getting quantitative and rigorous information on the rate function $\mathcal{I}$ is possible if we are able to get quantitative and rigorous information on the MLEs $\Lambda(p)$.

Remark 6.3.15. *Despite the presence of a supremum in (6.32), note that thanks to the convexity of Λ, rigorously enclosing Λ for a few specific values (and small intervals) of p can be enough to obtain the value $\mathcal{I}(0)$, which is of particular interest to us and simply given by*

$$\mathcal{I}(0) = -\inf_{p\in\mathbb{R}} \Lambda(p).$$

Indeed, if we find $p_1 < p_2 < p_3$ such that $\Lambda(p_1) > \Lambda(p_2)$ and $\Lambda(p_2) < \Lambda(p_3)$, then by convexity of Λ we know that its infimum is reached within the interval $[p_1, p_3]$, and therefore that $\mathcal{I}(0)$ is included in $-\Lambda([p_1, p_3])$.

In order to rigorously enclose $\Lambda(p)$ for a fixed p (and also for a small interval of p's, using interval arithmetic), we do not try to work directly with the definition (6.31), but instead leverage a different characterization of MLEs, namely that $\Lambda(p)$ is the principal eigenvalue of a so-called *tilted-generator* $\mathcal{L}_p$ [279], which is constructed from the generator $\mathcal{L}$ defined in (6.16), with additional zero order terms depending on p. In the specific case of (6.26), the titled generator writes

$$\mathcal{L}_p u = \frac{\sigma^2}{2}\partial_{xx} u + (\alpha x - x^3)\partial_x u + p(\alpha - 3x^2)u, \qquad x \in \mathbb{R}. \tag{6.33}$$

In summary, we have reduced the problem of rigorously enclosing the rate function $\mathcal{I}$ to that of rigorously enclosing eigenvalues of the operator $\mathcal{L}_p$. As already discussed several times in this manuscript, there exists computer-assisted techniques for rigorously enclosing eigenvalues of elliptic operators, especially self-adjoint ones, but non-self-adjoint elliptic problems can also be considered (as shown for instance in Section 6.3.2.2). While the operator $\mathcal{L}_p$ defined in (6.33) might not seem self-adjoint at first glance, it is in fact self adjoint on $L^2(\rho)$, where ρ is the

[3] This is the *correct* definition of the rate function. The more direct definition given in (6.29) should only be used for r larger than the asymptotic Lyapunov exponent λ, in which case it does coincide with the one given here.

invariant density (6.27) of the SDE (6.26). Equivalently, one can consider the isometry $u \mapsto \rho^{1/2}u$ between $L^2(\rho)$ and L^2, which conjugates $\mathcal{L}_p$ to a Schrödinger type operator H_p given by

$$H_p u = \frac{\sigma^2}{2}\partial_{xx}u - V_p(x)u,$$

which is now clearly self-adjoint on the flat L^2 space, and has the same spectrum as $\mathcal{L}_p$, where the potential V_p writes

$$V_p(x) = \frac{(x^3 - \alpha x)^2}{2\sigma^2} - (3x^2 - \alpha)\left(\frac{1}{2} - p\right).$$

Because the operator H_p is self-adjoint, but defined on the whole real line, the homotopy method presented in Section 1.3.2.3 is especially well-suited for obtaining rigorous and sharp bounds on its first eigenvalue. In particular, in contrast to the situation discussed in Section 6.3.2.2 where we had a non-self-adjoint problem, and therefore had to go via a zero-finding problem, the homotopy method directly gives us enclosures and the corresponding indices of the enclosed eigenvalues, therefore we do not have to check a posteriori that we indeed enclosed the right eigenvalue.

In order to use the homotopy method for the operator $-H_p$,[4] we need a suitable base problem (recall Definition 1.3.16), and the ability to numerically get accurate approximations of eigenfunctions of H_p. Here, both turn out to be rather straightforward. Indeed, the potential V_p grows like x^6 at infinity, therefore one can easily find a quadratic potential $V_p^{(0)}$ such that $V_p^{(0)}(x) \leq V_p(x)$ for all $x \in \mathbb{R}$, and consider the base problem

$$-H_p^{(0)} = -\frac{\sigma^2}{2}\partial_{xx} + V_p^{(0)}(x),$$

which is nothing but (a rescaled version of) the quantum harmonic oscillator, whose eigenvalues are known explicitly. Regarding approximate eigenfunctions, because the potential V_p is confining we expect eigenfunctions to be localized. We can therefore look for compactly supported eigenfunctions, discretized for instance using finite Chebyshev series. Moreover, the fact that eigenfunctions are well localized means that, even if V_p and $V_p^{(0)}$ behave quite differently at infinity, the base problem $-H_p^{(0)}$ will not be *too far away* from $-H_p$, in the sense that the large differences in the potentials at infinity will become insignificant against localized eigenfunctions.

Applying the homotopy method to rigorously enclose the first eigenvalue of $-H_p$, and hence of $\mathcal{L}_p$ from (6.33), is then rather straightforward, and yields the enclosures for $\mathcal{I}(0)$ reported in Figure 6.9. Similar computations, but for specific values of α closer to the minimum, yield Theorem 6.3.14. All these computations can be reproduced with the code available at [Code 7].

We note that a second example with different features compared to (6.26), namely a compact state space but multiplicative noise, is also studied in [B5]. The corresponding tilted generator $\mathcal{L}_p$ is no longer self-adjoint, but posed on a compact domain, which means the eigenvalue problem can be rigorously attacked via a zero-finding problem and the Newton–Kantorovich Theorem 1.2.2, as in Section 6.3.2.2. A notable consequence of going via a zero-finding problem and Theorem 1.2.2 is that we can then easily use the rigorous continuation tools introduced in Chapter 5. We are therefore able to get a much finer control on the dependency of Λ with respect to p, and for instance to rigorously enclose the asymptotic variance $\Lambda''(0)$ using Lemma 5.3.7. We again refer to [B5] for details, and to [Code 7] for the corresponding code.

[4] The minus sign is added for convenience, to get back to the setting of Section 1.3.2.3, where eigenvalues accumulate at $+\infty$.

6.4 Perspectives

- **A more natural setup for controlling truncation errors in gPC expansions.** Regarding Section 6.1, the natural setting for defining gPC expansions is $L^2(\rho)$, and it is in that metric that choosing the gPC expansions associated to the distribution of the random parameter is clearly optimal. However, all our computer-assisted proofs which control truncation errors for gPC expansions are done in the stronger ℓ^1_η norm, in which the distribution of the random parameter no longer plays any role. In particular, in that norm there is no longer any incentive for picking an expansion associated to the distribution of the random parameter, instead Chebyshev expansions are always the better choice (see [B8] for detailed comparisons). It would therefore be desirable to find an arguably more natural framework for rigorously controlling truncation errors of gPC expansions, in which selecting the proper basis could still be noticed.

- **Controlling truncation errors in gPC expansions beyond the Jacobi case.** On a somewhat related note, in Section 6.1, we only worked with gPC expansions associated with Jacobi polynomials, which in particular excludes the commonly used Hermite polynomials associated to Gaussian random variables. The main reason for this restriction is that Theorem 6.1.2 does not hold for Hermite expansions, therefore the question of rigorously quantifying a posteriori the truncation errors in that case remains open.

- **MAPs for non-gradient SDEs.** Regarding Section 6.2 and MEPs, a natural extension would be to derive a similar computer-assisted approach for minimal action paths, i.e., when the underlying ODE is no longer gradient. This means that MAPs no longer necessarily correspond to (concatenation of) connecting orbits of the original ODE, but one should be able to sometimes recover this characterization by looking at the extended system obtained from Hamilton's equations of motion associated to the Lagrangian (6.6) [146]. However, without the gradient structure, more complicated situations can also occur, for instance equilibria separated by a limit cycle, for which the description of MAPs is less straightforward [122].

- **Computer-assisted proofs for hypoelliptic equations.** Section 6.3 raises many questions, and suggests potential further investigations, of rather different nature. The most far-reaching one is that the study of Fokker–Planck operators associated to SDEs strongly calls for the development of computer-assisted proofs for solving hypoelliptic but non-elliptic equations, which would in fact be of interest beyond the study of stochastic systems. This is a very challenging question, but a possible angle of attack might be to first look specifically at the so-called kinetic Fokker–Planck equation, which has been very intensely studied within kinetic theory [304], and for which the explicit compactness estimates required for constructing an approximate inverse for Theorem 1.2.2 might be within reach. Some work in that direction is being started in collaboration with Maxime Herda.

- **Expanding the scope of the method for rigorously enclosing moment Lyapunov exponents.** On a related note, let us emphasize that the approach presented in Section 6.3.3 does already enable us to deal with questions related to hypoelliptic equations, but only if the quantity of interest can be expressed as an ergodic average. This is for instance the case of the (asymptotic) Lyapunov exponent, but not of the moment Lyapunov exponents that proved crucial in Section 6.3.4. This means that the rigorous quantitative study of the large deviation rate function described in Section 6.3.4 is for the moment only possible if the resulting tilted generator $\mathcal{L}_p$ is uniformly elliptic. Even without talking about genuinely hypoelliptic problems, being able to deal with non-uniformly elliptic problems, for instance coming from multiplicative noise, or with more general elliptic problems on unbounded domains, would already be of great interest. Below are a few more specific perspectives related to Section 6.3.

- **Using machine learning to find approximate solutions for the computer-assisted adjoint method.** In the computer-assisted adjoint method described in Section 6.3.3, the most challenging step is often to numerically find a reasonably accurate approximate solution $\bar{u}$ to equation (6.19). Since traditional numerical methods seem to suffer for this problem, at least in the highly non-elliptic cases, it might be of interest to use machine learning algorithms to find approximate solutions, which would possibly allow us to treat higher dimensional problems. The idea that neural networks could prove useful to find new approximate solutions that would then be validated a posteriori using computer-assisted proofs is not new, and was for instance put forward in [306] in the context of fluid dynamics.

- **Quantitative estimates on FTLEs.** In Section 6.3.4, we investigated fluctuations of FTLEs and obtained rigorous quantitative information on the rate function $\mathcal{I}$. While this rate function is definitely related to statistics of FTLEs, via large deviation estimates or through the characterization of an FTLE transition, having quantitative versions of large deviation estimates like (6.30) would be required in order to translate our quantitative statements on $\mathcal{I}$ into quantitative statements on the probability of having positive FTLEs.

- **Computer-assisted proofs of stochastic resonances.** Finally, we end with a perspective which belongs thematically to this chapter, but is still rather distinct from the problems mentioned there, namely a rigorous study of stochastic resonances using computer-assisted proofs. Very roughly speaking, the term stochastic resonance is used to describe a situation where a well-chosen level of noise makes a stochastic system behave in an almost deterministic-like manner, by producing rather regular oscillations that could not be observed in the absence of noise. Stochastic resonances can be found in a variety of contexts, and are believed to be important mechanisms in models related for instance to neuroscience or to climate [142, 31]. However, studying such phenomena mathematically is particularly challenging, if only because stochastic resonances typically appear for noise levels which are far from being arbitrarily small. With the recent development of computer-assisted proofs for the study of PDEs, and their links with SDEs, a rigorous study of some cases of stochastic resonance might be within reach. In particular, in an ongoing work with Hugo Chu, which relies on some of the tools developed in Section 3.3, we try to study stochastic resonance in the stochastic Duffing oscillator [76], by precisely describing the periodic invariant density, which means doing a computer-assisted proof for a periodic orbit of a parabolic PDE posed on an unbounded domain.

References

[1] H. Amann. Nonhomogeneous linear and quasilinear elliptic and parabolic boundary value problems. *Function spaces, differential operators and nonlinear analysis*, pages 9–126, 1993.

[2] K. Appel and W. Haken. Every planar map is four colorable. Part I: Discharging. *Illinois Journal of Mathematics*, 21(3):429–490, 1977.

[3] K. Appel, W. Haken, and J. Koch. Every planar map is four colorable. Part II: Reducibility. *Illinois Journal of Mathematics*, 21(3):491–567, 1977.

[4] G. Arioli, F. Gazzola, and H. Koch. Uniqueness and bifurcation branches for planar steady Navier–Stokes equations under Navier boundary conditions. *Journal of Mathematical Fluid Mechanics*, 23(3):1–20, 2021.

[5] G. Arioli and H. Koch. Computer-assisted methods for the study of stationary solutions in dissipative systems, applied to the Kuramoto-Sivashinski equation. *Arch. Ration. Mech. Anal.*, 197(3):1033–1051, 2010.

[6] G. Arioli and H. Koch. Integration of dissipative partial differential equations: a case study. *SIAM J. Appl. Dyn. Sys.*, 9(3):1119–1133, 2010.

[7] G. Arioli and H. Koch. Existence and stability of traveling pulse solutions of the FitzHugh-Nagumo equation. *Nonlinear Anal.*, 113:51–70, 2015.

[8] G. Arioli and H. Koch. Non-radial solutions for some semilinear elliptic equations on the disk. *Nonlinear Analysis*, 179:294–308, 2019.

[9] L. Arnold. *Random Dynamical Systems*. Springer Science & Business Media, 2013.

[10] L. Arnold, P. Imkeller, and N. S. Namachchivaya. The Asymptotic Stability of Weakly Perturbed Two Dimensional Hamiltonian Systems. In *Volume 6C: 18th Biennial Conference on Mechanical Vibration and Noise*, pages 2477–2486. American Society of Mechanical Engineers, 9 2001.

[11] L. Arnold and W. Kliemann. Large deviations of linear stochastic differential equations. In H. J. Engelbert and W. Schmidt, editors, *Stochastic Differential Systems*, pages 115–151, Berlin, Heidelberg, 1987. Springer Berlin Heidelberg.

[12] L. Arnold, G. Papanicolaou, and V. Wihstutz. Asymptotic Analysis of the Lyapunov Exponent and Rotation Number of the Random Oscillator and Applications. *SIAM Journal on Applied Mathematics*, 46(3):427–450, 6 1986.

[13] L. Arnold, N. Sri Namachchivaya, and K. R. Schenk-Hoppé. Toward an understanding of stochastic hopf bifurcation: a case study. *International Journal of Bifurcation and Chaos*, 6(11):1947–1975, 1996.

[14] S. Arrhenius. Über die Reaktionsgeschwindigkeit bei der Inversion von Rohrzucker durch Säuren. *Zeitschrift für physikalische Chemie*, 4(1):226–248, 1889.

[15] M. Aschbacher. *Sporadic groups*. Cambridge University Press, 1994.

[16] A. Avila and M. Lyubich. The full renormalization horseshoe for unimodal maps of higher degree: exponential contraction along hybrid classes. *Publications mathématiques de l'IHÉS*, 114:171–223, 2011.

[17] W. Bahsoun and C. Bose. Invariant densities and escape rates: rigorous and computable approximations in the l^∞-norm. *Nonlinear Analysis: Theory, Methods & Applications*, 74(13):4481–4495, 2011.

[18] W. Bahsoun, S. Galatolo, I. Nisoli, and X. Niu. A rigorous computational approach to linear response. *Nonlinearity*, 31(3):1073, 2018.

[19] C. Bataillon, F. Bouchon, C. Chainais-Hillairet, C. Desgranges, E. Hoarau, F. Martin, S. Perrin, M. Tupin, and J. Talandier. Corrosion modelling of iron based alloy in nuclear waste repository. *Electrochimica Acta*, 55(15):4451–4467, 2010.

[20] C. Bataillon, F. Bouchon, C. Chainais-Hillairet, J. Fuhrmann, E. Hoarau, and R. Touzani. Numerical methods for the simulation of a corrosion model with moving oxide layer. *Journal of Computational Physics*, 231(18):6213–6231, 2012.

[21] B. Batko, M. Gameiro, Y. Hung, W. Kalies, K. Mischaikow, and E. Vieira. Identifying nonlinear dynamics with high confidence from sparse data. *SIAM Journal on Applied Dynamical Systems*, 23(1):383–409, 2024.

[22] P. H. Baxendale. Statistical equilibrium and two-point motion for a stochastic flow of diffeomorphisms. *Spatial Stochastic Processes: A Festschrift in Honor of Ted Harris on his Seventieth Birthday*, pages 189–218, 1991.

[23] P. H. Baxendale. Asymptotic behaviour of stochastic flows of diffeomorphisms. In *Stochastic Processes and Their Applications: Proceedings of the International Conference held in Nagoya, July 2–6, 1985*, pages 1–19. Springer, 2006.

[24] P. H. Baxendale. Lyapunov exponents and shear-induced chaos for a Hopf bifurcation with additive noise. *Probability Theory and Related Fields*, 2024.

[25] P. H. Baxendale and L. Goukasian. Lyapunov Exponents for Small Random Perturbations of Hamiltonian Systems. *The Annals of Probability*, 30(1):101–134, 1 2002.

[26] J. Bedrossian, A. Blumenthal, and S. Punshon-Smith. A regularity method for lower bounds on the Lyapunov exponent for stochastic differential equations. *Inventiones mathematicae*, 227(2):429–516, 2022.

[27] J. Bedrossian, A. Blumenthal, and S. Punshon-Smith. Lower bounds on the Lyapunov exponents of stochastic differential equations. In *International Congress of Mathematicians*, volume 7, pages 5618–5654. EMS Press, 12 2023.

[28] J. Bedrossian and S. Punshon-Smith. Chaos in stochastic 2D Galerkin-Navier–Stokes. *Communications in Mathematical Physics*, 405(4):107, 2024.

[29] H. Behnke and G. F. Inclusions for eigenvalues of selfadjoint problems. In *Topics in Validated Computations*, volume 5 of *Studies in Computational Mathematics*, pages 277–322. North-Holland, Amsterdam, 1994.

[30] L. Benet, L. Ferranti, O. Hénot, R. Benoît, and D. Sanders. IntervalArithmetic.jl. https://github.com/JuliaIntervals/IntervalArithmetic.jl, 2023.

[31] R. Benzi, G. Parisi, A. Sutera, and A. Vulpiani. A theory of stochastic resonance in climatic change. *SIAM Journal on applied mathematics*, 43(3):565–578, 1983.

[32] N. Berglund. Kramers' law: validity, derivations and generalisations. *Markov Processes Relat. Fields*, 19(3):459–490, 2013.

[33] D. Blömker and A. Neamţu. Bifurcation theory for spdes: finite-time lyapunov exponents and amplitude equations. *SIAM Journal on Applied Dynamical Systems*, 22(3):2150–2179, 2023.

[34] A. Blumenthal, M. Engel, and A. Neamţu. On the pitchfork bifurcation for the chafee–infante equation with additive noise. *Probability Theory and Related Fields*, 187(3):603–627, 2023.

[35] B. Bogosel and D. Bucur. Polygonal Faber-Krahn inequality: Local minimality via validated computing. *arXiv preprint arXiv:2406.11575*, 2024.

[36] F. Bourgey, E. Gobet, and C. Rey. A comparative study of polynomial-type chaos expansions for indicator functions. *SIAM/ASA Journal on Uncertainty Quantification*, 10(4):1350–1383, 2022.

[37] A. Bovier, M. Eckhoff, V. Gayrard, and M. Klein. Metastability in reversible diffusion processes I: Sharp asymptotics for capacities and exit times. *Journal of the European Mathematical Society*, 6(4):399–424, 2004.

[38] A. Bovier, V. Gayrard, and M. Klein. Metastability in reversible diffusion processes II: Precise asymptotics for small eigenvalues. *Journal of the European Mathematical Society*, 7(1):69–99, 2005.

[39] Z. Bradshaw and T.-P. Tsai. Self-similar solutions to the Navier–Stokes equations: A survey of recent results. *arXiv preprint arXiv:1802.00038*, 2018.

[40] F. Bréhard, N. Brisebarre, and M. Joldeş. Validated and numerically efficient Chebyshev spectral methods for linear ordinary differential equations. *ACM Transactions on Mathematical Software (TOMS)*, 44(4):1–42, 2018.

[41] F. Bréhard, A. Mahboubi, and D. Pous. A certificate-based approach to formally verified approximations. In *ITP 2019-Tenth International Conference on Interactive Theorem Proving*, pages 1–19, 2019.

[42] B. Breuer, J. Horák, P. McKenna, and M. Plum. A computer-assisted existence and multiplicity proof for travelling waves in a nonlinearly supported beam. *J. Differential Equations*, 224(1):60–97, 2006.

[43] H. Brezis, L. A. Peletier, and D. Terman. A very singular solution of the heat equation with absorption. *Archive for Rational Mechanics and Analysis*, 95:185–209, 1986.

[44] T. Buckmaster, G. Cao-Labora, and J. Gómez-Serrano. Smooth imploding solutions for 3D compressible fluids. *arXiv preprint arXiv:2208.09445*, 2022.

[45] A. D. Burbanks, A. H. Osbaldestin, and J. A. Thurlby. Rigorous computer-assisted bounds on the period doubling renormalization fixed point and eigenfunctions in maps with critical point of degree 4. *Journal of Mathematical Physics*, 62(11), 2021.

[46] M. Burger, P. Laurençot, and A. Trescases. Delayed blow-up for chemotaxis models with local sensing. *Journal of the London Mathematical Society*, 103(4):1596–1617, 2021.

[47] T. Butler, C. Dawson, and T. Wildey. A posteriori error analysis of stochastic differential equations using polynomial chaos expansions. *SIAM Journal on Scientific Computing*, 33(3):1267–1291, 2011.

[48] X. Cabré, E. Fontich, and R. de la Llave. The parameterization method for invariant manifolds I: manifolds associated to non-resonant subspaces. *Indiana Univ. Math. J.*, 52(2):283–328, 2003.

[49] X. Cabré, E. Fontich, and R. de la Llave. The parameterization method for invariant manifolds II: Regularity with respect to parameters. *Indiana Univ. Math. J.*, 52(2):329–360, 2003.

[50] X. Cabré, E. Fontich, and R. de la Llave. The parameterization method for invariant manifolds III: Overview and applications. *J. Differential Equations*, 218(2):444–515, 2005.

[51] M. Cadiot. Constructive proofs of existence and stability of solitary waves in the capillary-gravity Whitham equation. *arXiv preprint arXiv:2403.18718*, 2024.

[52] M. Cadiot and D. Blanco. The 2D Gray–Scott system of equations: constructive proofs of existence of localized stationary patterns. *arXiv preprint arXiv:2404.08529*, 2024.

[53] M. Cadiot, J. Jaquette, J.-P. Lessard, and A. Takayasu. Validated matrix multiplication transform for orthogonal polynomials with applications to computer-assisted proofs for PDEs. *arXiv preprint arXiv:2411.18361*, 2024.

[54] M. Cadiot and J.-P. Lessard. Recent advances about the rigorous integration of parabolic PDEs via fully spectral Fourier-Chebyshev expansions. *In preparation*, 2025.

[55] M. Cadiot, J.-P. Lessard, and J.-C. Nave. Rigorous computation of solutions of semilinear PDEs on unbounded domains via spectral methods. *SIAM Journal on Applied Dynamical Systems*, 23(3):1966–2017, 2024.

[56] M. Cadiot, J.-P. Lessard, and J.-C. Nave. Stationary non-radial localized patterns in the planar Swift–Hohenberg PDE: constructive proofs of existence. *Journal of Differential Equations*, 414:555–608, 2025.

[57] M. Callaway, T. Doan, J. Lamb, and M. Rasmussen. The dichotomy spectrum for random dynamical systems and pitchfork bifurcations with additive noise. *Annales de l'Institut Henri Poincaré, Probabilités et Statistiques*, 53(4):1548–1574, 2017.

[58] R. Calleja, C. García-Azpeitia, O. Hénot, J.-P. Lessard, and J. D. Mireles James. From the lagrange triangle to the figure eight choreography: Proof of Marchal's conjecture. *arXiv preprint arXiv:2406.17564*, 2024.

[59] R. C. Calleja, A. Celletti, and R. De la Llave. A KAM theory for conformally symplectic systems: efficient algorithms and their validation. *Journal of Differential Equations*, 255(5):978–1049, 2013.

[60] M. Campanino and H. Epstein. On the existence of Feigenbaum's fixed point. *Commun. Math. Phys*, 79:261–302, 1981.

[61] C. Cancès, C. Chainais-Hillairet, B. Merlet, F. Raimondi, and J. Venel. Mathematical analysis of a thermodynamically consistent reduced model for iron corrosion. *Zeitschrift für angewandte Mathematik und Physik*, 74(3):96, 2023.

[62] E. Cancès, G. Dusson, Y. Maday, B. Stamm, and M. Vohralík. Guaranteed and robust a posteriori bounds for laplace eigenvalues and eigenvectors: conforming approximations. *SIAM Journal on Numerical Analysis*, 55(5):2228–2254, 2017.

[63] E. Cancès, G. Dusson, Y. Maday, B. Stamm, and M. Vohralík. Guaranteed a posteriori bounds for eigenvalues and eigenvectors: multiplicities and clusters. *Mathematics of Computation*, 89(326):2563–2611, 2020.

[64] C. Canuto, M. Y. Hussaini, A. Quarteroni, and T. A. Zang. *Spectral methods in fluid dynamics*. Springer Science & Business Media, 2012.

[65] M. J. Capiński and P. Zgliczyński. Cone conditions and covering relations fortopologically normally hyperbolic invariant manifolds. *Discrete and Continuous Dynamical Systems*, 30(3):641–670, 2011.

[66] R. Castelli, M. Gameiro, and J.-P. Lessard. Rigorous numerics for ill-posed PDEs: periodic orbits in the Boussinesq equation. *Arch. Ration. Mech. An.*, 228(1):129–157, 2018.

[67] A. Castro, D. Córdoba, and J. Gómez-Serrano. *Global smooth solutions for the inviscid SQG equation*, volume 266. American Mathematical Society, 2020.

[68] G. Castro-López and J. Gómez-Serrano. Existence of analytic non-convex v-states. *arXiv preprint arXiv:2411.12958*, 2024.

[69] C. Chainais-Hillairet and T. O. Gallouët. Study of a pseudo-stationary state for a corrosion model: Existence and numerical approximation. *Nonlinear Analysis: Real World Applications*, 31:38–56, 2016.

[70] C. Chainais-Hillairet and I. Lacroix-Violet. The existence of solutions to a corrosion model. *Applied Mathematics Letters*, 25(11):1784–1789, 2012.

[71] C. Chainais-Hillairet and I. Lacroix-Violet. On the existence of solutions for a drift-diffusion system arising in corrosion modeling. *Discrete and Continuous Dynamical Systems - B*, 20(1):77–92, 2015.

[72] D. Chemnitz and M. Engel. Positive Lyapunov exponent in the Hopf normal form with additive noise. *Communications in Mathematical Physics*, 402(2):1807–1843, 9 2023.

[73] J. Chen and T. Y. Hou. Stable nearly self-similar blowup of the 2D Boussinesq and 3D Euler equations with smooth data I: Analysis. *arXiv preprint arXiv:2210.07191*, 2022.

[74] J. Chen and T. Y. Hou. Stable nearly self-similar blowup of the 2D Boussinesq and 3D Euler equations with smooth data II: rigorous numerics. *Multiscale Modeling & Simulation*, 23(1):25–130, 2025.

[75] L. Chen and A. Jüngel. Analysis of a parabolic cross-diffusion population model without self-diffusion. *Journal of Differential Equations*, 224(1):39–59, 2006.

[76] A. M. Cherubini, J. S. Lamb, M. Rasmussen, and Y. Sato. A random dynamical systems perspective on stochastic resonance. *Nonlinearity*, 30(7):2835, 2017.

[77] K. Church and E. Queirolo. Computer-assisted proofs of Hopf bubbles and degenerate Hopf bifurcations. *Journal of Dynamics and Differential Equations*, pages 1–55, 2023.

[78] K. E. Church. Validated integration of differential equations with state-dependent delay. *Communications in Nonlinear Science and Numerical Simulation*, 115:106762, 2022.

[79] P. Collet, J. P. Eckmann, and O. Lanford. Universal properties of maps on an interval. *Communications in Mathematical Physics*, 76:211–254, 1980.

[80] P. Collet, S. Martinez, and J. San Martin. *Quasi-stationary distributions.* Probability and its Applications. Springer, Berlin, 2013.

[81] M. Coti Zelati and V. Navarro-Fernández. Three-dimensional exponential mixing and ideal kinematic dynamo with randomized ABC flows. *arXiv preprint arXiv:2407.18028*, 2024.

[82] H. Crauel and F. Flandoli. Additive noise destroys a pitchfork bifurcation. *Journal of Dynamics and Differential Equations*, 10(2):259–274, 1996.

[83] P. Cvitanović. Recurrent flows: the clockwork behind turbulence. *J. Fluid Mech.*, 726:1–4, 2013.

[84] J. Cyranka. Efficient and generic algorithm for rigorous integration forward in time of dPDEs: Part I. *Journal of Scientific Computing*, 59:28–52, 2014.

[85] J. Cyranka and J.-P. Lessard. Validated forward integration scheme for parabolic PDEs via chebyshev series. *Communications in Nonlinear Science and Numerical Simulation*, 109:106304, 2022.

[86] J. Cyranka and T. Wanner. Computer-assisted proof of heteroclinic connections in the one-dimensional Ohta–Kawasaki model. *SIAM Journal on Applied Dynamical Systems*, 17(1):694–731, 2018.

[87] J. Cyranka and P. Zgliczynski. Existence of globally attracting solutions for one-dimensional viscous Burgers equation with nonautonomous forcing — a computer assisted proof. *SIAM Journal on Applied Dynamical Systems*, 14(2):787–821, 2015.

[88] J. Dahne and J.-L. Figueras. Self-similar singular solutions to the nonlinear Schrödinger and the complex Ginzburg–Landau equations. *arXiv preprint arXiv:2410.05480*, 2024.

[89] J. Dahne, J. Gómez-Serrano, and K. Hou. A counterexample to payne's nodal line conjecture with few holes. *Communications in Nonlinear Science and Numerical Simulation*, 103:105957, 2021.

[90] H. Dankowicz and F. Schilder. *Recipes for continuation.* SIAM, 2013.

[91] J. Davenport, B. Poonen, J. Maynard, H. Helfgott, P. H. Tiep, and L. Cruz-Filipe. Machine-assisted proofs. In *Proceedings of the International Congress of Mathematicians: Rio de Janeiro 2018*, pages 1085–1110. World Scientific, 2018.

[92] S. Day, Y. Hiraoka, K. Mischaikow, and T. Ogawa. Rigorous numerics for global dynamics: A study of the Swift–Hohenberg equation. *SIAM Journal on Applied Dynamical Systems*, 4(1):1–31, 2005.

[93] S. Day, J.-P. Lessard, and K. Mischaikow. Validated continuation for equilibria of PDEs. *SIAM J. Numer. Anal.*, 45(4):1398–1424, 2007.

[94] R. de La Llave, A. Olvera, and N. P. Petrov. Combination laws for scaling exponents and relation to the geometry of renormalization operators: the principle of approximate combination of scaling exponents. *Journal of Statistical Physics*, 143(5):889–920, 2011.

[95] B. Derrida, A. Grevois, and Y. Pomeau. Universal metric properties of bifurcations of endomorphisms. *Journal of Physics A: Mathematical and General*, 12(3):269, 1979.

[96] L. Desvillettes, Y.-J. Kim, A. Trescases, and C. Yoon. A logarithmic chemotaxis model featuring global existence and aggregation. *Nonlinear Analysis: Real World Applications*, 50:562–582, 2019.

[97] L. Desvillettes, T. Lepoutre, A. Moussa, and A. Trescases. On the entropic structure of reaction-cross diffusion systems. *Communications in Partial Differential Equations*, 40(9):1705–1747, 2015.

[98] R. E. L. DeVille, N. S. Namachchivaya, and Z. Rapti. Stability of a stochastic two-dimensional non-Hamiltonian system. *SIAM Journal on Applied Mathematics*, 71(4):1458–1475, 1 2011.

[99] A. Dhooge, W. Govaerts, Y. A. Kuznetsov, H. G. E. Meijer, and B. Sautois. New features of the software MatCont for bifurcation analysis of dynamical systems. *Mathematical and Computer Modelling of Dynamical Systems*, 14(2):147–175, 2008.

[100] H. Dijkstra, L. Frankcombe, and H. Von der Heydt. A stochastic dynamical systems view of the Atlantic multidecadal oscillation. *Philos Trans A Math Phys Eng Sci.*, 366:2545–2560, 2008.

[101] T. S. Doan, M. Engel, J. S. W. Lamb, and M. Rasmussen. Hopf bifurcation with additive noise. *Nonlinearity*, 31(10):4567–4601, 2018.

[102] E. J. Doedel, A. R. Champneys, F. Dercole, T. F. Fairgrieve, Y. A. Kuznetsov, B. Oldeman, R. Paffenroth, B. Sandstede, X. Wang, and C. Zhang. AUTO-07P: Continuation and bifurcation software for ordinary differential equations, 2007.

[103] R. Donninger and B. Schörkhuber. Self-similar blowup for the cubic Schrödinger equation. *arXiv preprint arXiv:2406.16597*, 2024.

[104] G. W. Duchesne, J.-P. Lessard, and A. Takayasu. A rigorous integrator and global existence for higher-dimensional semilinear parabolic pdes via semigroup theory. *Journal of Scientific Computing*, 102(3):62, 2025.

[105] W. E, W. Ren, and E. Vanden-Eijnden. Minimum action method for the study of rare events. *Communications on pure and applied mathematics*, 57(5):637–656, 2004.

[106] W. E, W. Ren, and E. Vanden-Eijnden. Simplified and improved string method for computing the minimum energy paths in barrier-crossing events. *J. Chem. Phys.*, 126(16):164103, 2007.

[107] J. P. Eckmann, H. Epstein, and P. Wittwer. Fixed points of Feigenbaum's type for the equation $f^p(\lambda x) = \lambda f(x)$. *Communications in mathematical physics*, 93:495–516, 1984.

[108] J.-P. Eckmann and P. Wittwer. *Computer methods and Borel summability applied to Feigenbaum's equation*. Springer, 1985.

[109] J.-P. Eckmann and P. Wittwer. A complete proof of the Feigenbaum conjectures. *Journal of statistical physics*, 46(3):455–475, 1987.

[110] A. Enciso, J. Gómez-Serrano, and B. Vergara. Convexity of Whitham's highest cusped wave. *arXiv preprint arXiv:1810.10935*, 2018.

[111] M. Engel, J. S. W. Lamb, and M. Rasmussen. Conditioned Lyapunov exponents for random dynamical systems. *Trans. Amer. Math. Soc.*, 372(9):6343–6370, 2019.

[112] K. Engelborghs, T. Luzyanina, and D. Roose. Numerical bifurcation analysis of delay differential equations using DDE-BIFTOOL. *ACM Transactions on Mathematical Software (TOMS)*, 28(1):1–21, 2002.

[113] H. Epstein and J. Lascoux. Analyticity properties of the Feigenbaum function. *Communications in Mathematical Physics*, 81:437–453, 1981.

[114] M. Escobedo and O. Kavian. Variational problems related to self-similar solutions of the heat equation. *Nonlinear Analysis: Theory, Methods & Applications*, 11(10):1103–1133, 1987.

[115] H. Eyring. The activated complex in chemical reactions. *J. Chem. Phys.*, 3(2):107–115, 1935.

[116] C. L. Fefferman and R. de la Llave. Relativistic stability of matter (i). *Revista Matemática Iberoamericana*, 2(1-2):119–213, 1986.

[117] M. J. Feigenbaum. Quantitative universality for a class of nonlinear transformations. *Journal of statistical physics*, 19(1):25–52, 1978.

[118] J.-L. Figueras and R. de la Llave. Numerical computations and computer assisted proofs of periodic orbits of the Kuramoto–Sivashinsky equation. *SIAM J. Appl. Dyn. Sys.*, 16(2):834–852, 2017.

[119] J.-L. Figueras, A. Haro, and A. Luque. Rigorous computer-assisted application of KAM theory: a modern approach. *Foundations of Computational Mathematics*, 17:1123–1193, 2017.

[120] N. Filonov, M. Levitin, I. Polterovich, and D. A. Sher. Pólya's conjecture for Euclidean balls. *Inventiones mathematicae*, 234(1):129–169, 2023.

[121] F. Flandoli, B. Gess, and M. Scheutzow. Synchronization by noise. *Probability Theory and Related Fields*, 168:511–556, 2017.

[122] E. Fleurantin, K. Slyman, B. Barker, and C. K. Jones. A dynamical systems approach for most probable escape paths over periodic boundaries. *Physica D: Nonlinear Phenomena*, 454:133860, 2023.

[123] L. Fousse, G. Hanrot, V. Lefèvre, P. Pélissier, and P. Zimmermann. Mpfr: A multiple-precision binary floating-point library with correct rounding. *ACM Transactions on Mathematical Software (TOMS)*, 33(2), 2007.

[124] M. Freidlin and A. Wentzell. *Random Perturbations of Dynamical Systems*. Springer, New York, 3rd edition, 2013.

[125] X. Fu, L.-H. Tang, C. Liu, J.-D. Huang, T. Hwa, and P. Lenz. Stripe formation in bacterial systems with density-suppressed motility. *Physical review letters*, 108(19):198102, 2012.

[126] K. Fujie and J. Jiang. Comparison methods for a Keller–Segel-type model of pattern formations with density-suppressed motilities. *Calculus of Variations and Partial Differential Equations*, 60(3):92, 2021.

[127] D. Funaro. *Polynomial approximation of differential equations*, volume 8. Springer Science & Business Media, 2008.

[128] D. Funaro and O. Kavian. Approximation of some diffusion evolution equations in unbounded domains by Hermite functions. *Mathematics of Computation*, 57(196):597–619, 1991.

[129] D. Gabai, G. R. Meyerhoff, and N. Thurston. Homotopy hyperbolic 3-manifolds are hyperbolic. *Annals of Mathematics*, 157(2):335–431, 2003.

[130] S. Galatolo, M. Monge, and I. Nisoli. Existence of noise induced order, a computer aided proof. *Nonlinearity*, 33(9):4237, 2020.

[131] S. Galatolo, M. Monge, I. Nisoli, and F. Poloni. A general framework for the rigorous computation of invariant densities and the coarse-fine strategy. *Chaos, Solitons & Fractals*, 170:113329, 2023.

[132] S. Galatolo and I. Nisoli. An elementary approach to rigorous approximation of invariant measures. *SIAM Journal on Applied Dynamical Systems*, 13(2):958–985, 2014.

[133] G. P. Galdi. On bifurcating time-periodic flow of a Navier–Stokes liquid past a cylinder. *Arch. Ration. Mech. An.*, 222(1):285–315, 2016.

[134] G. P. Galdi and H. Sohr. Existence and uniqueness of time-periodic physically reasonable Navier–Stokes flow past a body. *Archive for rational mechanics and analysis*, 172:363–406, 2004.

[135] Z. Galias and P. Zgliczyński. Computer assisted proof of chaos in the Lorenz equations. *Physica D: Nonlinear Phenomena*, 115(3-4):165–188, 1998.

[136] I. Gallagher and A. Moussa. The Cauchy problem for quasi-linear parabolic systems revisited. *arXiv preprint arXiv:2407.08226*, 2024.

[137] M. Gameiro and J.-P. Lessard. A posteriori verification of invariant objects of evolution equations: periodic orbits in the Kuramoto–Sivashinsky PDE. *SIAM J. Appl. Dyn. Sys.*, 16(1):687–728, 2017.

[138] M. Gameiro, J.-P. Lessard, and A. Pugliese. Computation of smooth manifolds via rigorous multi-parameter continuation in infinite dimensions. *Foundations of Computational Mathematics*, 16(2):531–575, 2016.

[139] R. Ghanem and D. Ghosh. Efficient characterization of the random eigenvalue problem in a polynomial chaos decomposition. *International Journal for Numerical Methods in Engineering*, 72(4):486–504, 2007.

[140] R. G. Ghanem and P. D. Spanos. Stochastic Finite Element Method: Response Statistics. In *Stochastic Finite Elements: A Spectral Approach*, pages 101–119. Springer, 1991.

[141] J. Gimeno, J.-P. Lessard, J. D. Mireles James, and J. Yang. Persistence of periodic orbits under state-dependent delayed perturbations: computer-assisted proofs. *SIAM Journal on Applied Dynamical Systems*, 22(3):1743–1779, 2023.

[142] B. J. Gluckman, T. I. Netoff, E. J. Neel, W. L. Ditto, M. L. Spano, and S. J. Schiff. Stochastic resonance in a neuronal network from mammalian brain. *Physical Review Letters*, 77(19):4098, 1996.

[143] J. Gómez-Serrano. Computer-assisted proofs in PDE: a survey. *SeMA Journal*, 76(3):459–484, 2019.

[144] I. C. Gonnella, M. Khamlich, F. Pichi, and G. Rozza. A stochastic perturbation approach to nonlinear bifurcating problems. *arXiv preprint arXiv:2402.16803*, 2024.

[145] G. Gonthier et al. Formal proof–the four-color theorem. *Notices of the AMS*, 55(11):1382–1393, 2008.

[146] T. Grafke, T. Schäfer, and E. Vanden-Eijnden. Long term effects of small random perturbations on dynamical systems: Theoretical and computational tools. *Recent progress and modern challenges in applied mathematics, modeling and computational science*, pages 17–55, 2017.

[147] J. Guckenheimer and P. Holmes. *Nonlinear oscillations, dynamical systems, and bifurcations of vector fields*, volume 42. Springer Science & Business Media, 2013.

[148] J. Guerand, A. Menegaki, and A. Trescases. Global smooth solutions for triangular reaction-cross diffusion systems. *Bulletin des Sciences Mathématiques*, 189:103342, 2023.

[149] T. Hales, M. Adams, G. Bauer, T. D. Dang, J. Harrison, H. Le Truong, C. Kaliszyk, V. Magron, S. McLaughlin, T. T. Nguyen, et al. A formal proof of the Kepler conjecture. In *Forum of mathematics, Pi*, volume 5, page e2. Cambridge University Press, 2017.

[150] T. C. Hales. A proof of the Kepler conjecture. *Annals of mathematics*, pages 1065–1185, 2005.

[151] A. Haro, M. Canadell, J.-L. Figueras, A. Luque, and J.-M. Mondelo. The parameterization method for invariant manifolds. *Appl. Math. Sci*, 195, 2016.

[152] A. Haro and E. Sandin Vidal. Computer-assisted proofs of existence of fiberwise hyperbolic invariant tori in quasi-periodic systems via Fourier methods. *Discrete and Continuous Dynamical Systems-B*, 2024.

[153] K. Hashimoto, T. Kimura, T. Minamoto, and M. T. Nakao. Constructive error analysis of a full-discrete finite element method for the heat equation. *Japan Journal of Industrial and Applied Mathematics*, 36(3):777–790, 2019.

[154] K. Hashimoto, T. Kinoshita, and M. T. Nakao. Numerical verification of solutions for nonlinear parabolic problems. *Numerical Functional Analysis and Optimization*, 41(12):1495–1514, 2020.

[155] J. Hass and R. Schlafly. Double bubbles minimize. *Annals of Mathematics*, pages 459–515, 2000.

[156] G. Henkelman and H. Jónsson. A dimer method for finding saddle points on high dimensional potential surfaces using only first derivatives. *The Journal of chemical physics*, 111(15):7010–7022, 1999.

[157] G. Henkelman, B. P. Uberuaga, and H. Jónsson. A climbing image nudged elastic band method for finding saddle points and minimum energy paths. *The Journal of chemical physics*, 113(22):9901–9904, 2000.

[158] O. Hénot. On polynomial forms of nonlinear functional differential equations. *Journal of Computational Dynamics*, 8(3):307–323, 2021.

[159] O. Hénot, J.-P. Lessard, and J. Mireles James. Parameterization of unstable manifolds for DDEs: formal series solutions and validated error bounds. *Journal of Dynamics and Differential Equations*, 34(2):1285–1324, 2022.

[160] M. A. Herrero and J. J. Velázquez. A blow-up mechanism for a chemotaxis model. *Annali della Scuola Normale Superiore di Pisa-Classe di Scienze*, 24(4):633–683, 1997.

[161] M. Heymann and E. Vanden-Eijnden. The geometric minimum action method: A least action principle on the space of curves. *Communications on Pure and Applied Mathematics: A Journal Issued by the Courant Institute of Mathematical Sciences*, 61(8):1052–1117, 2008.

[162] M. Heymann and E. Vanden-Eijnden. Pathways of maximum likelihood for rare events in nonequilibrium systems: application to nucleation in the presence of shear. *Physical review letters*, 100(14):140601, 2008.

[163] L. T. Hoang, T. V. Nguyen, and T. V. Phan. Gradient estimates and global existence of smooth solutions to a cross-diffusion system. *SIAM Journal on Mathematical Analysis*, 47(3):2122–2177, 2015.

[164] W. Huang and K. Lu. Entropy, chaos, and weak horseshoe for infinite-dimensional random dynamical systems. *Communications on Pure and Applied Mathematics*, 70(10):1987–2036, 10 2017.

[165] M. Iida, M. Mimura, and H. Ninomiya. Diffusion, cross-diffusion and competitive interaction. *Journal of mathematical biology*, 53(4):617–641, 2006.

[166] G. Iooss. Existence et stabilité de la solution périodique secondaire intervenant dans les problèmes d'évolution du type Navier–Stokes. *Arch. Ration. Mech. An.*, 47(4):301–329, 1972.

[167] O. Ippei. Computer-assisted verification method for invariant densities and rates of decay of correlations. *SIAM Journal on Applied Dynamical Systems*, 10(2):788–816, 2011.

[168] V. Iudovich. The onset of auto-oscillations in a fluid. *PMM–J. Appl. Math. Mec.*, 35(4):587–603, 1971.

[169] H. Izuhara, M. Mimura, et al. Reaction-diffusion system approximation to the cross-diffusion competition system. *Hiroshima Mathematical Journal*, 38(2):315–347, 2008.

[170] J. Jaquette. A proof of Jones' conjecture. *Journal of Differential Equations*, 266(6):3818–3859, 2019.

[171] H.-Y. Jin, Y.-J. Kim, and Z.-A. Wang. Boundedness, stabilization, and pattern formation driven by density-suppressed motility. *SIAM Journal on Applied Mathematics*, 78(3):1632–1657, 2018.

[172] H.-Y. Jin and Z.-A. Wang. Critical mass on the Keller–Segel system with signal-dependent motility. *Proceedings of the American Mathematical Society*, 148(11):4855–4873, 2020.

[173] F. Johansson. Arb: efficient arbitrary-precision midpoint-radius interval arithmetic. *IEEE Transactions on Computers*, 66(8):1281–1292, 2017.

[174] D. Joseph and D. Sattinger. Bifurcating time periodic solutions and their stability. *Arch. Ration. Mech. An.*, 45(2):79–109, 1972.

[175] A. Jüngel. *Entropy methods for diffusive partial differential equations*, volume 804. Springer, 2016.

[176] S. Kaniel and M. Shinbrot. A reproductive property of the Navier–Stokes equations. *Arch. Ration. Mech. An.*, 24(5):363, 1967.

[177] L. V. Kantorovich. Functional analysis and applied mathematics. *Uspekhi Matematicheskikh Nauk*, 3(6):89–185, 1948.

[178] T. Kapela, M. Mrozek, D. Wilczak, and P. Zgliczyński. CAPD:: DynSys: a flexible C++ toolbox for rigorous numerical analysis of dynamical systems. *Communications in nonlinear science and numerical simulation*, 101:105578, 2021.

[179] O. Kavian. Remarks on the large time behaviour of a nonlinear diffusion equation. *Annales de l'Institut Henri Poincaré C, Analyse non linéaire*, 4(5):423–452, 1987.

[180] O. Kavian and F. B. Weissler. The pseudo-conformally invariant nonlinear Schrödinger equation. *Michigan Math. J*, 41:151–73, 1994.

[181] G. Kawahara and S. Kida. Periodic motion embedded in plane Couette turbulence: regeneration cycle and burst. *J. Fluid Mech.*, 449:291–300, 2001.

[182] M. Keane, R. Murray, and L.-S. Young. Computing invariant measures for expanding circle maps. *Nonlinearity*, 11(1):27, 1998.

[183] E. F. Keller and L. A. Segel. Initiation of slime mold aggregation viewed as an instability. *Journal of theoretical biology*, 26(3):399–415, 1970.

[184] E. F. Keller and L. A. Segel. Model for chemotaxis. *Journal of theoretical biology*, 30(2):225–234, 1971.

[185] S. Kepley and J. Mireles James. Chaotic motions in the restricted four body problem via Devaney's saddle-focus homoclinic tangle theorem. *Journal of Differential Equations*, 266(4):1709–1755, 2019.

[186] M. Kim, M. T. Nakao, Y. Watanabe, and T. Nishida. A numerical verification method of bifurcating solutions for 3-dimensional Rayleigh–Bénard problems. *Numer. Math.*, 111:389–406, 2009.

[187] K. Kishimoto and H. F. Weinberger. The spatial homogeneity of stable equilibria of some reaction-diffusion systems on convex domains. *Journal of Differential Equations*, 58(1):15–21, 1985.

[188] R. Klatte, U. Kulisch, A. Wiethoff, and M. Rauch. *C-XSC: A C++ class library for extended scientific computing*. Springer Science & Business Media, 2012.

[189] O. Knüppel. PROFIL/BIAS: a fast interval library [PROFIL/BIAS: eine schnelle Intervallbibliothek]. *Computing*, 53(3-4):277–287, 1994.

[190] K. Kobayashi. On the global uniqueness of Stokes' wave of extreme form. *IMA journal of applied mathematics*, 75(5):647–675, 2010.

[191] H. Kozono and M. Nakao. Periodic solutions of the Navier–Stokes equations in unbounded domains. *Tohoku Math. J.*, 48(1):33–50, 1996.

[192] H. A. Kramers. Brownian motion in a field of force and the diffusion model of chemical reactions. *Physica*, 7(4):284–304, 1940.

[193] Y. A. Kuznetsov. *Elements of applied bifurcation theory*, volume 112. Springer Science & Business Media, 2013.

[194] J. S. Lamb, G. Tenaglia, and D. Turaev. Horsehoes for a class of nonuniformly expanding random dynamical systems on the circle. *arXiv preprint arXiv:2304.03685*, 2023.

[195] O. E. Lanford III. A computer-assisted proof of the Feigenbaum conjectures. *Bulletin of the American Mathematical Society*, 6(3):427–434, 1982.

[196] O. Le Maître and O. M. Knio. *Spectral methods for uncertainty quantification: with applications to computational fluid dynamics*. Springer Science & Business Media, 2010.

[197] O. Le Maître, L. Mathelin, O. Knio, and M. Hussaini. Asynchronous time integration for polynomial chaos expansion of uncertain periodic dynamics. *Discrete Contin. Dyn. Syst*, 28:199–226, 2010.

[198] F. Ledrappier and L.-S. Young. Entropy formula for random transformations. *Probability theory and related fields*, 80(2):217–240, 1988.

[199] T. Lelièvre and F. Nier. Low temperature asymptotics for quasistationary distributions in a bounded domain. *Analysis & PDE*, 8(3):561–628, 2015.

[200] J.-P. Lessard. Recent advances about the uniqueness of the slowly oscillating periodic solutions of Wright's equation. *Journal of Differential Equations*, 248(5):992–1016, 2010.

[201] J.-P. Lessard and J. Mireles James. A rigorous implicit C^1 Chebyshev integrator for delay equations. *Journal of Dynamics and Differential Equations*, 33(4):1959–1988, 2021.

[202] J.-P. Lessard and J. D. Mireles James. Computer assisted Fourier analysis in sequence spaces of varying regularity. *SIAM Journal on Mathematical Analysis*, 49(1):530–561, 2017.

[203] J.-P. Lessard, J. D. Mireles James, and J. Ransford. Automatic differentiation for Fourier series and the radii polynomial approach. *Physica D: Nonlinear Phenomena*, 334:174–186, 2016.

[204] J.-P. Lessard and C. Reinhardt. Rigorous numerics for nonlinear differential equations using Chebyshev series. *SIAM J. Numer. Anal.*, 52(1):1–22, 2014.

[205] J.-P. Lessard, E. Sander, and T. Wanner. Rigorous continuation of bifurcation points in the diblock copolymer equation. *Journal of Computational Dynamics*, 4(1&2):71, 2017.

[206] K. K. Lin and L.-S. Young. Shear-induced chaos. *Nonlinearity*, 21(5):899–922, 2008.

[207] C. Liu, X. Fu, L. Liu, X. Ren, C. K. Chau, S. Li, L. Xiang, H. Zeng, G. Chen, L.-H. Tang, et al. Sequential establishment of stripe patterns in an expanding cell population. *Science*, 334(6053):238–241, 2011.

[208] X. Liu. *Guaranteed Computational Methods for Self-Adjoint Differential Eigenvalue Problems*. Springer Nature, 2024.

[209] X. Liu, M. T. Nakao, and S. Oishi. Computer-assisted proof for the stationary solution existence of the Navier–Stokes equation over 3D domains. *Communications in Nonlinear Science and Numerical Simulation*, 108:106223, 2022.

[210] Z. Liu and J. Xu. Large time behavior of solutions for density-suppressed motility system in higher dimensions. *Journal of Mathematical Analysis and Applications*, 475(2):1596–1613, 2019.

[211] C. Liverani et al. Rigorous numerical investigation of the statistical properties of piecewise expanding maps. a feasibility study. *Nonlinearity*, 14(3):463–490, 2001.

[212] M. Lyubich. Feigenbaum–Coullet–Tresser universality and Milnor's hairiness conjecture. *Annals of Mathematics*, pages 319–420, 1999.

[213] Y. Lou and W.-M. Ni. Diffusion, self-diffusion and cross-diffusion. *Journal of Differential Equations*, 131(1):79–131, 1996.

[214] Y. Lou, W.-M. Ni, and S. Yotsutani. On a limiting system in the Lotka–Volterra competition with cross-diffusion. *Discrete & Continuous Dynamical Systems-A*, 10(1&2):435, 2004.

[215] P. Maremonti. Existence and stability of time-periodic solutions to the Navier–Stokes equations in the whole space. *Nonlinearity*, 4(2):503–529, 1991.

[216] R. J. Mathar. Chebyshev series representation of Feigenbaum's period-doubling function. *arXiv preprint arXiv:1008.4608*, 2010.

[217] L. Mathelin and O. Le Maître. Dual-based a posteriori error estimate for stochastic finite element methods. *Communications in Applied Mathematics and Computational Science*, 2(1):83–115, 2007.

[218] P. McKenna, F. Pacella, M. Plum, and D. Roth. A uniqueness result for a semilinear elliptic problem: A computer-assisted proof. *Journal of Differential Equations*, 247(7):2140–2162, 2009.

[219] P. J. McKenna, F. Pacella, M. Plum, and D. Roth. A computer-assisted uniqueness proof for a semilinear elliptic boundary value problem. In *Inequalities and Applications 2010: Dedicated to the Memory of Wolfgang Walter*, pages 31–52. Springer, 2012.

[220] A. Melcher, G. Schneider, and H. Uecker. A Hopf-bifurcation theorem for the vorticity formulation of the Navier–Stokes equations in $\mathbb{R}^3$. *Communications in Partial Differential Equations*, 33(5):772–783, 2008.

[221] S. Méléard and D. Villemonais. Quasi-stationary distributions and population processes. *Probab. Surv.*, 9:340–410, 2012.

[222] G. Melquiond. Proving bounds on real-valued functions with computations. In *International Joint Conference on Automated Reasoning*, pages 2–17. Springer, 2008.

[223] F. Meyer, C. Rohde, and J. Giesselmann. A posteriori error analysis for random scalar conservation laws using the stochastic Galerkin method. *IMA Journal of Numerical Analysis*, 40(2):1094–1121, 2020.

[224] M. Mimura and K. Kawasaki. Spatial segregation in competitive interaction-diffusion equations. *Journal of Mathematical Biology*, 9(1):49–64, 1980.

[225] M. Mimura, Y. Nishiura, A. Tesei, and T. Tsujikawa. Coexistence problem for two competing species models with density-dependent diffusion. *Hiroshima Mathematical Journal*, 14(2):425–449, 1984.

[226] J. D. Mireles James. Validated numerics for equilibriua of analytic vector fields: invariant manifolds and connecting orbits. *Rigorous Numerics in Dynamics, Proc. Sympos. Appl. Math., Amer. Math. Soc*, 74:27–79, 2017.

[227] J. D. Mireles James and K. Mischaikow. Computational proofs in dynamics. In *Encyclopedia of Applied Computational Mathematics*, pages 288–295. Springer Berlin Heidelberg, 2015.

[228] K. Mischaikow and M. Mrozek. Chaos in the Lorenz equations: a computer-assisted proof. *Bulletin of the American Mathematical Society*, 32(1):66–72, 1995.

[229] K. Mischaikow and M. Mrozek. Conley index. *Handbook of dynamical systems*, 2:393–460, 2002.

[230] A. Molteni. An efficient method for the computation of the Feigenbaum constants to high precision. *arXiv preprint arXiv:1602.02357*, 2016.

[231] R. E. Moore. A test for existence of solutions to nonlinear systems. *SIAM Journal on Numerical Analysis*, 14(4):611–615, 1977.

[232] R. E. Moore, R. B. Kearfott, and M. J. Cloud. *Introduction to interval analysis*. SIAM, 2009.

[233] K. Müller and L. D. Brown. Location of saddle points and minimum energy paths by a constrained simplex optimization procedure. *Theoretica chimica acta*, 53(1):75–93, 1979.

[234] K. Nagatou, M. Nakao, and M. Wakayama. Verified numerical computations for eigenvalues of non-commutative harmonic oscillators. *Numerical Functional Analysis and Optimization*, 23(5-6):633–650, 2002.

[235] K. Nagatou, M. Plum, and M. T. Nakao. Eigenvalue excluding for perturbed-periodic one-dimensional Schrödinger operators. *Proceedings of the Royal Society A: Mathematical, Physical and Engineering Sciences*, 468(2138):545–562, 2012.

[236] M. T. Nakao. A numerical approach to the proof of existence of solutions for elliptic problems. *Japan Journal of Applied Mathematics*, 5(2):313, 1988.

[237] M. T. Nakao. Solving nonlinear parabolic problems with result verification. Part I: one-space dimensional case. *Journal of Computational and Applied Mathematics*, 38(1-3):323–334, 1991.

[238] M. T. Nakao, M. Plum, and Y. Watanabe. *Numerical Verification Methods and Computer-Assisted Proofs for Partial Differential Equations*, volume 53 of *Springer Series in Computational Mathematics*. Springer Singapore, 2019.

[239] M. Nauenberg. Fractal boundary of domain of analyticity of the Feigenbaum function and relation to the Mandelbrot set. *Journal of statistical physics*, 47:459–475, 1987.

[240] A. Neumaier. Complete search in continuous global optimization and constraint satisfaction. *Acta numerica*, 13:271–369, 2004.

[241] W.-M. Ni. Diffusion, cross-diffusion, and their spike-layer steady states. *Notices of the AMS*, 45(1):9–18, 1998.

[242] N. Nigam, B. Siudeja, and B. Young. A proof via finite elements for Schiffer's conjecture on a regular pentagon. *Foundations of Computational Mathematics*, 20:1475–1504, 2020.

[243] S. Oishi. Numerical verification of existence and inclusion of solutions for nonlinear operator equations. *Journal of Computational and Applied Mathematics*, 60(1-2):171–185, 1995.

[244] F. W. Olver, D. W. Lozier, R. F. Boisvert, and C. W. Clark. *NIST handbook of mathematical functions*. Cambridge University Press, 2010.

[245] J. M. Ortega. The Newton-Kantorovich theorem. *The American Mathematical Monthly*, 75(6):658–660, 1968.

[246] L. A. Peletier, D. Terman, and F. Weissler. On the equation $\Delta u + \frac{x}{2} \cdot \nabla u + f(u) = 0$. *Archive for Rational Mechanics and Analysis*, 94(1):83–99, 1986.

[247] M. Plum. Eigenvalue inclusions for second-order ordinary differential operators by a numerical homotopy method. *Zeitschrift für angewandte Mathematik und Physik ZAMP*, 41(2):205–226, 1990.

[248] M. Plum. Explicit H^2-estimates and pointwise bounds for solutions of second-order elliptic boundary value problems. *Journal of Mathematical Analysis and Applications*, 165(1):36–61, 1992.

[249] M. Plum. Existence and enclosure results for continua of solutions of parameter-dependent nonlinear boundary value problems. *Journal of Computational and Applied Mathematics*, 60(1-2):187–200, 1995.

[250] M. Plum and C. Wieners. New solutions of the Gelfand problem. *Journal of mathematical analysis and applications*, 269(2):588–606, 2002.

[251] D. Potts, G. Steidl, and M. Tasche. Fast algorithms for discrete polynomial transforms. *Mathematics of Computation of the American Mathematical Society*, 67(224):1577–1590, 1998.

[252] G. Raugel. Global attractors in partial differential equations. *Handbook of dynamical systems*, 2:885–982, 2002.

[253] C. Reinhardt and J. Mireles James. Fourier–Taylor parameterization of unstable manifolds for parabolic partial differential equations: formalism, implementation and rigorous validation. *Indagationes Mathematicae*, 30(1):39–80, 2019.

[254] N. Revol. Introduction to the IEEE 1788-2015 standard for interval arithmetic. In *Numerical Software Verification: 10th International Workshop, NSV 2017, Heidelberg, Germany, July 22-23, 2017, Proceedings 10*, pages 14–21. Springer, 2017.

[255] N. Revol and F. Rouillier. Motivations for an arbitrary precision interval arithmetic and the MPFI library. *Reliable computing*, 11(4):275–290, 2005.

[256] P. Rizzi, E. Sander, and T. Wanner. Cyclic symmetry induced pitchfork bifurcations in the diblock copolymer model. *Discrete and Continuous Dynamical Systems-B*, 29(2):666–701, 2024.

[257] D. Ruelle and F. Takens. On the nature of turbulence. *Les rencontres physiciens-mathématiciens de Strasbourg-RCP25*, 12:1–44, 1971.

[258] S. Rump. INTLAB - INTerval LABoratory. In T. Csendes, editor, *Developments in Reliable Computing*, pages 77–104. Kluwer Academic Publishers, Dordrecht, 1999. http://www.tuhh.de/ti3/rump/.

[259] S. M. Rump. Verification methods: Rigorous results using floating-point arithmetic. *Acta Numer*, 19:287–449, 2010.

[260] K. Ryu and I. Ahn. Coexistence theorem of steady states for nonlinear self-cross diffusion systems with competitive dynamics. *Journal of mathematical analysis and applications*, 283(1):46–65, 2003.

[261] B. Salvy. Linear differential equations as a data structure. *Foundations of Computational Mathematics*, 19(5):1071–1112, 2019.

[262] E. Sander and T. Wanner. Equilibrium validation in models for pattern formation based on Sobolev embeddings. *Discrete and Continuous Dynamical Systems-B*, 26(1):603–632, 2020.

[263] Y. Sato, T. S. Doan, J. S. Lamb, and M. Rasmussen. Dynamical characterization of stochastic bifurcations in a random logistic map. *arXiv preprint arXiv:1811.03994*, 2018.

[264] M. Schick, V. Heuveline, and O. Le Maitre. A Newton–Galerkin method for fluid flow exhibiting uncertain periodic dynamics. *SIAM/ASA Journal on Uncertainty Quantification*, 2(1):153–173, 2014.

[265] R. E. Schwartz. Obtuse triangular billiards II: One hundred degrees worth of periodic trajectories. *Experimental Mathematics*, 18(2):137–171, 2009.

[266] J. Serrin. A note on the exstencie of periodic solutions of the Navier–Stokes equations. *Arch. Ration. Mech. An.*, 3(2):120–122, 1959.

[267] D. Sheppard, R. Terrell, and G. Henkelman. Optimization methods for finding minimum energy paths. *J. Chem. Phys.*, 128(13):134106, 2008.

[268] N. Shigesada, K. Kawasaki, and E. Teramoto. Spatial segregation of interacting species. *Journal of theoretical biology*, 79(1):83–99, 1979.

[269] T. J. Sullivan. *Introduction to uncertainty quantification*, volume 63. Springer, 2015.

[270] R. Szczelina and P. Zgliczyński. Algorithm for rigorous integration of delay differential equations and the computer-assisted proof of periodic orbits in the Mackey–Glass equation. *Foundations of Computational Mathematics*, 18:1299–1332, 2018.

[271] R. Szczelina and P. Zgliczyński. High-order lohner-type algorithm for rigorous computation of Poincaré maps in systems of delay differential equations with several delays. *Foundations of Computational Mathematics*, 24(4):1389–1454, 2024.

[272] R. Szwarc. Orthogonal polynomials and Banach algebras. *Inzell Lectures on Orthogonal Polynomials. Advances in the Theory of Special Functions and Orthogonal Polynomials, Nova Science Publishers*, 2:103–139, 2005.

[273] A. Takayasu, J.-P. Lessard, J. Jaquette, and H. Okamoto. Rigorous numerics for nonlinear heat equations in the complex plane of time. *Numerische Mathematik*, pages 1–58, 2022.

[274] A. Takayasu, X. Liu, and S. Oishi. Verified computations to semilinear elliptic boundary value problems on arbitrary polygonal domains. *Nonlinear Theory and Its Applications, IEICE*, 4(1):34–61, 2013.

[275] A. Takayasu, M. Mizuguchi, T. Kubo, and S. Oishi. Accurate method of verified computing for solutions of semilinear heat equations. *Reliable Computing*, 25:75, 2017.

[276] A. Takeshita. On the reproductive property of the 2-dimensional Navier–Stokes equations. *J. Fac. Sci. Univ. Tokyo Sect. I*, 16:297–311, 1969.

[277] A. Tantet, M. D. Chekroun, H. A. Dijkstra, and J. D. Neelin. Ruelle–Pollicott resonances of stochastic systems in reduced state space. part II: Stochastic Hopf bifurcation. *J. Stat. Phys.*, 179(5-6):1403–1448, 2020.

[278] G. I. Taylor and A. E. Green. Mechanism of the production of small eddies from large ones. *P. Roy. Soc. Lond. A Mat.*, 158(895):499–521, 1937.

[279] H. Touchette. Introduction to dynamical large deviations of Markov processes. *Physica A: Statistical Mechanics and its Applications*, 504:5–19, 2018.

[280] L. N. Trefethen. *Approximation theory and approximation practice*, volume 128. Siam, 2013.

[281] C. Tresser and P. Coullet. Itérations d'endomorphismes et groupe de renormalisation. *C.R. Acad. Sci. Paris Sér. A*, 287(7):577—-580, 1978.

[282] W. Tucker. A rigorous ODE solver and Smale's 14th problem. *Foundations of Computational Mathematics*, 2(1):53–117, 2002.

[283] W. Tucker. *Validated numerics: a short introduction to rigorous computations*. Princeton University Press, 2011.

[284] H. Uecker, D. Wetzel, and J. D. Rademacher. pde2path-A Matlab package for continuation and bifurcation in 2D elliptic systems. *Numerical Mathematics: Theory, Methods and Applications*, 7(1):58–106, 2014.

[285] M. Urabe. Galerkin's procedure for nonlinear periodic systems. *Archive for Rational Mechanics and Analysis*, 20(2):120–152, 1965.

[286] J. B. van den Berg. Introduction to rigorous numerics in dynamics: general functional analytic setup and an example that forces chaos. *Rigorous Numerics in Dynamics, Proc. Sympos. Appl. Math., Amer. Math. Soc*, 74:1–25, 2017.

[287] J. B. van den Berg, C. M. Groothedde, and J. Williams. Rigorous computation of a radially symmetric localized solution in a Ginzburg–Landau problem. *SIAM Journal on Applied Dynamical Systems*, 14(1):423–447, 2015.

[288] J. B. van den Berg, O. Hénot, and J.-P. Lessard. Constructive proofs for localised radial solutions of semilinear elliptic systems on $\mathbb{R}^d$. *Nonlinearity*, 36(12):6476, 2023.

[289] J. B. van den Berg and J. Jaquette. A proof of Wright's conjecture. *Journal of Differential Equations*, 264(12):7412–7462, 2018.

[290] J. B. van den Berg, J. Jaquette, and J. Mireles James. Validated numerical approximation of stable manifolds for parabolic partial differential equations. *Journal of Dynamics and Differential Equations*, pages 1–61, 2022.

[291] J. B. van den Berg and J.-P. Lessard. Rigorous numerics in dynamics. *Notices Amer. Math. Soc.*, 62(9), 2015.

[292] J. B. van den Berg, J.-P. Lessard, and K. Mischaikow. Global smooth solution curves using rigorous branch following. *Mathematics of computation*, 79(271):1565–1584, 2010.

[293] J. B. Van den Berg, J.-P. Lessard, and E. Queirolo. Rigorous verification of Hopf bifurcations via desingularization and continuation. *SIAM Journal on Applied Dynamical Systems*, 20(2):573–607, 2021.

[294] J. B. van den Berg and E. Queirolo. A general framework for validated continuation of periodic orbits in systems of polynomial ODEs. *Journal of Computational Dynamics*, 8(1):59, 2021.

[295] J. B. van den Berg and R. Sheombarsing. Validated computations for connecting orbits in polynomial vector fields. *Indagationes Mathematicae*, 31(2):310–373, 2020.

[296] J. B. van den Berg and R. Sheombarsing. Rigorous numerics for ODEs using Chebyshev series and domain decomposition. *Journal of Computational Dynamics*, 8(3):353, 2021.

[297] J. B. van den Berg and J. F. Williams. Validation of the bifurcation diagram in the 2D Ohta–Kawasaki problem. *Nonlinearity*, 30(4):1584, 2017.

[298] J. B. van den Berg and J. F. Williams. Rigorously computing symmetric stationary states of the Ohta–Kawasaki problem in three dimensions. *SIAM Journal on Mathematical Analysis*, 51(1):131–158, 2019.

[299] L. van der Aalst, J. B. van den Berg, and J.-P. Lessard. Periodic localized traveling waves in the two-dimensional suspension bridge equation. *arXiv preprint arXiv:2405.19759*, 2024.

[300] L. van Veen. *Computational Modelling of Bifurcations and Instabilities in Fluid Dynamics*, chapter A brief history of simple invariant solutions in turbulence, pages 217–232. Springer, 2019.

[301] L. van Veen and G. Kawahara. Homoclinic tangle on the edge of shear turbulence. *Physical review letters*, 107(11):114501, 2011.

[302] S. Varadhan. *Large Deviations and Applications*. SIAM, 1984.

[303] M. Viana. *Lectures on Lyapunov exponents*, volume 145. Cambridge University Press, 2014.

[304] C. Villani. *Hypocoercivity*, volume 202. American Mathematical Society, 2009.

[305] J. Wang and M. Wang. Boundedness in the higher-dimensional Keller–Segel model with signal-dependent motility and logistic growth. *Journal of Mathematical Physics*, 60(1), 2019.

[306] Y. Wang, C.-Y. Lai, J. Gómez-Serrano, and T. Buckmaster. Asymptotic self-similar blow-up profile for three-dimensional axisymmetric euler equations using neural networks. *Physical Review Letters*, 130(24):244002, 2023.

[307] T. Wanner. Computer-assisted bifurcation diagram validation and applications in materials science. In *Proc. Sympos. Appl. Math. Rigorous Numerics in Dynamics.*, volume 74, pages 123–174. Amer. Math. Soc., 2018.

[308] Y. Watanabe. A computer-assisted proof for the Kolmogorov flows of incompressible viscous fluid. *J. Comp. Appl. Math.*, 223:953–966, 2009.

[309] Y. Watanabe. An efficient verification method for the Kolmogorov problem of incompressible fluid. *J. Comp. Appl. Math.*, 302:157–170, 2016.

[310] Y. Watanabe, M. Plum, and M. T. Nakao. A computer-assisted instability proof for the Orr–Sommerfeld problem with Poiseuille flow. *ZAMM-Journal of Applied Mathematics and Mechanics/Zeitschrift für Angewandte Mathematik und Mechanik: Applied Mathematics and Mechanics*, 89(1):5–18, 2009.

[311] Y. Watanabe, N. Yamamoto, and M. T. Nakao. A numerical verification method of solutions for the Navier–Stokes equations. *Reliab. Comput.*, 5:347–357, 1999.

[312] F. B. Weissler. Rapidly decaying solutions of an ordinary differential equation with applications to semilinear elliptic and parabolic partial differential equations. *Archive for Rational Mechanics and Analysis*, 91:247–266, 1986.

[313] S. Wieczorek. Stochastic bifurcation in noise-driven lasers and Hopf oscillators. *Physical Review E*, 79(3):036209, 2009.

[314] N. Wiener. The homogeneous chaos. *American Journal of Mathematics*, 60(4):897–936, 1938.

[315] D. Wilczak and P. Zgliczyński. A geometric method for infinite-dimensional chaos: Symbolic dynamics for the Kuramoto–Sivashinsky PDE on the line. *Journal of Differential Equations*, 269(10):8509–8548, 2020.

[316] D. Wilczak and P. Zgliczyński. Symbolic dynamics for the Kuramoto–Sivashinsky PDE on the line II. *arXiv preprint arXiv:2405.17087*, 2024.

[317] C. Wormell. Spectral Galerkin methods for transfer operators in uniformly expanding dynamics. *Numerische Mathematik*, 142:421–463, 2019.

[318] J. Wunderlich. *Computer-assisted Existence Proofs for Navier–Stokes Equations on an Unbounded Strip with Obstacle*. PhD thesis, Dissertation, Karlsruhe, Karlsruher Institut für Technologie (KIT), 2022, 2022.

[319] D. Xiu. Fast numerical methods for stochastic computations: a review. *Communications in computational physics*, 5(2-4):242–272, 2009.

[320] D. Xiu and G. E. Karniadakis. The Wiener–Askey polynomial chaos for stochastic differential equations. *SIAM journal on scientific computing*, 24(2):619–644, 2002.

[321] N. Yamamoto. A numerical verification method for solutions of boundary value problems with local uniqueness by Banach's fixed-point theorem. *SIAM J. Numer. Anal.*, 35:2004–2013, 1998.

[322] M. Yamazaki. The Navier–Stokes equations in the weak-L^n space with time-dependent external force. *Mathematische Annalen*, 317(4):635–675, 2000.

[323] E. Yanagida. Uniqueness of rapidly decaying solutions to the Haraux–Weissler equation. *journal of differential equations*, 127(2):561–570, 1996.

[324] C. Yoon and Y.-J. Kim. Global existence and aggregation in a Keller–Segel model with Fokker–Planck diffusion. *Acta Applicandae Mathematicae*, 149:101–123, 2017.

[325] L.-S. Young. Mathematical theory of Lyapunov exponents. *Journal of Physics A: Mathematical and Theoretical*, 46(25):254001, 2013.

[326] P. Zgliczynski. C^1 Lohner algorithm. *Foundations of computational mathematics*, 2:429–465, 2002.

[327] P. Zgliczynski. Rigorous numerics for dissipative partial differential equations II. Periodic orbit for the Kuramoto–Sivashinsky PDE—a computer-assisted proof. *Found. Comp. Math.*, 4(2):157–185, 2004.

[328] P. Zgliczynski. Covering relations, cone conditions and the stable manifold theorem. *J. Differential Equations*, 246(5):1774–1819, 2009.

[329] P. Zgliczyński. Rigorous numerics for dissipative PDEs III. An effective algorithm for rigorous integration of dissipative PDEs. *Topological Methods in Nonlinear Analysis*, pages 197–262, 2010.

[330] P. Zgliczynski and M. Gidea. Covering relations for multidimensional dynamical systems. *J. Differential Equations*, 202(1):32–58, 2004.

[331] P. Zgliczynski and K. Mischaikow. Rigorous numerics for partial differential equations: The Kuramoto–Sivashinsky equation. *Foundations of Computational Mathematics*, 1(3):255–288, 2001.

Institut Polytechnique de Paris
91120 Palaiseau, France